Research

Research and Service Experience with Environmentally-Assisted Cracking in Carbon and Low-Alloy Steels in High-Temperature Water

Hans-Peter Seifert
Stefan Ritter

November 2005

SKi

SKI perspective

Background

Carbon and low alloy steels are widely used for pressure-boundary components such as piping and pressure vessels in nuclear power plants. Along with other ageing mechanisms such as fatigue, erosion or flow-accelerated corrosion and irradiation embrittlement, environmentally assisted cracking has been identified as a possible degradation process for components manufactured from such materials.

Early laboratory investigations clearly demonstrated that environmentally assisted cracking might occur in low-alloy reactor pressure vessel and piping steels in high temperature water under certain critical conditions and revealed significant effects of simulated reactor environments on fatigue crack initiation/growth, as well as the possibility of crack growth through stress corrosion cracking under static loading conditions. Based on these investigations, the question of conservatism and adequacy of the relevant nuclear codes, and thus of the safety margins for critical components such as the reactor pressure vessel, arose and has resulted in intensive experimental and theoretical investigations on environmentally assisted cracking over the last three decades. This research led initially to a revision of ASME XI (1980) and, more recently, to a new pressurized water reactor (PWR) code case N-643 (2000) (which was revised in 2003), as well as to different proposals for incorporating environmental effects in ASME III.

Purpose of the project

Some years ago SKI and the Swedish utilities sponsored a project following some alarming results on stress corrosion crack growths rates in reactor pressure vessel steels. The aim of the project was to investigate the risk for stress corrosion cracking in the Swedish reactor pressure vessels. Within this project, the susceptibility of different reactor pressure vessel steels to stress corrosion cracking in BWR water has been investigated using 72 bolt loaded C(T) specimens, which were exposed to BWR normal and hydrogen water chemistry environments. Twelve C(T) specimens were multipass clad with either Inconel 182 or stainless steel AISI 308L and post weld heat treated to simulate cladding or attachment welds.

In only one of the Inconel 182 clad specimens, where the pre-fatigue crack tip was located in the pressure vessel steel base metal far beyond its heat affected zone, was marked crack growth observed in the pressure vessel steel. This was an unexpected result, so further fractographic and metallographic investigations have been performed by VTT, Finland, in order to clarify the reasons for this unique observation.

The cracking in this specific specimen was found to be due to environmentally assisted cracking in the reactor pressure vessel steel that could not be related to any mistreatment of specimen, welding defects, testing artefacts or microstructural anomalies. Although the area fraction of inclusions was high, it was within the range reported in literature for materials with increased environmentally assisted cracking susceptibility due to MnS-inclusions and no completely satisfactory explanation for this unexpected result could be forwarded.

SKI deemed it necessary to initiate further work to try and put these results in perspective of the latest knowledge in this area. Leading experts in this field from the Paul Scherrer Institute (PSI) were therefore asked by SKI to prepare a State-of-the-Art report on environmentally

assisted cracking of low-alloy reactor pressure vessel steels and to critically review and reassess the Swedish work in this area in a second report (see SKI report 2005:61). These two documents intended to support SKI with decision making as to whether or not there is a substantial risk for stress or strain-induced corrosion cracking in Swedish nuclear reactor pressure vessels, if for example a crack propagates through the cladding or an attachment weld to the underlying low alloy steel.

Results

In this report, the most relevant aspects of research and service experience with environmentally assisted cracking of carbon and low-alloy steels in high-temperature water are reviewed, with special emphasis on the primary pressure-boundary components of boiling water reactors. The main factors controlling the susceptibility to environmentally assisted cracking under light water reactor conditions are discussed with respect to crack initiation and crack growth. The adequacy and conservatism of the current BWRVIP-60 stress corrosion cracking disposition curves, ASME III fatigue design curves, and ASME XI reference fatigue crack growth curves, as well as of the GE environmentally assisted crack growth model are evaluated in the context of recent research results. The operating experience is summarized and compared to the experimental/mechanistic background knowledge. Finally, open questions and possible topics for further research are identified.

In spite of the absence of stress corrosion cracking in the field, several unfavourable critical parameter combinations, which can lead to sustained, fast stress corrosion cracking with crack growth rates well above the BWRVIP-60 stress corrosion cracking disposition curves have been identified. Many of them appear atypical for current BWR plant operation with properly manufactured carbon and low alloy steel components, but some could occur during service, at least temporarily under faulted conditions or in components with fabrication deficiencies. In the opinion of PSI, although there are open questions and potential for improvements in all fields, from a safety perspective, the special emphasis of research should be placed on these conditions, and in particular, on an improved identification/quantification of the boundaries/thresholds for the transition from low to high/accelerated stress corrosion cracking crack growth rates. In this context, PSI consider that research should be focused on the effects of chloride transients and dynamic strain ageing/yield stress on the stress corrosion crack growth behaviour of carbon and low alloy steel and of weld heat-affected zone materials under BWR normal water chemistry conditions. Additionally, the mitigation effect of hydrogen water chemistry or noble metal chemical addition should be evaluated under these critical conditions.

Effects on SKI work

The conclusions below are made using both this study and the study presented in SKI 2005:61 and also are valid for both.

Both studies are a step towards understanding the behaviour of carbon and low-alloy steels in the environment prevailing in nuclear power plants. Understanding the underlying cause of environmentally assisted cracking is necessary, to be able to mitigate it and to have an effective inspection program where it is needed.

The laboratory experiences presented in this report prevail that chloride transients have an increasing effect on crack growth rate due to stress corrosion cracking in carbon and low alloy

steels. The overwhelming part of crack growth in that only specimen showing high crack rate growth (see SKI 2005:61) seems to have occurred during a chloride transient. The explanation given by PSI that chloride transient is the cause of excessive crack growth rate appears to be reasonable.

Even in such cases only very limited stress corrosion cracking or strain induced stress corrosion cracking is expected as long as prolonged and severe chloride excursions are avoided and the number of transients are limited.

Prolonged and severe or numerous chloride transients are not expected to occur in nuclear power plants operating properly. In addition the pressure vessel steels used in Swedish nuclear power plants contain a low sulphurous content which also is favourable in terms of crack growth due to stress corrosion cracking. The risk of excessive crack growth in pressure vessel steels in Swedish nuclear power plants, due to stress corrosion cracking or strain induced corrosion cracking is therefore estimated to be low.

Although it is of scientific interest to investigate the effect of chloride excursions on stress corrosion cracking crack growth in reactor pressure vessel steels under BWR normal water chemistry conditions, and in particular the possibility of long-term effects after severe and prolonged transients, there is no practical interest of that for the time being.

Project information

Behnaz Aghili has been responsible for the project at SKI.
SKI reference: SKI 2005/309/200341002.

Research

Research and Service Experience with Environmentally-Assisted Cracking in Carbon and Low-Alloy Steels in High-Temperature Water

Hans-Peter Seifert
Stefan Ritter

Paul Scherrer Institute
Laboratory for Materials Behaviour
Nuclear Energy and Safety Research Department
5232 Villigen PSI
SWITZERLAND
E-Mail: hans-peter.seifert@psi.ch

November 2005

Executive Summary

In the following report, the most relevant aspects of research and service experience with environmentally-assisted cracking (EAC) of carbon (C) and low-alloy steels (LAS) in high-temperature (HT) water are reviewed, with special emphasis on the primary pressure-boundary components of boiling water reactors (BWRs). The main factors controlling the susceptibility to EAC under light water reactor (LWR) conditions are discussed with respect to crack initiation and crack growth. The adequacy and conservatism of the current BWRVIP-60 stress corrosion cracking (SCC) disposition lines (DLs), ASME III fatigue design curves, and ASME XI reference fatigue crack growth curves, as well as of the GE EAC crack growth model are evaluated in the context of recent research results. The operating experience is summarized and compared to the experimental/mechanistic background knowledge. Finally, open questions and possible topics for further research are identified.

Laboratory investigations revealed significant effects of simulated reactor environments on fatigue crack initiation/growth, as well as the possibility of SCC crack growth for certain specific critical combinations of environmental, material and loading parameters. During the last three decades, the major factors of influence and EAC susceptibility conditions have been readily identified. Most parameter effects on EAC initiation and growth are adequately known with acceptable reproducibility and reasonably understood by mechanistic models. Tools for incorporating environmental effects in ASME III fatigue design curves have been developed/ qualified and should be applied in spite of the high degree of conservatism in fatigue evaluation procedures. The BWRVIP-60 SCC DLs and ASME XI reference fatigue crack growth curves are usually conservative and adequate under most BWR operation circumstances.

The operating experience of C & LAS primary pressure-boundary components in LWRs is very good worldwide. However, isolated instances of EAC have occurred, particularly in BWR service, most often in piping and, rarely in the reactor pressure vessel (RPV) itself. Oxidizing conditions, usually dissolved oxygen (DO), and relevant dynamic straining were always involved. These cases were either attributed to strain-induced corrosion cracking (SICC) or corrosion fatigue (CF) and could be readily rationalized by the experimental background knowledge. Both service experience and experimental/mechanistic background knowledge confirm the high resistance of C & LAS to SCC under stationary power operation and static loading conditions and clearly reveal, that slow, positive (tensile) straining, with associated plastic yielding and sufficiently oxidizing conditions are essential for EAC initiation in HT water. Based on the experimental/mechanistic background knowledge and service experience different remedial and mitigation actions have been qualified and successfully applied, which further reduced the low EAC cracking frequency in the field.

In spite of the absence of SCC in the field, several unfavourable critical parameter combinations, which can lead to sustained, fast SCC with crack growth rates (CGRs) well above the BWRVIP-60 SCC DLs have been identified. Many of them appear atypical for current BWR plant operation with properly manufactured C & LAS components, but some might occur during service, at least temporarily under faulted conditions or in components with fabrication deficiencies. Although there are open questions and potentials for improvements in all fields, from a safety perspective, the special emphasis of research should be placed to these conditions, and in particular, to an improved identification/quantification of the boundaries/thresholds for the transition from low to high/accelerated SCC CGRs. In this context, research should be focused on the effects of chloride transients and dynamic strain ageing (DSA)/yield stress (YS) on the SCC crack growth behaviour of C & LAS and of weld heat-affected zone (HAZ) materials under BWR/normal water chemistry (NWC) conditions. Additionally, the mitigation effect of hydrogen water chemistry (HWC) or noble metal chemical addition (NMCA) should be evaluated under these critical conditions.

Table of Contents

0 Abbreviations and Symbols

Abbreviations:

ABB	Asea Brown Boveri
ASME BPV	ASME Boiler and Pressure Vessel Code
ASTM	American Society of Testing and Materials
ASTM E 399	Test method for plane-strain fracture toughness of metallic materials
BWR	Boiling water reactor
BWRVIP	Boiling Water Reactor Vessel and Internals Project
C(T)	Compact tension specimen
CF	Corrosion fatigue
CGR	Crack growth rate
CMOD	Crack-mouth opening displacement
COD$_{LL}$	Crack opening displacement at the load line
DCPD	Direct current potential drop method
DL	Disposition line
DO	Dissolved oxygen
DSA	Dynamic strain ageing
EAC	Environmentally-assisted cracking
ECP	Electrochemical corrosion potential
EPRI	Electric Power Research Institute
FRAD	Film rupture/anodic dissolution mechanism
GE	General Electric
HWC	Hydrogen water chemistry
IG	Intergranular
KTA	Kerntechnischer Ausschuss, Germany
LAS	Low-alloy steel
LCF	Low-cycle fatigue
LF	Low-frequency
LFCF	Low-frequency corrosion fatigue (test)
LWR	Light water reactor
MPA	Staatliche Materialprüfungsanstalt, University of Stuttgart, Germany
n	Neutron
NDT	Non-destructive testing
NMCA	Noble metal chemical addition
NRI	Nuclear Research Institute, Řež, Czech Republic

NWC	Normal water chemistry
PPU	Periodical partial unloading
PSI	Paul Scherrer Institute, Villigen, Switzerland
PWHT	Post-weld heat treatment
PWR	Pressurized water reactor
RPV	Reactor pressure vessel
SCC	Stress corrosion cracking
SEM	Scanning electron microscope
SHE	Standard-hydrogen electrode
SICC	Strain-induced corrosion cracking
SKI	Swedish Nuclear Power Inspectorate, Stockholm, Sweden
SRL	Slow rising load (test)
SS	Stainless steel
SSR	Slow strain rate (test)
SSY	Small-scale yielding
TG	Transgranular
UTS	Ultimate tensile strength
VGB	Technische Vereinigung der Grosskraftwerksbetreiber, Germany
VTT	Technical Research Centre of Finland, Espoo, Finland
YS	Yield stress
Z	Reduction of area

Symbols and Units:

Symbol	Unit	Designations
Δa	µm or mm	Crack advance
a	mm	Crack length
$\Delta a/\Delta N$	µm/cycle	Crack advance per fatigue cycle
da/dt	m/s	Time-based crack growth rate: time-derivate of a(t)
da/dt_{Air}	m/s	Time-based fatigue crack growth rate in air
da/dt_{EAC}	m/s	Time-based CF crack growth rate in high-temperature water
DO	ppb or ppm	Concentration of dissolved oxygen
Δa_{SICC}	µm or mm	Corrosion-assisted crack advance by SICC
Δa_{EAC}	µm or mm	Corrosion-assisted crack advance by EAC
CMOD	µm	Crack-mouth opening displacement
$dCOD_{LL}/dt$	mm/s	Crack opening displacement rate at load line
ε	[%]	Strain
$d\varepsilon/dt$	s^{-1}	Strain rate
$d\varepsilon_{CT}/dt$	s^{-1}	Crack-tip strain rate
dK_I/dt	$MPa \cdot m^{1/2}/h$	Stress intensity factor rate
ΔK	$MPa \cdot m^{1/2}$	$\Delta K = K_I^{max} - K_I^{min}$: Total stress intensity factor range
ΔK_{th}	$MPa \cdot m^{1/2}$	ΔK threshold for fatigue
Δt_D	h or s	Decline time (decreasing load)
Δt_H	h or s	Hold time (constant load at maximum peak load)
Δt_R	h or s	Rise time (rising load)
ECP	mV_{SHE}	Electrochemical corrosion potential
ν	Hz	Frequency
κ	µS/cm	Specific electric conductivity
K_I	$MPa \cdot m^{1/2}$	Stress intensity factor
$K_{I,ASTM}$	$MPa \cdot m^{1/2}$	ASTM E 399 limit for K_I
$K_{I,i}$	$MPa \cdot m^{1/2}$	K_I value at crack initiation by SICC in SRL tests
K_{IJ}	$MPa \cdot m^{1/2}$	K_I value at the onset of ductile crack growth in inert environment
N	–	Cycle number
R	–	Load-ratio: $R = P_{min} / P_{max}$
T	°C	Temperature
Z	[%]	Reduction of area

1 Introduction

1.1 Background and Goals of the Report

Some years ago SKI and the Swedish utilities sponsored a project following the alarming results on stress corrosion CGRs in RPV steels, which were published in the late eighties and early nineties [1]. The aim of this project was to demonstrate that the risk for SCC in the Swedish RPVs is minimal. Within this project, the susceptibility of different RPV steels to SCC in BWR water has been investigated with 72 bolt loaded C(T) specimens, which were exposed to BWR NWC environment during a five-year period in Oskarshamn 3, and to BWR HWC environment during a four-year period in Oskarshamn 2 [2]. Twelve C(T) specimens were multipass cladded with either Inconel 182 or stainless steel AISI 308L and post weld heat treated (PWHT) at 620 °C for 8 h to simulate cladding or attachment welds.

All non-cladded specimens revealed no or only minor (< 0.24 mm) crack growth, which usually appeared as a ditch on the fracture surfaces. However, some specimens with Inconel 182 cladding tested in BWR NWC environment revealed clear, but minor crack growth into the HAZ of the RPV steel. Marked crack growth of 2.43 mm in the pressure vessel steel was only observed in one of the Inconel 182 cladded specimens, where the pre-fatigue crack tip was located in the pressure vessel steel base metal far beyond its HAZ (specimen 402). Due to this unexpected results, further fractographic and metallographic investigations have been performed by VTT on five of the 72 modified C(T) specimens in total in order to clarify the reasons for this unexpected cracking and the results of these investigations were presented in the VTT report [3].

The cracking in the C(T) specimen 402 was found to be due to EAC in the RPV steel and could not be related to any mistreatment of specimen/welding defects, testing artefacts or microstructural anomalies. Although the area fraction of inclusions was high, within the range reported in literature for materials with increased EAC susceptibility due to MnS-inclusions, no completely satisfactory explanation for this unexpected result could be forwarded. Paul Scherrer Institute (PSI) was therefore asked by SKI to prepare a State-of-the-Art report on EAC of low-alloy RPV steels and to critically review and reassess the Swedish work in this area in a second report [4]. These two documents shall support SKI with decision making as whether or not there is a substantial risk for stress or strain-induced corrosion cracking in Swedish nuclear RPVs, if for example a crack in the cladding or an attachment weld propagates to the underlying LAS.

1.2 Structure of the Report

In this extended status report, the most relevant aspects of research and service experience with EAC of C & LAS in HT water are reviewed, with special emphasis on the primary pressure-boundary components of BWR. The main factors controlling EAC susceptibility under LWR conditions are discussed with regard to both crack initiation and crack growth. The adequacy and conservatism of the current BWRVIP-60 SCC DLs, ASME III fatigue design curves and ASME Section XI reference fatigue crack growth curves are evaluated in the context of recent research results. The relevant operating experience is summarized and compared with the background knowledge, which has been accumulated in laboratory experiments over the last 30 years. Finally, open questions and challenges for future research are identified.

This extended review report has a modular structure, since it covers a very wide range of quite different aspects ranging from mechanisms/models to field experience. Individual Sections can be read and readily understood without knowing the details of the other ones. For this reason, text parts of some Sections may appear as repetitive to a certain extent, when reading the complete report.

2 EAC of C & LAS in High-Temperature Water

2.1 Introducing Remarks on EAC of C & LAS in High-Temperature Water

C & LAS are widely used for pressure-boundary components such as piping and pressure vessels in fossil and nuclear power plants (NPPs). Along with other ageing mechanisms such as fatigue, erosion or flow-accelerated corrosion and irradiation embrittlement, EAC has been identified as a possible degradation process for C & LAS components. CF and SICC in de-aerators, feedwater piping and tanks, etc. continue to be the damage mechanisms responsible for the largest percentage of availability loss in fossil power plants [5]. Although CF and SICC are less significant in NPP, they have occurred and are perceived to be damage mechanisms which need to be considered for older plants, especially for those considering lifetime extension [5].

Early laboratory investigations clearly demonstrated that EAC might occur in low-alloy RPV and piping steels in HT water under certain critical conditions and revealed significant effects of simulated reactor environments on fatigue crack initiation/growth, as well as the possibility of crack growth through stress corrosion cracking (SCC) under static loading conditions. Based on these investigations, the question of conservatism and adequacy of the relevant nuclear codes, and thus of the safety margins for critical components such as the RPV, arose and has resulted in intensive experimental and theoretical investigations on EAC during the last three decades. This research led initially to a revision of ASME XI (1980) and, more recently, to a new pressurized water reactor (PWR) code case N-643 (2000) (which was revised in 2003), as well as to different proposals for incorporating environmental effects in ASME III. The accumulated operating experience and experimental background knowledge have been reviewed in several papers and reports during this period. [5 – 16]

2.2 Basic Types of EAC in C & LAS in High-Temperature Water

EAC is used as a general term to cover the full spectrum of corrosion cracking from SCC to CF. EAC can be further classified by the crack propagation mechanism, crack path, etc. but currently no internationally accepted consensus definition for the different cracking types exists. In case of C & LAS and nuclear applications, differentiation of cracking mechanism is usually performed according to the type of mechanical loading involved. SICC, which involves slow, dynamic straining with localized plastic deformation of material, but where obvious cyclic loading is absent, or restricted to a limited number of infrequent events such as plant start-up and shut-down, is increasingly used as an appropriate term to describe the area of overlap between SCC and CF. The different EAC types and the currently available guidelines for evaluating and assessing EAC initiation and growth in LAS are summarized in Table 1. The basic types of EAC can be assigned approximately to different LWR operational states: SICC and low-frequency (LF) CF are characteristic for operating transients, such as plant start-up/shut-down. SCC is characteristic for transient-free, steady-state power operation, when predominantly static loading of the RPV and piping prevails. [13]

Mechanism	Environmentally-assisted cracking (EAC)		
	SCC Stress corrosion cracking	**SICC** Strain-induced corrosion cracking	**CF** Corrosion fatigue
Type of loading	Static	Slow monotonically rising or very low-cycle	Cyclic: low-cycle, high-cycle
LWR operation condition	Transient-free, steady-state power operation	Start-up/shut-down, thermal stratification	Thermal fatigue, thermal stratification, …
Characterization of crack growth	BWRVIP-60 disposition lines	?	ASME XI, Code Case N-643 (PWR)
Characterization of crack initiation	? $(\sigma > YS)$	Susceptibility conditions: ECP_{crit}, $d\varepsilon/dt_{crit}$, ε_{crit}	ASME III, F_{env}-approach

Table 1: Basic types of EAC in C & LAS and relevant nuclear codes.

3   EAC Test Methods and their Relevance to LWR Components

EAC initiation in C & LAS in HT water has usually been studied by slow strain rate (SSR), low-cycle fatigue (LCF), and to a significantly lesser extent by constant load/deformation tests with smooth or notched specimens. Tests with (fatigue) pre-cracked specimens under cyclic, slow rising, static or periodical partial unloading (PPU) conditions were typically applied to evaluate the EAC crack growth behaviour. In Table 2 an overview on the most popular EAC test methods and their relevance to LWR components is given [17].

Type of specimen	SCC		CERT	SICC *)	Corrosion fatigue	
	Unnotched	Precracked	Unnotched	Unnotched	Unnotched	Precracked
Loading				LCF		
Result						
Objective. application	Susceptibility, material selection	Safety margins	Susceptibility, material select., environmental parameters	Optimization of start-up procedure	Design	Evaluation of Δa and safety margins
Height of loading	Variable (up to full plastic load)	Linear elastic	Increasing to fracture	Variable (up to full plastic load)	Variable (up to full plastic load)	Linear elastic
Applicable to the compon. behaviour	Yes	Yes, if cond. of LEFM are fulfilled	Qualitative indications	Yes	Yes	Yes
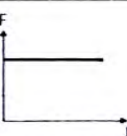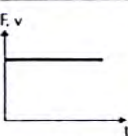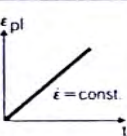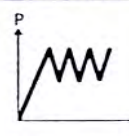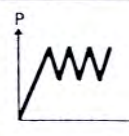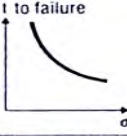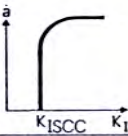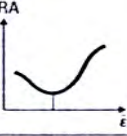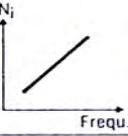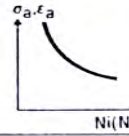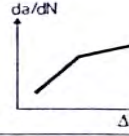
Table 2: Basic EAC test methods and their relevance to LWR components/power operation.

4 Major Factors of Influences for EAC in C & LAS in HT Water

EAC initiation ("susceptibility") and growth in C & LAS are governed by a complex interaction of interrelated environmental, material, and loading parameters, which synergistically control the local crack-tip strain rate and environment (see Section 10.4). The amplitude of individual parameter effects is strongly dependent on the values of the other system parameters. Parameter influences and thresholds should therefore be regarded as specific system parameters (i.e., only valid for a specific and limited range of corrosion system conditions), rather than as universal parameters and may be dependent on testing or component history. [18]

The major parameters of influence on EAC in LAS which have been identified so far are summarized in Table 3 [18]. The effect of these parameters on EAC is discussed in the following Sections and in Ref. [11 – 13]. In most studies, the effect of an individual system parameter has not been studied under constant process conditions. Furthermore, the effect of system parameters on crack initiation/thresholds and crack growth processes cannot be clearly separated in many cases. Crack initiation and growth may be controlled by different microscopic processes and may therefore show a different response to the various system parameters, although usually very similar effects are observed. Because of significant variations, e.g., in ECP, steel sulphur content and mechanical loading conditions from study to study and test to test, and the limited amount and large scatter (in particular around true or apparent thresholds) of literature data, complete interpretation is sometimes difficult and no clear conclusion can be drawn for some parameters. Cessation/crack arrest phenomena and initiation problems in the LAS-HT water system are other important reasons for some apparent discrepancy between some literature data. Table 4 is a summary of several key parameters of influence whose role is either well established/reasonably understood, or not yet clear/partially contradictory/insufficiently characterized from the author's point of view [18].

Environmental Parameters	Material Parameters	Loading Parameters
• ECP and DO • Temperature • Cl^-, SO_4^{2-}, S^{2-}, HS^- • Flow rate	• S-content, morphology, size, spatial distribution and chemical composition of MnS • DSA, concentration of interstitial C and N • Hardness/yield stress if > 350 HV5/ 800 MPa	• Frequency, loading or strain rate • Level of load, K_I, stress, strain, ΔK • Type of loading • Residual stress

Table 3: Major influencing factors for EAC in C & LAS [18, 19].

Well characterized and established	Insufficiently characterized and understood
• Oxygen content and ECP • Sulphate-concentration of environment • Steel sulphur content, MnS-inclusions • Susceptibility conditions (crack initiation) • Strain/load rate/frequency effects • Stationary conditions	• Temperature, flow rate, chloride, pitting and irradiation • Microstructure (weld filler, HAZ, heat treatment, ...) • Dynamic strain ageing, yield stress • Crack initiation and growth mechanism • Transient (water chemistry, non-isothermal) conditions • Overload and load sequence effects, short crack growth

Table 4: Assessment of different influencing parameters for EAC of LAS [18].

4.1 Environmental Parameters

4.1.1 *Temperature*

Crack Initiation: The effect of temperature on SCC initiation has not been investigated so far. From SSR tests with smooth tensile specimens, a maximum SICC susceptibility can be derived between 180 °C and 270 °C (see Figure 2a) [21 – 25], depending on dissolved oxygen content, ECP, strain rate, strain, and steel sulphur content. A minimum oxygen concentration is needed in this temperature range to exceed the critical cracking potential ECP_{crit} [25]. DSA (see Sections 4.2.4 and 10.2) may be an important reason for this maximum of susceptibility and for variations in temperature trends between different alloys [18, 26, 27].
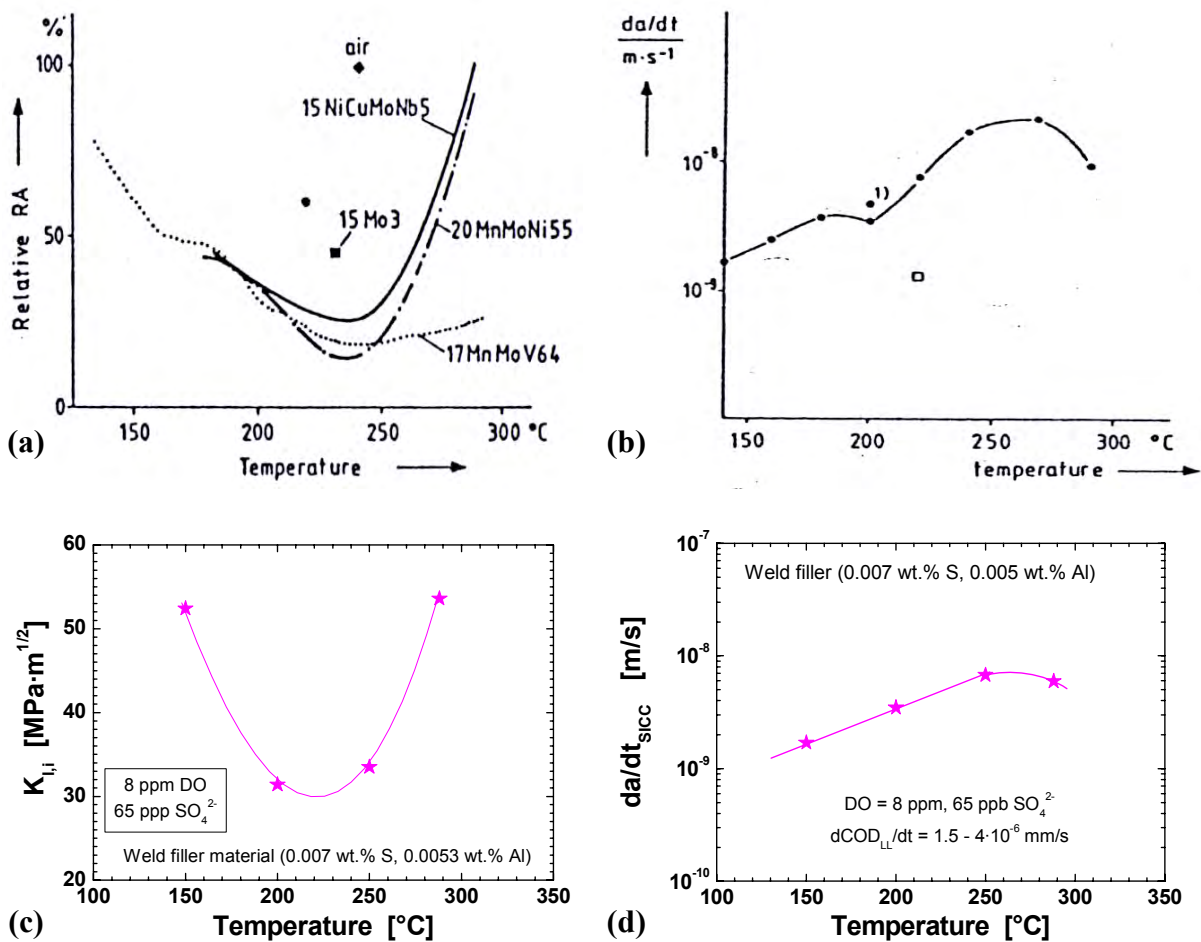
Figure 2: Maximum SICC susceptibility at intermediate temperatures in SSR tests (a) with smooth specimens and in slow rising load (SRL) tests with pre-cracked specimens (c). Effect of temperature on SICC crack growth in SSR (b) and SRL tests (d). [23, 28]

In LCF tests, fatigue life decreases linearly with temperature above 150 °C and up to 320 °C [29 – 31], when the other threshold conditions (strain rate, strain, DO, sulphur content) for environmental effects are satisfied (see Section 9.2.1). Fatigue life is insensitive to temperatures below 150 °C or when any other threshold condition is not satisfied [29 – 31].

Although the SICC and CF susceptibility of C & LAS are low at temperatures < 100 °C, the few tests in this regime indicate that EAC crack growth may still occur [1, 21, 22].

Crack Growth: The SCC CGRs increased with increasing temperature [1, 32] in static autoclave tests (Figure 3a). An activation energy of 42 KJ/mol has been determined with plateau-CGRs under these aggressive environmental (high impurity content) and extreme loading conditions (with severe violation of small-scale yielding (SSY) conditions) [1, 32]. In high-purity water, C & LAS usually show a very low susceptibility to sustained SCC growth between 150 to 320 °C [33 – 36], which makes it impossible to determine activation energies and temperature trends under these conditions. A maximum of SCC CGR has been observed at high K_I values at intermediate temperatures (200 to 250 °C) in LAS with a high DSA susceptibility (Figure 3b), whereas comparable LAS with a low susceptibility revealed no or very minor SCC over the whole temperature range from 150 to 300 °C [36].
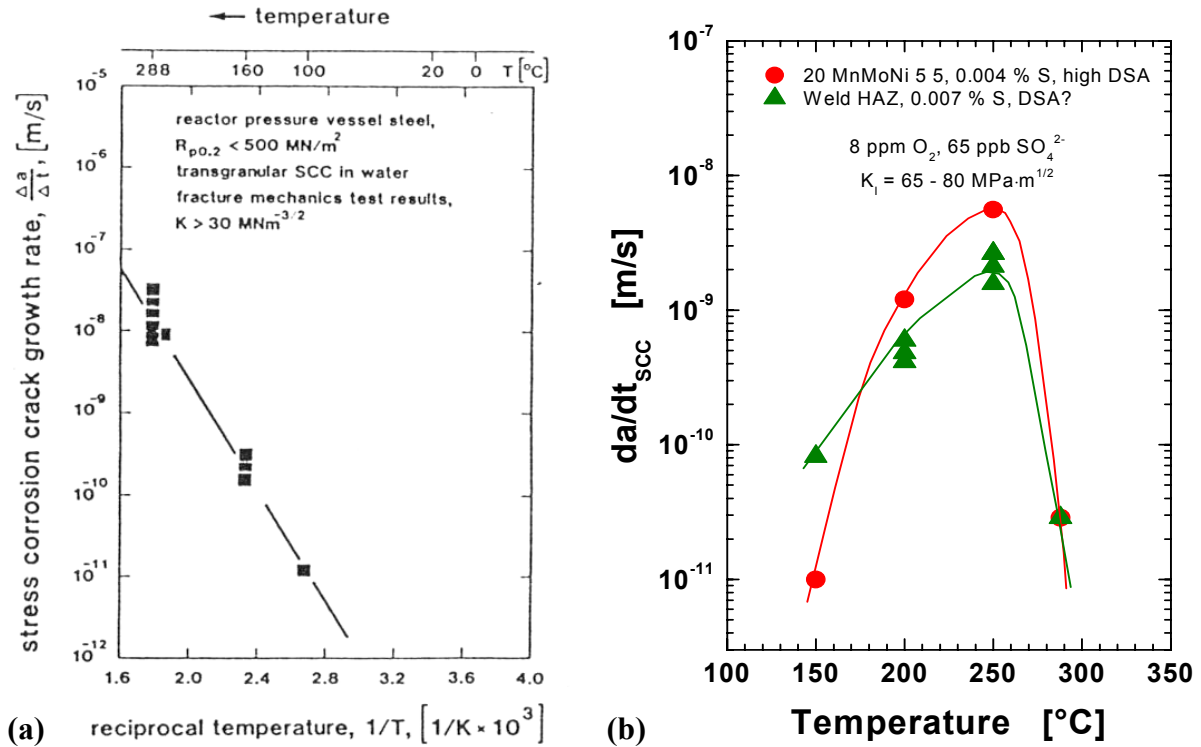
Figure 3: Temperature dependence of SCC CGRs in static autoclave tests (a) [1, 37]. Maximum of SCC CGRs at intermediate temperatures in LAS with a high DSA susceptibility (b) [36].

In SSR [21 – 24] and SRL tests [28] in oxygenated HT water, increasing SICC CGRs were observed with increasing temperatures between 150 and 288 °C, with a maximum or plateau at/above 250 °C (Figures 2b and d).

The CF crack growth behaviour under cyclic loading conditions shows two major trends: Under conditions where no or only minor acceleration of fatigue crack occurs (i.e., if low-sulphur crack-tip environment conditions prevail, e.g., at frequencies > 10 Hz or at frequencies $\leq 10^{-3}$ Hz and low ECPs (PWR or BWR/HWC), at high flow rates with flushing of the crack-tip environment), generally only moderate temperature effects are observed, which are similar to those in air. If significant acceleration of fatigue crack growth occurs (i.e., if high-sulphur crack-tip environment conditions prevail, e.g., under BWR/NWC conditions at loading frequencies between 10^{-4} to 1 Hz) CF CGRs between 150 and 300 °C were either monotonically increasing with temperature or showing a maximum at intermediate temperatures between 180 to 270 °C [11, 38 – 51] (see Figures 4 and 5) in most cases. Under these conditions, an apparent activation energy of 40 to 50 KJ/mol was observed between 150 and 288 °C at loading frequencies < 10^{-2} Hz [51].
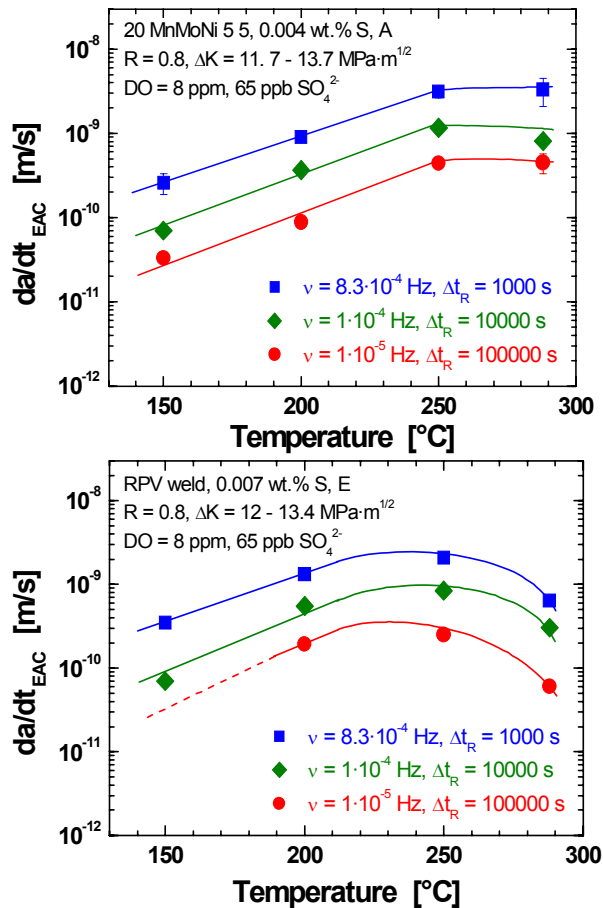
Figure 4: Effect of temperature on CF crack growth under BWR/NWC conditions (where high-sulphur crack-tip environment conditions prevail) [51].

DSA and the temperature dependence of different EAC crack growth thresholds (ΔK_{EAC}, ν_{crit}, etc.) are probably the two major reasons for deviations form these two temperature trends and for a more complex behaviour. A change in crack growth mechanism (film rupture/anodic dissolution (FRAD) to hydrogen-assisted EAC (HAEAC), true CF to stress CF, e.g., in the temperature range from 100 to 180 °C) may be a further contributing factor and may explain a minimum of CGR in this regime as observed in some few cases [42, 45]. DSA may explain a CGR maximum at intermediate temperatures for certain strain rates by both, its effect on CGR and on thresholds. Differences in the free nitrogen and carbon content of the steel may explain the quite different temperature response sometimes observed in otherwise similar alloys. It has been proposed, that both plateau thresholds ΔK_{EAC} and plateau CF CGRs increase with increasing temperature [40]. The region of EAC might therefore be significantly extended at lower and intermediate temperatures compared to 290 °C (Figure 5). A lower plateau threshold ΔK_{EAC} or critical frequency at lower temperatures may explain a negative temperature dependence of EAC above a certain temperature in the case where the $\Delta K/\nu$ of the tests do exceed the thresholds $\Delta K_{EAC}/\nu_{crit}$ at lower temperatures, but not at higher temperatures.
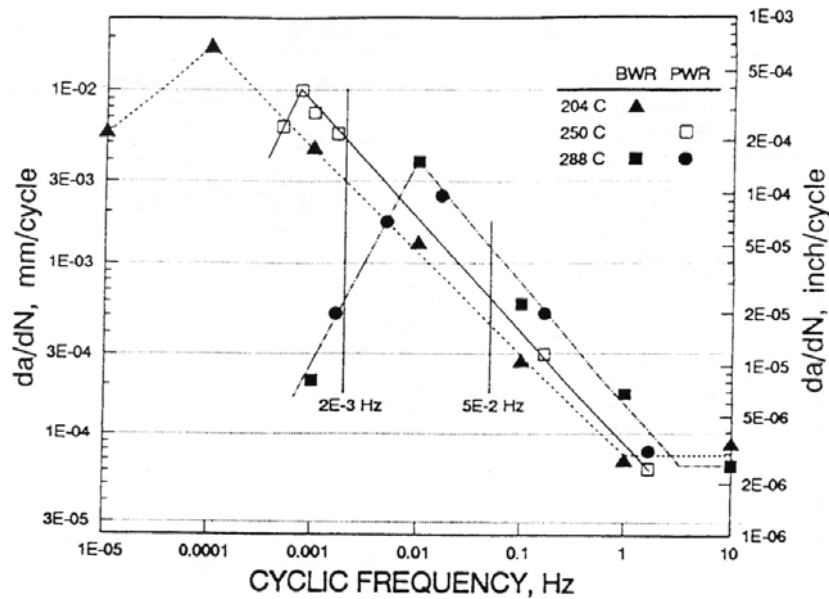
Figure 5: Effect of loading frequency and temperature on CF CGR [11]. $2 \cdot 10^{-3}$ Hz: Maximum at 250 °C. $5 \cdot 10^{-2}$ Hz: CF CGR monotonically increases with temperature.

Non-Isothermal Conditions: Most plant transients involve non-isothermal conditions, which can be in- and out-of-phase with mechanical loading. There is only very limited testing under non-isothermal conditions, which indicated that the fatigue life of non-isothermal tests were comparable to that of isothermal tests with an average temperature of the thermal cycling (see Figure 82 on p. 85). Since environmental effects on fatigue life are moderate and independent of temperature below 150 °C, the mean temperature was determined as the average value of 150 °C or the minimum temperature, whichever is higher, and the maximum temperature. The fatigue life under in-phase condition was comparable to that of out-of-phase cycling in most tests [52, 53], although one would rather expect a longer life for out-of phase tests, because environmental effects are usually occurring during the tensile portion of fatigue cycles and the applied strains usually have to exceed certain thresholds for environmental effects to occur.

There is only one single study on CF crack growth in a high-sulphur LAS in PWR environment under non-isothermal and out-of-phase conditions, with temperature cycling between 243 and 149 °C [54]. Significant non-steady-state cracking was observed. CGRs were initially high, approximately equivalent to the high EAC rates at 243 °C, but over a 57 day period of non-steady behaviour, the CGR steadily dropped to the non-EAC rates normally expected at 149 °C in this material. On a long-term perspective the CGR under non-isothermal conditions behaved as if the test was being conducted at 149 °C. Although no generic conclusion can be derived from this study, it illustrates the complex non-steady crack growth behaviour, which may occur under non-isothermal conditions.

4.1.2 Corrosion Potential (ECP) and Dissolved Oxygen Content (DO)

The ECP can have a strong effect on EAC initiation and growth over a wide range of corrosion system conditions and is more fundamental for EAC than the concentration or types of oxidizing (O_2, H_2O_2) and reducing (H_2) species [9, 55], which govern the ECP. Although there is a non-linear relationship between ECP and DO (Figure 6), the effects of DO and ECP are very similar. Therefore, the following discussion is primarily focused on ECP effects.

16
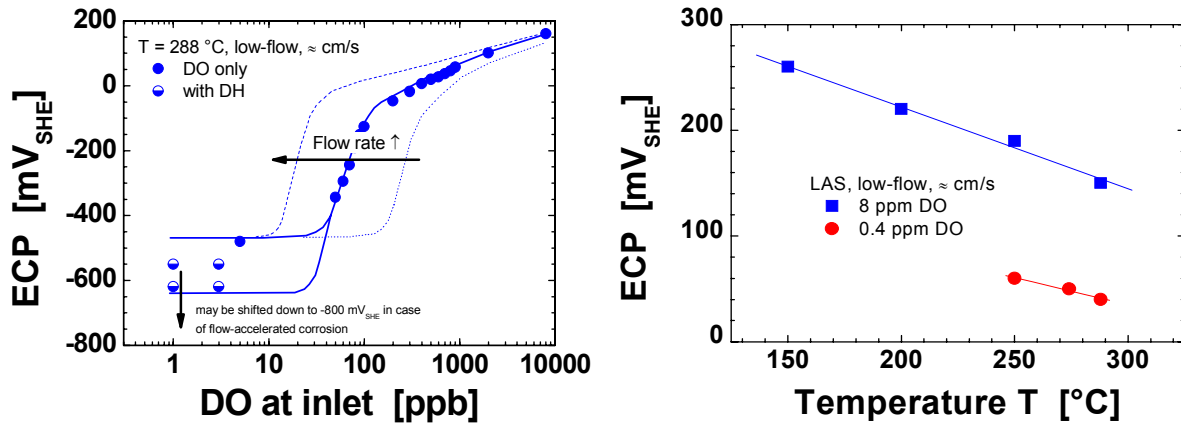
Figure 6: Relationship between ECP and DO/temperature.

Crack Initiation: Because of the very low SCC susceptibility of C & LAS in high-purity water under static loading conditions, no ECP trend on SCC initiation could be established.

In high-purity water, no SICC was usually observed in SSR tests below a certain critical cracking potential ECP_{crit} of approximately -200 mV_{SHE}. Depending on flow rate, temperature, and material, 5 to 100 ppb DO was sufficient to exceed the critical cracking potential of ca. -200 mV_{SHE} [9, 21 – 24, 56, 57]. The critical potential ECP_{crit} is dependent on temperature, steel sulphur content, bulk sulphur-anion concentration and strain rate (see Figures 7 – 9, 17). ECP_{crit} decreased with increasing sulphur content of the steel [56 – 59] (Figure 8) and with increasing sulphate or chloride content of the environment [56, 57, 60] (see Figure 9). Above the critical cracking potential, the SICC susceptibility increases with increasing ECPs and usually saturates at high ECPs. The SICC cracking region at high potentials is significantly extended with respect to low potentials, in the sense that lower critical strains or sulphur contents are required to initiate SICC.

In LCF tests with smooth specimens, when all threshold conditions are satisfied, fatigue life decreases above a DO of 50 ppb and the effect seems to saturate at 500 ppb DO (Figure 83). Fatigue life is insensitive to DO levels below 50 ppb (e.g., PWR or BWR/HWC) or when any other threshold condition is not satisfied. [29 – 31, 61]
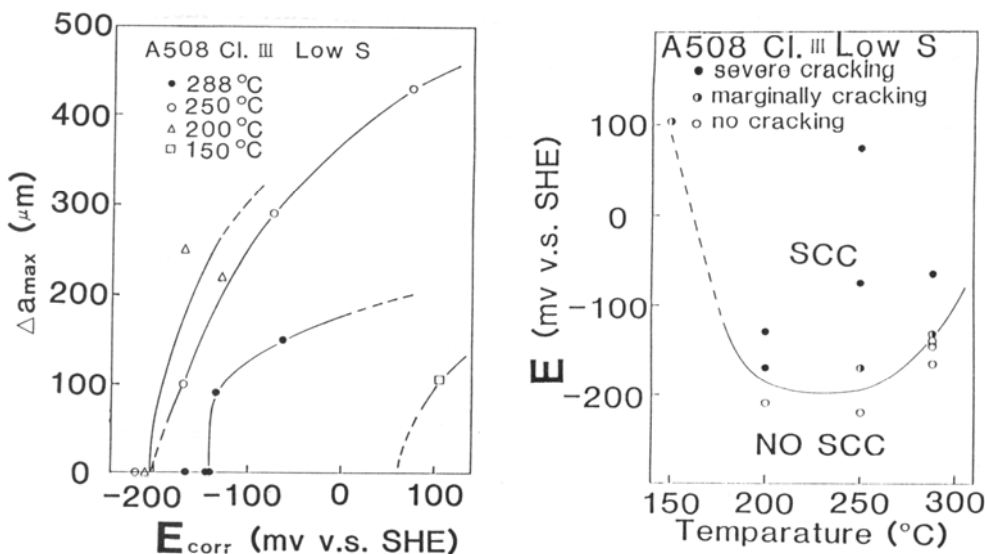
Figure 7: Effect of temperature on critical cracking potential. Maximum susceptibility around 200 to 250 °C [56, 57].

17
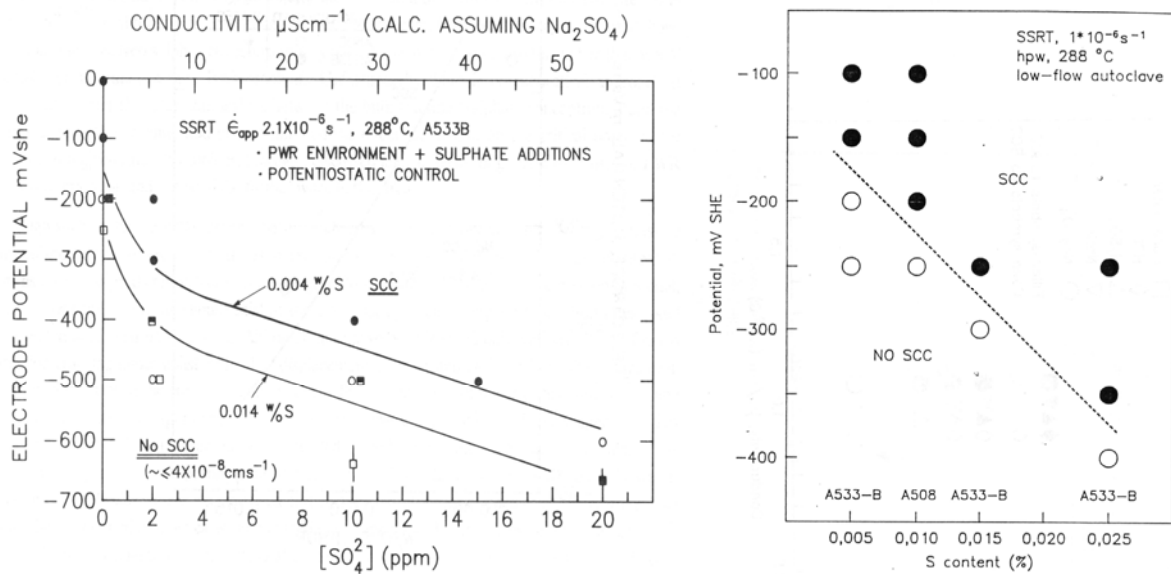
Figure 8: Effect of bulk sulphate concentration [56, 57] and steel sulphur content [60] on ECP$_{crit}$ in oxygenated HT water.
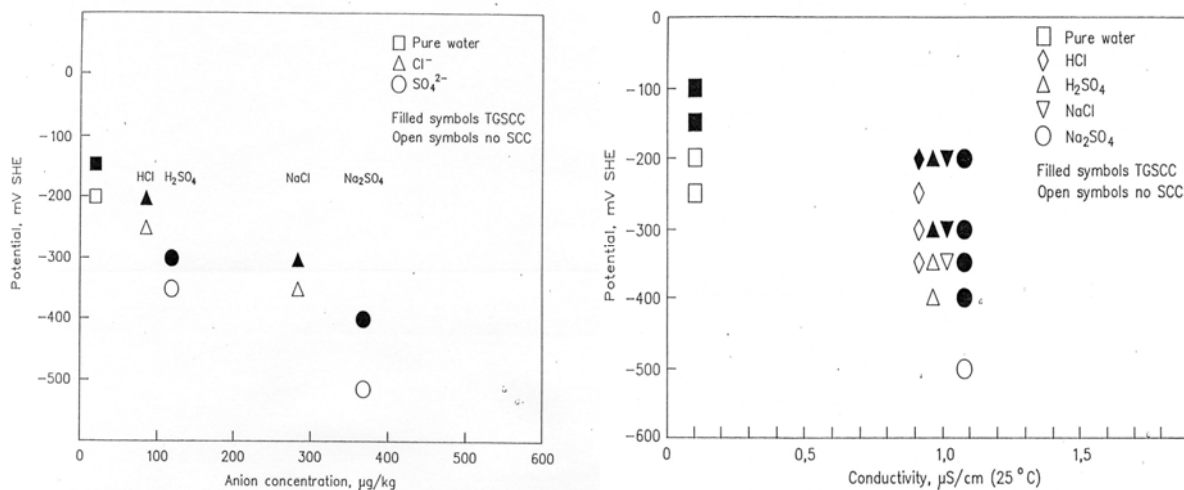
Figure 9: Effect of sulphate and chloride on the critical potential [60].

Crack Growth: The range of system conditions where EAC crack <u>growth</u> from incipient cracks may occur is significantly extended compared to the initiation susceptibility conditions for smooth defect-free surfaces. E.g., accelerated CF crack growth has been observed in high-purity PWR water at low ECP below -500 mV$_{SHE}$ under certain cyclic loading conditions (10^{-2} to 10 Hz) [5, 8, 11 – 13], where no environmental reduction of LCF life occurred [29].

Even under highly oxidizing conditions (ECP = +200 mV$_{SHE}$), SCC crack growth could not be sustained in C & LAS in chloride-free HT water at 270 to 290 °C up to rather high stress intensity factors K$_I$ of 60 MPa·m$^{1/2}$ [33 – 36]. Because, of this very low SCC crack growth susceptibility, no relationship between ECP and crack growth could be established.

A strong effect of ECP on SICC crack growth has been observed in slow rising load (SRL) tests, where fast SICC crack growth could only be established at high ECPs ≥ 50 mV$_{SHE}$ (Figure 10). Below this ECP, SICC crack growth in high-purity water was very localized in nature and could only be detected by post-test fractography. [28, 35]
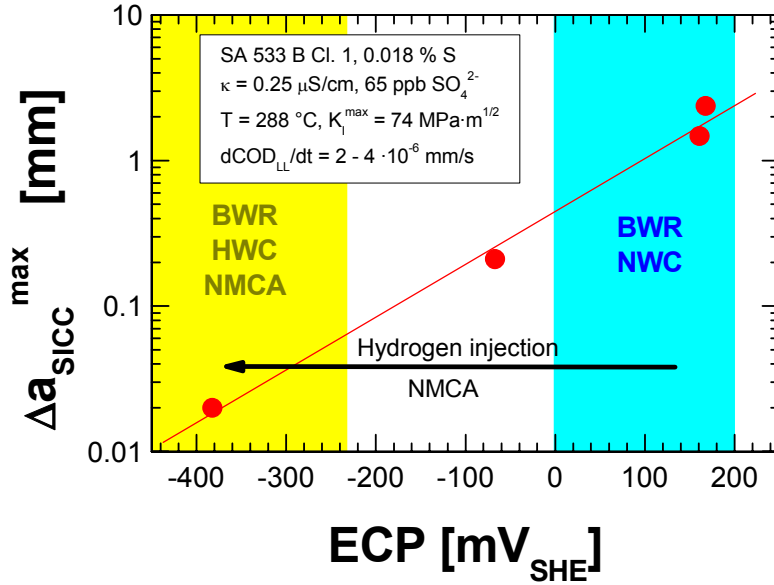
Figure 10: Effect of ECP on SICC crack growth in SRL tests under identical loading conditions [28, 35].

The effect of ECP on CF crack growth is exemplarily illustrated by Figures 11 (cycle-based CGR) and 12 (time-based CGR) [63]. Depending on the loading conditions, the ECP/DO either had a very pronounced or only a moderate effect on CF crack growth. Below a loading frequency of 10 Hz, environmental acceleration of fatigue crack growth was observed for all ECP/DO and the cycle-based CGR $\Delta a/\Delta N_{EAC}$ were increasing with decreasing loading frequency following roughly the high-sulphur CF CGR line of the GE-model down to a frequency of 10^{-2} Hz. In this frequency range, the same CF CGR $\Delta a/\Delta N_{EAC}$ were observed at a given frequency for low and high ECP/DO values. The slightly lower CF CGR $\Delta a/\Delta N_{EAC}$ at 400 to 8000 ppb were related to the slightly lower loading level in these tests. Below a critical frequency ν_{crit} of 10^{-2} (< 5 ppb DO) and 10^{-3} Hz (200 ppb DO), the cyclic CGR $\Delta a/\Delta N_{EAC}$ dropped again down to low-sulphur CF CGR slightly above the air fatigue CGR, since high-sulphur crack-tip environment conditions could not be sustained anymore. On the other hand, in oxygenated HT water with a DO content of 400 or 8000 ppb, fast CF crack growth with CGR close to the high-sulphur CF CGR could be sustained down to the lowest loading frequency tested (10^{-5} Hz). Below 10^{-2} Hz, significantly different cycle-based CGR $\Delta a/\Delta N_{EAC}$ were observed at the different ECP and DO values.

The ECP mainly affected the transition from high to low CF CGR, which appeared as critical frequencies $\nu_{crit} = f(\Delta K, R)$ and ΔK-thresholds $\Delta K_{EAC} = f(\nu, R)$ in the cycle-based form and as a critical air fatigue CGR $da/dt_{Air,crit}$ in the time-domain form. The critical CGR, frequencies and ΔK_{EAC}-thresholds were shifted to lower values with increasing ECP (or DO).
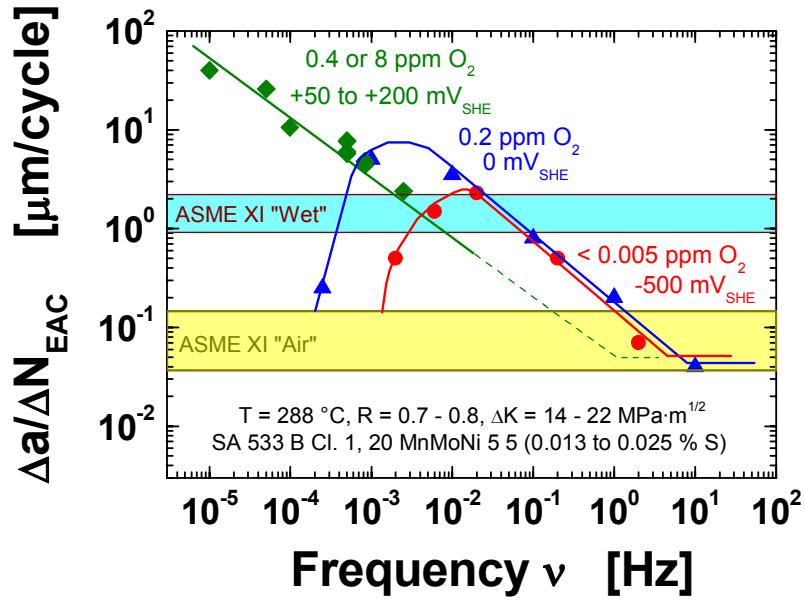
Figure 11: Effect of DO/ECP and loading frequency on $\Delta a/\Delta N_{EAC}$ and comparison to the corresponding ASME XI reference fatigue CGRs for the specified loading conditions [62].
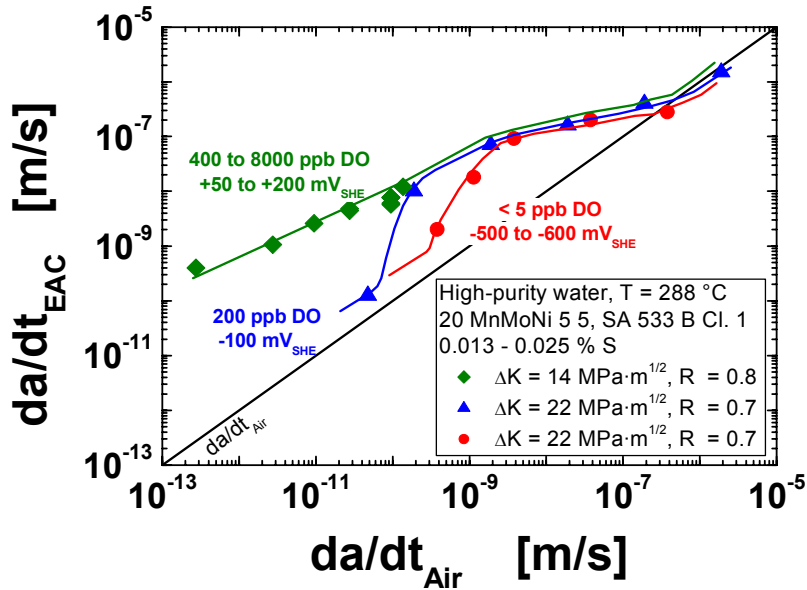
Figure 12: Effect of DO/ECP and loading frequency on the time-based CGR da/dt$_{EAC}$ [62].

CF tests with NWC (0.4 ppm DO) → HWC (0.15 ppm DH) → NWC (0.4 ppm DO)-transients always revealed a significant drop of the CF CGR (by a factor of 10 or larger) under low-frequency fatigue loading conditions (≤ 0.01 Hz) a few hours after adding hydrogen and changing to low potentials (< -200 mV$_{SHE}$) [63]. A few 10 hours after returning to oxidizing NWC conditions, the CF CGR again reached the same high-sulphur CF CGR as before the HWC-transient. This is exemplarily shown in Figure 13. In some cases at very low loading frequencies, the high-sulphur CF CGR could only be re-established after a temporary increase of loading frequency after changing back to NWC conditions.
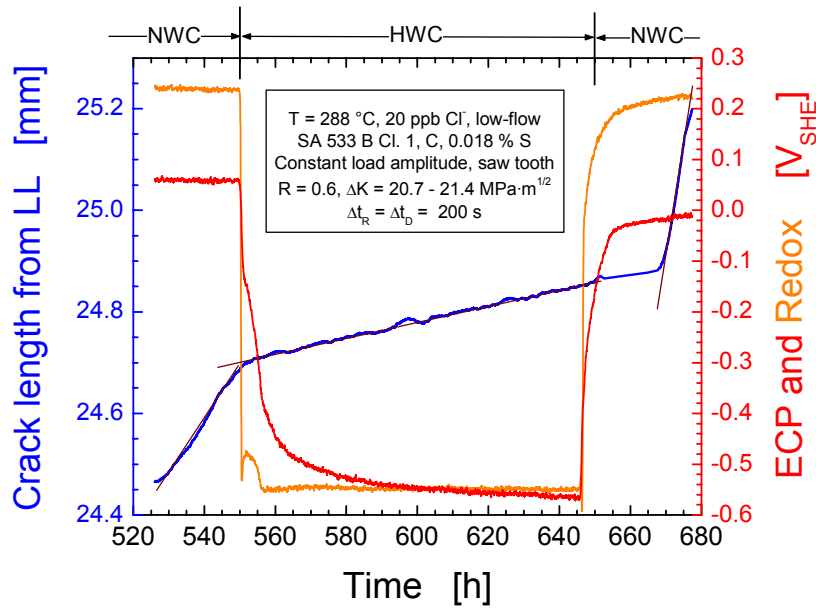
Figure 13: Example of LFCF crack growth during a NWC → HWC → NWC-transient [63].

In Figure 14, the PSI results at different loading conditions are compared to similar investigations of Andresen [64] including noble metal coated specimens [65] and to the predictions of the GE-model [66]. By changing from oxygenated (or stoichiometric excess of oxygen in case of NMCA) to hydrogenated (or stoichiometric excess of hydrogen in case of NMCA) water chemistry conditions, the CF CGR always dropped from the PSI NWC CF regression curve, which is close to the high-sulphur CF curve, down to the low-sulphur CF CGR of the GE-model. HWC/NMCA resulted in a significant reduction of CF CGR by a factor of 10 to 50 under the tested low-frequency loading conditions, where the ASME XI wet reference fatigue CGRs were significantly exceeded under NWC conditions (Figure 11). On the other hand, no or only a very moderate reduction of CF CGR by HWC is expected in the loading frequency range of 10^{-2} to 10^{-1} Hz (see Figures 11 and 14), since high-sulphur crack-tip environment conditions may also prevail in this frequency range in deoxygenated HT water (by the exposure and dissolution of new fresh MnS-inclusions by the fast growing crack and the relatively slow transport of the sulphides out of the crack by diffusion). Above 1 to 10 Hz, environmental effects disappear and fatigue crack growth is dominated by pure mechanical fatigue under NWC and HWC conditions.

In Figure 15, the stationary low-frequency ($5 \cdot 10^{-4}$ to $4 \cdot 10^{-2}$ Hz) cyclic CF CGR $\Delta a/\Delta N_{EAC}$ during NWC and HWC/NMCA phases are compared to the ASME XI reference fatigue crack growth curves. Under these conditions, $\Delta a/\Delta N_{EAC}$ significantly exceeded the ASME XI wet reference fatigue crack growth curve under NWC conditions, but dropped well below this curve under HWC conditions. Thus HWC or NMCA seem to be very promising methods to reduce LFCF CGRs.
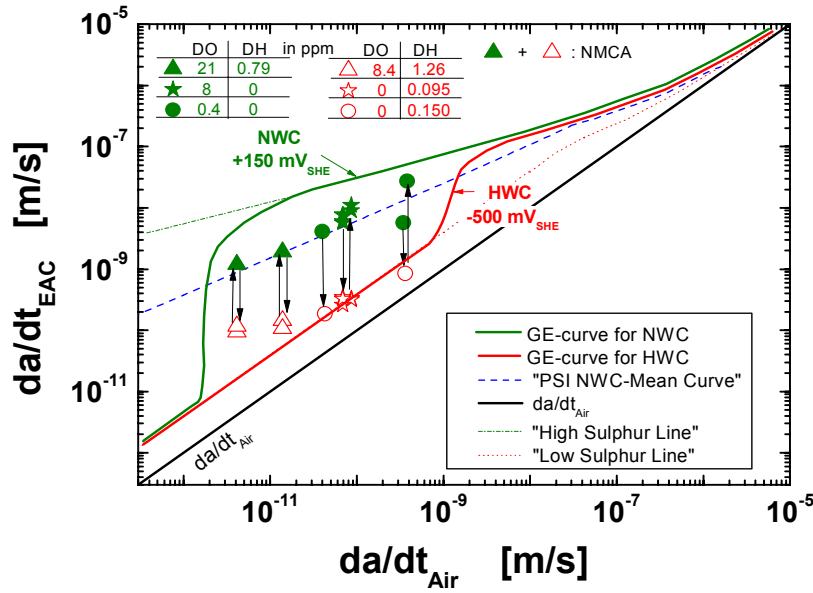
Figure 14: Reduction of time-based CF CGR da/dt$_{EAC}$ by changing from NWC to HWC/ NMCA [63].
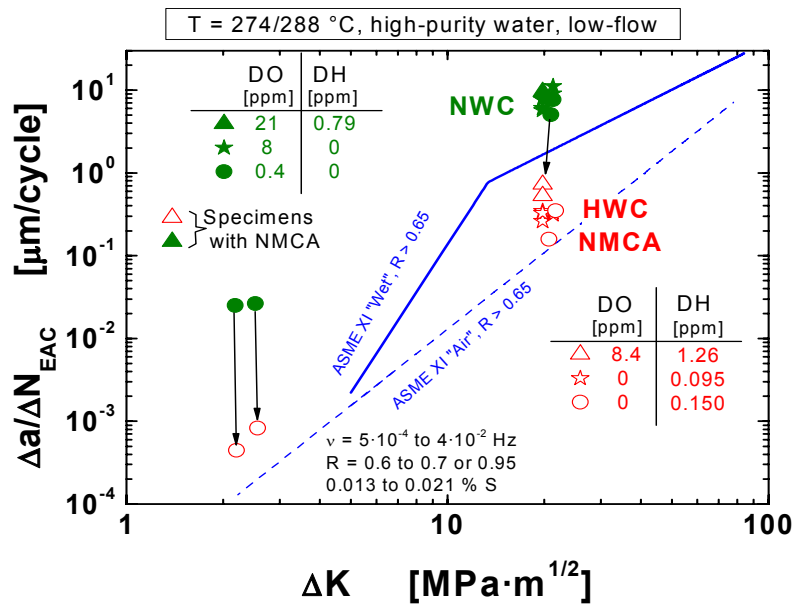
Figure 15: Comparison of stationary LFCF CGR Δa/ΔN$_{EAC}$ during NWC and HWC/NMCA phases with the corresponding ASME XI reference fatigue CGR curves [63].

4.1.3 Sulphate and Chloride

The concentration of sulphate and chloride (and of other harmful anionic species) may have a relevant effect on EAC initiation [56, 57, 59, 60] (see Figure 9) and crack growth [67 – 69] (see Figures 16b, 17 and 23). The amplitude of the effect strongly depends on the ECP [70] and other system parameters.

Crack Initiation: Limited static load tests with smooth specimens in oxygenated HT water indicate that SCC initiation may occur after relative short incubation periods with respect to LWR lifetimes at significantly increased chloride and sulphate levels under quasi-stagnant conditions at stress levels in the range or slightly above the HT yield stress [71].

SSR tests clearly indicate, that the critical cracking potential ECP_{crit} for SICC is shifted to lower values with increasing sulphate and chloride content of the environment (Figure 9) [56, 57, 59, 60].

Limited LCF testing also indicates, that sulphate addition may reduce fatigue lifetime with respect to high-purity water. Furthermore, LCF testing with stepwise changes of environmental conditions [72 – 75] indicates that even a few cycles under aggressive environmental conditions may have a disproportionably strong effect on reducing fatigue lifetime (Figure 84 on p. 86 in Section 9.2.2).

Crack Growth: Even at very high sulphate levels of up to 1400 ppb no accelerated SCC crack growth at K_I levels < 60 MPa·m$^{1/2}$ was observed under highly oxidizing BWR/NWC conditions (Figure 16a) and all SCC CGRs were conservatively covered by the BWRVIP-60 SCC DL 2 for water chemistry transients [3, 76]. On the other hand, 5 to 10 ppb of chloride were already sufficient to induce accelerated SCC in LAS under highly oxidizing BWR/NWC conditions (Figures 16b to 18) with CGRs well above the BWRVIP-60 SCC DL 2 [67 – 69].
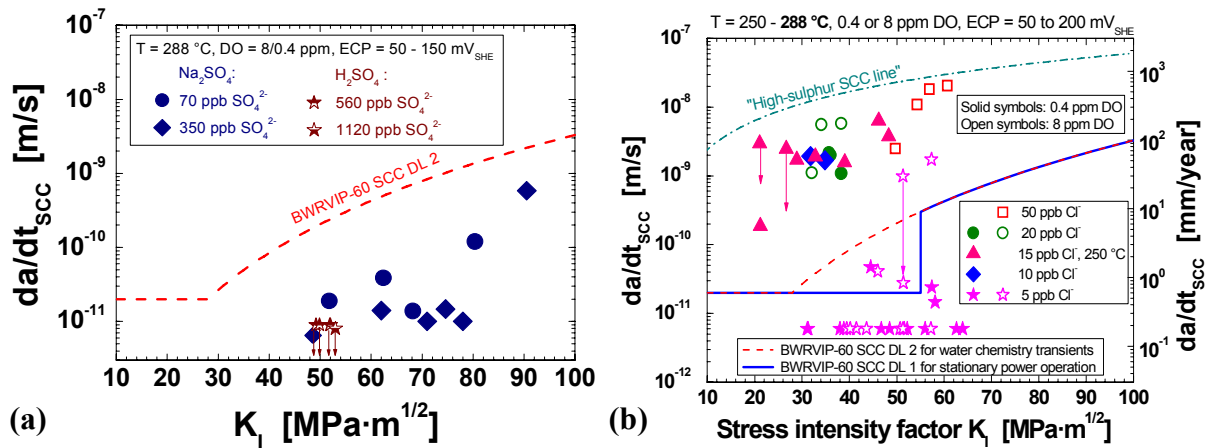
Figure 16: Comparison of SCC CGRs during sulphate (a) and chloride transients (b) with the BWRVIP-60 SCC DL 2 for water chemistry transients.
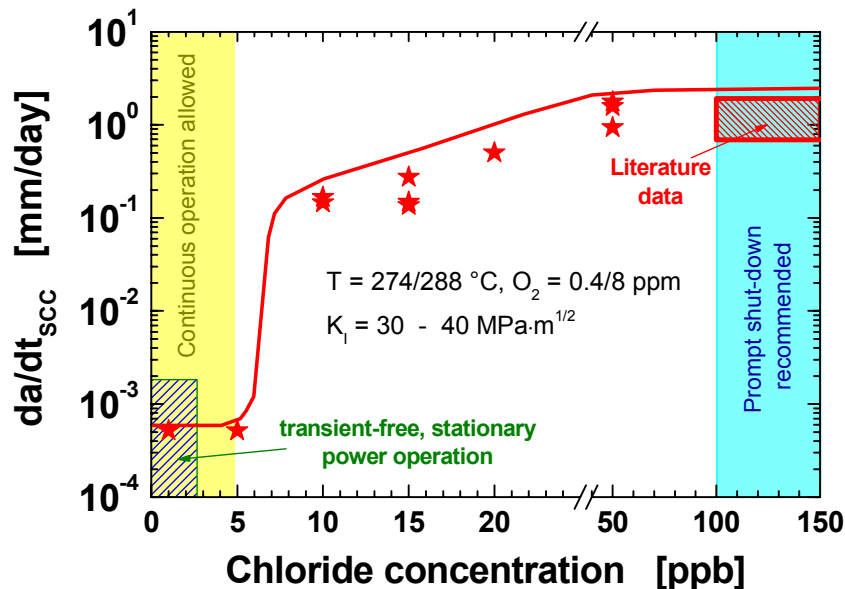
Figure 17: Chloride-induced acceleration of SCC crack growth in oxygenated HT water.

The critical chloride concentration for the onset of accelerated SCC in C & LAS strongly increased with decreasing ECP, as shown in Figure 18 [69]. The critical ECP for accelerated SCC, on the other hand strongly increased with decreasing chloride concentration.

Under test conditions, where high-sulphur crack-tip environment and accelerated CF crack growth prevailed, the addition of sulphate or chloride, even in very high amounts, did not result in an acceleration of CF crack growth (Figures 19 and 28) [62]. On the other hand, under system conditions, where low-sulphur crack-tip environment conditions with minor acceleration of CF CGRs prevailed, the addition of a sufficient amount of sulphate or chloride may result in relevant acceleration of crack growth and CGR could reach high-sulphur CF rates. Under typical PWR (or BWR/HWC) conditions, the addition of 1 to 3 ppm sulphate was required to accelerate CF crack growth [77] (see Figure 23 on p. 27 in Section 4.1.5).
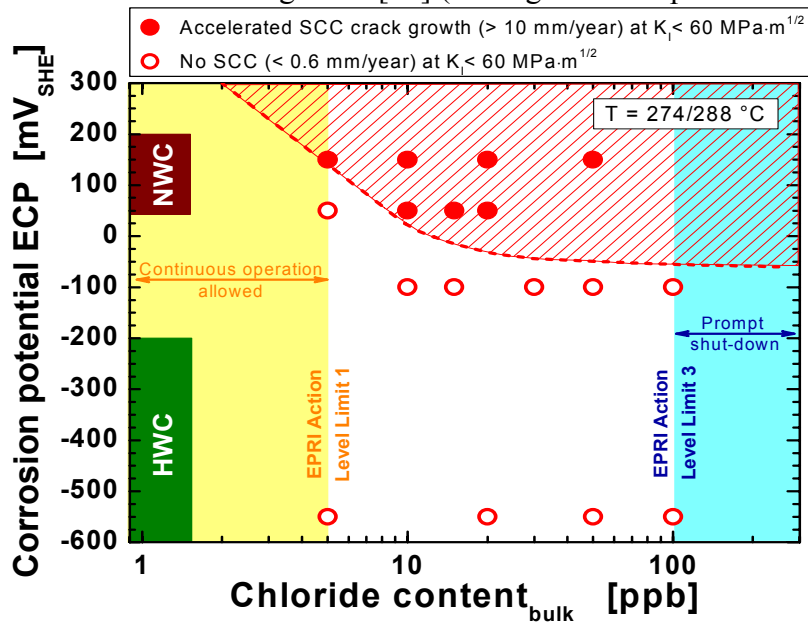
Figure 18: Effect of chloride and ECP on SCC crack growth in C & LAS [69].
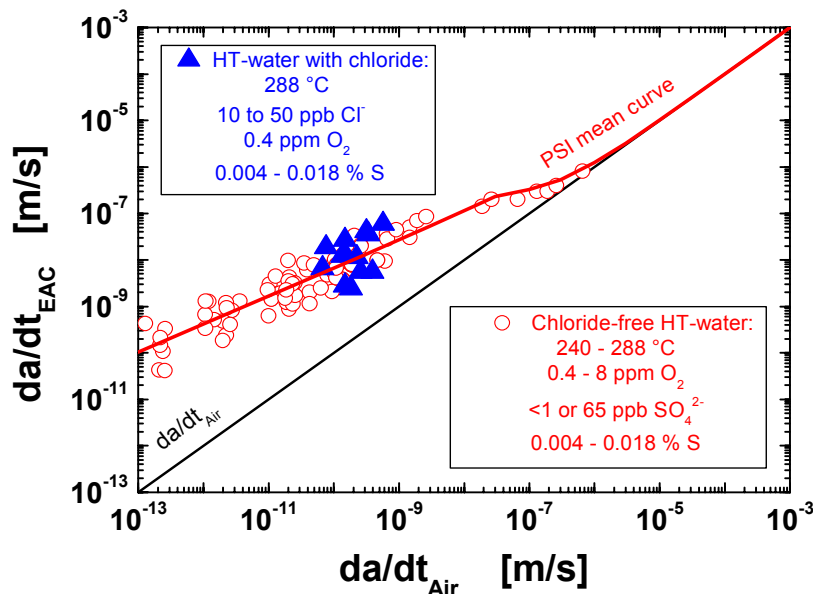
Figure 19: Comparable time-based CF CGR da/dt$_{EAC}$ in chloride-free and chloride-containing oxygenated HT water under conditions, where high-sulphur crack-tip environment conditions prevail.

4.1.4 pH, H₃BO₃/LiOH, H₂ and H₂O₂

The CF crack growth behaviour in nitrogenated and hydrogenated high-purity HT water, or water with H_3BO_3 (nuclear purity grade) and LiOH additions with different room-temperature pH's was comparable over a wide range of system conditions, thus not arising any immediate concern for these parameters under typical PWR plant conditions [9, 11 – 13, 78]. H_2O_2 and O_2 generation by radiolysis is suppressed by the large H_2 overpressure in PWRs during stationary power operation. If the ECP in PWR water was raised by polarisation or by O_2 or H_2O_2 additions, e.g., to simulate some transient conditions or specific component locations, the CF crack growth behaviour was identical to that under BWR/NWC conditions at similar ECPs [9, 13].

BWRs are always operated by near-neutral high-purity HT water. The EAC behaviour in oxygenated HT water was comparable to that in HT water with oxygen/hydrogen mixtures at temperatures > 150 °C as long as the ECPs were similar (Figure 20). The low ECPs with significant stoichiometric excess H_2 (e.g., HWC) have always resulted in a significant reduction of SCC and CF CGRs with respect to highly oxidizing NWC conditions (Figures 14 and 15) [63]. At temperatures < 150 °C, negative hydrogen effects on EAC, e.g., in the high hardness coarse grain zone of weld HAZ, cannot be fully excluded.

EAC experiments in the test reactor at NRI, in Řež within a VGB project with pre-irradiated RPV steels in an in-pile loop under n- and γ-irradiation with an additional H_2O_2 generation channel in the reactor core to generate a defined H_2O_2 concentration at the specimen surface, and in an out-of-pile loop outside the radiation field basically revealed the same EAC behaviour at comparable ECPs [79]. These results clearly show that the ECP is more fundamental for EAC than the type of chemical species, which control the value of ECP.
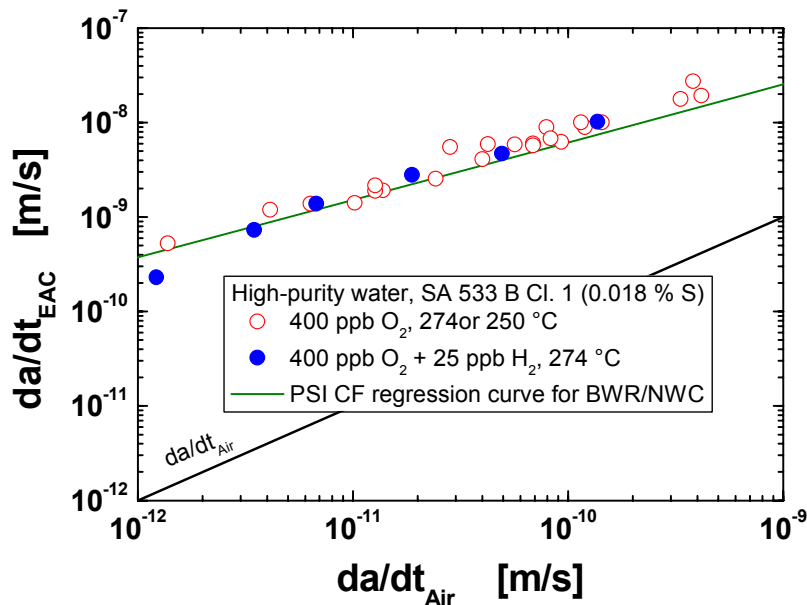
Figure 20: Similar CF CGRs in HT water with oxygen and oxygen/hydrogen mixtures with stoichiometric oxygen excess.

4.1.5 Flow Rate

Possible convection effects by external fluid flow across the crack-mouth and by "fatigue pumping" (trough the relative displacements of the crack flanks between maximum and minimum stress portions of a fatigue cycle) are briefly discussed and reviewed in [13, 80].

High flow rates may be beneficial for both EAC initiation at smooth surfaces and EAC growth of long cracks in C & LAS in high-purity water with very low levels of harmful impurities (Cl⁻, SO_4^{2-}, H_2S, HS⁻, S²⁻). No negative effect of high flow rate on EAC in LAS under LWR conditions has been observed so far. SICC initiation in SSR tests may be significantly retarded [81, 82] or even completely suppressed and LCF life is increased by increasing the flow rate from quasi-stagnant or low-flow to turbulent flow conditions [31, 83]. The beneficial effects of increased flow rate on LCF life are higher for slow strain rates/strain amplitudes, high DO content and higher steel sulphur contents, thus under conditions, where the strongest reduction of LCF life is typically observed. CF growth may be stopped or significantly slowed down by turbulent high flow rates (see Figures 21 to 23) [84 – 92]. Studies by Lenz et al. [84], e.g., suggest that, to some degree, EAC CGRs under cyclic fatigue loading and BWR conditions appeared to be inversely proportional to the water velocity past the crack-mouth. In some cases higher flow rate increased the ECP at intermediate DO levels (see also Figure 6), but still resulted in a reduction of CF CGRs.
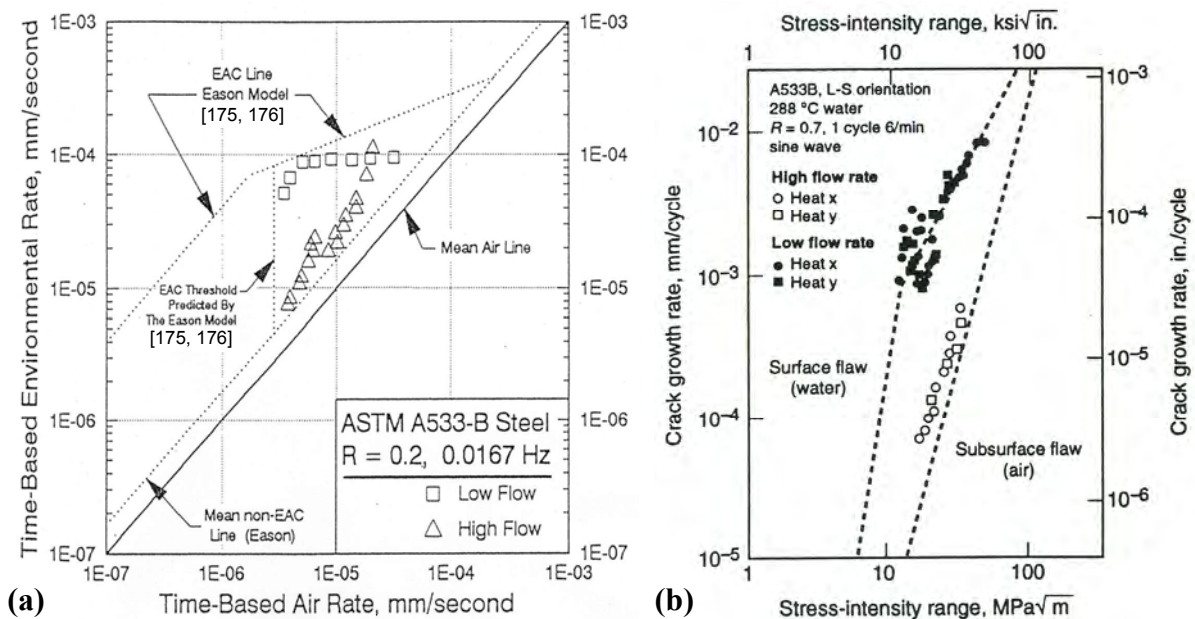
Figure 21: Effect of water flow rate upon the CF CGR response of LAS in PWR environments in the time-domain (a) [12] and cycle-based form (b) [92].

The high turbulent flow rate mitigates or avoids the evolution of an aggressive occluded water chemistry in small surface defects and pits, which seems to be a necessary pre-requisite for accelerated EAC initiation at smooth surfaces. The crack growth of long cracks may be relevantly slowed down or even stopped if relevant dilution or complete flushing out of the aggressive crack electrolyte occurs.
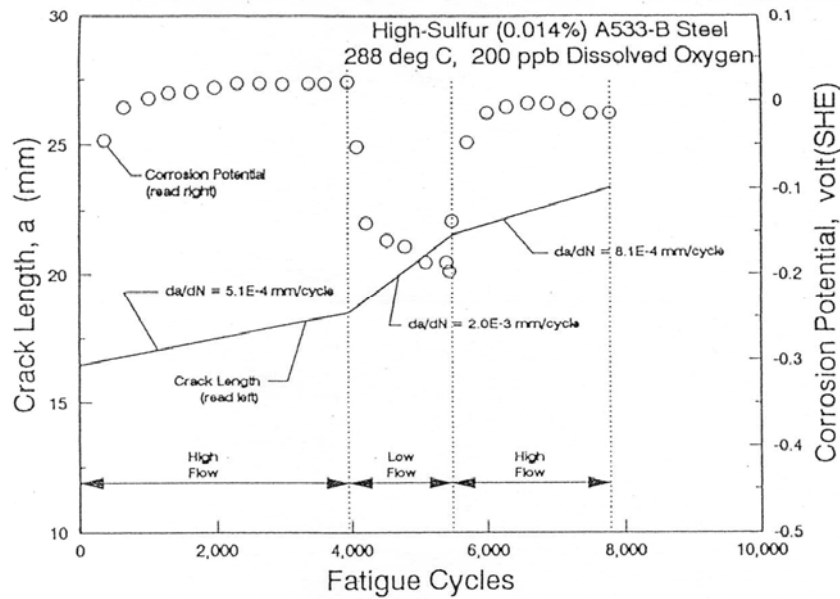
Figure 22: Crack length and corrosion potential vs. time for a LAS tested under cyclic load in 288 °C water containing 200 ppb oxygen. Higher flow velocity increased the ECP, but reduced the CGR [87].
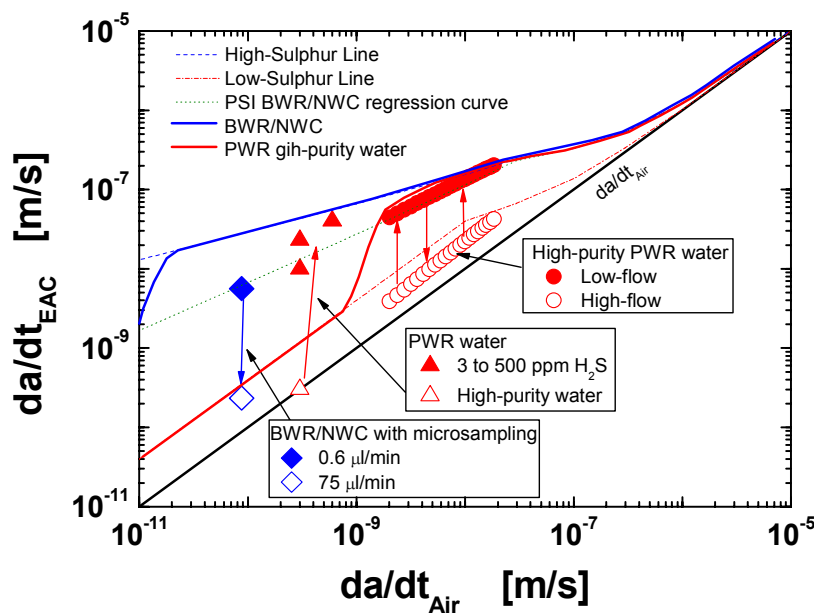
Figure 23: Experimental results, which illustrate how CF CGRs drop from high-sulphur to low-sulphur rates (GE-model) by flushing of the aggressive crack-tip environment by external flow across the crack-mouth (from Figure 21, [12, 92]) or by high microsampling rates [64]. The addition of a large amount of H_2S, on the other hand, can shift the CF CGRs under PWR conditions, where sulphur enrichment by migration is absent, from air or low-sulphur rates close to high-sulphur rates (GE-model) [77]. These data clearly confirm that the aggressive crack-tip environment chemistry controls EAC crack growth.

The flushing of crack-tip electrolyte is more efficient for small cracks and under cyclic loading conditions and depends on factors such as crack surface roughness, crack path, oxides in the crack, ratio of crack-mouth opening displacement (CMOD) to crack length (crack opening angle), flow rate, orientation of flow and on (cyclic) loading conditions (frequency, R-

ratio). High flow rate, large CMOD, high loading frequency, and low load ratio favour the flushing of the aggressive crack-tip environment. The beneficial effect of high flow rate on EAC crack growth is usually slightly overestimated, in particular for static loading conditions and for deep cracks. Most investigations on the effect of flow rate have employed cyclic loading conditions with relative high frequencies ($\geq 10^{-2}$ Hz) and specimens with through-thickness cracks, e.g., C(T)-type specimens. The higher CMOD of these specimens compared to more realistic and more tight surface cracks for similar crack lengths and K_I levels, and the fact that the crack enclave is open to three sides make crack-tip flushing more favourable in this specimen type. Experiments with tight and relatively deep (up to 15 mm), semi-elliptical surface cracks under cyclic fatigue loading conditions clearly demonstrated, that high flow rates of several m/s could mitigate EAC CGR [88, 89]. The important case of a tight surface crack penetrating the cladding/Inconel 182 attachment welds and reaching to the adjacent RPV base metal has not been investigated so far. It is expected that intergranular (IG), respectively interdentritic crack path by SCC in the stainless steel or Inconel 182 cladding could relevantly reduce the interaction between fluid flow past the crack-mouth and the crack-tip environment.

Most of the experimental studies have been performed under "quasi-stagnant" or low flow conditions (< cm/s). Since the formation of aggressive occluded water chemistry is favoured in creviced regions under these conditions, the experimental studies are generally regarded to be conservative. As noted in the review of service experience in Section 11.1, several cracking incidents have been associated with low flow or stagnant conditions, apparently confirming this aspect. In most regions of the rector turbulent conditions with comparably high flow rates in the range of several m/s exist.

4.1.6 Effect of Irradiation

Irradiation can affect the EAC behaviour of low-alloy RPV steels in two major ways, by an increase of the oxidizing power of the environment due to radiolysis of the reactor coolant by n- and γ-irradiation, and by the change of the microstructure and mechanical properties by n-irradiation (n-embrittlement).

Change of the Oxidizing Power of the Environment by Irradiation: This aspect is mainly of relevance for BWRs, whereas in PWRs, the large hydrogen overpressure during stationary power operation suppresses the build-up of oxygen and hydrogen peroxide arising from the water radiolysis. Radiolytic decomposition of the reactor coolant mainly occurs in the high n- and γ-flux region of the reactor core. In LWRs core radiolysis is dominated by the interaction of neutrons with water, and it always produces stoichiometric quantities of reductants (H_2) and oxidants (H_2O_2, O_2). γ-radiation produces some radiolysis (about 20000 times less than neutrons in BWRs), but it is more important in aiding the recombination of reductants and oxidants in the outer annulus (downcomer) of the BWR. ECPs of structural materials are governed by the "stable" radiolysis products H_2, H_2O_2, and O_2. BWR/NWC reactor water always contains a stoichiometric excess of oxidants mostly because of the limited volatility of H_2O_2, whereas both H_2 and O_2 partition to the live steam. Stability of hydrogen peroxide decreases with increasing temperature. The heterogeneous (at component surfaces) and homogeneous decomposition of hydrogen peroxide to oxygen and water produces changes in water chemistry, and greatly complicates their measurement in BWRs and their control and measurement in laboratory systems. The highest concentration is postulated to exist in the coolant within the reactor core zone. A decrease in concentration proportional to the distance travelled by the coolant after exiting the reactor core is expected for the remaining water containing regions within the RPV. The concentration of radiolytic products and the ECP of structural materials

can be readily calculated by radiolysis codes and ECP models and may strongly depend on reactor design, location within the RPV and water chemistry.

Probably the biggest issues in interpreting lab data and simulating BWR potentials relate to the presence of H_2 and H_2O_2, not just to O_2 as in most lab experiments. At low oxidant concentrations significant ECP shifts have been observed in the lab by H_2O_2 addition compared to the ECP measured at the same oxygen level. But at moderate and high oxidant concentrations, the effect of H_2O_2 is not remarkable [93, 94]. Recent measurements of ECP (mainly on stainless steels) in BWRs suggests that the normal free corrosion potential is only slightly elevated by about 100 mV due to irradiation. This is mainly caused by the presence of oxidizing species other than oxygen, particularly hydrogen peroxide. In tests under proton irradiation with stainless steels only small shifts (some few 10 mV) in corrosion potentials on external surfaces and at the crack-tip have been observed over a wide range of water chemistry conditions [95, 96], compared to tests without irradiation, confirming the above mentioned aspect.

An ECP of at maximum $\approx +100$ to $+200$ mV could be expected on the stainless steel cladding or on attachment welds on the inner RPV surface. The slightly increased ECP can be simulated in tests by a higher DO content. As mentioned in Section 4.1.4, EAC crack growth from incipient cracks was very similar in HT water with oxygen, oxygen/hydrogen mixtures or hydrogen peroxide as long as the ECPs were comparable. Thus, the higher ECP can be readily simulated by an increased DO level. The situation might change for crack initiation from smooth surfaces, where oxide film composition/structure on the surface may be different in water with moderate and high levels of oxidants.

Change of Material Properties by Irradiation: Neutron-irradiation embrittlement of low-alloy RPV steels reduces their toughness and ductility (and thus the critical crack sizes) and increases their hardness and yield stress (which might affect the EAC behaviour at high strength levels).

Due to the large core-to-RPV wall annulus in BWRs, the irradiation effects are minimal, especially for modern optimized low-alloy RPV steels with improved n-embrittlement resistance. For example, typical end of life fluencies for a 40 year operating period are 2 to $5 \cdot 10^{23}$ n/m^2 (E > 1 MeV) for PWRs and approximately 10^{22} n/m^2 (E > 1 MeV) for BWRs. Relevant changes of mechanical properties can be observed above fluencies of $> 10^{18}$ n/m^2. This concerns the late state of design life. n-embrittlement is more relevant for PWR, but this aspect is somehow compensated by the very low ECPs, which are significantly below the critical cracking potentials for SICC, even if ECP shifts would occur under irradiation. Nevertheless, accelerated CF crack growth is even possible at these low ECPs under some very specific loading and material combinations.

Experiments with Irradiated Materials and/or Irradiation: Some few tests with spot-check character were carried out on pre-irradiated and non-irradiated pressure vessel steels in air and HT water with and without irradiation [79, 97 – 105] (see e.g., Figure 24). These experiments have so far not indicated any cause for concern on irradiation effects on EAC in C & LAS. The air fatigue, corrosion, and EAC behaviour of irradiated materials did not significantly differ from that of un-irradiated ones. The general lack of observations of significant effects of low strength low-alloy steel composition, microstructure (except sulphur content and inclusion morphology) and yield strength/hardness (as long as ≤ 700 to 800 MPa) (see Section 4.3.2) does not give rise to any theoretical reason to suspect a strong influence of irradiation. The small ECP-shift due to irradiation is unlikely to have more than a slight accelerating effect relative to oxygenated high-temperature water on crack propagation rates. This ECP-shift can readily be simulated, at least for pre-cracked specimens (see Section 4.1.4), in loop experiments by an increased oxygen content. Furthermore, the few cracking incidents in

BWR RPVs can be readily rationalized by the EAC laboratory data base without irradiation and there is no direct indication that these cracking incidents could have been accelerated or promoted by irradiation.
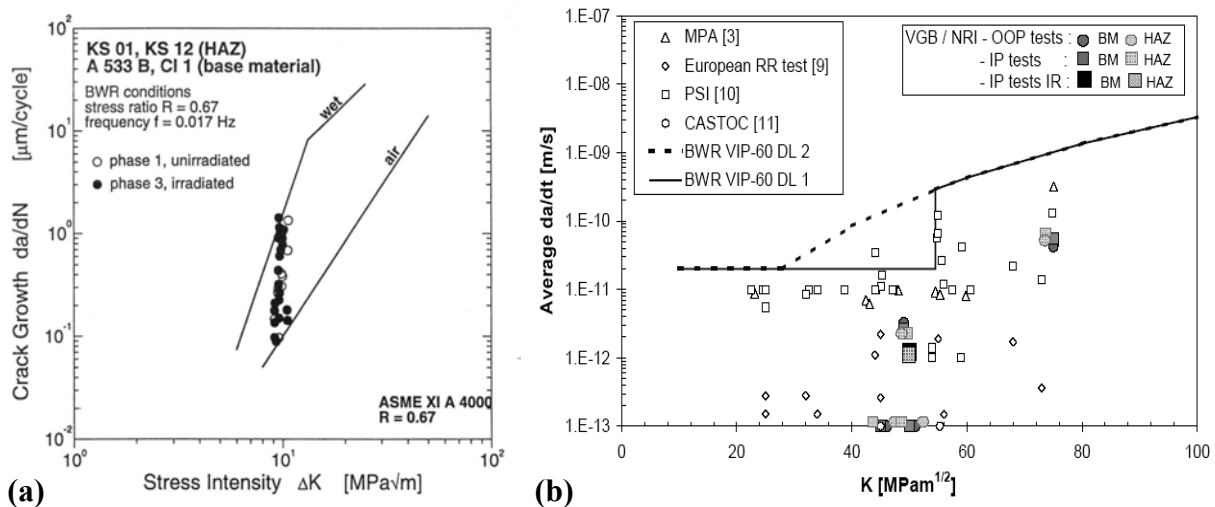
Figure 24: Absence of significant irradiation effects on CF CGRs (a) [105] and SCC CGRs (b) [79] in irradiated RPV steels in high-temperature water in EAC experiments in test reactors.

A major effect of irradiation on EAC propagation rates in RPV steels is therefore not expected, but a slight accelerating effect cannot be completely excluded. A recent research project at NRI, in Řež sponsored by the VGB, where pre-irradiated (end of life fluence) and non-irradiated pre-cracked low-alloy RPV (base metal and HAZ) specimens were tested under cyclic and constant active load under BWR conditions in in-pile and out-of pile loops in a test reactor did <u>not</u> reveal a higher EAC susceptibility of irradiated RPV steels [79, 104].

4.2 Material Parameters

4.2.1 Sulphur Content and MnS-Inclusions

The sulphur content of the steel, the size, type (chemical composition), morphology and spatial distribution of MnS-inclusions are the material parameters having the strongest effect on EAC susceptibility [6 – 9, 11, 38, 56, 57, 106 – 112]. It has been shown that EAC initiation [21, 22, 29 – 31], EAC growth [9, 21, 22, 38, 56, 57, 113, 114] and the pitting behaviour [6, 7] of LAS are affected by the presence of MnS-inclusions. EAC in C & LAS is basically controlled by the sulphur-anion concentration in the crack-tip environment, which has to exceed a critical threshold for accelerated EAC to occur. The effects of steel sulphur content are therefore <u>synergistic</u> with environmental and loading variables, such as sulphur-anion concentration in the bulk environment, ECP (DO content), flow rate, and loading frequency/level (see Sections 10, 10.3 and 10.4 for a detailed discussion).

Metallurgical Aspects: Although the majority of the embedded inclusions appear to be mainly MnS, few of them are stoichiometric MnS, and some inclusions are FeS or mixed (Mn,Fe)S. The variations in sulphide compositions may be related to the steel-making process [115], and different sulphide compositions may produce different levels of electrochemical attack [116 – 118]. MnS is readily soluble in acidic water, FeS and NiS are somewhat less soluble, and CrS is "sparingly" soluble [119]. The dissolution of embedded sulphides intersected by the growing crack results in sulphide-anions (S^{2-}, HS^-) in the crack-tip environment.

The local sulphur content and morphology of MnS-inclusions depend on the steel making (→ segregation) and fabrication process of the plate (forming: hot rolling, forging, etc.) and they can significantly differ in large plates [120]. Sulphur strongly accumulates in the liquid phase during the solidification process. MnS is a relatively low melting compound, and hence migrates in the molten state toward the centre of a solidifying ingot. The concentration of sulphides is generally higher in the centre of the plate. In segregation zones local sulphur content can be several times larger than the mean bulk sulphur content [121]. Sulphides tend to be rod-like in unidirectionally-rolled plates, and disk-like in cross-rolled plates, while in forgings the sulphides tend to be more spherical. Modern RPV steels have both, a smaller sulphur content and a more homogeneous sulphur distribution than older ones.

The orientation (T-L, L-T, T-S, etc.) and location of the specimens may therefore be further important factors and may be an important source of scatter of experimental EAC data. It has been reported, that the T-L orientation produces higher CF CGR than the L-T orientation which, in turn, produces higher CF CGR than the L-S orientation [122], while in another reference, the rates for the L-S, L-T and T-L orientation were found to be essentially similar [123]. The size and morphology of the MnS-inclusions seem to be as important as the sulphur content itself [9]. Plate-like or rod-shaped sulphides are often reported to be more detrimental than spherical inclusions. This all suggests that steel making process and product form (plate vs. forging vs. weld) may play a role in EAC susceptibility. The low apparent EAC susceptibility of welds is attributed to the very small, uniformly-distributed sulphides, as well as to the compositional differences between wrought steels and welds [9].

As mentioned above, the bulk sulphur content as generally provided on material certifications is not an optimum indicator of the EAC susceptibility of a given steel. Other attributes (shape, size, etc.) may be as least as important as the sulphur content. A promising parameter is the area fraction of MnS-inclusions, which correlated well with the EAC susceptibility of the materials in some investigations [124, 125].
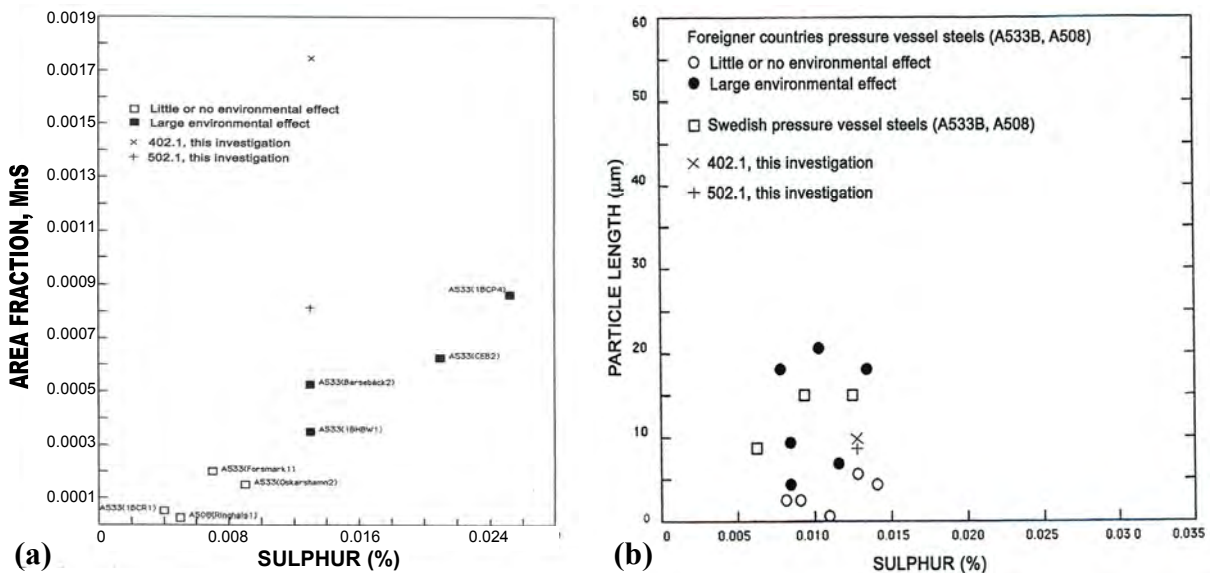
Figure 25: Correlation between EAC susceptibility and area fraction (a) and length of MnS-inclusions (b) [124, 125].

Crack Initiation: In smooth specimens SICC initiation and pitting often occurs at MnS-inclusions which intersect the steel surface [24, 58, 112, 126]. In high sulphur steels generally more MnS-inclusions intersect the steel surface, which increases the probability for crack initiation. Kunyia [127] showed that whilst SICC rates where the same for low and medium sul-

31

phur steels, the number of initiation sites was greater in the latter case. Hurst et al. [129] showed that if specimen orientation was such as to maximise access of the environment to the crevice created by decohesion of an outcropping sulphide inclusion, localized SICC could be observed in a stagnant autoclave in nominally deoxygenated conditions. If the MnS-inclusions, intersecting the steel surface, were removed before starting an SSR test, no SICC in high-purity water was observed [111]. Under highly oxidizing conditions at low or intermediate temperatures and low flow rate conditions, where pitting and the formation of an aggressive occluded water chemistry is strongly favoured [6, 111], initiation occurs often at pits and the effect of MnS is less dominant. Furthermore, strain localization by DSA further facilitates EAC initiation in the intermediate temperature range.

SICC susceptibility generally decreases with decreasing steel sulphur content. A high steel sulphur content is usually extending the range of SICC conditions (ECP, DO, bulk sulphur-anion content, strain rates, etc.) and shifting the thresholds to less severe conditions [9]. The critical cracking potential for SICC in SSR tests, e.g., decreased with increasing steel sulphur content [56, 57, 58, 60] (Figure 8). In SRL tests with pre-cracked specimens in oxygenated HT water, SICC initiation in low-sulphur steels occurred at lower $K_{I,i}$ values than in high-sulphur steels, whereas the subsequent SICC rates were very similar for given loading conditions (Figure 26) [28]. The situation may be different at intermediate temperatures, where DSA effects may even dominate steel sulphur effects on SICC initiation [128].
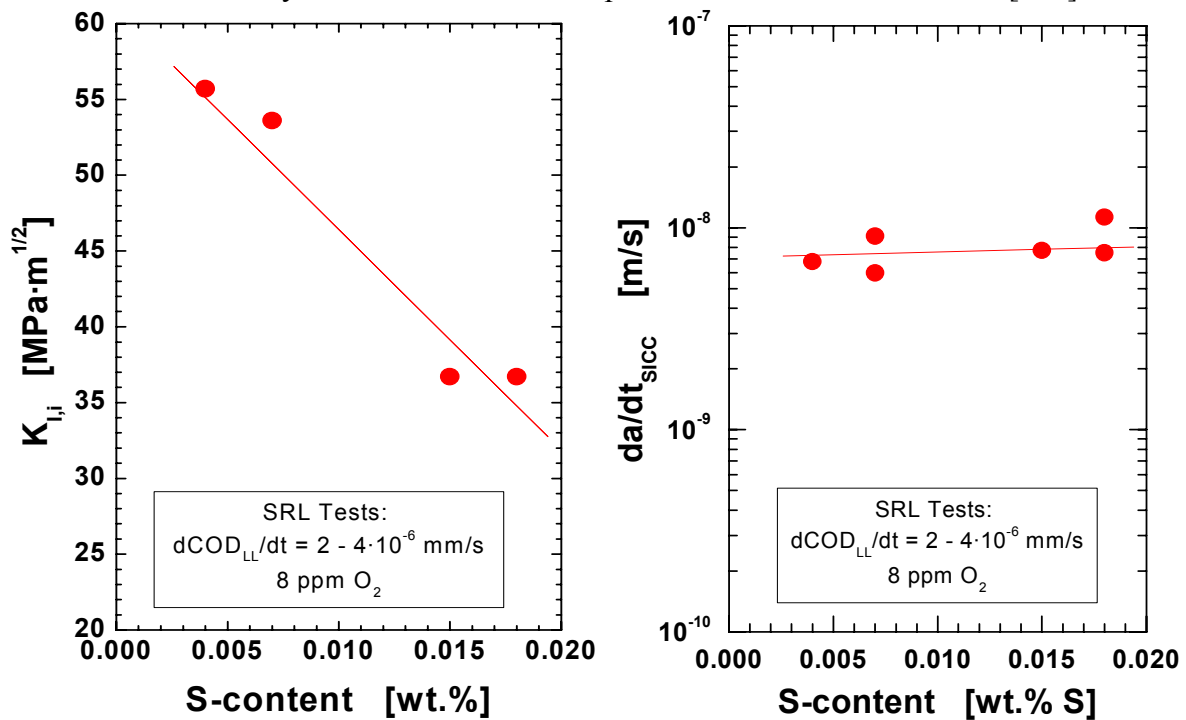
Figure 26: Effect of steel sulphur content on SICC initiation and crack growth in SRL tests with pre-cracked specimens in oxygenated HT water at 288 °C [128].

In LCF tests, the effect of sulphur content on fatigue life depends on the DO content of the water. When the threshold conditions are satisfied and for a DO content of 1 ppm, the fatigue life decreases with increasing sulphur content [29 – 31]. Limited data suggest that environmental effects on fatigue life saturate at a sulphur content of 0.015 wt.%. At high DO levels, e.g., > 1 ppm, the fatigue life seems to be insensitive to sulphur content in the range of 0.002 – 0.015 wt.% [29 – 31]. If any of the threshold conditions is not satisfied, environmental effects are minimal and relatively insensitive to changes in sulphur content.

Crack Growth: The effect of steel sulphur content is less pronounced for crack growth than for crack initiation, in particular under oxidizing BWR conditions. In pre-cracked specimens, a large area of dissolvable MnS-inclusions, intersected by the crack plane and front, are available and the restricted mass transport in the crack crevice favours the formation of sulphur-anion-rich crack-tip environment.

Since SCC crack growth could not be sustained in C & LAS in chloride-free, oxygenated HT water at 288 °C up to relatively high K_I values of 60 MPa·m$^{1/2}$, no effect of steel sulphur content could be derived in this K_I range. Nevertheless, above 60 MPa·m$^{1/2}$ there were some indications that the transition from these low to high SCC CGRs was shifted to lower K_I values with increasing steel sulphur content and that high-sulphur steels tended to produce higher SCC CGRs in this region [35].

Usually it was more difficult to initiate SICC in low-sulphur steels, but SICC CGRs in SRL tests in oxygenated HT water of different LAS were comparable over a wide range of loading conditions (Figure 26) [28, 128].

Under system conditions, where high-sulphur crack-tip conditions prevailed (e.g., at high ECP, relatively high loading frequencies or high sulphate/sulphide contents of the environment, etc.), the CF CGRs of different C & LAS were very similar over a wide range of loading and environmental conditions (Figures 27 and 28) [28, 51, 62]. A different trend in the CF crack growth behaviour under highly oxidizing conditions only appeared at intermediate temperatures (200 to 250 °C) and/or very low loading frequencies $\leq 3 \cdot 10^{-5}$ Hz (Figure 29) [51, 62]. At 250 °C and at a loading frequency of 10^{-5} Hz the cycle-based CGR $\Delta a/\Delta N_{EAC}$ increased with increasing DSA susceptibility, which even seemed to dominate the effect of steel sulphur content. RPV steels with a low sulphur content of 0.004 wt.% S and high DSA susceptibility revealed a higher cycle-based CGR $\Delta a/\Delta N_{EAC}$ under these conditions than a high sulphur steel (0.018 wt.% S) with a moderate DSA susceptibility (Figure 29). With increasing loading frequency, the difference between the materials disappeared. At a loading frequency of $8.3 \cdot 10^{-4}$ Hz all materials revealed very similar CF CGRs. At 288 °C and a loading frequency of 10^{-5} Hz on the other hand, the cycle-based CGR $\Delta a/\Delta N_{EAC}$ seemed to better correlate to the steel sulphur content than to the DSA susceptibility and increased with increasing sulphur concentration (Figure 29).

A more pronounced effect of steel sulphur content was observed under PWR or BWR/HWC conditions (lower ECP), where high-sulphur crack-tip environment conditions are more difficult to be achieved or sustained. In this case, the accelerated CF rates could be sustained to lower loading frequencies or ΔK values at 288 °C in high-sulphur steels for given ECP conditions [124].
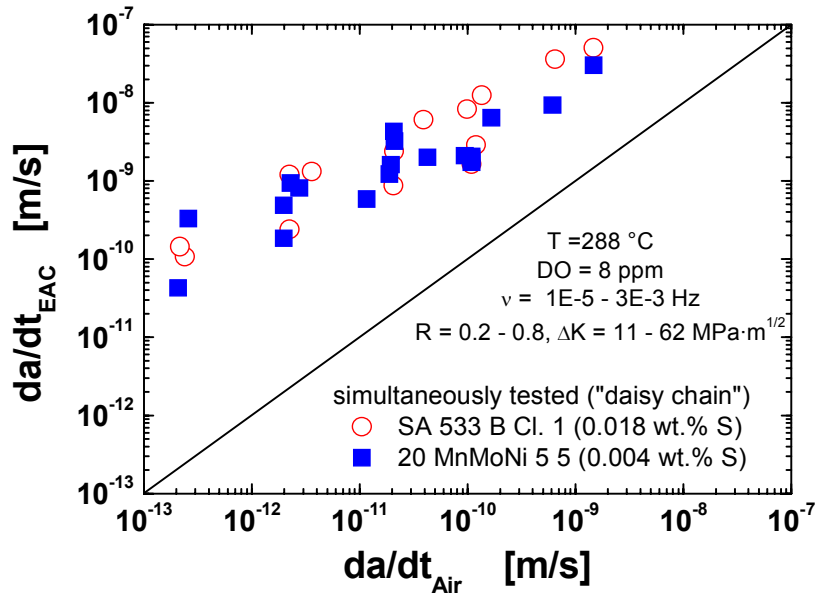
Figure 27: Comparable CF CGRs in simultaneously tested low- and high-sulphur steels under highly oxidizing conditions, where high-sulphur crack-tip conditions prevailed [28].
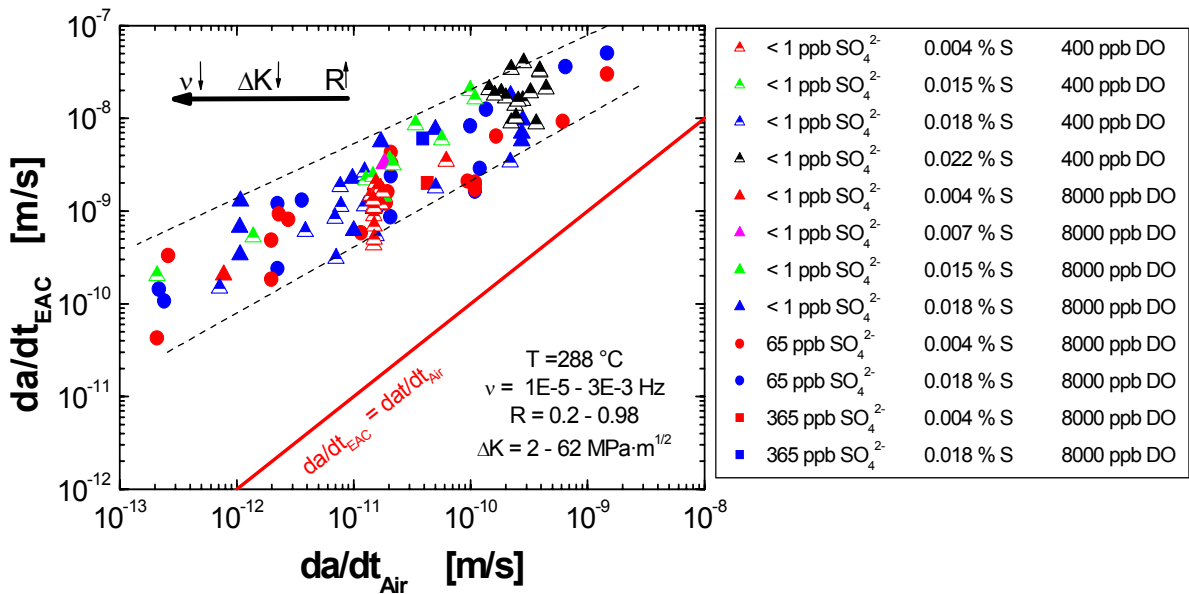
Figure 28: Comparable CF CGRs over a wide range of material, loading and environmental conditions in oxygenated HT water at 288 °C as long as high-sulphur crack-tip environment prevailed [62].
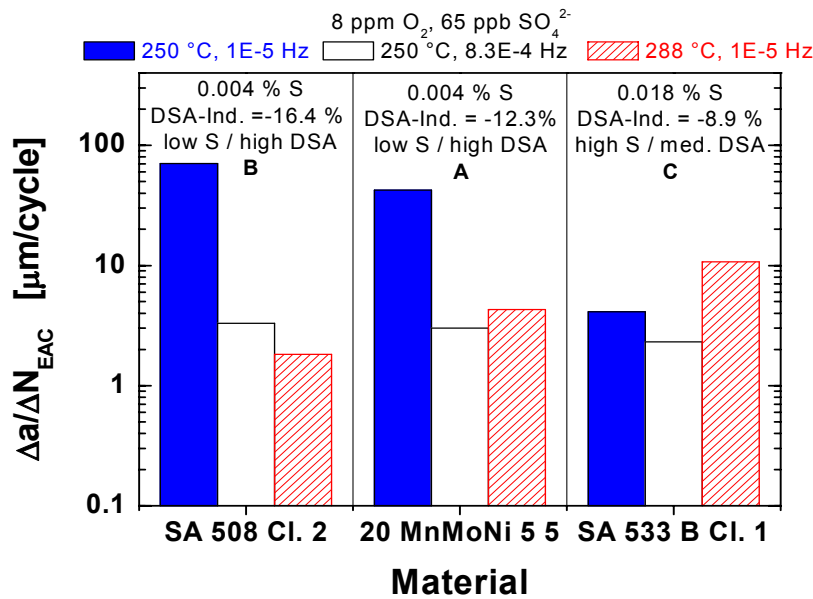
Figure 29: Comparison of cycle-based CF CGRs $\Delta a/\Delta N_{EAC}$ from CF tests with three RPV steels with different steel sulphur content and DSA susceptibility [51, 62].

Sulphur Threshold: Steels with a sulphur-content of less than 0.003 wt.% show a very low susceptibility to EAC crack growth over a wide range of environmental and loading conditions and are often regarded as "immune", but SICC has even been observed in SSR tests in extremely low sulphur (0.001 wt.% S) forging material in oxygenated HT water at DO contents > 100 ppb in the temperature range form 150 to 250 °C [2, 22]. Furthermore, the low sulphur content results in a higher toughness, larger critical crack sizes, and higher safety margins. But the beneficial effect of a low steel sulphur content concerning EAC may disappear under suitable combinations of corrosion system parameters (e.g., high ECP and/or high sulphur-anion concentration in the bulk environment and/or or under suitable strain rate/temperature conditions) [34, 62].

4.2.2 Yield Stress

Hydrogen-Assisted SCC (HASCC): A distinct effect of yield stress (YS) on SCC has been observed in many corrosion systems, in particular in the context of HASCC. Hydrogen-assisted (intergranular (IG)/transgranular (TG)) SCC in high-purity HT water has been observed in high strength LAS (which are used, e.g., for turbine discs) with a high YS > 800 MPa and high hardness (> 350 HV5) at least up to a temperature of 200 °C [129, 130]. The susceptibility is high below 100 °C and increasing with increasing strength level, increasing grain size, and decreasing temperature [129, 130]. In high strength LAS, K_{ISCC} is usually decreasing and SCC CGRs are increasing with YS [130 – 132] at temperatures < 150 °C.

The C & LAS used in LWR for pressure-boundary components are operated at temperatures > 150 to 200 °C and have significantly lower YS, if they were in the proper material conditions. The relevance of HASCC is therefore restricted to some specific material and operation conditions for these components. The macroscopic peak Vickers hardness of the weld HAZ in LAS components can be limited to values below 350 HV5 by PWHT and stress relieving, although locally the microhardness can still exceed this value. IG/TG SCC has been observed in quenched (and in some cases tempered) low-alloy RPV steels (with martensitic/bainitic microstructure), which have been austenitized at high temperatures with significant austenite grain growth [133, 134]. A higher SCC susceptibility may therefore be postulated for the peak hardness coarse-grain region of weld HAZ, in particular in combination

with a high steel sulphur content, especially if welding and PWHT have not been properly carried out or in the case of repair welding without any PWHT. Cold work (bending), which also results in an increase of YS is restricted to small diameter C & LAS piping, and the degree of cold work, which can be accepted without any heat treatment is strictly limited.

YS Effects in Low and Moderate Strength C & LAS at Temperatures > 150 °C: The effect of YS on EAC in the LAS-HT water system has not been studied systematically. The limited data revealed the following trends:

Crack Initiation: A very similar reduction of LCF life and similar SICC behaviour in SSR tests with smooth specimens of C & LAS and of cold worked LAS with different YS levels has been observed, suggesting that under these loading conditions YS only has a moderate effect [31]. LCF life in air of carbon steels is typically a factor of 1.5 lower than for LAS with higher YS. Although the cyclic-hardening behaviour and microstructures of C & LAS and cold worked LAS significantly differ, the effects of HT water on LCF life reduction is very similar for both classes of materials. The amplitude of fatigue life reduction was only affected by steel sulphur content. Very limited data by Venz et al. [135] suggest that cold work does not significantly affect LCF life.

Crack Growth: The limited data suggest, that there is only a moderate effect of YS and hardness on SCC, SICC and CF crack growth up to a relatively high critical YS/Vickers hardness level of 700 to 900 MPa and 350 HV5 (Figures 30 and 31). Above this critical YS/hardness, the SCC and SICC CGRs seemed to increase with increasing YS level, but CF CGRs were still comparable (Figure 31) [128, 136]. It is expected that the transition region from low- to high-sulphur CF and SCC CGRs is shifted to lower loading frequencies and ΔK- or K_I values with increasing YS (see also Figures 94 and 104).
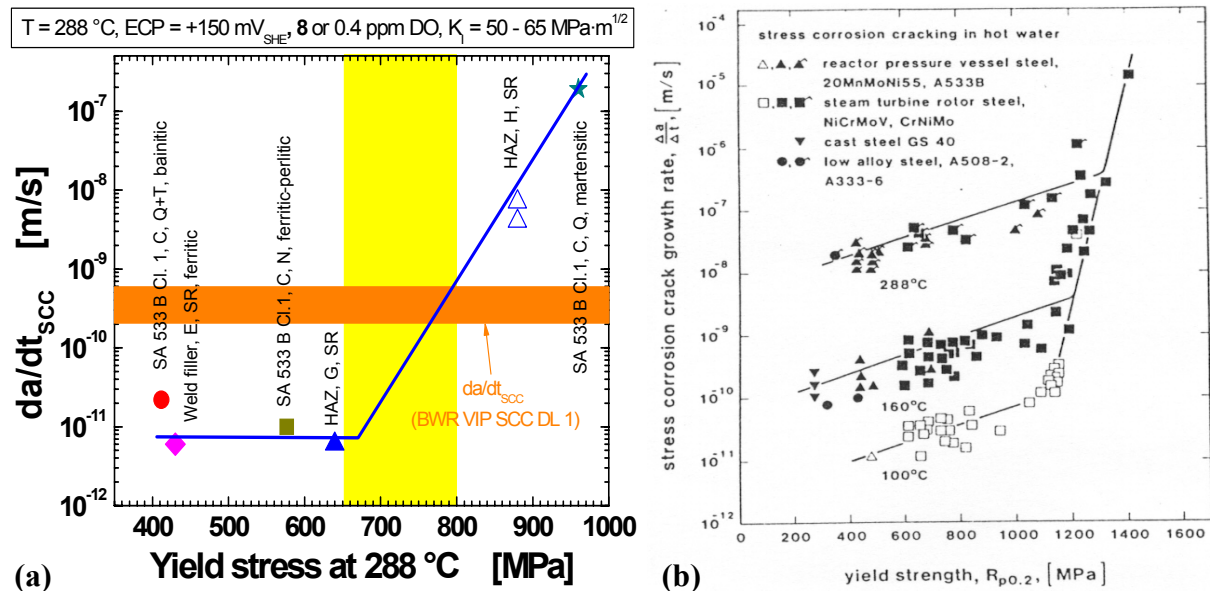
Figure 30: Effect of YS on SCC CGRs in different LAS in recirculation/refreshed [128] (a) and in static ("no flow") autoclave tests (b) [132].

36
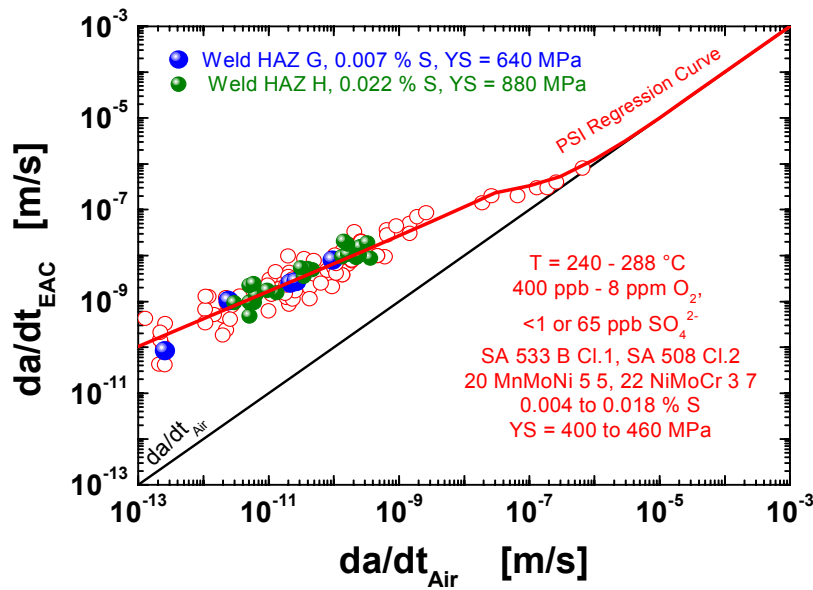
Figure 31: No significant effect of YS on cyclic CF crack growth [136].

Possible Explanation for YS Effects: In case of HASCC, a higher YS results in a higher hydrostatic stress at the crack-tip and, thereby, a better chance to achieve the necessary critical hydrogen supersaturation in this region. Possible effects of YS on EAC in carbon and low-alloy primary pressure-boundary component steels in HT water at temperatures > 150 °C may be better rationalized by the effect of YS on (crack-tip) strain rate. A higher YS (and work hardening rate) results in a smaller plastic zone size and steeper strain gradient at the tip of a growing crack, and therefore in a higher crack-tip strain rate with crack growth for given loading conditions [137, 138]. Additionally, higher YS usually results in more distinct low-temperature creep for a given stress to YS ratio, in particular for incipient cracks, where the peak tensile stress at the crack-tip is approximately three times the YS under plane-strain conditions [136]. There may be opposite YS trends for EAC initiation from smooth surfaces and from incipient cracks. It has been suggested that a low YS facilitates SICC initiation from smooth surfaces, since it is easier to attain a high plastic strain at the water-wetted surface in the field. On the other hand a higher YS results in more low-temperature creep at a given stress to YS ratio, which may be important for SCC initiation under static loading conditions.

4.2.3 Microstructure

Steel sulphur content/MnS-inclusions and DSA susceptibility (see Section 4.2.4) in the DSA-temperature-strain rate range seem to be the only material parameters, which may have very pronounced effects on EAC in C & LAS.

As long as sulphur content and MnS-inclusion morphology were similar and YS level was in the range from 200 to 600 MPa, the EAC crack growth behaviour and CGRs of different C & LAS were very similar over a wide range of system conditions and are not dependent on their microstructural state (Figure 32) [51, 62]. Similarly, the EAC crack growth behaviour and CGRs of weld filler and weld HAZ materials (if hardness was limited to values < 350 HV5) were generally very similar to those of the corresponding wrought metals over a wide range of system conditions (Figures 30a and 31). Pronounced effects are only expected in the transition region from low- to high-sulphur EAC CGRs.
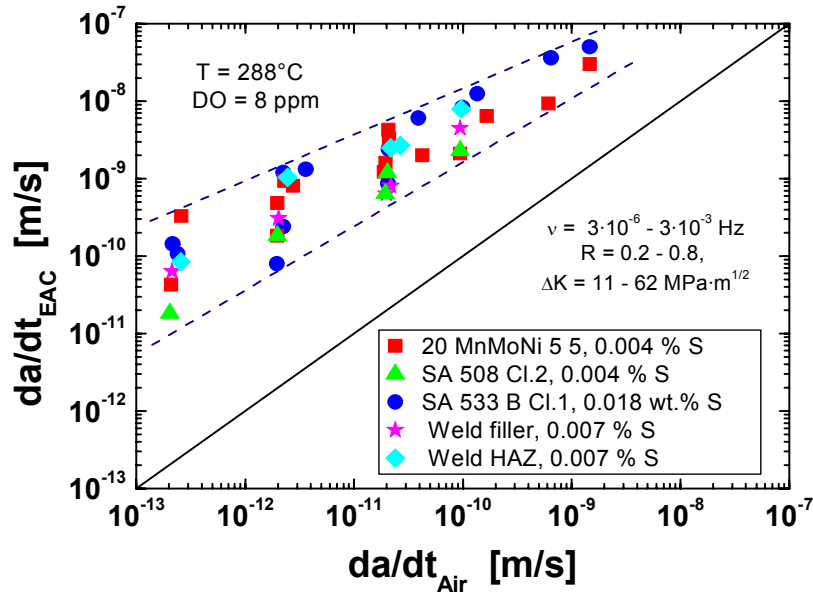
Figure 32: Similar CF CGRs for different alloys/microstructures in oxygenated HT water.

4.2.4 Dynamic Strain Ageing

The DSA phenomenon is observed in C & LAS during plastic straining at sufficiently slow strain rates ($< \approx 10^{-2}$ s^{-1}) in the temperature range from 100 to 350 °C. Similar temperature/strain rate conditions typically occur in C & LAS primary pressure-boundary components during BWR plant transients (e.g., start-up/shut-down, turbine trips, hot stand-by with thermal stratification, etc.) and the stationary operating temperature of BWR RPVs (274 to 288 °C) and of the feedwater piping system (200 to 220 °C) is very close to the peak DSA effect region. Although the role of DSA in EAC has not yet been extensively studied, many EAC data strongly suggest that the susceptibility of C & LAS to EAC coincides with evidence of DSA, both in terms of temperature and strain rate. DSA effects in EAC of C & LAS may be related to its influence on crack-tip strain rate/strain and to the strain localization process (see Section 10.2). The physical metallurgy of DSA is summarized in [13, 27]. In the following paragraphs the most important phenomenological, microscopic, and material aspects of DSA are briefly summarized, followed by a short discussion of the experimental evidence for possible interactions between DSA and EAC in C & LAS in HT water.

Phenomenological and Microscopic Aspects of DSA: DSA in C & LAS is an elastic interaction between the strain fields of solute interstitials as N and C and moving dislocations. In the DSA temperature range (100 to 350 °C) this interaction macroscopically results in a maximum in ultimate tensile strength (UTS), hardness and strain hardening rate, in a minimum of ductility (elongation to fracture, A and reduction of area, Z), and in a negative strain rate sensitivity (Figure 33). Additionally, serrations in the stress-strain cure may occur. The YS is affected by static strain ageing rather than DSA, resulting in a plateau or small peak in YS in the temperature range of DSA. The DSA effect increases with increasing concentration of free, interstitial N and C and is most pronounced if the diffusion rate of N/C (which is dependent on temperature) and the dislocation velocity (which is dependent on strain rate or loading rate/frequency) are similar. Parameters, which affect the concentration of free N and C and their diffusion rate have therefore a strong effect on the DSA behaviour. The temperature range of DSA peak effect decreases with decreasing strain rate. Microscopically, DSA results in an inhomogeneous localisation of plastic deformation, an increase of planar deformation and dislocation density and in deformation bands.
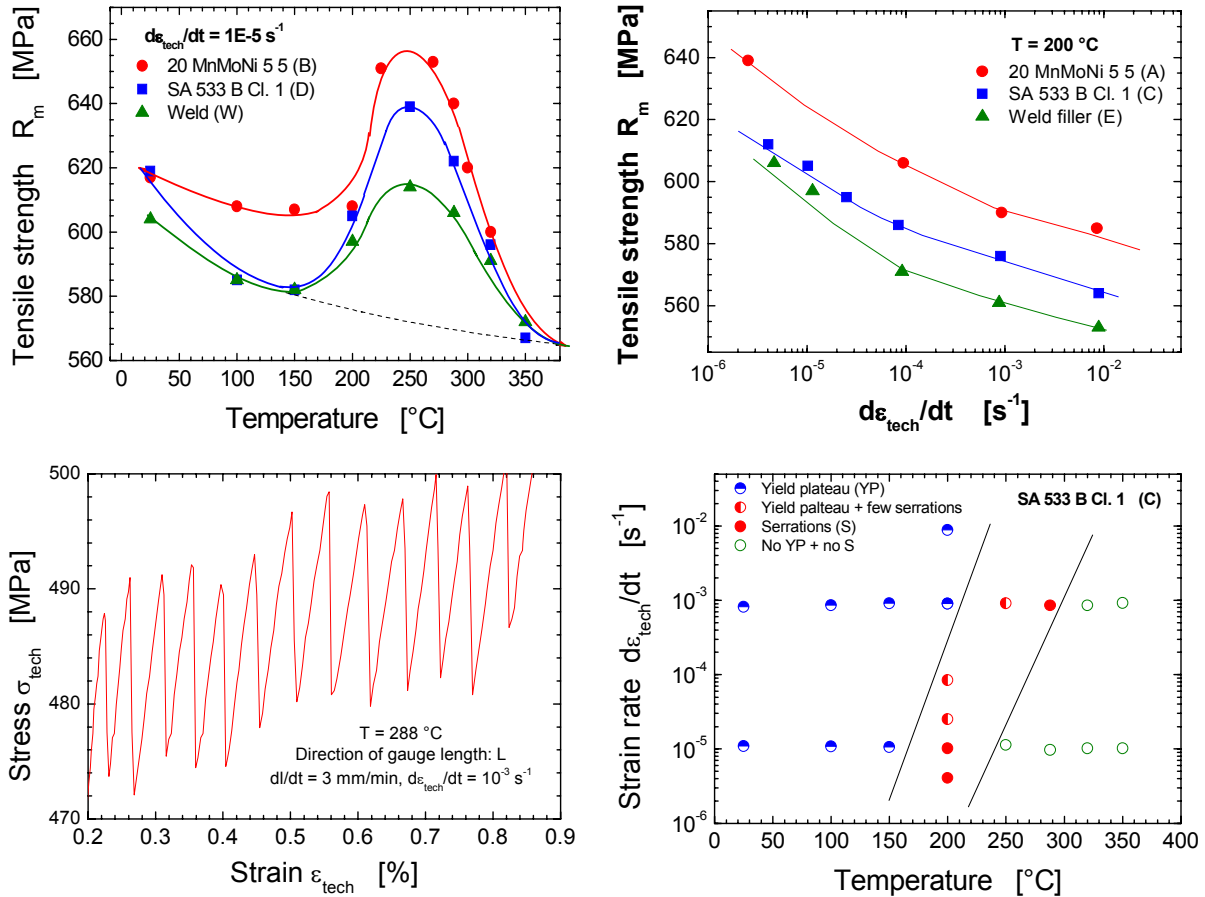
Figure 33: Typical features of DSA in C & LAS in tensile tests in air [128].

Important Material Aspects: The free N and C contents are not specified in the relevant nuclear guidelines and regulations (KTA, ASME BVP) and can strongly vary from steel to steel. The concentration of free interstitial nitrogen and carbon strongly depend on the steel making (killing) or welding process, the thermal history or heat-treatment (annealing-, PWHT- or stress relieving temperature), on the chemical composition (C_{tot}, N_{tot}, Al, V, Ti, Cr, Mo, O, Mn, …) and on the (immobile) forest dislocation density of the steel. Alloying elements, which have a strong affinity to N or C, such as Al, Cr and Mo, and form nitrides or carbides may result in a reduction of the residual concentration of free N and C. A high forest dislocation density (cold work, HAZ, as-welded (quenched) materials) acts as a sink for N and C and also reduces the free N and C content, which can pin fresh moving dislocations. Parameters, which would affect the interstitial diffusion might result in a temperature or strain rate shift of the typical DSA range. The onset of serrations in the stress-strain curve is not very sensitive to the microstructure or composition of C & LAS. An exemption is the Mn content, which seems to influence the diffusion process of N and C by forming Mn-N and Mn-C pairs increasing thus the activation energy for the diffusion process [135] and shifting the onset of DSA range to higher temperatures. Large differences in the activation energy for the disappearance of DSA suggest that it is also a function of steel composition.

Silicon killed air poured C & LAS show a much more pronounced DSA effect than aluminium killed vacuum ladle degassed steels, since in aluminium killed steels, aluminium nitrides are formed and the remaining free interstitial N content is very low.

During the welding process uptake of small amounts of O and N can occur. Weld metal often have a very little Al but high O contents. Because of its very high affinity to O, Al first combines to O (aluminium oxide precipitates) in welds, which reduces the beneficial effect of

the aluminium. During fast cooling after welding, incomplete precipitation of carbides and nitrides occurs resulting in an increased or even supersaturated concentration of free C and N in the as-welded condition. During PWHT the concentration of free C and N is increasingly reduced by increasing PWHT temperature trough carbide/nitride precipitation. Welds might reveal increased concentrations of interstitial N and therefore be more susceptible to EAC in the DSA temperature/strain rate range than generally thought so far. The better resistance of the weld material outside the DSA range reported in some references has been mainly attributed to the different morphology of MnS-inclusions in the welds (very small spherical inclusions).

In the HAZ near to the fusion line with high peak temperatures slightly below the melting point (partial) dissolution of carbides and (incomplete) re-precipitation during subsequent cooling occurs, which can result in a supersaturated state. During the following PWHT precipitation of further carbides occurs. The interstitial C is strongly dependent on the stability of the carbides, on the peak temperature, heating and cooling rates and on the PWHT-treatments applied. The most severe DSA effects might be expected for materials in the as-welded condition without PWHT (e.g., repair welding), but on the other hand the high forest dislocation density in this material state may have an opposite and mitigating effect.

Experimental Evidence for Interactions between DSA and EAC in C & LAS: EAC in C & LAS has been observed under temperature/strain rate conditions, or in materials where no (or only minor) DSA effects were present. DSA is therefore not a pre-requisite for EAC and is best regarded as an additional contributor to the EAC growth process. The available EAC data strongly suggest that the susceptibility of LAS to EAC coincides with evidence of DSA, both in terms of temperature and strain rate (Figures 34 and 35). [13, 26, 27]
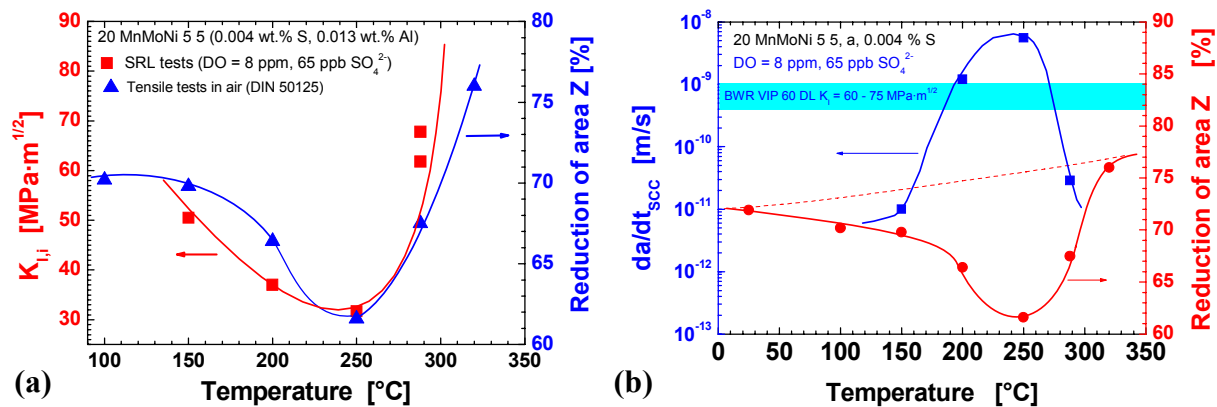
Figure 34: Coincidence between maximum in SICC susceptibility (a) [28] and in SCC CGRs (b) [36] with DSA in terms of temperature.

DSA generally results in an extension of the susceptibility region and may especially affect the temperature and strain rate dependence of EAC. In the DSA temperature range, e.g., the reduction of LCF life in HT water did not saturate at 10^{-5} s^{-1} and further decreased monotonically down to the lowest tested strain rate of 10^{-7} s^{-1} in case of a LAS with distinct DSA susceptibility [75]. The most pronounced effects of DSA on EAC are typically observed close to crack growth thresholds (e.g., for SCC under static load [36, 139] (Figures 34 and 35) or for CF close to critical frequencies [51, 62] under cyclic load (Figures 29 and 36). Under these conditions, EAC better correlated with DSA susceptibility than with steel sulphur content. Under system conditions, where fast EAC crack growth can be easily sustained, only minor or moderate effects of DSA are observed generally (Figure 37).
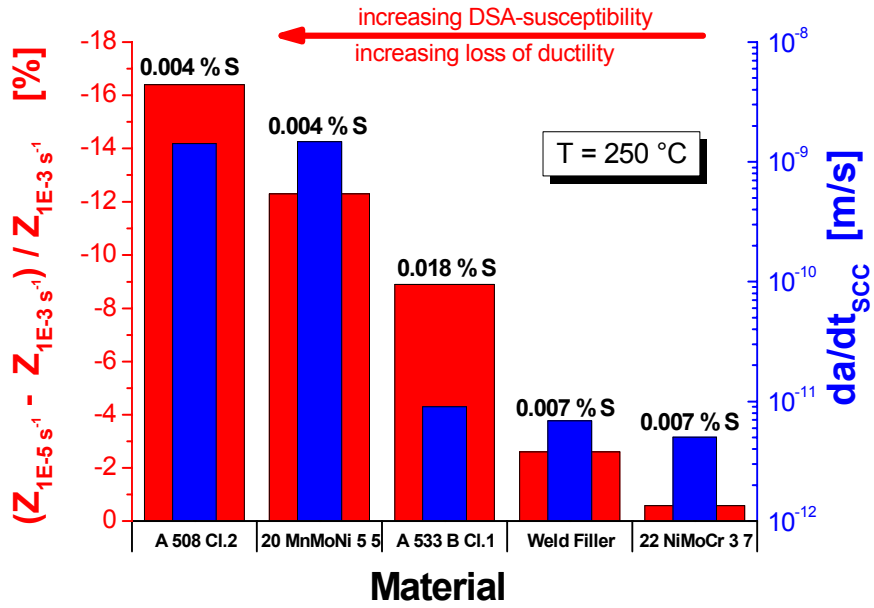
Figure 35: Good correlation between degree of DSA susceptibility and SCC CGR at intermediate temperatures in different LAS [36].

(a)   **(b)**
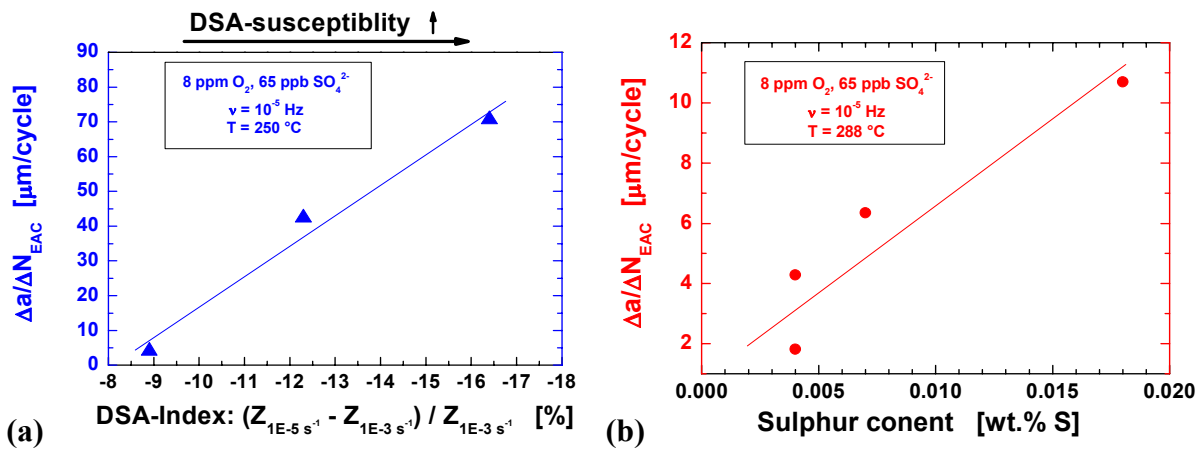
Figure 36: Good correlation between DSA susceptibility and steel sulphur content (a) and with cycle-based CF CGRs (b) at 250 and 288 °C at $1\cdot10^{-5}$ Hz close to the critical frequency for oxygenated HT water [51, 62, 128].
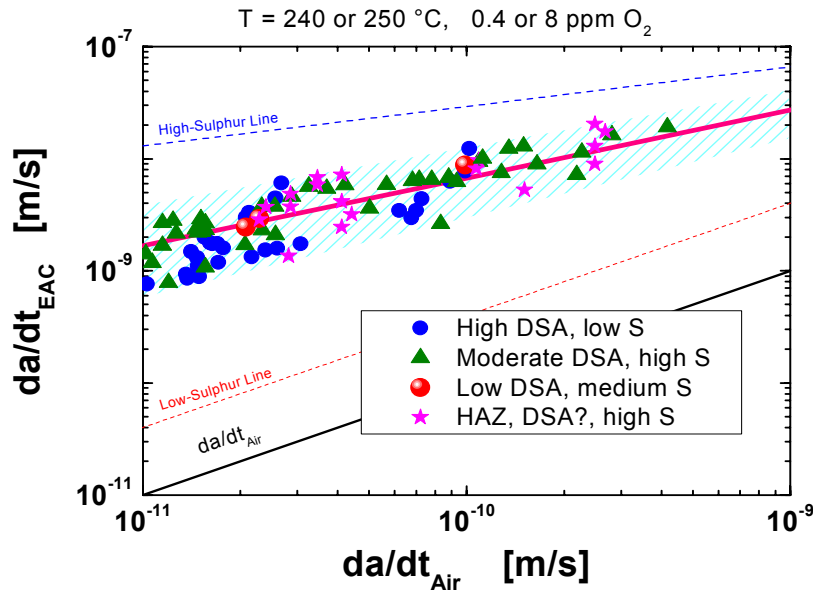
Figure 37: Similar CF CGR for LAS with different DSA susceptibilities and steel sulphur contents in oxygenated HT water at loading frequencies $> 1\cdot10^{-4}$ Hz.

These results clearly show that the concentration of free, interstitial N/C, which mainly governs the DSA susceptibility in C & LAS, might therefore be just as relevant for EAC susceptibility as the steel sulphur content and even overwhelm sulphur effects under certain conditions in the DSA temperature/strain rate region [36, 51, 62, 139]. Differences in DSA susceptibility of otherwise identical LAS may explain some of the observed data scatter and different temperature trends. DSA also draws attention to weld filler (low Al and high N_{free} content) and weld HAZ materials (eventual, incomplete precipitation of carbon/nitrogen during cooling-down/PWHT), which therefore could be more susceptible to EAC than thought so far. DSA also offers an explanation for the TG quasi-cleavage fracture appearance with feather morphology (see Section 7.2) and the increasing fracture surface roughness of EAC at intermediate temperatures.

Although chemical composition may give a rough indication for the DSA susceptibility of different materials, it normally has to be determined either by internal friction measurements or tensile tests at different temperatures/strain rates. A simple method is required for non-destructive determination of DSA susceptibility of operating C & LAS components.

4.2.5 Low-Temperature Creep

Low-temperature creep in C & LAS is thermally activated dislocation glide and low-temperature creep strain rate increases exponentially with applied tensile stress. Since strain hardening is dominating recovery processes, low-temperature creep strain rate/strain after initial loading usually decreases/increases according to a reciprocal/logarithmic time law [140]. Furthermore, low-temperature creep seems to be enhanced by free N [141] (and Mn content) and high YS/cold work/pre-strain level [142 – 146].

The effect of low-temperature creep has not been directly studied in case of C & LAS. It seems that low-temperature creep may be very important for SCC initiation under static loading conditions for both smooth and pre-cracked specimens and that it may control SCC crack growth in C & LAS in high-purity HT water (see Figure 43 on p. 51). A macroscopic stress above the YS and a slow positive strain rate at the water-touched surface are necessary for SCC initiation. If exhaustion of low-temperature creep was allowed to occur before statically loaded smooth or pre-cracked specimens were exposed to HT water, then no SCC was ob-

served [13]. Low-temperature creep is less important for SCC crack growth, in particular un-der aggressive test conditions (e.g., increased chloride levels), where crack-tip strain rate is dominated by the growth contribution. It is stressed that in case of severe violation of SSY conditions and ligament yielding in specimens, sustained low-temperature creep in air and sustained SCC is observed in high-purity water, but test results from such specimens cannot be transferred to the thick-walled components.

4.2.6 Other Material Aspects

Surface conditions (roughness, cold work, residual stress, oxide film, pitting) may have an effect on EAC initiation, but have only been investigated in the context of LCF initiation to a very limited extent [31] (see Section 9.2.2).

In some C & LAS, segregation of phosphorous (and of other metalloids) to prior austen-ite grain boundaries during annealing/PWHT (temper embrittlement) or during prolonged op-eration periods in the temperature range from 300 to 350 °C has been observed [147 – 148]. The resulting decohesion or increased electrochemical activity of grain boundaries might also affect EAC in C & LAS, although so far there is no direct evidence that phosphorous might significantly affect EAC in these materials. Phosphorous segregation has been the reason for some mixed IG/TG EAC cracking in some Western RPV steels in HT water [149]. The ob-served EAC CGRs were similar as in other steels with purely TG EAC, thus not indicating any significant acceleration of EAC by this effect [149].

Tests with thermal ageing at 400 °C for 3000 h resulted in precipitation of severe carbide bands along the rolling direction of RPV steels and a reduced LCF life in simulated BWR en-vironment with respect to the non-aged state [150]. It is not clear if this ageing process could also occur during prolonged periods at lower temperatures of 290 to 350 °C or not. Most data from the literature suggest that there is no thermal embrittlement in typical RPV steels at tem-peratures of up to 350 °C for times as great as 100000 h [148].

Recent cracking incidents in carbon steels in CANDU reactor cold bent feeder lines oper-ating at 310 °C [151] and older cracking incidents in cold bent pipes in fossil-fired plants [152], which were related to low-temperature creep crack growth in combination with DSA or temper embrittlement and possible environmental effects in some cases, have arisen the ques-tion, if low-temperature creep crack growth might also occur in PWR RPV or pressurizers. A recent publication seems to support this idea [153], but the extreme material and loading con-ditions of theses tests do not allow any conclusion concerning RPV or pressure vessels. The applied stresses or reference stresses were very high (near to the UTS) compared to plant de-sign conditions. The simulated coarse grain HAZ had a Vickers hardness of 430 HV10 and a grain size of 144 μm. Peak hardness of coarse grain zone in weld HAZ can be limited to val-ues below 350 HV5 by PWHT. Even locally, micro hardness hardly reaches such high hard-ness values even in poor quality welds. At PSI, very fast SCC was observed under such mate-rial conditions in HT water at much lower K_I values [128], where low-temperature creep crack growth is not observed. Cold work (bending) and the degree of cold work, which can be accepted without any heat treatment is strictly limited. Service experience has not indicated any problem here.

4.3 Loading Parameters

Both EAC initiation and growth in C & LAS show a high sensitivity to strain rate (or crack-tip strain rate in case of incipient cracks). <u>Slow dynamic</u> straining with a <u>positive</u> strain rate (<u>tensile loading with an open crack enclave and access of the environment to the crack-tip</u>) in the range of 10^{-7} to 10^{-3} s^{-1} with associated <u>plastic yielding</u> above a critical strain threshold is essential for crack initiation [23, 29 – 31, 39, 106, 107, 129] and subsequent crack

growth. The strain rate effect may be rationalized by oxide film rupture frequency/repassivation in both anodic dissolution or HASCC mechanisms. DSA may be an alternative explanation or additional contributing factor for the strain rate dependence of EAC. Critical strains for EAC have often been related to the oxide film rupture strain [5].

4.3.1 *Strain Rate and Loading Rate/Frequency*

Crack Initiation: In static test with smooth tensile test specimens, crack initiation is only observed at stress levels above the HT YS [39, 127]. If complete exhaustion of low-temperature creep is allowed to occur before the specimens are exposed to high-purity, HT water, no SCC is observed in smooth and pre-cracked specimens under pure static loading conditions, thus indicating non-classical SCC behaviour and confirming the importance of dynamic straining for EAC of LAS in HT water [13].

In SSR tests, above a strain rate of 10^{-3} to 10^{-2} s^{-1}, no significant environmental effects are observed and specimens fail without any EAC and reduction of ductility with respect to corresponding tests in air. Below a strain rate of 10^{-3} s^{-1}, the SICC susceptibility increases with decreasing strain rate with a possible maximum of SICC susceptibility between 10^{-7} to 10^{-4} s^{-1} depending on other relevant system parameters, as ECP (oxygen content), temperature, steel sulphur content and bulk sulphate concentration of the environment [23, 24, 56, 57, 129] (Figure 38). At the moment, it is not fully clear if SICC susceptibility saturates below 10^{-7} s^{-1} or if it is decreasing again at very slow strain rates (which eventually would imply lower strain rate threshold > 0). No reliable experiments have been performed so far at these extremely slow strain rates. Similarly, in SRL tests in oxygenated HT water with pre-cracked specimen, the stress intensity factor at the point of crack initiation $K_{I,i}$ (and therefore susceptibility) increased with decreasing loading rate, with a possible minimum (maximum of susceptibility) at very low loading rates (Figure 39a).

(a)   **(b)**
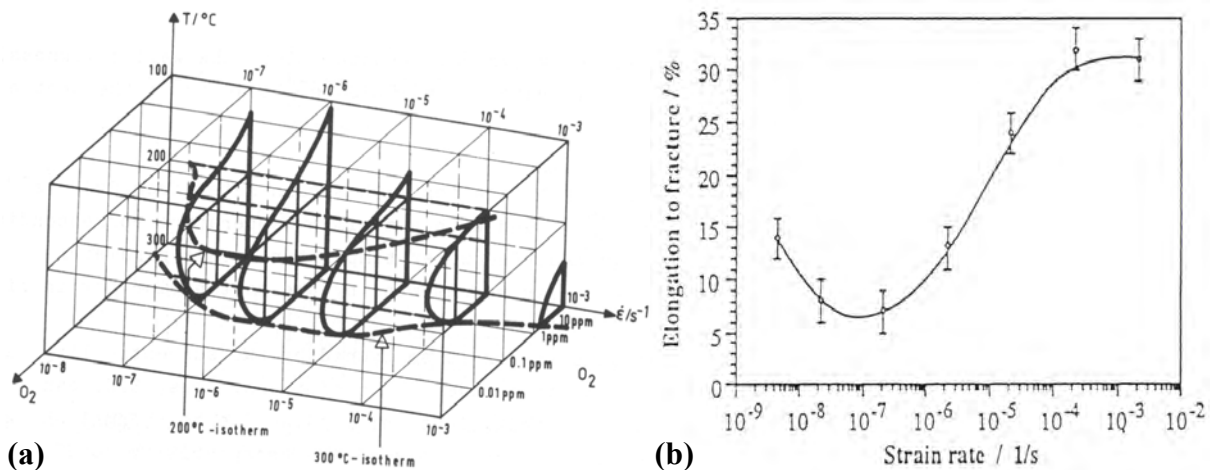
Figure 38: Effect of strain rate, temperature and DO content on SICC susceptibility of LAS [23] (a) and of strain rate [107] on SICC susceptibility in the RPV steel 22 NiMoCr 3 7 (0.016 wt.% S) in HT water at 288 °C with a DO content of 0.4 ppm (b).

When all other threshold conditions are satisfied, fatigue life in LCF tests decreases according to a power law relationship below 10^{-2} s^{-1} and the effect of environment on life saturates at 10^{-5} s^{-1} in most tests (Figure 81). In some other investigations in the DSA temperature range, fatigue life did not saturate and further decreased monotonically down to the lowest tested strain rate of 10^{-7} s^{-1}. Above 10^{-2} s^{-1} no environmental effects are observed and strain rate effects are consistent with those in air. [29 – 31]
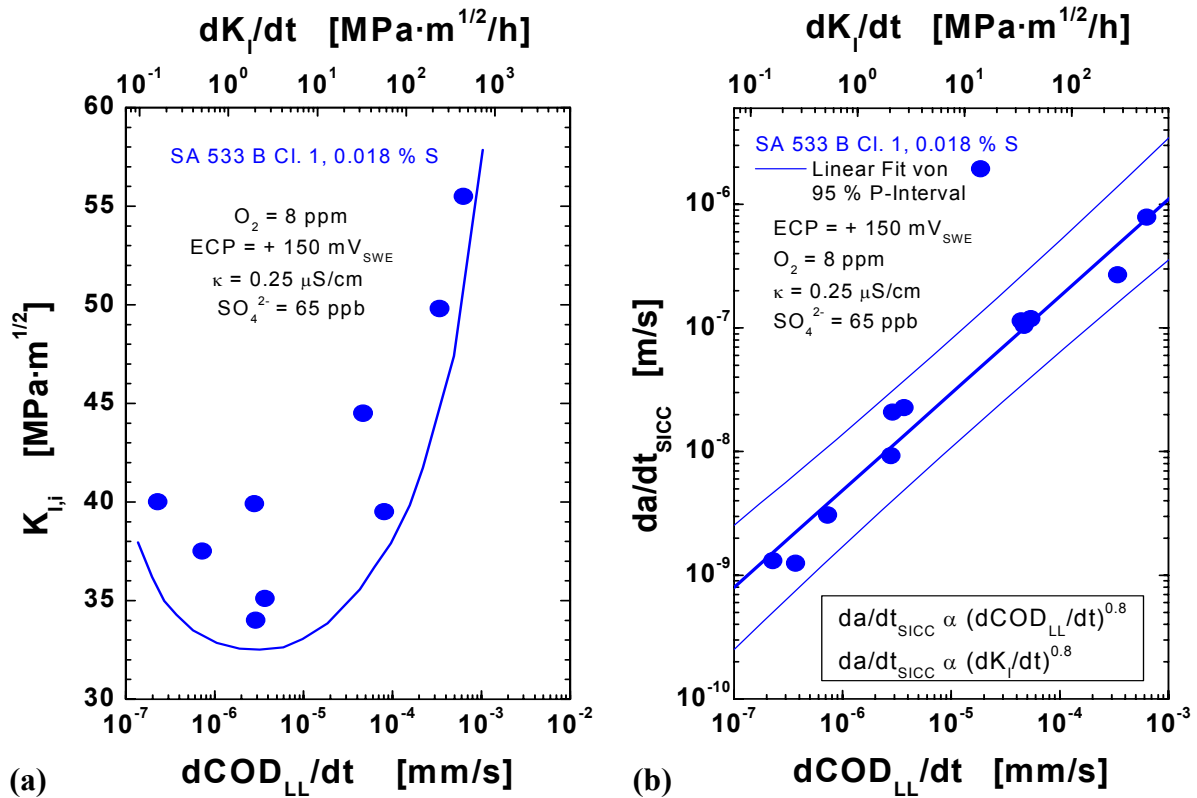
Figure 39: Effect of loading rate on SICC initiation (a) and growth (b) in SRL tests with a high-sulphur steel in oxygenated HT water [28].

Crack Growth: In contrast to EAC susceptibility, which increases with decreasing strain rate/loading rate, the EAC CGR increases with increasing crack-tip strain rate/loading rate.

In SRL tests in oxygenated HT water, where high-sulphur conditions prevailed, the SICC CGRs increased with increasing loading rate dK_I/dt according to a power law relationship with an exponent of 0.8 (Figure 39b), thus slightly slower than a linear increase. SICC was observed under these highly oxidizing conditions down to the lowest tested loading rate of 0.1 MPa·m$^{1/2}$/h, which is well below slowest plant transients [28]. At the present time it is not clear if a lower strain rate/loading rate threshold for SICC exists or not. At very high loading rates > 1000 MPa·m$^{1/2}$/h no SICC was observed up to the onset of pure mechanical ductile crack growth at K_{IJ}.

Very similarly, in cyclic load tests in oxygenated HT water, where high-sulphur conditions prevailed, the time-based CGR da/dt_{EAC} increased with increasing loading rate and approached the air fatigue CGRs at loading frequencies > 1 to 100 Hz depending on R and ΔK values. The CF crack advance per cycle $\Delta a/\Delta N_{EAC}$ increased with decreasing frequency (Figures 5, 11, 58, and 105), whereas the time-based CGR da/dt_{EAC} decreased with decreasing frequency (Figure 40). Sustained CF crack growth has been observed down to the lowest tested loading frequencies of $3 \cdot 10^{-6}$ Hz under highly oxidizing conditions. Depending on temperature and material a power law relationship ($\Delta a/\Delta N_{EAC} = A \cdot \nu^{-n}$) between crack advance per cycle $\Delta a/\Delta N_{EAC}$ and loading frequency ν is usually observed in the loading frequency range from 10^{-5} to 10^{-2} Hz with an exponent of 0.4 to 0.65 (typically 0.5 to 0.6). This exponent is generally only slightly smaller than the corresponding value of 0.65 of the GE-model for high-sulphur crack-tip environment conditions. Under conditions, where low-sulphur conditions prevailed, e.g., at low ECPs and low loading frequencies, the crack advance per cycle

45

$\Delta a/\Delta N_{EAC}$ was not dependent on loading frequency ν and only slightly higher (a factor of 2 to 5) than the corresponding air rates under identical loading conditions [28, 51, 62].
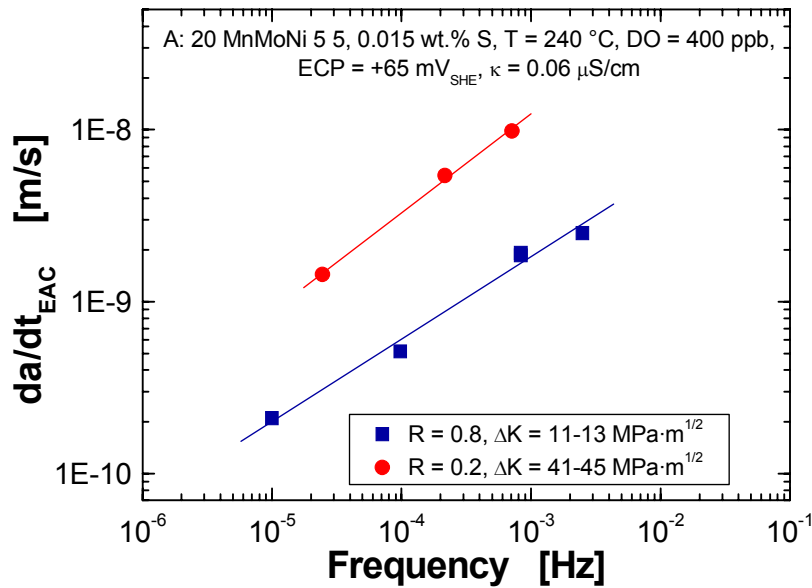
Figure 40: Effect of loading frequency on time-based CF CGRs.

4.3.2   *Strain, K_I and $\Delta K/R$ Level*

Crack Initiation: In static test with smooth tensile test specimens, crack initiation is only observed at stress levels above the high-temperature YS [39, 127]. Because of the limited data, it is not possible to derive critical strains for SCC initiation.

Slow straining in the purely elastic region in SSR tests does not lead to cracking in HT water. Microplasticity at microstructural inhomogeneities below the YS is not sufficient to induce crack initiation. The critical strains for crack initiation derived from SSR tests with smooth tensile test specimens were generally in the range of 1 to 5 % depending on applied strain rate, ECP (DO content), temperature, sulphur content of steel, and sulphate concentration of environment and surface state [9, 106, 107].

In LCF tests significant environmental effects on fatigue life have not been observed at strains below 0.1 – 0.3 % [29 – 31], showing that a certain extent of "macroscopic" yielding is a necessary pre-requisite for environmental effects. In the ASME III Code proposals, a strain threshold of 0.042 and 0.07 % is suggested for C & LAS.

The primary design stresses are normally limited to values below the HT YS (YS/S, S: safety factor). Therefore, in general plastic yielding in service is only observed in regions of increased (local) stress (e.g., at notches or welding defects) and/or for high secondary (thermal) stresses or superimposed residual stresses. Dynamic straining primarily arises during transient LWR operation conditions (thermal and pressurization cycles during start-up/shut-down, stand-by, thermal stratification/stripping). Strain localization by DSA may be helpful to overcome these strain limits. In case of static loading conditions, low-temperature creep in highly stressed regions (notches, welding defects, etc.) is the only source of strain rate before crack initiation occurs. After crack initiation, the crack growth itself is an important source of crack-tip strain rate.

Crack Growth: Effect of load level (K_I, ΔK, R) on EAC crack growth is discussed in Section 6. Loading aspects, which have not yet been investigated, but may have a relevant effect on flaw tolerance evaluations, cover overload (pressure test), load sequence effects and (oxide-, surface roughness- or plasticity-induced) crack closure effects (during unloading).

5 EAC Susceptibility Conditions

5.1 Susceptibility Conditions for SCC

Table 5 shows an early assessment scheme for SCC initiation (susceptibility) and crack growth for LAS under BWR/NWC conditions according to Hickling [71]. SCC initiation from smooth, defect-free surfaces under static load is generally only observed for stresses at the water-wetted surface above the HT YS, quasi-stagnant flow conditions, and increased concentration levels of anionic impurities such as SO_4^{2-} or Cl^-. If complete exhaustion of low-temperature creep was allowed to occur before the specimens were exposed to high-purity, HT water, no SCC was observed, thus indicating non-classical SCC behaviour and confirming the importance of dynamic straining for EAC of LAS in HT water [13].

Operating medium: HT water or steam condensate with T > 170 °C						
O_2 [ppm]	Flow conditions	κ [µS/cm]	Crack initiation by SCC?	Derivation	Crack growth by SCC?	Derivation
< 0.2	typical for reactor	typical i.e. ≤ 0.1	no susceptibility	1	no susceptibility	1
< 0.2	quasi-stagnant	approx. 0.2	no susceptibility	1	no susceptibility	2
< 0.2	quasi-stagnant	Raised (e.g. by impurities)	X(for stress levels at the water-wetted surface in the region of the HT yield point)	2	possibility cannot be excluded, perhaps after incubation time	3
0.2 – 0.4	typical for reactor	typical, i.e. approx. 0.2	no susceptibility	1	no susceptibility	1
0.2 – 0.4	quasi-stagnant	approx. 0.2	X(for stress levels at the water-wetted surface > HT yield point)	2	possibility cannot be excluded, perhaps after incubation time	2
0.2 – 0.4	quasi-stagnant	raised (e.g. by impurities)	X(for stress levels at the water-wetted surface in the region of the HT yield point)	2	possibility cannot be excluded, perhaps after incubation time	2
>> 0.4	typical for reactor	typical, i.e. approx. 0.2	in general, no susceptibility (? at stress levels >> HT yield point)	1 3	susceptibility is suppressed through flow	2
>> 0.4	quasi-stagnant	< 1 (approx. 0.2)	X(for stress levels at the water-wetted surface ≥ HT yield point)	2	possibility cannot be excluded, perhaps after incubation time	2
>> 0.4	quasi-stagnant	raised (e.g. by impurities)	X(for stress levels at the water-wetted in the region of the HT yield point)	2	possibility cannot be excluded, perhaps after incubation time	2

X possibility cannot be excluded, perhaps after long incubation time

Derivation: 1: from experiments in more aggressive environments, 2: from appropriate autoclave experiments, 3: no direct experimental evidence

Table 5: Assessment scheme for SCC susceptibility of C & LAS [71].

Based on experimental experience, SCC initiation during stationary, transient-free BWR/NWC power operation from defect-free surfaces appears to be extremely unlikely. Even for the unlikely case of SCC initiation, the SCC CGR would be very slow for stress intensity factors $K_I < 60$ MPa·m$^{1/2}$ (see Section 6.1).

5.2 Susceptibility Conditions for SICC and CF

SSR and LCF tests with smooth specimens have clearly shown that EAC may occur in LAS (YS of 300 to 600 MPa, sulphur content of $\leq$ 0.020 wt.% S) in oxygenated, high-purity HT water (κ < 0.3 μS/cm), if the following conditions are simultaneously attained over a sufficiently long period of time [13, 21 – 23, 29 – 31, 106, 107, 154]:

- **Corrosion potential ECP > ECP$_{crit}$ = -200 mV$_{SHE}$.** Depending on flow rate, material (sulphur content, susceptibility to DSA) and temperature, a DO content of 20 to 100 ppb is sufficient to exceed this threshold. The susceptibility generally increases with increasing ECP (or DO content).

- **Strain rate in a critical range: $0 < d\varepsilon/dt_{crit,min} \leq d\varepsilon/dt \leq d\varepsilon/dt_{crit,max} = 10^{-3}$ s^{-1}.** The susceptibility increases with decreasing strain rate dε/dt. In most LCF investigations, a saturation of fatigue life is observed below a strain rate of 10^{-5} s^{-1}. SSR tests indicate a maximum of susceptibility between 10^{-5} and 10^{-7} s^{-1}, depending on DO content and temperature, and a decrease of susceptibility at very slow strain rates $\leq 10^{-8}$ s^{-1} [23, 107].

- **(Local) macroscopic strain above the elastic limit: $\varepsilon \geq \varepsilon_{crit}$ = 0.1 % ($\sigma_{crit} > R_p$).** The susceptibility strongly increases with increasing strain.

- Temperature T > 150 °C. SSR tests indicate a maximum of susceptibility around 240 °C. LCF experiments showed almost a linear increase of susceptibility (decrease of fatigue life) between 150 and 300 °C. Unpublished SSR studies indicate that SICC may be observed down to at least 100 °C [22].

- Sulphur content > 0.003 wt.% S. Susceptibility increases with increasing sulphur content, but the experimental evidence for a sulphur threshold is weak. At combinations of suitable temperatures and sufficiently high ECP, SICC was observed even in extremely low-sulphur steels (0.001 wt.% S) [22]. Furthermore, a distinct susceptibility to DSA or a low YS may favour crack initiation by SICC [13].

If one of these conjoint threshold conditions is not satisfied, SICC initiation is extremely unlikely and no or only minor environmental reduction of fatigue life is observed in HT water. In high-purity water, a high flow rate may completely suppress SICC susceptibility and significantly retard fatigue crack initiation (in particular for small/slow strain/strain rates) compared to quasi-stagnant conditions, since the risk for formation of aggressive occluded water chemistry in small surface defects (which would promote EAC) is significantly reduced by convection.

The range of system conditions where EAC crack growth from incipient cracks may occur is significantly extended compared to the initiation susceptibility conditions specified above. E.g., CF crack growth has been observed in high-purity PWR water at ECPs below -500 mV$_{SHE}$ under certain cyclic loading conditions (10^{-2} to 10 Hz) [5, 8, 11 – 13] and also at temperatures well below 100 °C [20, 155].

6 EAC Crack Growth

EAC crack growth in C & LAS is basically governed by the <u>crack-tip strain rate</u> and the activity of <u>sulphur anions</u> in the <u>crack-tip environment</u> (see Section 10.4) [13, 16, 66, 156]. The onset and extent of EAC is crucially dependent on <u>simultaneously</u> maintaining a slow, positive crack-tip strain rate and a critical sulphur anion activity in the crack-tip environment. If these two conjoint requirements are not met, no SCC and SICC, or only minor environmental acceleration of fatigue crack growth are generally observed. In the following three Sections the effect of loading conditions on EAC crack growth under static or near static (periodical partial unloading (PPU) or ripple loading), slow rising and cyclic loading conditions is summarized. Additionally, data quality and screening aspects are briefly discussed in the context of SCC under static loading conditions.

6.1 SCC Crack Growth

6.1.1 SCC Crack Growth under Static Loading Conditions

The stress intensity factor threshold K_{ISCC} for SCC, below which SCC CGRs are technically insignificant, depends on strain rate (initial loading procedure) and on other system parameters such as ECP, temperature, sulphur content of steel, sulphate/chloride concentration of environment, etc. For nominal static loading conditions apparent K_{ISCC} values ranging from 20 to 60 $MPa \cdot m^{1/2}$ [1, 32 – 35, 157, 159] have been reported in oxygenated HT water (simulated BWR conditions). In PSI tests in oxygenated HT water with 15 ppb of chloride at 250 °C sustained, fast SCC was observed down to K_I values of 20 $MPa \cdot m^{1/2}$ [128]. Lower thresholds down to 12 $MPa \cdot m^{1/2}$ were observed in surface-cracked specimens with significant plastic yielding [158], making K_I calculations invalid. The very limited number of tests with K_I values < 20 $MPa \cdot m^{1/2}$ (mainly static autoclave tests under aggressive environmental conditions) has not revealed any SCC [1, 32, 37]. Although, the existence of such a true K_{ISCC} threshold is very questionable, for practical reasons there is some interest to define such a limit for flaw tolerance evaluations. Combined slow rising-constant load or low-frequency fatigue-constant load experiments (Figure 41) in high-purity or sulphate-containing oxygenated HT water, where the constant load phase started with an actively growing TG EAC crack ($3 \cdot 10^{-10}$ to $3 \cdot 10^{-7}$ m/s), indicated that SCC cannot be sustained below 20 to 30 $MPa \cdot m^{1/2}$ and almost instantaneous crack arrest occurs [34 – 36, 128].

The effect of K_I on SCC crack growth in chloride-free oxygenated HT water under well-controlled conditions is summarized in Figure 42 and Table 6. Between 30 and 60 $MPa \cdot m^{1/2}$ the SCC crack growth in C & LAS in the temperature range from 274 to 288 °C either slowed down to CGRs of less than 0.6 mm/year or arrested within a few hundred hours under constant load [34 – 36, 128]. The SCC crack growth under these conditions (if it occurred at all) was usually very localized (some few isolated locations with very limited crack growth, often around MnS-inclusions which were intersected by the crack front) and could usually only be detected by post-test fractography with some few exceptions. Because of the extremely low susceptibility to SCC crack growth under these conditions, no effect of K_I on SCC CGRs could be resolved below 60 $MPa \cdot m^{1/2}$. Sustained (with respect to operational time scales) SCC crack growth has only been observed above 60 $MPa \cdot m^{1/2}$ [17, 33 – 36]. Above 60 $MPa \cdot m^{1/2}$ the SCC CGRs tended to increase with increasing K_I values, although in many cases they were still decaying with time following roughly a reciprocal time law (logarithmic law for crack growth, Figure 43) [35, 128]. Stationary SCC crack growth was only observed at extremely high loading conditions ($K_I \geq 80$ $MPa \cdot m^{1/2}$) if the K_I or the load approached either the K_{IJ} value of the material or the plastic limit load or for severe violation of SSY conditions [34 – 36, 128].
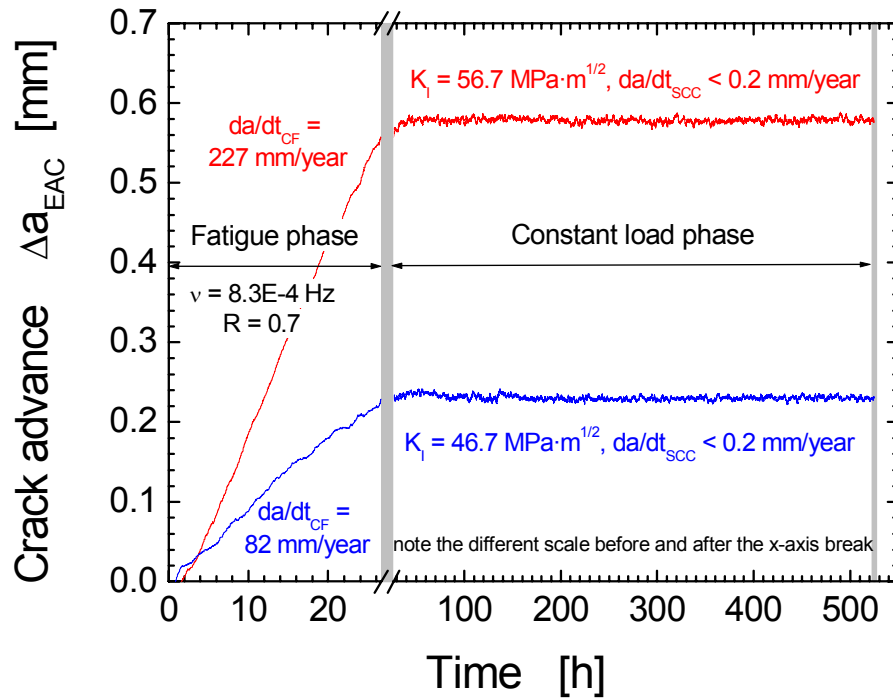
Figure 41: Example of combined LFCF-constant load tests in oxygenated high-purity HT water, which confirms cessation of SCC briefly after switching to constant load [36, 76].
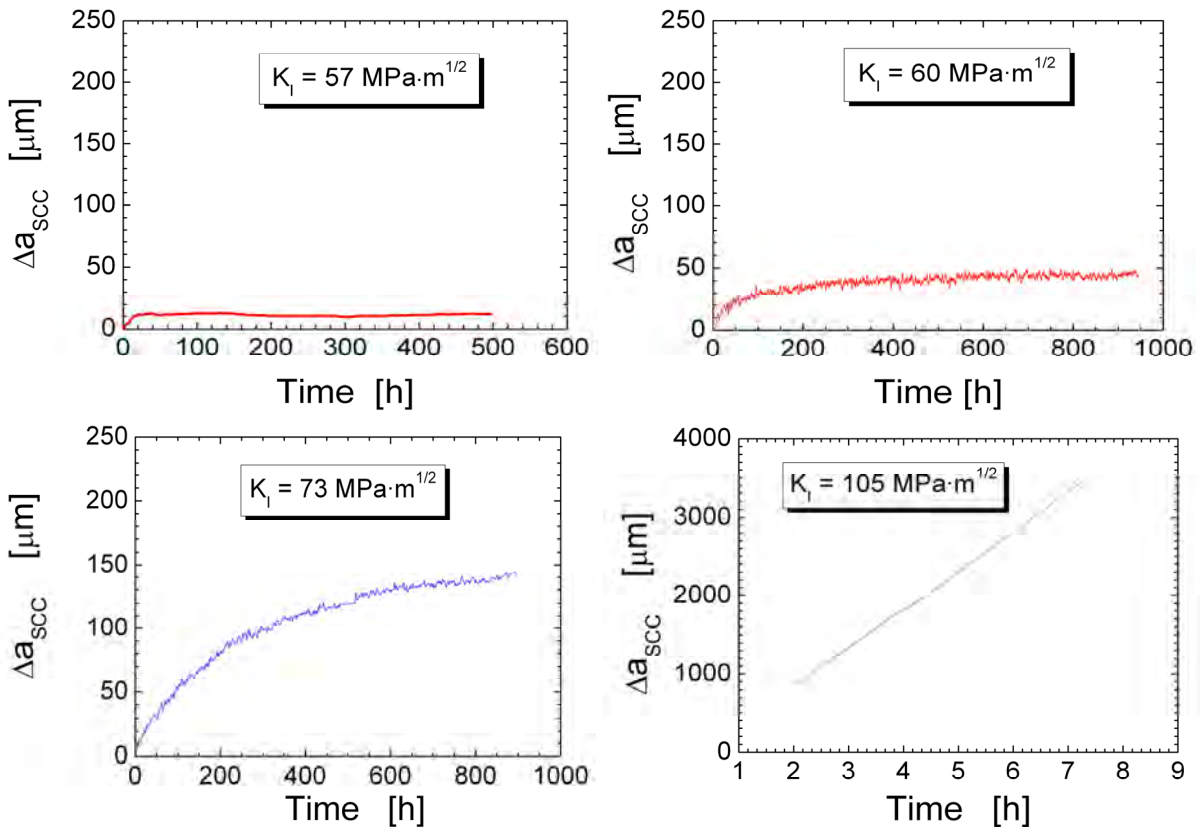
Figure 42: Examples of SCC crack growth in high-sulphur RPV steel (0.018 wt.% S) at 288 °C and different K_I levels under aggressive environmental conditions (8 ppm DO, 65 ppb SO_4^{2-}) after switching from LFCF to constant load [34 – 36, 128].

K_I [MPa·m$^{1/2}$]	Region	SCC crack growth under constant load	SCC		
			$\Delta a_{SCC}/\Delta t_{CL}$ Δt_{CL} = 1000 h [m/s]	da/dt$_{DCPD}$(t) t = 1000 h [m/s]	
< 30	SSY	No crack growth	< 10^{-11} *	< 10^{-11} *	
30 – 60	≈ SSY	Strictly limited in time ≈10^1 h – ≈10^2 h	< 2·10^{-11}	< 10^{-11} *	
60 – 80	Transition region	Limited in time ≈10^2 h – ≈10^3 h	< 10^{-10}	< 3·10^{-11}	
≥ 80 $K_I \rightarrow K_{IJ}$**	Ligament yielding	Yes, sustained, stationary in some cases	> 3·10^{-10} < 3·10^{-7}	> 3·10^{-10} < 3·10^{-7}	

*) ≤ detection limit, **) $K_{IJ} = (J_I \cdot E/(1-\nu^2))^{1/2}$

Sulphur [wt.%]	SICC or CF da/dt (t = 0) [m/s]	T [°C]	κ [µS/cm]	Cl$^-$ [ppb]	SO$_4^{2-}$ [ppb]	ECP [mV$_{SHE}$]	DO [ppm]
0.004 – 0.018	3·10^{-10} – 3·10^{-7}	288	0.06 – 0.25	< 5	1 – 65	-50 – +200	0.2 – 8

Table 6: Summary of PSI constant load SCC results in chloride-free oxygenated HT water at 274 to 288 °C [35, 36, 128].
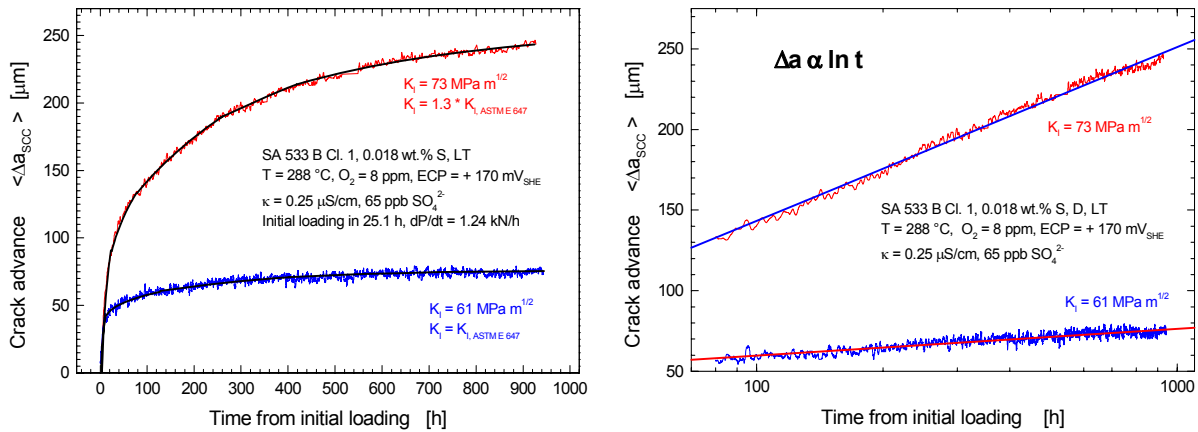
Figure 43: Decay of SCC crack growth according to logarithmic time law, which indicates that SCC and crack-tip strain rate are controlled by low-temperature creep under these specific conditions [35].

Although, there were not enough testing data at high K_I values without severe violation of SSY conditions, it is expected that the transition from low to high SCC CGRs is shifted to lower K_I values with increasing steel sulphur content, ECP, DSA susceptibility, YS level, etc. [35].

As long as K_I and the Vickers hardness/steel sulphur content were limited to values ≤ 60 MPa·m$^{1/2}$ and < 350 HV5/0.02 wt.% S, all materials (base metal, weld metal and HAZ) revealed a very similar SCC crack growth behaviour at 274 to 288 °C with CGRs well below the BWRVIP-60 SCC DL 1 (Figure 44 and Section 9.1) [36, 128]. The PSI data thus support the adequacy and conservative character of the interim disposition lines for the RPV during stationary power operation [36, 128]. The conservative character at 288 °C was further con-firmed by European Round Robin tests [76, 160, 161]. Under reducing PWR or BWR/HWC conditions (Figure 79) no SCC crack growth was observed up to very high K_I values of al-most 100 MPa·m$^{1/2}$ or up to K_{IJ} [9, 162].
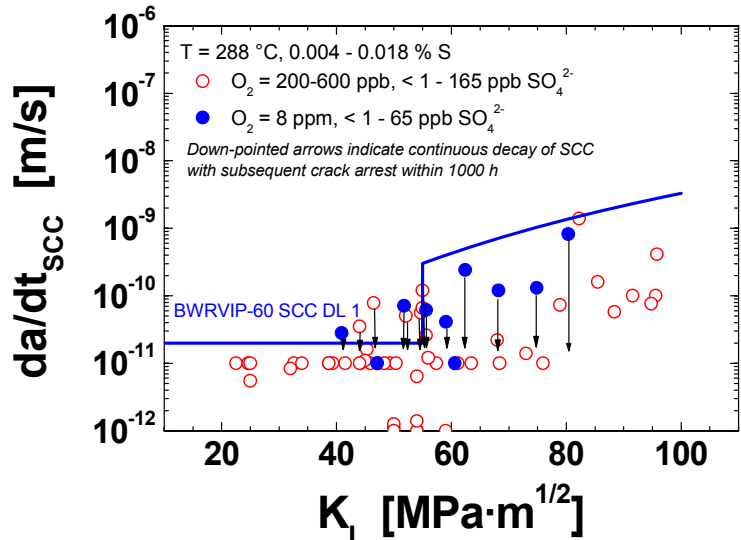
Figure 44: Confirmation of the conservative character of the BWRVIP-60 SCC DL 1 for stationary, transient-free BWR power operation by combined SRL/low-frequency fatigue-constant load tests in chloride-free, oxygenated HT water at 288 °C at PSI [35, 36, 128].

Stationary SCC in chloride-free, oxygenated HT water at K_I levels < 70 MPa·m$^{1/2}$ with CGRs above the BWRVIP-60 SCC DL 1 was observed at intermediate temperatures (180 – 270 °C) in RPV materials which show a distinct susceptibility to DSA [36, 128, 139, 163] and at 288 °C in case of excessive hardness (> 350 HV5) (e.g., in bad weld HAZs) [36, 130], in particular in combination with a high steel sulphur content (Figure 45). As discussed in Section 4.1.3, small amounts of chloride in the range of 5 to 10 ppb under highly oxidizing BWR/NWC conditions may also result in accelerated SCC close to the high-sulphur SCC line of the GE-model [16] down to very low K_I levels of 20 MPa·m$^{1/2}$ (Figure 16b on p. 23 in Section 4.1.3) [36, 67 – 69, 128]. The tests with chloride indicated only a very moderate increase of SCC CGRs with K_I between 20 and 60 MPa·m$^{1/2}$.
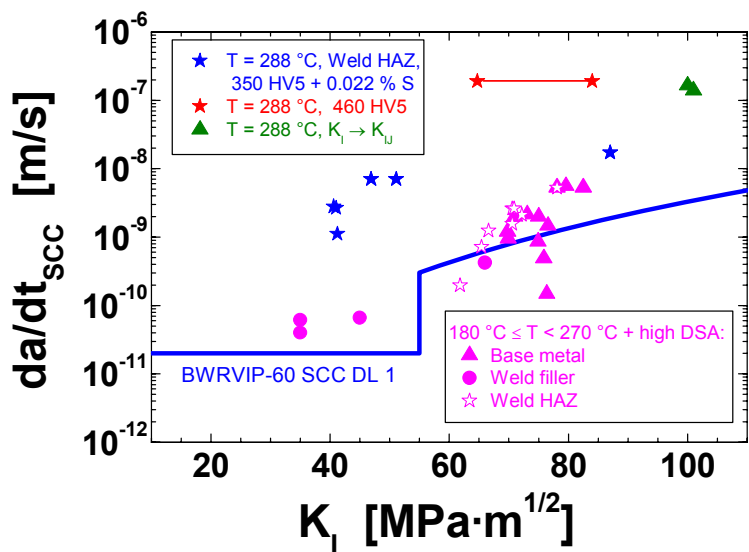
Figure 45: Test results with stationary SCC CGRs above the BWRVIP-60 SCC DL 1 in chloride-free, oxygenated HT water. The BWRVIP-60 SCC DL 1 may be exceeded in case of intermediate temperatures and a high DSA susceptibility [36, 139, 163] of the steel or in case of excessive hardness ≥ 350 HV5 in the weld HAZ region [36, 130].

53

6.1.2 SCC Crack Growth under Periodical Partial Unloading Conditions

The SCC crack growth behaviour under PPU conditions was investigated in oxygenated, high-purity HT water with a DO content of 0.4 or 8 ppm at temperatures of 288 or 250/240 °C with different RPV steels and weld HAZ materials [36, 76, 128]. Additional tests were performed with HT water containing 65 to 365 ppb sulphate and 5 to 50 ppb chloride. PPU at high and low load ratios of 0.8, 0.7, and 0.2 was applied. The hold time at constant maximum load Δt_H was varied from 0 to 10^5 s at fixed rise times Δt_R of 100 to 4000 s. The $K_{I,max}$ values were varied from 30 to 70 MPa·m$^{1/2}$.

For $K_{I,max}$ values ≤ 60 MPa·m$^{1/2}$ and chloride contents < 5 ppb, the time-based CGR da/dt$_{EAC}$ always decreased with increasing hold time Δt_H for all material and loading conditions (Figure 46a). Above a hold time of 1 to 20 h (depending on $K_{I,max}$ values, rise times Δt_R, temperatures, ECP, etc.) the EAC CGRs generally dropped below the current BWRVIP-60 SCC DLs 1 and 2 (Figure 46b), thus further confirming their conservative character. At hold times ≥ 5 to 20 h the time-based EAC CGR generally dropped below the detection limit of the DCPD of $6 \cdot 10^{-12}$ m/s indicating crack arrest for long hold times. This behaviour is fundamentally different from that in stainless steels and nickel alloys, where time-based CGRs in PPU tests are approaching the pure constant load SCC CGRs for long hold times under those environmental and loading conditions. [36, 76, 128]
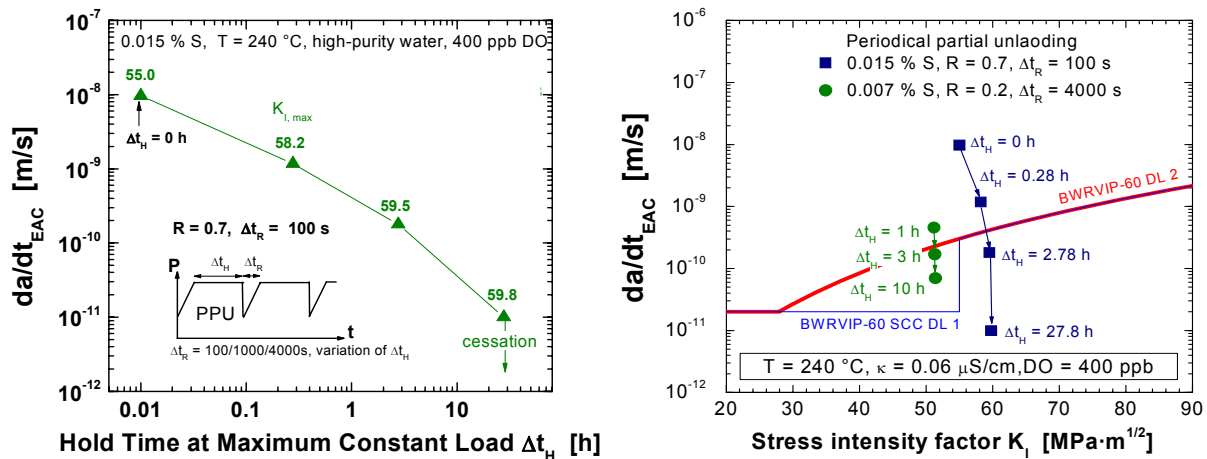
Figure 46: Effect of hold time on time-based EAC CGRs in PPU tests and comparison with the BWRVIP-60 SCC DLs [36, 76, 128].

For $K_{I,max}$ values ≤ 60 MPa·m$^{1/2}$ and chloride contents < 5 ppb, the crack advance per cycle $\Delta a/\Delta N_{EAC}$ did not depend on the hold time for a fixed rise time (Figure 47b) and was identical to that under cyclic saw tooth loading conditions with the same rise time. This behaviour could be related to the absence of any relevant SCC crack growth at constant load under these conditions. As shown in Figure 47a, EAC crack growth only occurred during the rising load phase without any SCC during the subsequent constant load phase of the PPU cycle [67, 68, 76, 128]. An increase of $\Delta a/\Delta N_{EAC}$ with hold time Δt_H was only observed under some very specific system conditions, where sustained SCC was usually observed at constant load tests in LAS [128], e.g., for chloride contents ≥ 5 ppb, high $K_{I,max}$ values > 60 to 70 MPa·m$^{1/2}$, high hardness ≥ 350 HV5 or at intermediate temperatures in materials with a high DSA susceptibility. On the other hand, in some cases, in particular at low $K_{I,max}$ values and low load ratios, a decrease of $\Delta a/\Delta N_{EAC}$ with increasing hold time Δt_H and cessation of EAC has been observed for long hold times $\geq 3.6 \cdot 10^4$ s, which was probably caused by oxide- or surface roughness-induced crack closure [128]. The PPU tests therefore confirmed the observed EAC cracking behaviour in combined rising load/LF fatigue-constant load tests (see Section 6.1.1).
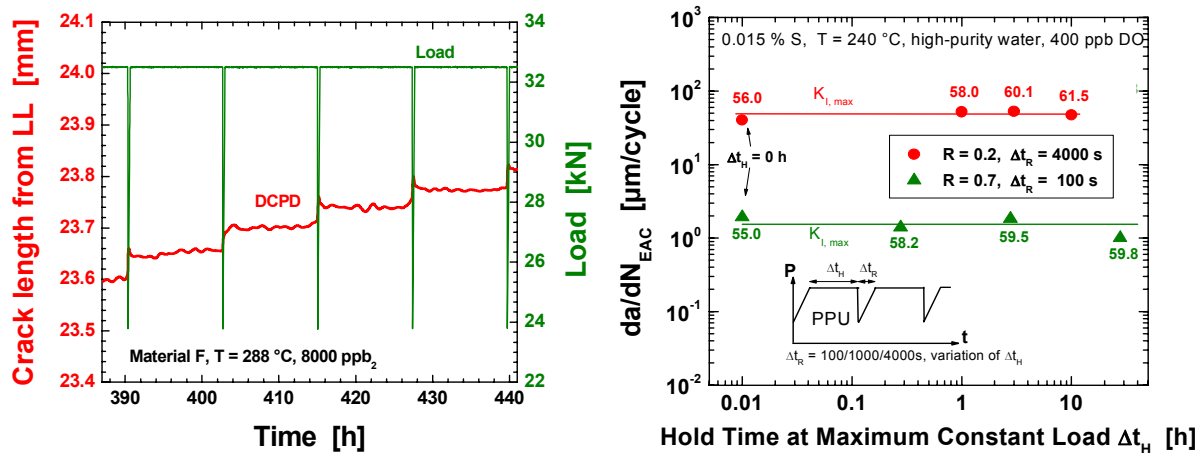
Figure 47: EAC crack growth during PPU and effect of hold time Δt_H on the crack advance per PPU cycle. Both plots clearly show that the crack is only growing during the rising load phase by SICC without any significant SCC contribution during the constant load phases of the PPU cycles [67, 76, 128].

6.1.3   *SCC Crack Growth under Ripple Loading Conditions*

The effect of small, low-frequency load fluctuations at very high load ratios (R ≥ 0.95) near to the fatigue threshold ΔK_{th} of 1 to 2 MPa·m$^{1/2}$ (ripple loading) was investigated using different RPV steels with low and high sulphur content and a weld HAZ material. The tests were conducted in high-purity (< 1 ppb SO_4^{2-}, κ ≤ 0.06 μS/cm), HT water at 288, 274 and 250 °C with a DO content of 8 (+150 to +200 mV$_{SHE}$) and 0.4 ppm (+50 mV$_{SHE}$). The load fluctuations corresponded to a load ratio of 0.947 to 0.97 and a stress intensity factor amplitude ΔK of 3.3 to 1.5 MPa·m$^{1/2}$. Constant load amplitude with load control and an asymmetrical saw tooth waveform were applied. The loading frequency was stepwise decreased from $5 \cdot 10^{-2}$ to 10^{-5} Hz.

In Figure 48 the CGR of the ripple load tests [36, 128] are compared to the BWRVIP-60 SCC DL 2. In all materials sustained, stationary EAC crack growth was observed in HT water with a DO content of 8 and 0.4 ppm in the loading frequency range form 10^{-2} to 10^{-4} Hz. The SCC CGRs thereby reached values from 30 up to 160 mm/year at stress intensity factors between 30 and 76 MPa·m$^{1/2}$. In some experimental phases the CGRs temporarily slowed down to very small CGR in the range of 0.1 to 1 mm/year, but fast crack growth re-initiated again after a large number of fatigue cycles. The temporary slow down or retardation of CGR might be a result of crack closure effects. At lower loading frequencies around 10^{-5} Hz, cessation of the SCC crack growth and subsequent crack arrest was observed (Figure 49). Investigations of Argonne National Laboratories (ANL) [164] revealed a very similar SCC behaviour under ripple loading conditions with CGRs of up to 250 mm/year in the stress intensity factor range of 30 to 70 MPa·m$^{1/2}$. Furthermore, in several tests the crack growth consisted of long periods with low CGRs followed by shorter periods with transient, high CGRs.

At ΔK values ≥ 2 MPa·m$^{1/2}$ the ripple loading in the frequency range of 10^{-2} to 10^{-4} Hz resulted in an acceleration of SCC crack growth by a factor of up to 150 compared to pure static loading conditions at identical K_I levels and environmental conditions (see Figure 48). The fracture surface revealed a relatively rough, TG cleavage-like appearance without any indications of striations, which is typical for SCC or SICC in LAS. In contrast to that, the ripple loading in an inert environment results in very smooth hair-line cracks. The maximum EAC CGRs under ripple loading conditions were similar for a DO of 0.4 and 8 ppm and for the different materials, and did not significantly depend on the stress intensity factor in the range of

30 to 76 MPa·m$^{1/2}$. The high-sulphur RPV steel revealed fast EAC over a wider parameter range than the low-sulphur alloys and the SCC CGRs were generally slightly higher. Even for small stress intensity factors of 30 MPa·m$^{1/2}$ and a DO content of 0.4 ppm, the maximum EAC CGR significantly exceeded the BWRVIP-60 SCC DL 2. If the ΔK value was reduced to values $\leq 1.5 - 2$ MPa·m$^{1/2}$, the EAC CGRs dropped below the BWRVIP-60 SCC DL 1 and subsequent crack arrest was observed in many cases. This result indicated an apparent EAC threshold ΔK_{EAC} of $1.5 - 2$ MPa·m$^{1/2}$ for corrosion fatigue in HT water (see also Figure 55 in Section 6.3.1). This threshold could eventually be further reduced by higher loading frequencies in the range of 0.1 to 100 Hz.
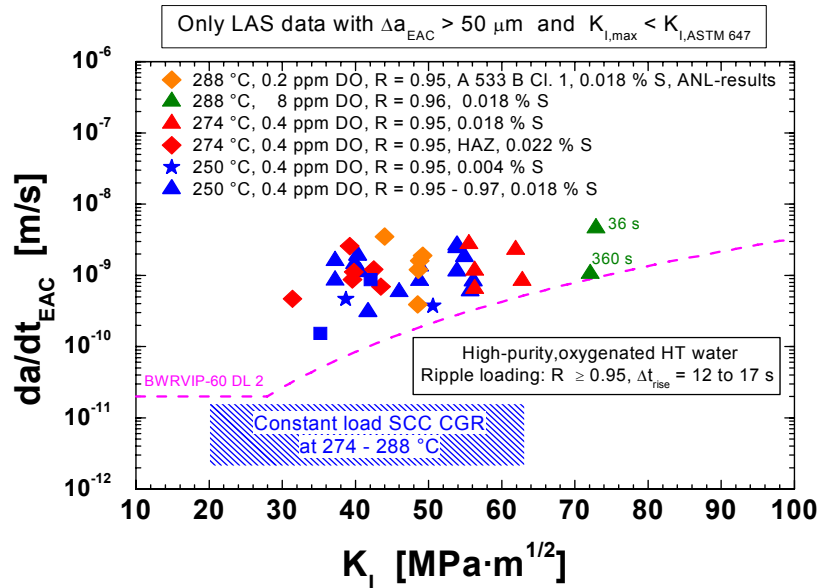
Figure 48: Comparison of time-based EAC CGRs in oxygenated, high-purity HT water in different RPV steels under ripple loading conditions (R ≥ 0.95) with BWRVIP-60 SCC DL 2 for load and water chemistry transients [36, 128].
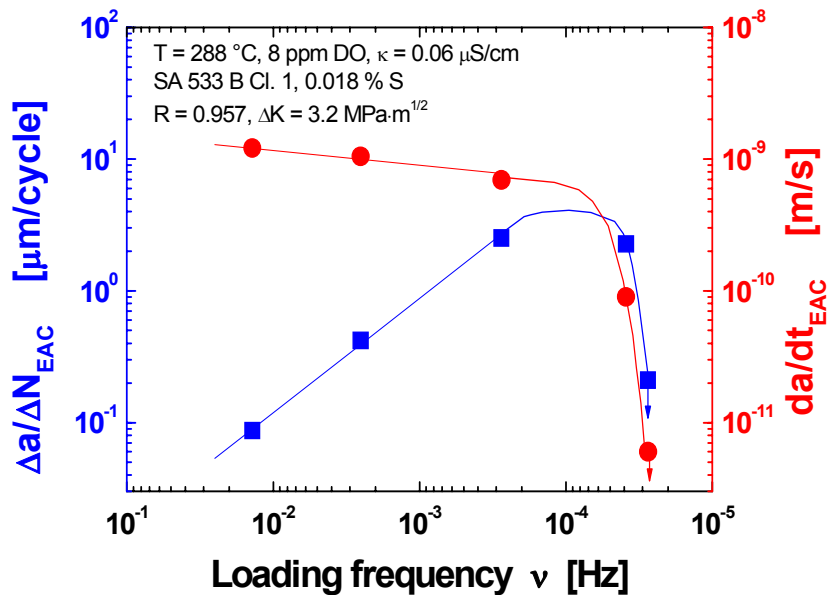
Figure 49: Effect of loading frequency on time-based and cycle-based EAC CGRs in a high-sulphur RPV steel in oxygenated, high-purity HT water under ripple loading conditions at R = 0.957. Cessation of EAC is observed below a loading frequency of 10^{-4} Hz [128, 165].

Detailed analysis of the ripple load experiments have clearly shown that EAC under these loading conditions may be regarded as normal corrosion fatigue at small ΔK and high load ratio R without any significant SCC contribution (Figure 50). Possible SCC contribution in chloride-free HT water cannot be excluded at high K_I values > 60 MPa·m$^{1/2}$, intermediate temperatures and materials with a high DSA susceptibility or in case of excessive hardness in weld HAZs.
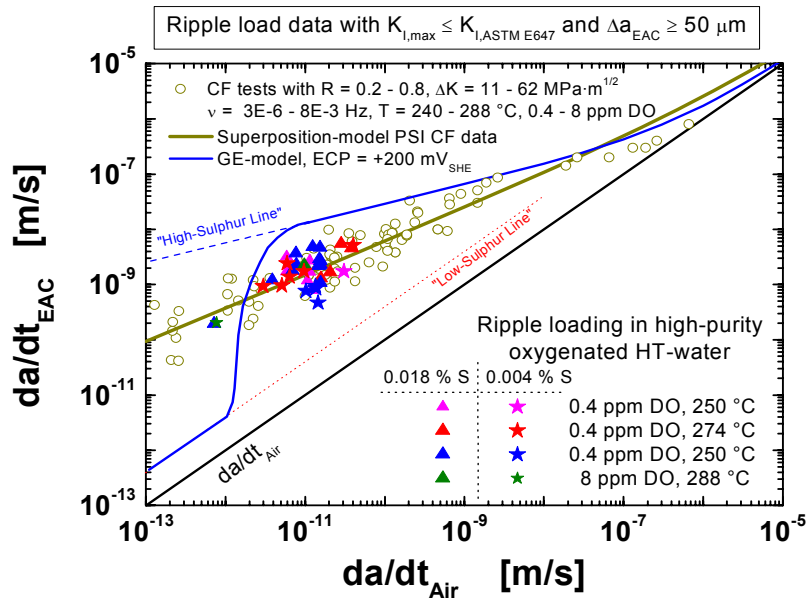
Figure 50: Comparison of time-based ripple load EAC CGRs with results of LFCF tests at lower R values of 0.2 to 0.8. The time-domain analysis confirms that EAC under ripple loading conditions can be rationalized as normal CF [165].

6.1.4 Data Quality Aspects and Screening

Figure 51 shows a compilation of literature SCC CGR data of C & LAS under simulated BWR conditions in oxygenated HT water. The tremendous scatter of 3 to 5 orders of magnitude with CGRs ranging from 30 μm/year to 3 m/year under nominally similar testing conditions (Figure 51) [35] makes rational life prediction impossible. The SCC behaviour of C & LAS in oxygenated HT water and its relevance to BWR power operation, in particular its possible effect on both RPV structural integrity and safety, has therefore been a subject of controversial discussions for many years.

There is no simple physical/metallurgical reason why the inherent scatter of SCC CGRs (arising, e.g., from material heterogeneity and variability) under constant, reproducible test conditions should be larger than one order of magnitude. A larger scatter can be expected close to EAC thresholds (e.g., in transition region from high- to low-sulphur EAC CGRs)

Attempts have been made to reduce this tremendous scatter by data reduction methods, taking into account the different quality and method of performance of the experiments [167]. It was shown that, in older investigations, system parameters having a strong influence on crack growth were neither sufficiently controlled and monitored, nor documented. Thus, the transferability and relevance of many of these data to pressure-boundary components and to BWR power operation cannot be satisfactorily evaluated. Only a few, well characterized and reproducible experiments, which fulfil current quality requirements on testing [168, 169], have been identified in the literature (Figure 52). This evaluation therefore clearly revealed a lack of reliable and hard SCC CGR data, in particular under plant relevant conditions, which can be used for the definition of SCC disposition lines and flaw tolerance evaluations.
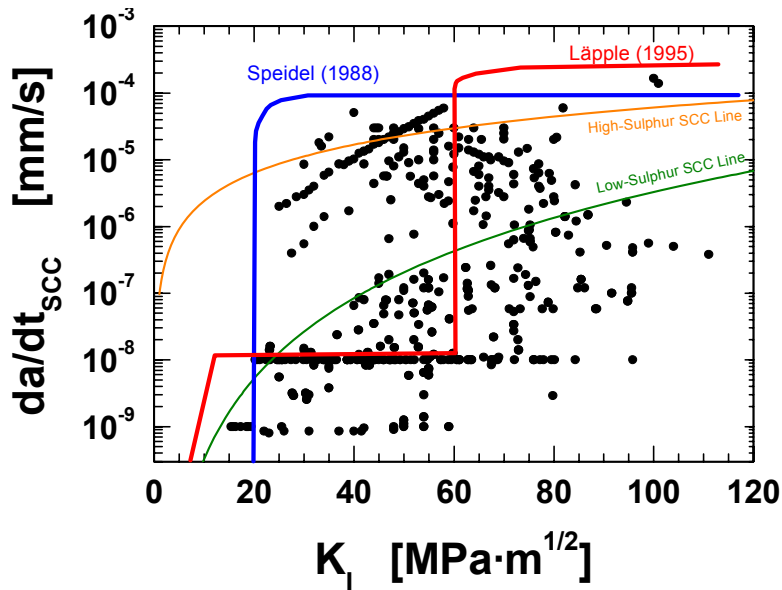
Figure 51: Compilation of literature data on apparent SCC CGRs of low-alloy, pressure-boundary component steels in oxygenated, HT water at 288/240 °C ("simulated BWR conditions") [35]. Additionally an upper bounding line according to Speidel [1] and an envelope of results from MPA Stuttgart [166] are plotted.
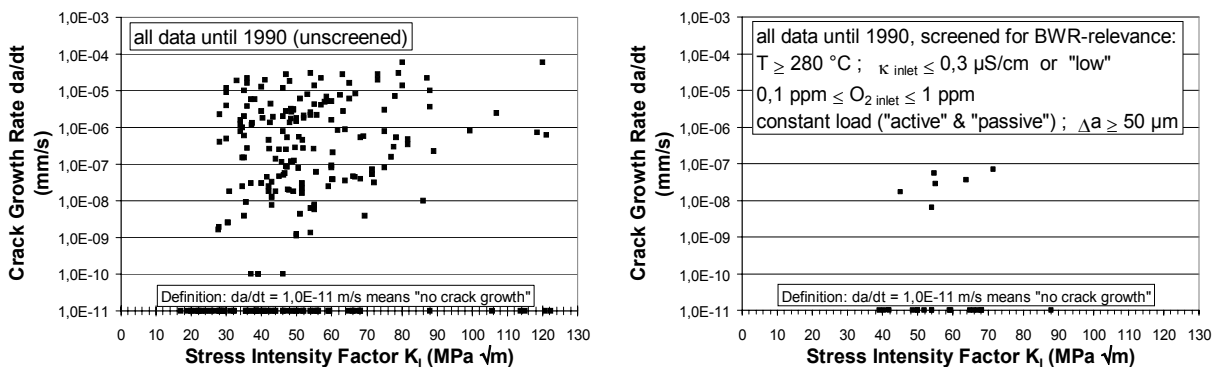
Figure 52: Data reduction with different testing quality criteria revealing a significant lack of reliable data under plant relevant conditions [167].

As discussed in Sections 6.1.1 and 9.1, the recently performed, well-qualified experiments at MPA Stuttgart [33], at PSI [34 – 36] and in the context of European Round Robin tests [76, 160, 161], as well as reactor site testing by ABB [2, 4] and GE [170], have shown very low susceptibility to SCC crack growth under static loading conditions in oxygenated high-purity HT water/BWR environments at temperatures around 288 °C up to high K_I values of 50 to 60 MPa·m$^{1/2}$.

The re-analysis of the available old SCC data by PSI revealed a plenty and wide field of different factors and reasons for the apparent scatter of these data base, which are discussed in [13]. A lot of scatter can be attributed at least in part to the term SCC which can be understood either in a narrow sense (EAC under purely static mechanical loading) or as part of the broader spectrum of EAC (including the transition to SICC and LFCF). In fact many of the high SCC CGR data were performed under non-static loading conditions (e.g., under frequent PPU conditions for crack length measurements by compliance method, SRL tests), which can result in very high EAC CGRs as shown, e.g., in Sections 6.1 and 6.2, but which are not related to SCC growth under constant load. PSI has demonstrated how CGR measurements by post-test fractography without DCPD can result in tremendous errors in some situations [35].

In those cases were sufficient background information on testing characteristics was available ("assessable data"), the low-sulphur SCC line of the GE-model [16, 171] either conservatively bounded all of these data points under nominal BWR conditions or plausible reasons for the deviations from this behaviour based on the accumulated well accepted experimental/mechanistic EAC background knowledge for the system LAS/HT water could be given. If testing conditions and procedures were carefully taken into account, the observed data and parameter trends fit excellently to EAC cracking behaviour described in this report. The high SCC CGR data under pure static loading conditions were either related to tests with severe violation of SSY conditions, aggressive environmental conditions (e.g., tests in static autoclaves with inadequate water chemistry control and therefore increased levels of chloride and sulphate) or extreme material conditions (e.g., excessive hardness) which cannot be transferred to thick-walled and properly manufactured primary LAS primary pressure-boundary components or appear atypical for current stationary BWR power operation practice.

6.2 SICC Crack Growth under Slow Rising Loading Conditions

In slow rising displacement/load or J-R-tests at different displacement/loading rates, the lowest K_I values where SICC initiation and cracking has been observed in oxygenated HT water were in the range from 23 to 40 MPa·m$^{1/2}$ [20, 28, 35, 157, 172 – 174] depending on the steel sulphur content and the environmental conditions. This threshold decreases with decreasing load/strain rate [28], but it is not yet clear if the threshold saturates or increases again at very slow loading rates (see Figure 39a on p. 44 in Section 4.3.1). At low ECPs (PWR, BWR/HWC) it was not possible to initiate or sustain SICC growth in SRL tests [28, 35].

In SRL tests at PSI under highly oxidizing BWR/NWC conditions (ECP $\geq$ +50 mV$_{SHE}$, DO $\geq$ 0.4 ppm) above the K_I value of 25 MPa·m$^{1/2}$ the SICC CGRs in the loading rate range of 0.05 to 500 MPa·m$^{1/2}$/h increased with increasing loading rate dK_I/dt according to a power law relationship with an exponent of 0.8 (see Figure 39b on p. 44 in Section 4.3.1), but as a first approximate the rates were not dependent on the actual K_I values of 60 MPa·m$^{1/2}$. High SICC growth rates between 10^{-9} and $8 \cdot 10^{-7}$ m/s were observed under SRL and highly oxidizing BWR/NWC conditions. Under these conditions maximum SICC CGRs can be described as follows:

$$\mathbf{da/dt_{SICC} = 6 \cdot 10^{-9} \cdot (dK_I/dt)^{0.8} \neq f(K_I)} \qquad \text{in m/s and MPa·m}^{1/2}\text{/h} \qquad (1)$$

$$\text{for } 25 \text{ MPa·m}^{1/2} \leq K_I \leq 60 \text{ MPa·m}^{1/2}, \ 0.05 \text{ MPa·m}^{1/2}\text{/h} \leq dK_I/dt \leq 500 \text{ MPa·m}^{1/2}\text{/h}$$

$$\text{and}$$

$$\text{ECP} \geq + 50 \text{mV}_{SHE}, \ 250 \text{ °C} \leq T \leq 288 \text{ °C}$$

6.3 CF Crack Growth under Cyclic Loading Conditions

In the following two Sections, CF crack growth is discussed in the cycle-based and time-based form. The cycle-based analysis (Section 6.3.1) is the common way in fatigue Codes and flaw tolerance evaluations. In the cycle-based form, a complex relationship is observed between $\Delta a/\Delta N_{EAC}$ and loading parameters such as ΔK, load ratio R and loading frequency ν. Each load ratio R/frequency ν combination results here in a different $\Delta a/\Delta N_{EAC}$ vs. ΔK curve for one given ECP/steel sulphur combination. The time-based analysis (6.3.2), on the other hand, is much simpler and therefore more convenient for analysis of corrosion fatigue.

The following discussion is focused to effect of loading parameters in the temperature range of 240 to 288 °C under BWR conditions at different ECPs. Material and environmental effects on CF crack growth have been discussed in Section 4 for specific cases.

6.3.1 Corrosion Fatigue Crack Growth in the Cycle-Based Form

For the sake of comprehensibility and clarity, the complex relationship between $\Delta a/\Delta N_{EAC}$ and ΔK including the effect of loading frequency and ECP, as predicted by the GE-model [16, 66, 114], is first discussed and shown in Figures 53 and 54.
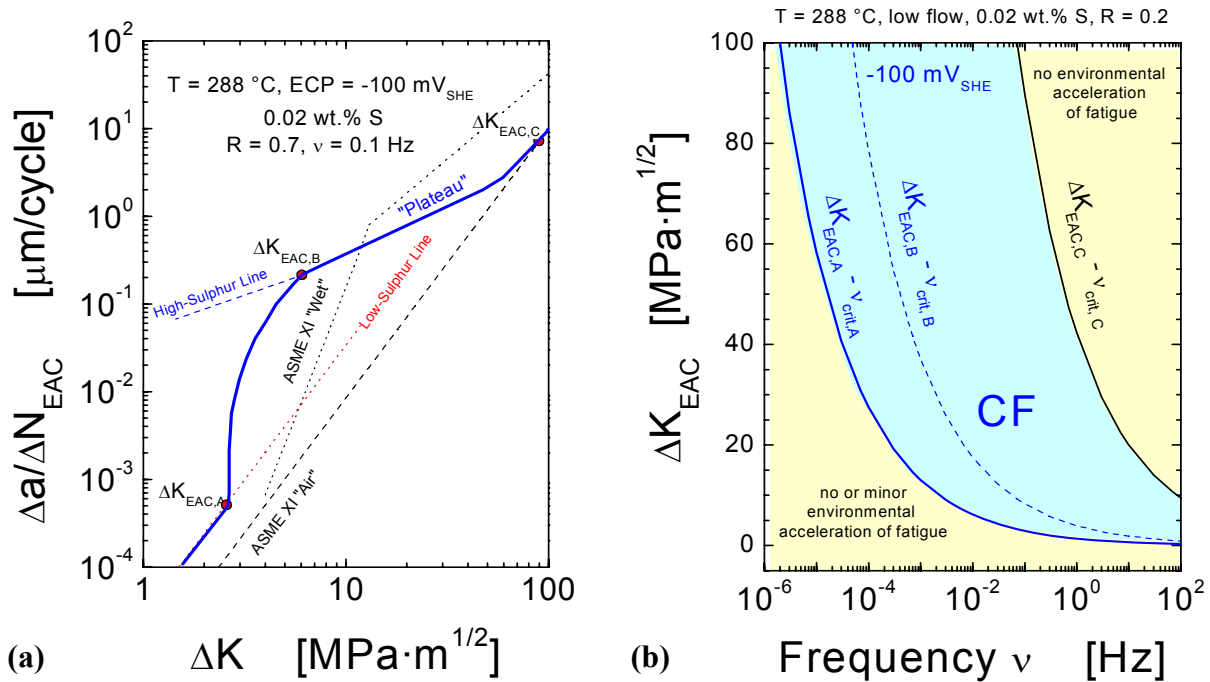
Figure 53: $\Delta a/\Delta N_{EAC}$ ΔK relationship and ΔK_{EAC} thresholds at a loading frequency of 10^{-1} Hz/load ratio of 0.7 and an ECP of -100 mV$_{SHE}$ (a) and ΔK_{EAC}-frequency relationships for a load ratio of 0.2 at an ECP of -100 mV$_{SHE}$ (b) according to the GE-model [16, 66, 114].
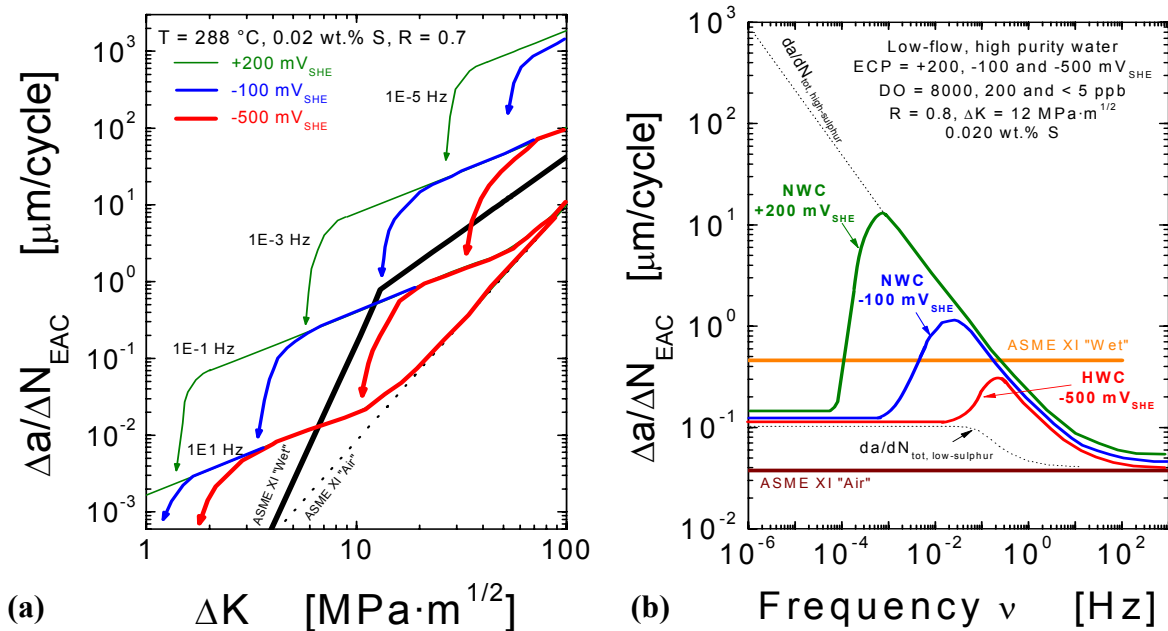
Figure 54: Effect of ΔK (a) and loading frequency ν (b) on the cycle-based CGR $\Delta a/\Delta N_{EAC}$ in oxygenated, high-purity HT water at three different ECP/DO-levels according to the GE-model [16, 66, 114]. Additionally, the model predictions are compared to the corresponding ASME XI reference fatigue CGR curves for the given loading conditions.

According to the GE-model, the $\Delta a/\Delta N_{EAC}$ vs. ΔK curve can be roughly approximated by a bilinear curve. In contrast to the time-based form (Figure 56), each load ratio R/frequency ν combination results in a different $\Delta a/\Delta N_{EAC}$ vs. ΔK curve for one given ECP/steel sulphur combination in the cycle-based from. Accelerated CF is only observed in a limited frequency and ΔK range. Based on the GE-model (Figures 53 and 54), it is expected that ΔK_{EAC} thresholds and plateau CGR (2nd slope region) are shifted to lower values with increasing loading frequencies and load ratios. The threshold $\Delta K_{EAC,A}$ and $\Delta K_{EAC,B}$ are furthermore shifted to lower ΔK values with increasing ECP and steel sulphur content, in contrast to the plateau CGR (2nd slope region), which is not affect by these two parameters.

The effects of ΔK, R and loading frequency observed in experiments in HT water fit very well to the predictions of the GE-model [62]. Above an upper critical loading frequency of about 1 to 100 Hz and/or at very high ΔK values, no environmental acceleration of fatigue crack growth was observed and fatigue CGR in HT water and air were identical. Below this upper critical frequency (which is dependent on ΔK and R) the cycle-based CGR $\Delta a/\Delta N_{EAC}$ were similar for all ECP/DO/material conditions and increasing with decreasing loading frequency (approximately parallel to the high-sulphur CF line of the GE-model) down to a lower critical frequency, where a maximum in cycle-based CGRs $\Delta a/\Delta N_{EAC}$ and environmental acceleration of fatigue crack growth was observed (Figure 11). Below this lower critical frequency, no or only minor environmental acceleration (by factor of 2 to 5) was observed and cycle-based CGRs $\Delta a/\Delta N_{EAC}$ quickly dropped down to low-sulphur CF CGRs by further decreasing the loading frequency. This lower critical frequency was strongly dependent on DO/ECP and shifted to lower values with increasing ECP/DO, steel sulphur content and ΔK, as well as by decreasing temperatures (with a possible peak at intermediate temperatures) [11]. Depending on ΔK, R and material a lower critical frequency of 10^{-3} to 10^{-1} Hz (< 5 ppb DO, PWR, BWR/HWC), 10^{-4} to 10^{-2} Hz (200 ppb DO, BWR/NWC) and < 10^{-5} to 10^{-6} Hz (DO $\geq$ 400 ppb, BWR/NWC transients or simulation of realistic in-pile ECPs) has typically been observed at 288 °C.

Under system conditions, where no or minor environmental acceleration of fatigue crack growth ($\leq$ a factor of 5) was observed (i.e., below the lower and above the upper critical frequency), a similar Paris-exponent m ($\Delta a/\Delta N_{EAC} = B \cdot \Delta K^m$) of $\approx$ 3 was observed in HT water as in air and the $\Delta a/\Delta N_{EAC}$ vs. ΔK curve was approximately parallel to the corresponding air fatigue CGR curve. Under these conditions, $\Delta a/\Delta N_{EAC}$ was hardly affected by loading frequency. This behaviour has sometimes been designated as true corrosion fatigue [62, 128].

Under system conditions, where strong environmental acceleration of fatigue crack growth ($\geq$ factor of 10) was observed (i.e., between the lower and upper critical frequency), a plateau-like range was observed in the $\Delta a/\Delta N_{EAC}$ vs. ΔK curve above a plateau threshold ΔK_{EAC} with a relatively small Paris-exponent m between 1 and 2 (Figure 55). This plateau intersected the air fatigue curve at high ΔK values. The plateau CGR $\Delta a/\Delta N_{EAC}$ and the plateau threshold ΔK_{EAC} increased with decreasing loading frequency. A power law relationship ($\Delta a/\Delta N_{EAC} = A \cdot \nu^n$) between plateau $\Delta a/\Delta N_{EAC}$ and loading frequency ν was observed in this frequency range (Figure 11) with an exponent of -0.4 to -0.65 (typically 0.5 to 0.6). The ΔK_{EAC} thresholds were strongly dependent on ECP/DO and were decreasing with increasing load ratio, loading frequency and ECP/DO. Under highly oxidizing BWR/NWC conditions (ECP $\geq$ +50 mV$_{SHE}$, DO $\geq$ 0.4 ppm) and suitable loading conditions, fast CF could be sustained down to the lowest tested loading frequency of $3 \cdot 10^{-6}$ Hz and to a CF-threshold ΔK_{EAC} of 1.5 to 2 MPa·m$^{1/2}$ [36, 62, 165], which is significantly smaller than the apparent thresholds of the ASME XI wet reference fatigue CGR curves (Figure 55a).
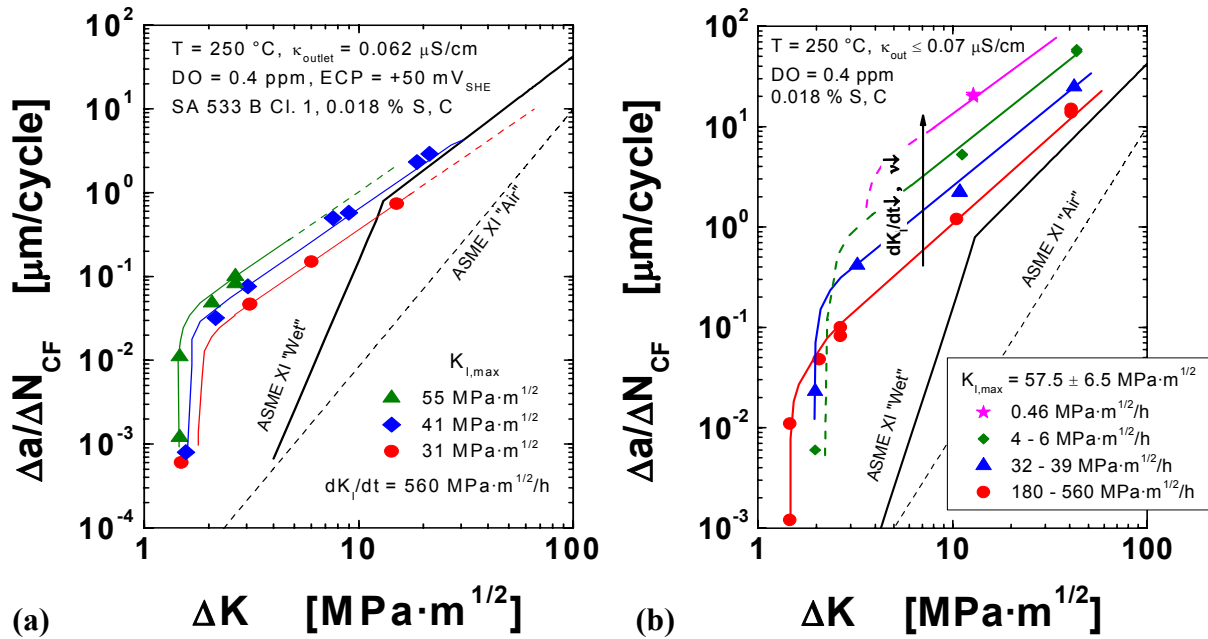
Figure 55: Effect of ΔK (a) and loading rate dK_I/dt (b) on $\Delta a/\Delta N_{EAC}$ in material C for increasing load ratio/decreasing ΔK tests at constant $K_{I,max}$ and dK_I/dt and comparison to the corresponding ASME XI reference fatigue CGR for the specified loading conditions [62].

Very similar CF CGRs were observed in different materials at various ECP/DO levels for given loading conditions, if loading frequency was above/below the highest/lowest lower critical frequency of the different material/environment combinations, i.e. as long as either only high- or low-sulphur crack-tip environment conditions prevailed. The ECP/DO and steel sulphur content thus mainly affected CF in the transition region from high- to low-sulphur CF CGRs, which appeared as critical frequencies $\nu_{crit} = f(\Delta K, R)$ and ΔK thresholds $\Delta K_{EAC} = f(\nu, R)$ in the cycle-based and as a critical air fatigue CGR $da/dt_{Air,crit}$ in the time-domain form (Figure 59). The critical CGRs, frequencies, and ΔK_{EAC} thresholds were shifted to lower values with increasing ECP (or DO content). Literature data/model predictions furthermore suggest, that they are shifted to lower values with decreasing temperature, increasing ΔK, steel sulphur content/DSA susceptibility of the material and sulphate/sulphide/chloride content of the environment [62].

6.3.2 Corrosion Fatigue Crack Growth in the Time-Based Form

According to the GE-model [16, 66, 114], the CF crack growth in C & LAS can be described by one single curve in the time-based form for a given ECP/steel sulphur combination as shown in a time domain plot in Figure 56. Figure 57 shows such a time-domain plot of CF CGR from experiments which covered a wide range of environmental (240 to 288 °C (range with maximum CF CGR), 0.4 to 8 ppm DO, $\kappa = 0.06$ to 0.25 μS/cm, <1 to 65 ppb SO_4^{2-}), material (0.004 to 0.018 wt.% S) and loading parameters ($\Delta K = 11$ to 62 MPa·m$^{1/2}$, R = 0.2 to 0.8, $\nu = 3 \cdot 10^{-6}$ to $8 \cdot 10^{-3}$ Hz) [51, 62, 128]. Despite the wide range of parameters, all CF CGR data were lying in a relatively small scatter band of one half to one order of magnitude. The experimental data basically confirms the predicted behaviour, although the transition curve at high ECPs seems to be not conservative with respect to the experimental data. Time-domain analysis of CF CGR data is therefore very attractive for the development of CF crack growth curves for codes.
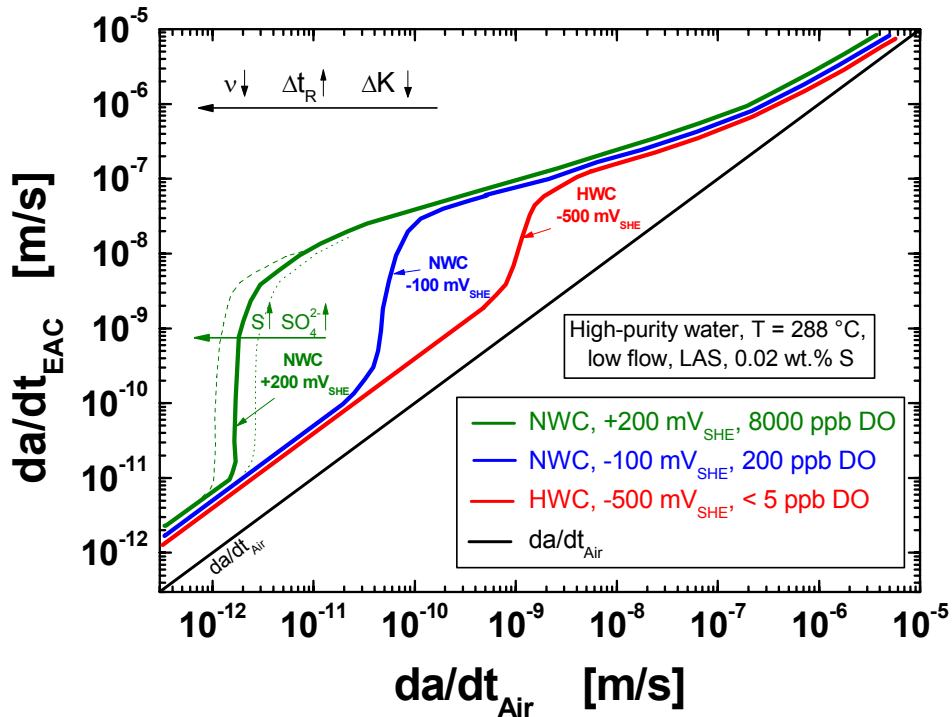
Figure 56: Comparison of the time-based CF CGR da/dt_{EAC} in oxygenated, high-purity HT water at different ECP levels according to the GE-model [16, 66, 114] with the corresponding fatigue CGR in air da/dt_{Air} under otherwise identical loading and system conditions (= time-domain plot).
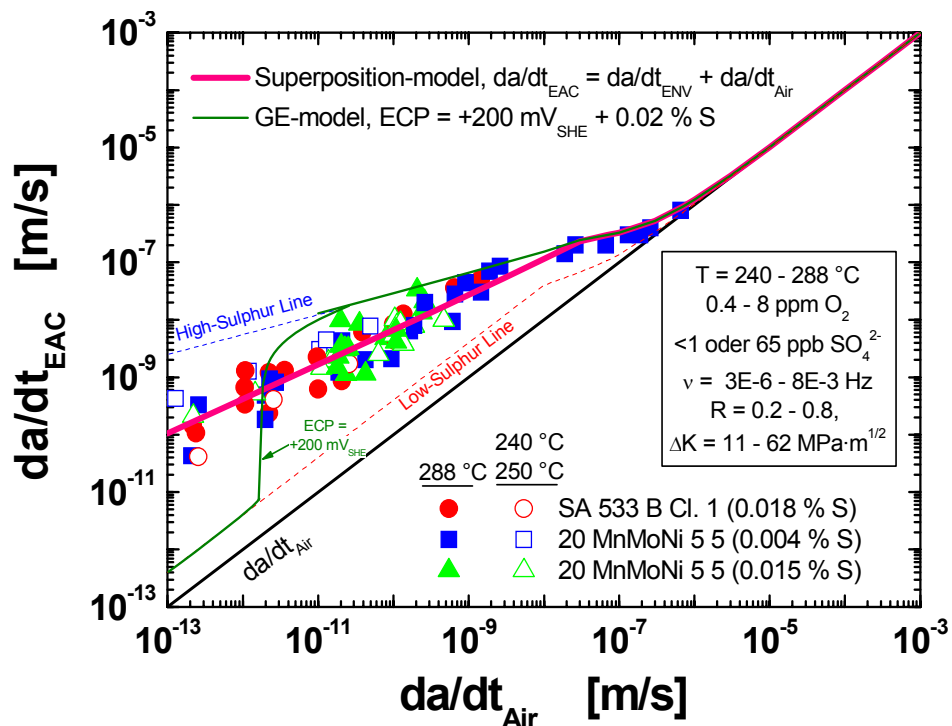
Figure 57: Time-domain analysis of CF test data in oxygenated HT water with a simple superposition-model (Section 6.3.3) and comparison with the GE-model [16, 66, 114].

6.3.3 Superposition Model for CF Crack Growth in C & LAS in HT Water

In the following paragraphs, a very simple superposition-model for the evolution of engineering reference fatigue crack growth curves in HT water is outlined, which is based on the time domain analysis and considers some of the basic ideas of the GE-model and some of the most dominant experimental parameter effects (ECP, frequency), but ignores material (steel sulphur content) aspects in the present form:

In this model, the cycle-based CGR in HT water $\Delta a/\Delta N_{EAC}$ is just a simple linear superposition of the cycle-based CGR in air $\Delta a/\Delta N_{Air}$ by pure mechanical fatigue and of the corrosion-assisted CGR $\Delta a/\Delta N_{ENV}$. The first contribution is a purely cyclic-controlled process and independent of loading frequency. The second contribution only occurs during the rising load part of the fatigue cycle and is strongly dependent on crack-tip strain rate $d\varepsilon/dt_{CT}$ (high-sulphur behaviour: $da/dt_{ENV}\ \alpha\cdot(d\varepsilon/dt_{CT})^n$, low-sulphur behaviour: $da/dt_{ENV}\ \alpha\cdot(d\varepsilon/dt_{CT})$, saturation of da/dt_{ENV} at high $d\varepsilon/dt_{CT}$ in both cases ($\rightarrow$ continuous dissolution)) and loading frequency. Under cyclic loading conditions it is assumed, that the crack-tip strain rate is proportional to the experimentally derived and known fatigue CGR in air ($d\varepsilon/dt_{CT}\ \alpha\ da/dt_{Air}$) under otherwise identical loading conditions. For the onset of fast EAC ("critical sulphur-anion concentration criteria", see Sections 10.3 and 10.4), the fatigue CGR in air da/dt_{Air} has to exceed a critical CGR $da/dt_{Air,crit}$, which is strongly dependent on the ECP. Based on these assumptions, the CF crack growth in HT water can be described by the following equations, which are the basis of the so-called "time-domain analysis method":

$$da/dt_{EAC} = da/dt_{ENV} + da/dt_{Air} \tag{2}$$

$$da/dt_{Air} = f(\Delta t_R, \Delta K, R),\ \text{e.g., ASME XI air CGR equation} \tag{3}$$

da/dt_{ENV}:

- $da/dt_{Air} < da/dt_{Air,crit} = f(ECP)$: $\qquad da/dt_{ENV} = 3\cdot da/dt_{Air}$ (4)
- $da/dt_{Air,crit} = f(ECP) \le da/dt_{Air} < 3.7\cdot10^{-8}$ m/s: $\quad da/dt_{ENV} = C\cdot(da/dt_{Air})^m$ (5)
- $da/dt_{Air} \ge 3.7\cdot10^{-8}$ m/s: $\qquad da/dt_{ENV} = 2.3\cdot10^{-7}$ m/s (6)

These equations can be easily transformed in a cycle-based form by dividing them by the rise time Δt_R or multiplying them by the doubled loading frequency $2\cdot\nu$. In contrast to the time-based form, the cycle-based form ($\Delta a/\Delta N_{EAC}$ vs. ΔK) splits into different curves for each ν-R combination. The parameters C, m and $da/dt_{Air,crit}$ have to be determined by regression analysis of conservative experiments (e.g. by adequate materials (high-sulphur content and high DSA susceptibility), decreasing frequency and high load ratio tests, 200 – 290 °C, etc.) for different important ECP regimes, (e.g., BWR/NWC, BWR/HWC and PWR conditions). In contrast to $da/dt_{Air,crit}$, C and m are not dependent on ECP (Figures 56 and 59). Based on $da/dt_{Air,crit}$, thresholds $\Delta K_{EAC} = f(\nu, R)$ and critical frequencies $\nu_{crit} = f(\Delta K, R)$ for the onset of EAC can be derived. The corrosion fatigue crack growth behaviour of LAS in oxygenated, HT water can therefore be reasonably described by the proposed model and by one single curve in the time-based form for a given ECP value. Furthermore, it directly considers frequency and ECP effects and inherently defines "immunity conditions", where environmental effects on fatigue crack growth can be excluded or neglected. In the time-base form, this superposition model can be easily extended by an SCC crack growth part.

Such a time-domain analysis for a large data base of CF tests [62, 128] in oxygenated HT water (simulated BWR/NWC operating conditions) is shown in Figure 57. The air fatigue CGRs da/dt_{Air} have been calculated according to Eason [175, 176]. Despite the wide range of parameters, all CF CGR data were lying in a relatively small scatter band of one half to one order of magnitude and within a factor of 5 of the calculated regression curve. The data indi-

cated a critical CGR $da/dt_{Air,crit} < 10^{-13}$ m/s under highly oxidizing BWR/NWC conditions ($+50 \leq ECP \leq +200$ mV$_{SHE}$).

For 10^{-13} m/s $\leq da/dt_{Air} < 3.7 \cdot 10^{-8}$ m/s, the time-based CF CGRs in Figure 57 can be described by the following regression equations:

$$da/dt_{Air} = (7.87 \cdot 10^{-11}/\Delta t_R) \cdot (\Delta K/(2.88-R))^{3.07} \qquad (7)$$

$$da/dt_{EAC} = 6.6 \cdot 10^{-3} \cdot (da/dt_{Air})^{0.6} + da/dt_{Air} \qquad (8)$$

$$\text{in m/s, s and MPa} \cdot \text{m}^{1/2}$$

In Figure 58, the predictions based on equation (8) are compared to experimental data [128]. A reasonably good correlation is observed for these testing conditions.
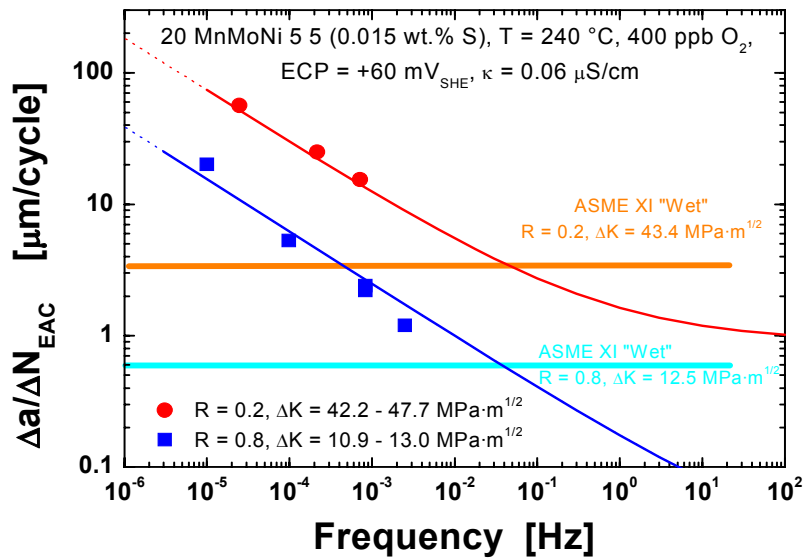
Figure 58: Good correlation between superposition model and experimental data about the effect of loading frequency [128].

Currently, a test matrix is running at PSI to identify $da/dt_{Air,crit}$ in different ECP regimes in conservative way. Preliminary results can be seen in a time-domain plot in Figure 59 for an ECP of +50 to +200, -100, and -500 mV$_{SHE}$.
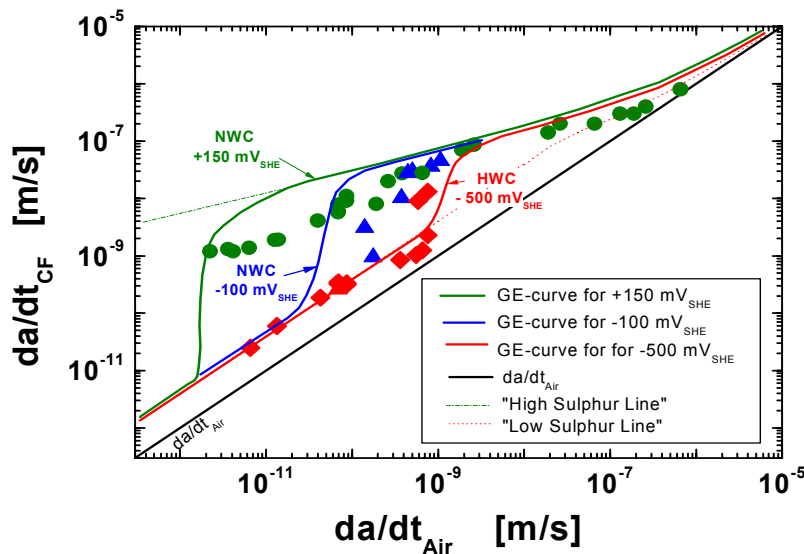
Figure 59: Experimental evidence for critical CGR $da/dt_{Air,cirt}$ at different ECP regimes for a high-sulphur RPV steel.

7 Metallographical and Fractographical Aspects of EAC in C & LAS

7.1 EAC Crack Initiation

SICC cracks in SSR tests at smooth defect free surfaces usually initiate at MnS-inclusions, which intersect the steel surface or at corrosion pits (see Section 8) [24, 58, 112, 126]. In high-sulphur steels generally more MnS-inclusions intersect the steel surface, and in fact, the number of initiation sites was often greater for high-sulphur steels [127]. Under highly oxidizing conditions at low or intermediate temperatures and low flow rate conditions, where pitting and the formation of an aggressive occluded water chemistry is strongly favoured [6, 111], initiation often occurs at pits and the effect of MnS is less dominant. Furthermore, strain localization by DSA further facilitates EAC initiation in the intermediate temperature range.

In LCF tests with C & LAS in HT water, as in air, cracks initiated and formed either along slip bands, carbide particles, or at the ferrite-pearlite phase boundary, but rarely at micropits or MnS-inclusions. Furthermore, the environment has no significant effect on the frequency of cracks. For similar loading conditions, the number of cracks in specimens tested in air and highly oxygenated water were identical, although fatigue life in water was lower by a factor of 10. Fatigue lives of the pre-oxidized specimens, which contained a plenty of micropits, were identical to those of unoxidized specimens in air. Specimens, which were first subjected to highly oxygenated water and slow strain rates at a strain amplitude of 0.4 % for a certain cycle number and then tested in either air or highly oxygenated water at a higher strain rate, revealed no reduction in fatigue live. They were thus not confirming that high DO and slow strain rate might enhance formation of cracks in LCF tests in HT water. These results suggest that the reduction in fatigue life in highly oxygenated water is primarily due to environmental effects on fatigue crack propagation. Environment appears to have little or no effect on formation of micro-cracks on the surface. [29]

The effect of pitting is not yet fully clear. Although micro-pitting seemed not to affect LCF [29], limited testing in another investigation with pre-pitting in oxygenated high-conductivity water revealed a relevant reduction of fatigue live in air and HT water [75]. There might be might a more pronounced effect of pitting or MnS-inclusions at smaller strain amplitudes and strain rates, where mechanical damage part becomes less dominant in LCF. Several service SICC cracking incidents (see Section 11) were related to severe pitting during prolonged shut-down periods, thus showing that pitting might affect SICC initiation under these less severe loading conditions.

7.2 Crack Path of EAC in C & LAS in HT water

The crack path in EAC of C & LAS in HT water is usually perpendicular to the direction of maximum tensile stress and is predominantly TG in nature (Figure 60) over a very wide range of loading (static to cyclic, SCC to CF), environmental (BWR/NWC and HWC, PWR) and material conditions (C & LAS; bainitic, ferritic-pearlitic and ferritic microstructure; wrought, weld filler and weld HAZ materials; low- and high sulphur steels; low to medium strength LAS) [128, 177, 178]. In C & LAS with ferritic-pearlitic microstructure, the TG crack propagates trough both, soft ferritic grains and hard pearlitic regions in HT water, but preferentially along soft ferrite grains in air [29].
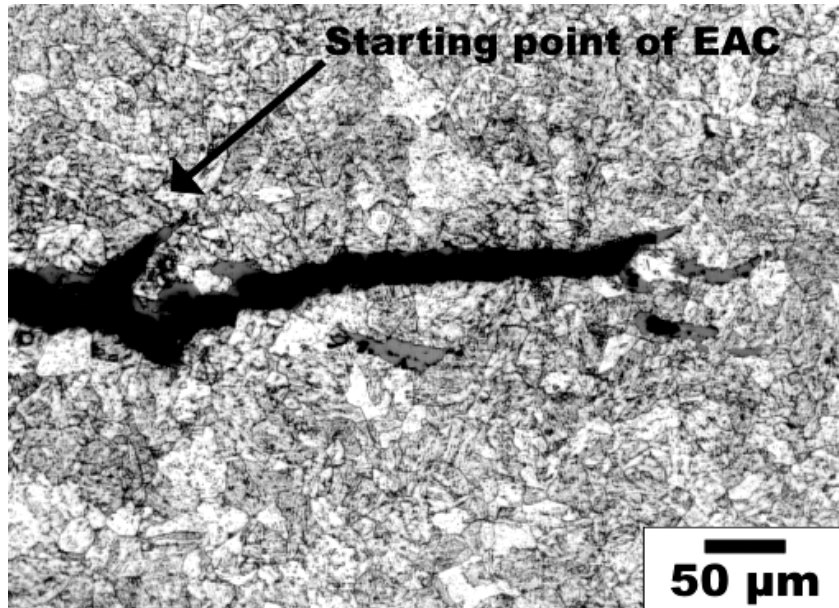
Figure 60: Typical example of TG crack path of EAC in C & LAS in HT water (light microscope micrograph of a metallographic cross-section).

IG or mixed TG/IG cracking (Figure 61) only occurred in some very specific and isolated cases, e.g., in high strength LAS [130], in peak hardness coarse grain zone of (poor quality) weld HAZ with excessive Vickers hardness > 350 HV5 [131], in highly cold-worked carbon steels (bended pipes) [151] or in quenched (non-tempered and non-stress-relieved) LAS [131, 133]. Most of these conditions appear as atypical for properly manufactured and fabricated C & LAS primary pressure-boundary components. Phosphorous (and other metalloid elements) segregation to prior austenite grain boundaries ("temper embrittlement") can be another reason for IG cracking in LAS (Figure 61) [147, 148]. Some IG cracking was related to hydrogen-assisted SCC or to strain localization process. The tendency for IG cracking increased with increasing strength level/hardness, grain size and decreasing temperature.

Minor micro- and macro-branching was sometimes observed, but is not a distinct or characteristic feature of EAC in C & LAS. The tendency for branching was higher under static than under cyclic loading conditions and was more frequently observed at intermediate/lower temperatures or, in particular, in case of overloading of specimens with severe violation of SSY conditions, where cracks were growing at 45 ° angle with respect to specimen mid-plane. Most of the "branching" under SSY conditions was rather related to multiple crack initiation (and therefore multiple crack planes) at several initiation sites on different levels at the crack front than to classical bifurcation of a single crack (which is often observed in case of IG cracking).
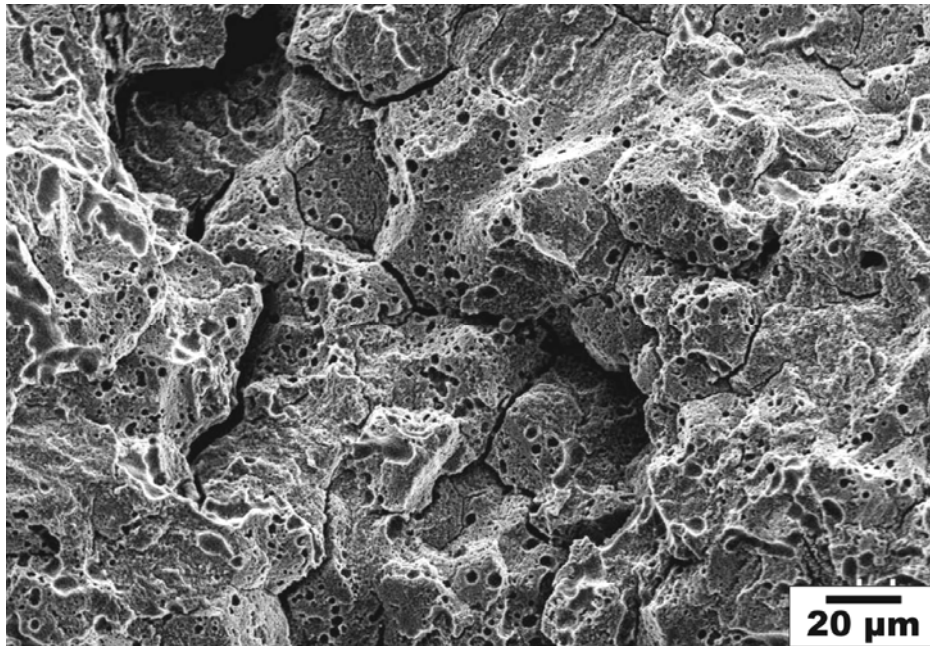
Figure 61: Local IG cracking in RPV steel with local phosphorous segregation [149].

7.3 Fractographical Appearance of EAC in C & LAS in HT water

7.3.1 Loss of Micro-Fractographic Information by Oxide Film Growth

C & LAS which have been exposed to HT water are covered by thick double-layer oxide film [179] with a complex structure and composition, which depends on DO, temperature, flow rate, etc. After cooling to room temperature, the crack flanks in the oxygen-depleted crack crevice are usually covered by a Fe_3O_4 or mixed $Fe_3O_4/FeS/FeS_2$ film (in case of strongly accelerated EAC) with complex structure. To reveal the micro-fractographic details, the oxide film is usually removed by galvanostatic reduction in an Endox-bath [180].

There is a significant loss of fractographic information by general corrosion in C & LAS at extended exposure periods in HT water compared to stainless steels or Ni-base alloys (Figure 62). The growth of the inner oxide film at the metal/oxide interface results in a smoothening of the fracture surface topography and the destruction of the micro-fractographic details like feather facets, striations or cleavage facets with river pattern, in particular, if aggressive high-sulphur crack-tip environment conditions prevail. The degree of information loss increases with increasing exposure time and aggressiveness of the environment. The feather morphology/striations can usually only be detected by SEM, if the exposure time to HT water of the specific location on the fracture surface is less than 200 to 1000 h, depending on the test conditions. If EAC crack growth is sustained up to the end of the test, micro-fractographic details can still bee seen close to the final crack front. Crack closure in case of high fracture surface roughness or significant out-of-mid-plane cracking during unloading may sometimes modify this micro-fractographic appearance. But even after very prolonged exposure times (e.g., service cracking incidents), EAC can be readily differentiated from pure fatigue by the different macro-fractographic appearance, which is not destroyed by oxidation. A differentiation between SCC, SICC, and LFCF, on the other hand, is quite difficult based on fractography only. Shut-down corrosion can further increase the information loss and impede analysis. In spite of this possible loss of information, fractographical investigations can provide some helpful additional information about EAC processes. Some typical fractographic "features" are briefly summarized in the following sub-sections and some (secondary electron) SEM micrographs are shown.
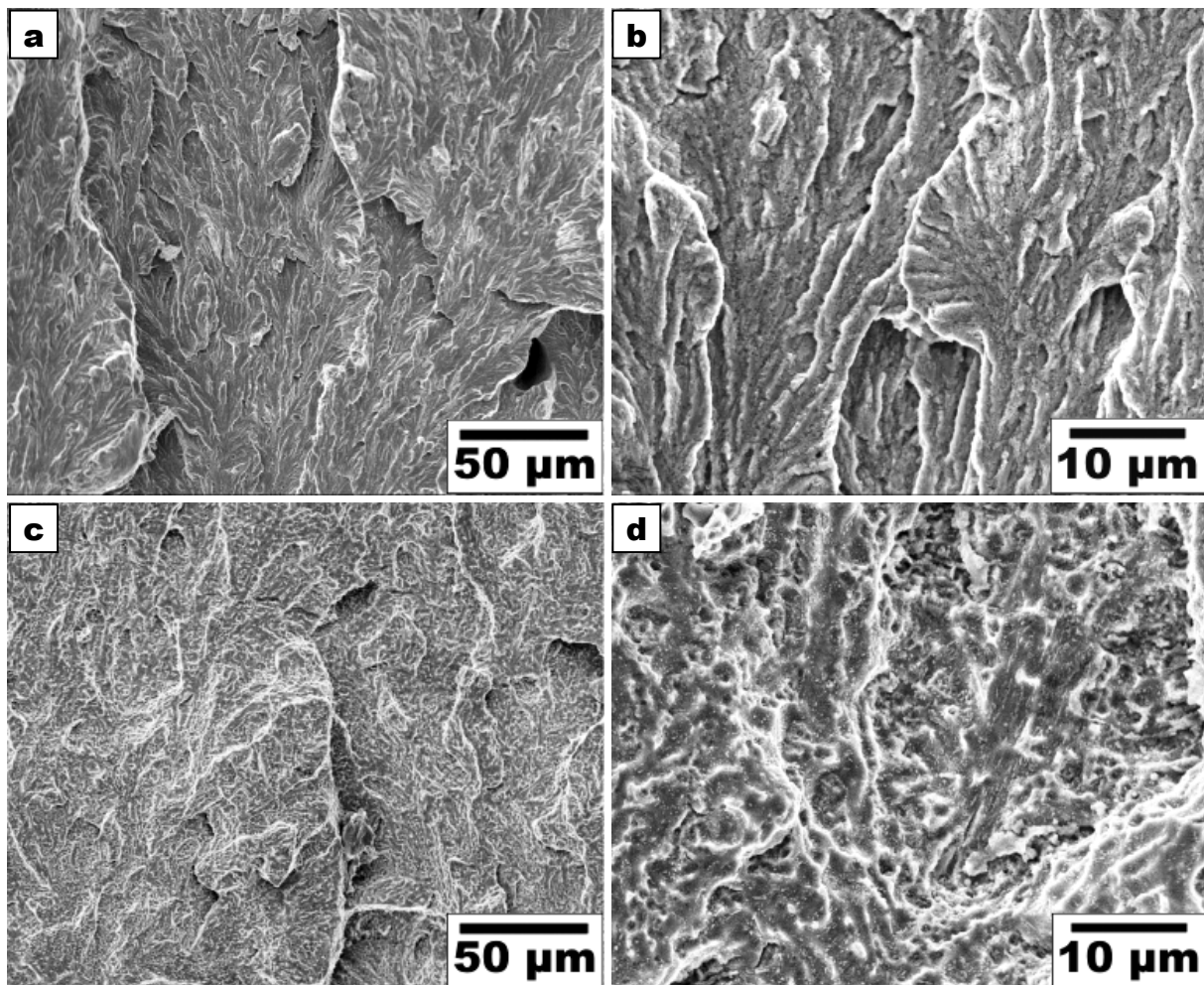
Figure 62: (a) and (b): "Fresh" fracture surface with micro-fractographic information (< 200 h exposure time to HT water). (c) and (d): Heavily corroded fracture surface without micro-fractographic information (> 500 h exposure time to HT water).

7.3.2 Typical Appearance of the Fracture Surface

EAC in C & LAS in HT water in the temperature range from 150 to 320 °C, where main environmental effects occur, usually has a TG quasi-cleavage appearance with feather morphology (Figures 62a, 62b, 63 and 64) [128, 177, 178]. The feather facets/tear ridges with a spacing of some few μm are parallel to the local crack growth direction (Figure 63) and may be the result of plastic strain localization and shear processes. The general fracture appearance is similar for SCC, SICC and CF (in case of strong environmental acceleration of fatigue crack growth), thus confirming that EAC is governed by the same basic process for all three loading modes. In case of cyclic loading conditions the fracture surface may also contain both ductile (Figure 65) and brittle fatigue striations (Figure 66), which are perpendicular to the local crack growth direction. The striations are usually only seen at loading frequencies $\geq 10^{-3}$ Hz.
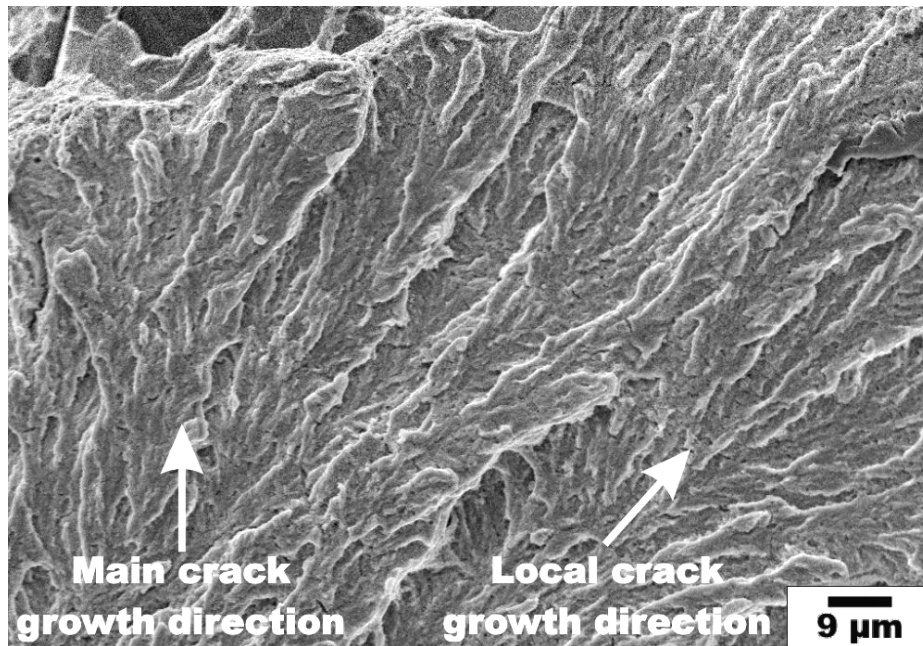
Figure 63: Typical quasi-cleavage appearance of the fracture surface with feather morphology.
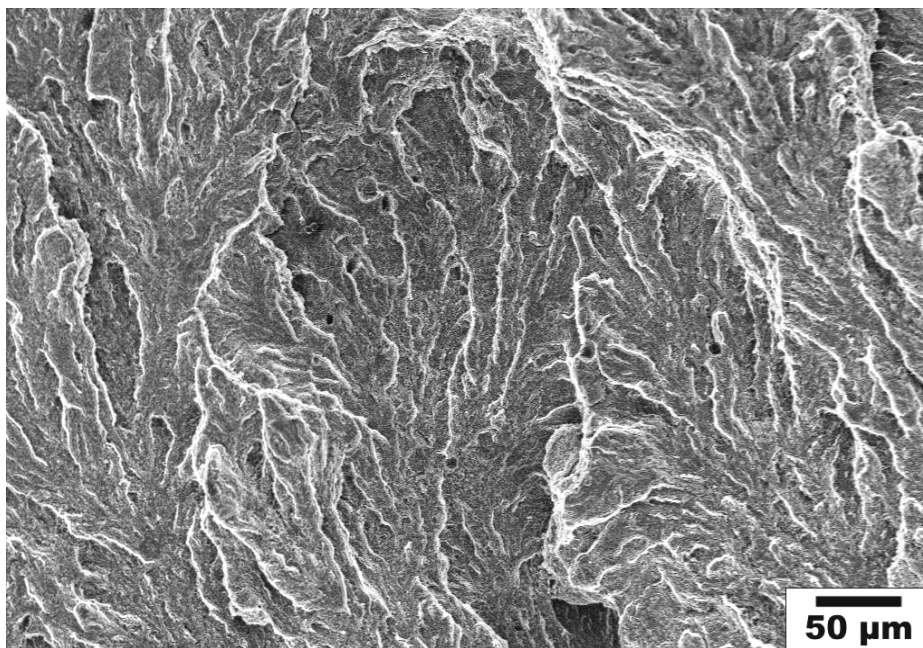
Figure 64: Typical quasi-cleavage appearance of the fracture surface with feather morphology.

The fracture surface usually has a terrace-like structure (Figure 67), because of multiple crack initiation. Individual crack terraces are often fan-shaped, and sometimes initiate from MnS-inclusions, which intersect the crack front (Figure 68). The ligaments/steps between the individual crack planes may fail (usually with retardation) by fatigue, EAC or ductile shearing or may even remain un-cracked. The retarded failure of such un-cracked ligaments in SCC tests has also been confirmed by DCPD measurements. Figure 69 shows a schematic of the observed fracture surface.
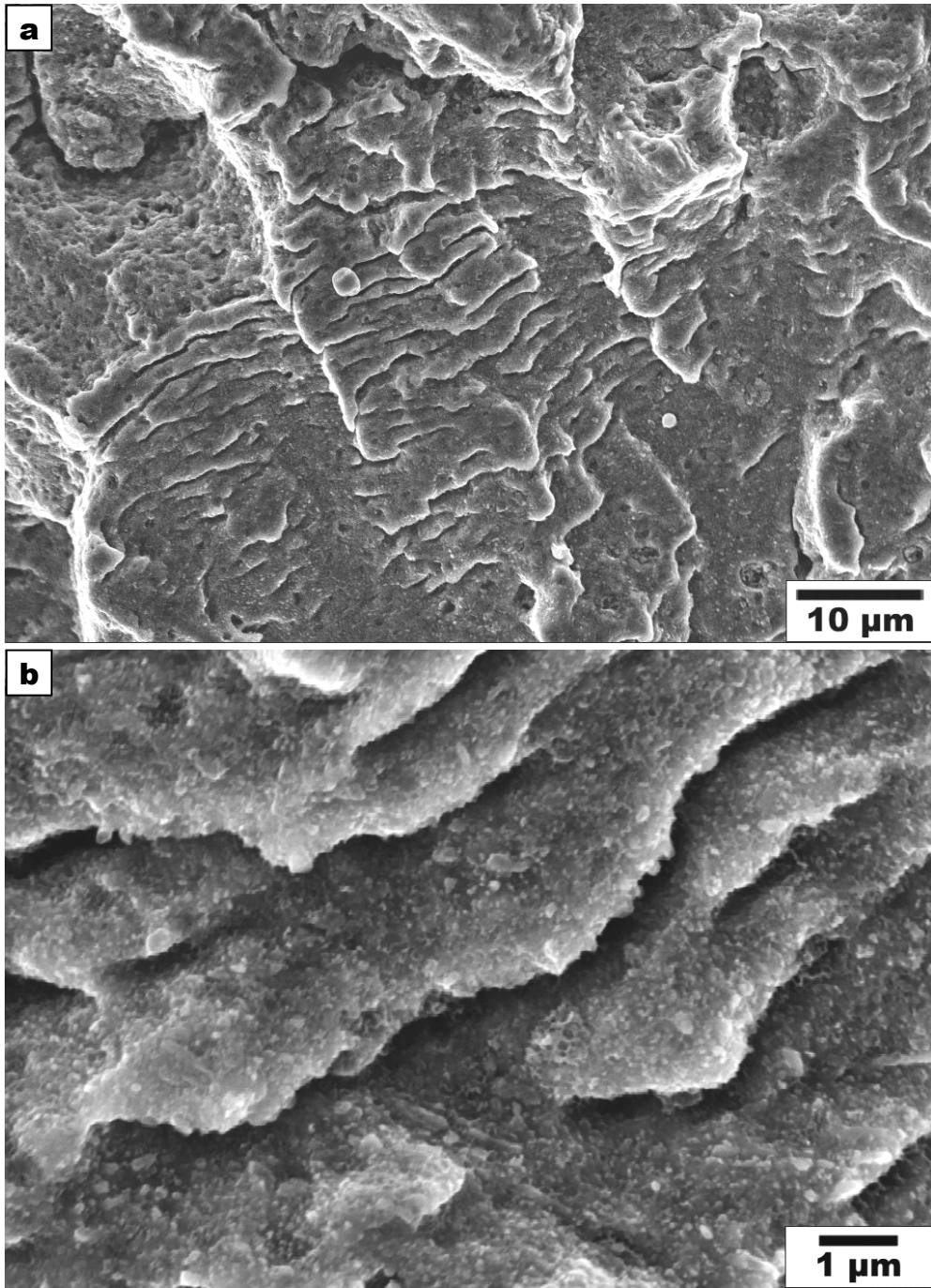
Figure 65: Ductile fatigue striations (irregular, deep striations).
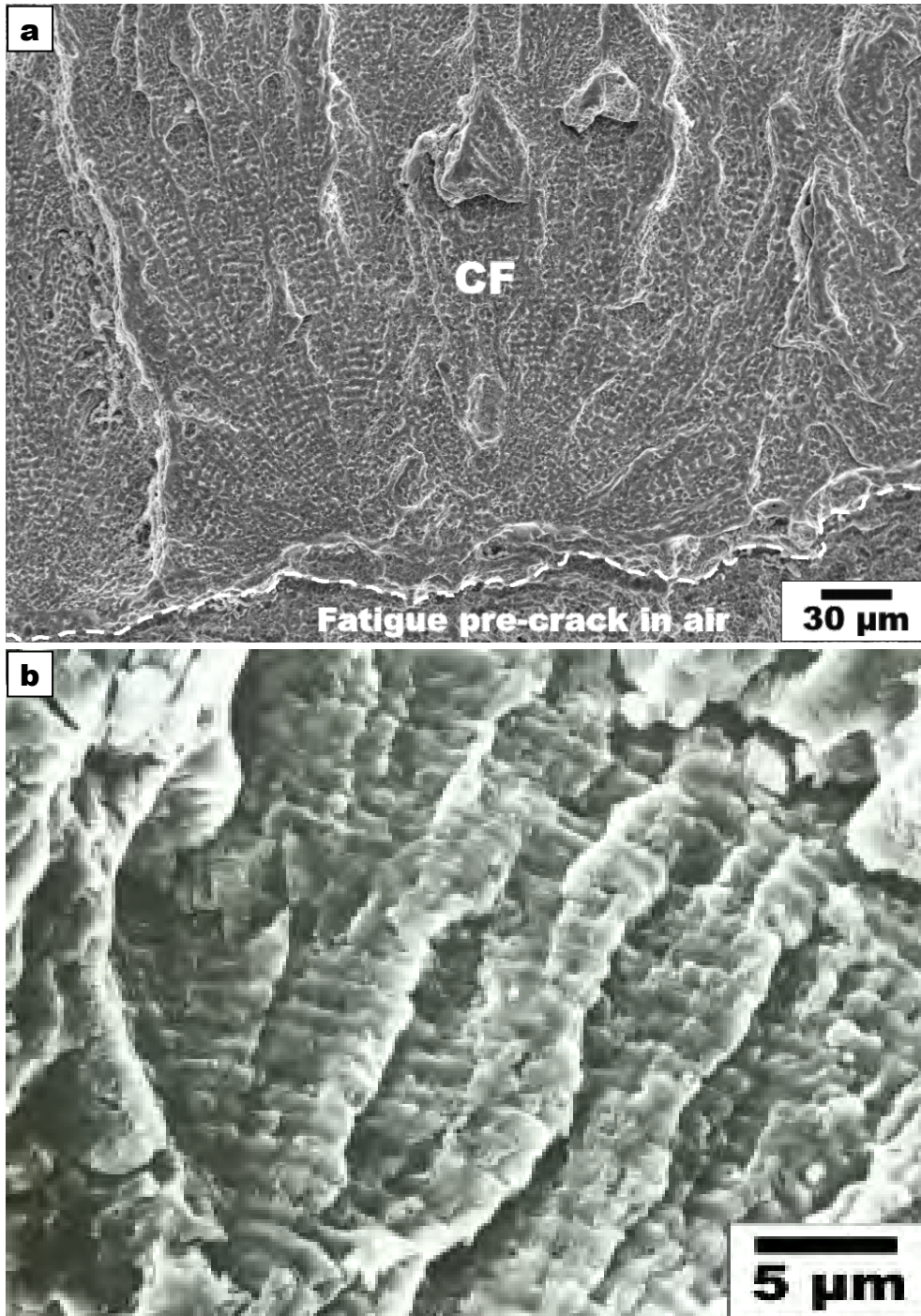
Figure 66: Brittle fatigue striations (regular, shallow striations with feather facets/tear ridges parallel to local crack growth direction) [128, 177].
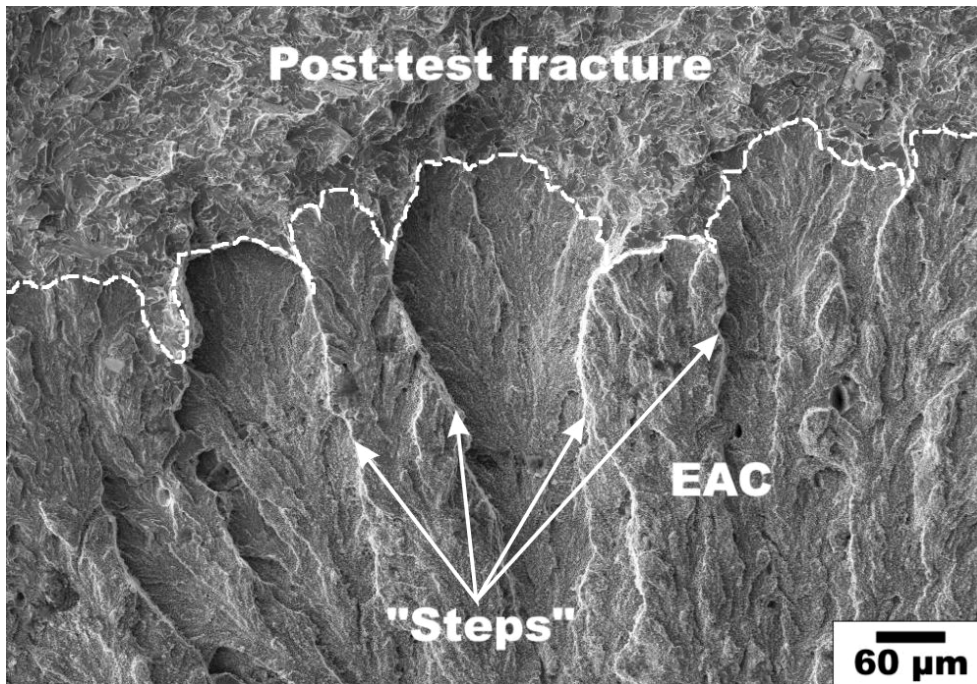
Figure 67: Terrace-like structure of the fracture surface.
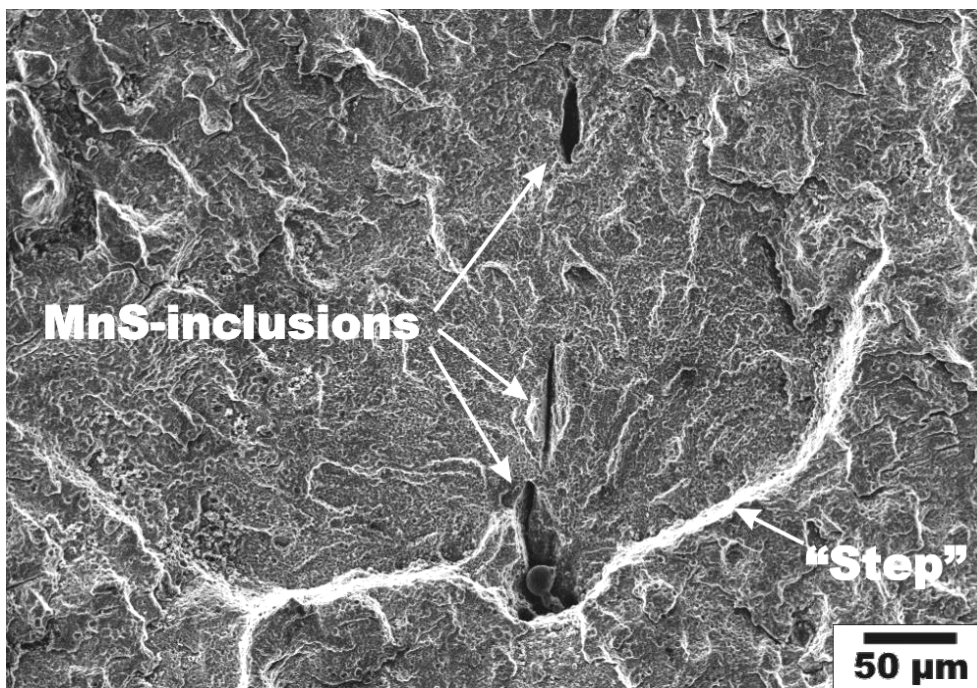
Figure 68: A crack terrace initiated from MnS-inclusions.
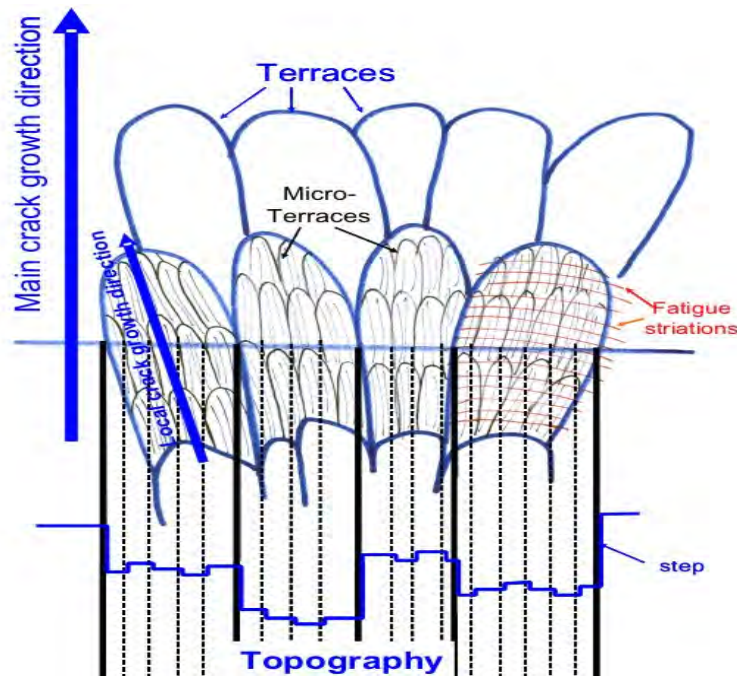
Figure 69: Schematic of the terrace-like structure of the fracture surface.

The roughness of the fracture surface and feather morphology usually increases with increasing environmental acceleration of fatigue crack growth, load level (ΔK, K_I) and DSA susceptibility as well as with decreasing external loading rate and temperature with a peak at intermediate temperatures of 200 to 250 °C.

Under cyclic loading conditions in case of minor environmental acceleration of fatigue crack growth (i.e., in case of low-sulphur crack-tip environment conditions or high loading frequencies ≥ 0.1 Hz), the fracture surface generally has an air-fatigue-like appearance with ductile striations. The spacing of the ductile striations is usually higher than in air and the striations are perpendicular to the macroscopic crack growth direction. The fracture surface is rather smooth and the crack front very even without any crack pinning.

With increasing environmental acceleration of fatigue crack growth and decreasing loading frequency (10^{-2} to 10^{-4} Hz), the spacing between the striations becomes larger, the surface roughness increases and local crack growth direction starts to deviate from the macroscopic crack growth direction. An increasing amount of brittle fatigue striation appears with increasing environmental acceleration. Mixed ductile and brittle striations may co-exist on the same facture surface in direct neighbourhood. Sometimes, brittle striations originate from MnS-inclusions, but they are not necessarily related to them. In case of very high environmental acceleration (i.e., high-sulphur crack-tip environment conditions) and very low loading frequencies ≤ $5 \cdot 10^{-4}$ Hz, ductile striations completely disappear and the fracture surface becomes more and more striation-less. The local crack growth direction on individual crack terraces strongly deviates from the macroscopic crack growth direction and may significantly differ even in neighbouring crack terraces. The fracture surface has a high roughness and the crack front becomes highly uneven and contains an increasing number of large un-cracked ligaments (Figure 70). In some cases, crack growth becomes localized and is restricted to some few isolated regions at the crack front, often related to large MnS-inclusions, which intersect the crack front (Figure 71). Local crack pinning is usually not related to distinct microstructural features like secondary phase inclusions With increasing surface roughness, local roughness/oxide film induced crack closure is increasingly observed, in particular at low load ratios, which can result in local crack pinning and even crack arrest in extreme cases.
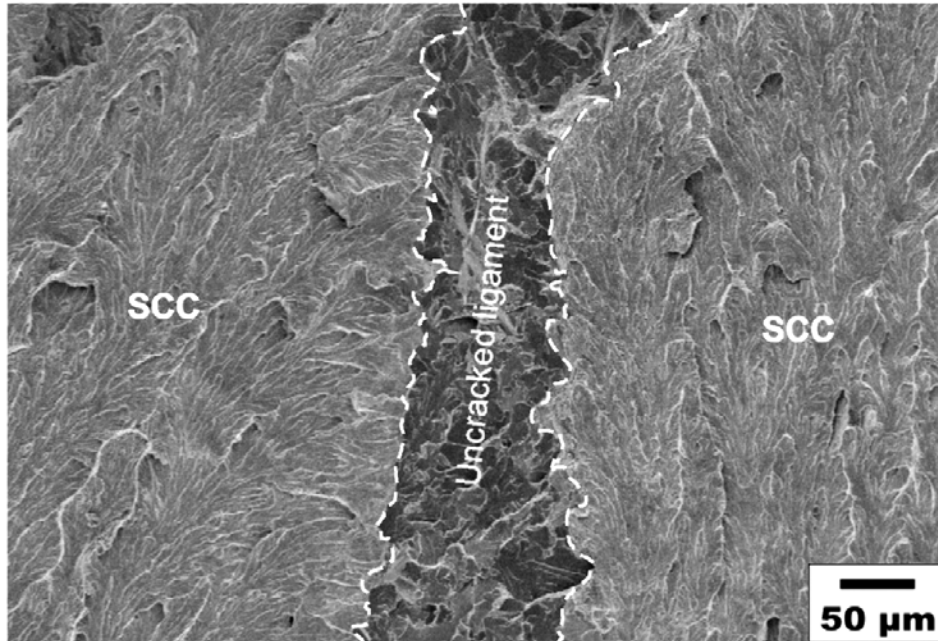
Figure 70: Large un-cracked ligament, which didn't fail until the end of the test.
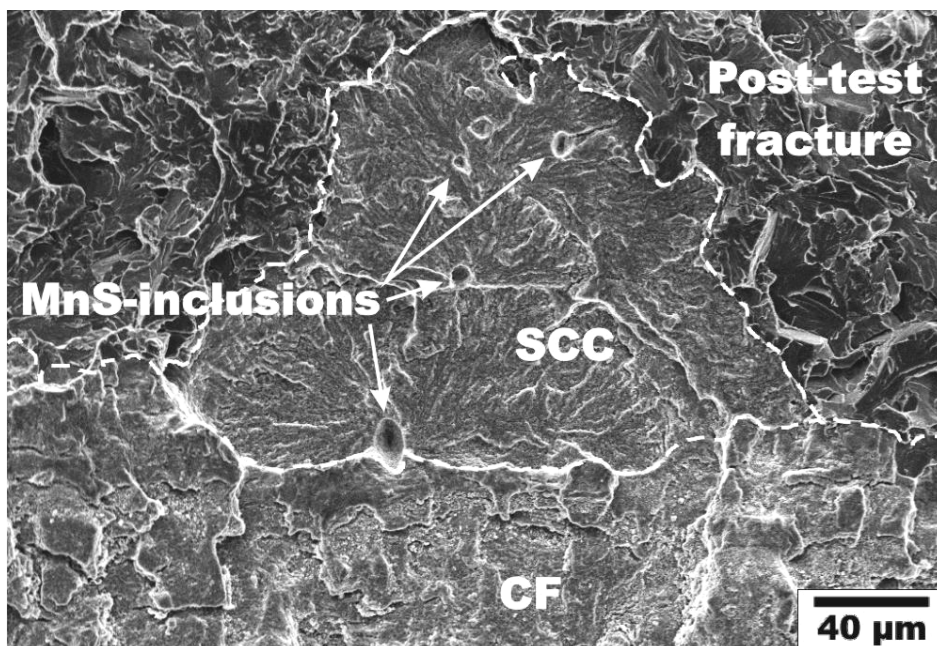
Figure 71: Localized crack growth under constant load (SCC) due to MnS-inclusions, intersected by the crack front.

SCC often can be differentiated from CF at loading frequencies $> 10^{-3}$ Hz by an increased roughness of the fracture surface, fan-shaped facets resulting in a more uneven crack front (Figure 72) and the absence of striations (Figure 73). Under very low-frequency fatigue loading and highly oxidizing conditions, on the other hand, the fracture surface appearance of CF is almost identical to that of SICC and SCC and can hardly be differentiated from each other.

In Table 7 the major aspects of fractographic appearance for CF, SICC, and SCC are briefly summarized.
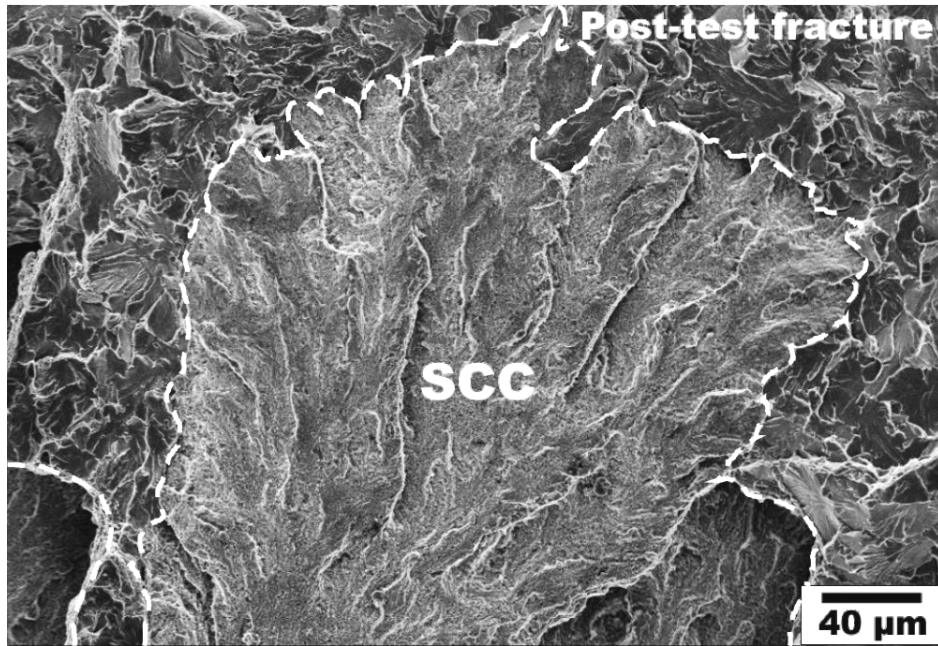
Figure 72: Fan-shaped facets, resulting in an uneven crack front, typical for SCC.
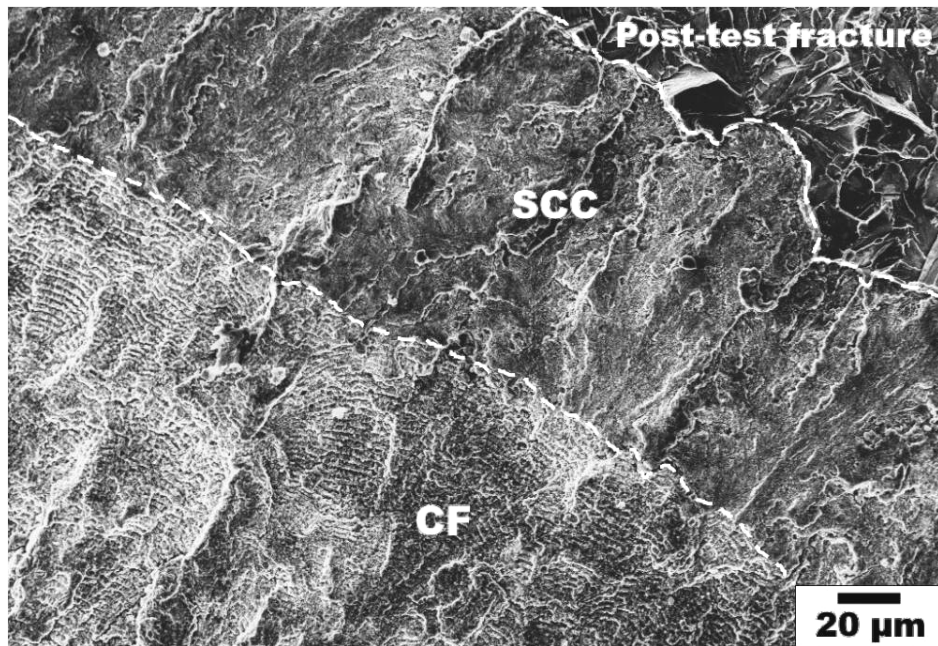
Figure 73: Transition from brittle striations (CF) to SCC.

Type of EAC	CF	SICC	SCC
Loading	cyclic $\nu > 10^{-3}$ Hz	Cyclic, $\nu < 5 \cdot 10^{-4}$ Hz rising load	constant load ripple load (CF)
Surface roughness/ topography	low $\Delta K \uparrow,\ T \downarrow,\ \nu \downarrow \rightarrow r \uparrow$	medium $\Delta K \uparrow,\ T \downarrow,\ \nu \downarrow \rightarrow r \uparrow$	high $K_I \uparrow,\ T \downarrow \rightarrow r \uparrow$
Direction of local crack growth	parallel to main CGD	slight deviations from main CGD, fan-shaped	strong deviations from main CGD, fan-shaped
Shape of crack front	straight	straight to irregular	irregular, local
Feather morphology	**yes**, if $t_{oxidation} \leq \approx 200$ h parallel to main CGD	**yes**, if $t_{oxidation} \leq \approx 200$ h parallel to main CGD	**yes**, if $t_{oxidation} \leq \approx 200$ h parallel to main CGD
Striations	**yes**, if $\nu \geq \approx 10^{-3}$ Hz + $t_{oxidation} \leq \approx 10^{2}$ h perpendic. to local CGD	**no**	**no**
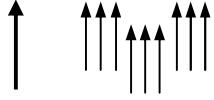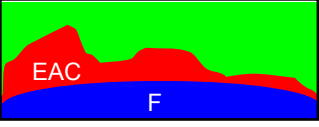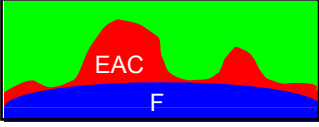
Table 7: Summary of the major aspects of fractographical appearance for CF, SICC and SCC (CGD = crack growth direction, F = fatigue pre-crack in air, r = roughness).

7.3.3 Role of MnS-Inclusions

Fractography suggests that dissolution of MnS-inclusions is rather slow and sluggish in HT water and dependent on their chemical composition. MnS-inclusions, which have completely dissolved leave distinct and characteristic traces, which can be easily identified in the SEM and by EDX (Figure 74). In lab tests, MnS-inclusions, which have only been partially dissolved, can bee seen in some cases (Figure 75). The effect of MnS-inclusions is less pronounced on crack growth than on crack initiation, since a large area of MnS-inclusions, which are intersected by the crack flanks and front is available to create a sulphur-anion-rich environment, which is essential for EAC. MnS-inclusions, which intersect the crack front may act as crack initiation sites, but there is no clear trend that they are the preferred location for crack initiation.

The effect of MnS-inclusions on crack growth becomes more important with decreasing ECP (e.g., PWR or BWR/HWC conditions, where sulphur-anion enrichment by migration is absent), load level, frequency, and steel sulphur content as well as with increasing purity of the water. Under mild or moderate test conditions, EAC in low-sulphur steels is often restricted to some few isolated regions at the crack front, which are usually related to MnS-inclusions, which intersect the crack front. In high-sulphur steels, EAC usually spreads over the whole crack front and is more even. Nevertheless, the local maximum EAC CGR in low-sulphur steels is comparable to the EAC rates in high-sulphur steels in many cases [128].
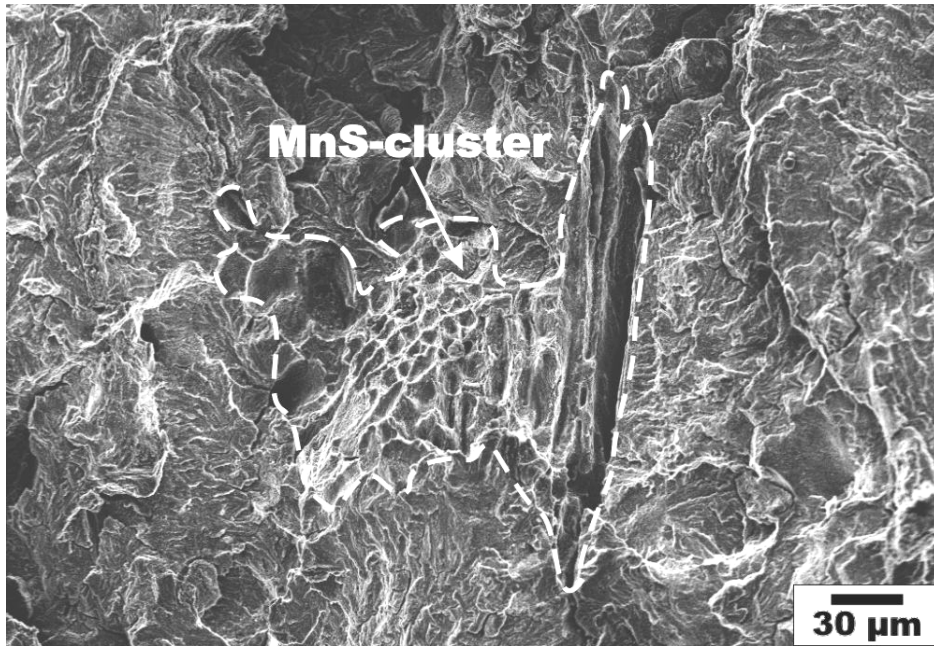
Figure 74: Traces of completely dissolved MnS-inclusions (MnS-cluster).
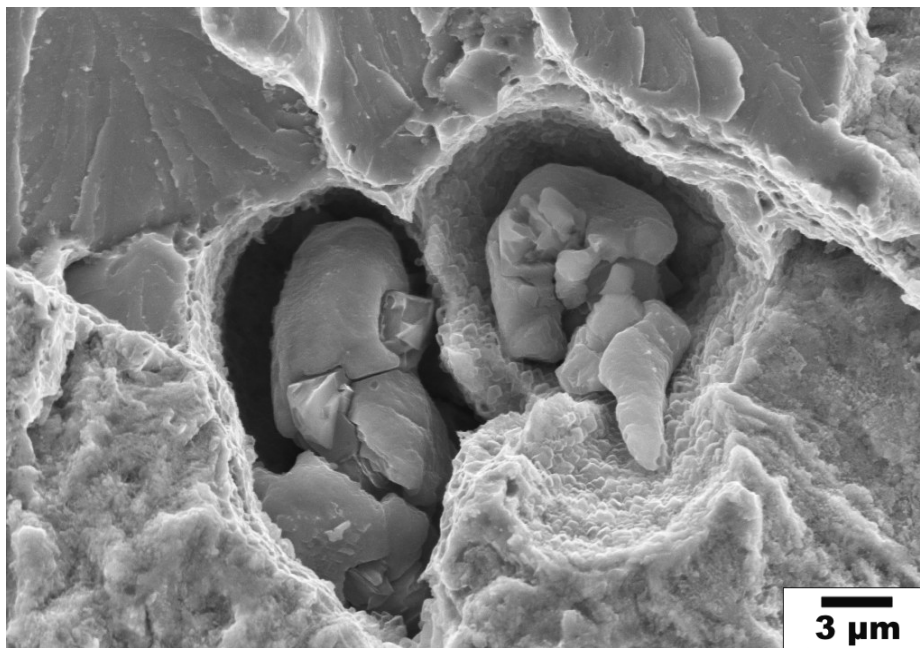
Figure 75: MnS-inclusions, which have only been partially dissolved (at the crack-tip).

7.3.4 Conclusion concerning EAC Crack Growth Mechanism

The similar fractographical appearance suggests that SCC, SICC and CF may be related to the same basic time-dependent EAC process. In case of CF, there is a further cycle-based contribution from mechanical fatigue, which can be regarded as additive and dominates at high loading frequencies. The crack growth mechanism cannot be derived directly from fractography, but probably it involves a complex mixed mode process, which includes oxide film rupture, anodic dissolution and localization of plastic deformation. To clarify the role of plastic deformation, TEM investigations should be included. Below a temperature of 100 to 180 °C, there might be a change in crack growth mechanism and fracture surface appearance. Since low-temperature EAC fracture surfaces were not available to PSI, no conclusion can be derived concerning this aspect.

78

8 Pitting in C & LAS in HT Water

SICC cracks at smooth defect free surfaces typically initiate at corrosion pits or at MnS-inclusion, which intersect the steel surface. Pitting in C & LAS is favoured by high oxygen concentrations and low temperatures as well as by dynamic straining (see Figure 76) or an aggressive water chemistry (high concentration of harmful anionic species like sulphate and chloride) [6, 7, 15]. Pits are often formed at MnS-inclusions, which intersect the steel surface, in particular under mild system conditions. Low-flow conditions which promote the build-up of an aggressive occluded water chemistry in these small surfaces defects strongly favours SICC initiation at the pit ground.
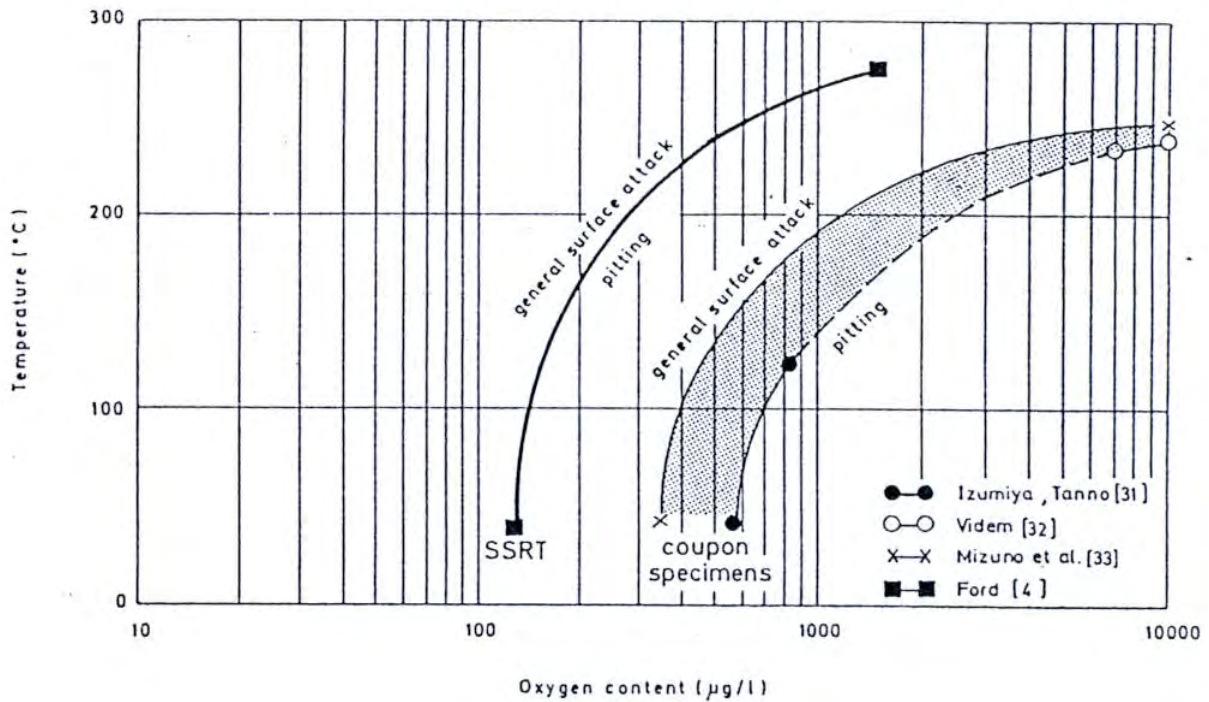
Figure 76: Effect of DO content, temperature and strain rate on pitting in LAS [6, 7, 15].

9 Adequacy/Conservatism of Codes/DLs with Respect to EAC

9.1 BWRVIP-60 and VGB SCC Disposition Lines

Careful re-analysis of older data, as well as recently performed, well-qualified experiments at MPA Stuttgart [33], at PSI [34 – 36] and in the context of European Round Robin tests [76, 160, 161], as well as reactor site testing by ABB [2, 4] and GE [170] have shown very low susceptibility to SCC crack growth under static loading conditions in oxygenated high-purity HT water/BWR environments at temperatures around 288 °C up to high K_I values of 50 to 60 MPa·m$^{1/2}$. Based on these test results and other well-qualified data for simulated BWR environment [33 – 36, 76, 128, 160, 161, 170, 181], DLs for SCC crack growth in C & LAS during BWR power operation were proposed by an international group of experts working within the framework of the EPRI BWRVIP project and accepted by the US Nuclear Regulatory Commission (NRC) as an interim position (Figure 77) [170, 182].
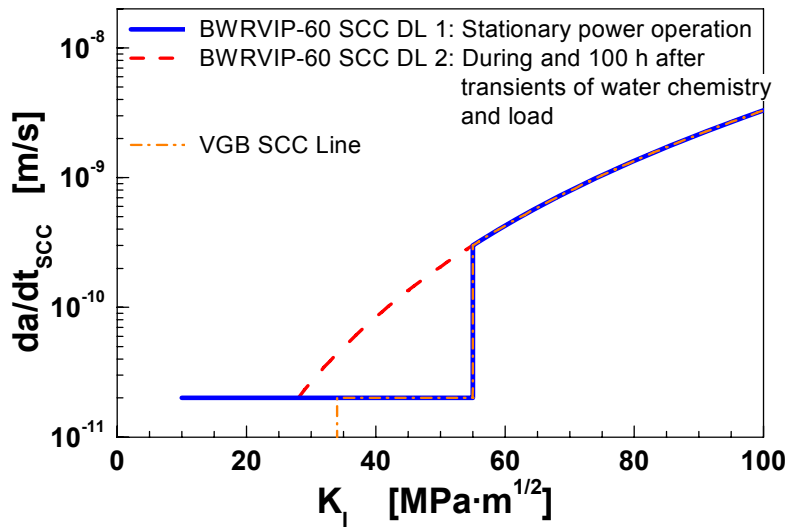
Figure 77: BWRVIP-60 [170, 183] and VGB [183] SCC DLs for C & LAS in BWR environment.

The BWRVIP-60 SCC DL 1 applies to crack growth in LAS under static loading and transient-free, stationary BWR/NWC or HWC power operation conditions. The BWRVIP-60 SCC DL 2, on the other hand, may be used for estimating SCC crack growth during and 100 h after transients in water chemistry (> EPRI action level 1 limit of EPRI BWR water chemistry guidelines, see Table 8) or load transients not covered by fatigue evaluation procedures. VGB has suggested a modified curve based on the BWRVIP-60 SCC DL 1, but which includes a K_{ISCC} threshold of 34 MPa·m$^{1/2}$ [183]. This threshold was derived from SRL tests with pre-cracked specimens with high sulphur RPV steels under aggressive environmental conditions (8 ppm DO, 65 ppb SO_4^{2-}) and different loading rates at PSI [28, 35, 128], where SICC initiation has only been observed above this value in this kind of experiment.

Control Parameter	Action Level 1	Action Level 2	Action Level 3
Conductivity [µS/cm]	> 0.3	> 1.0	> 5.0
Sulphate [ppb]	> 5	> 20	> 100
Chloride [ppb]	> 5	> 20	> 100

Table 8: Summary of action levels for reactor water during stationary BWR power operation from EPRI BWR water chemistry guidelines [184, 185]. Apart from action level 2 for HWC, which is 50 ppb, the Swedish guidelines [186] are identical to those of EPRI.

The conservative character of the first DL for SCC crack growth in LAS has been confirmed by several independent studies [32 – 36, 181] for 270 to 288 °C and RPV base (≤ 0.02 wt.% S) and weld filler/HAZ materials (Vickers hardness < 350 HV5) if the water chemistry is maintained within current BWR/NWC operational practice (< EPRI action level 1) (see Figure 44 in Section 6.1.1) and K_I value is below 60 MPa·m$^{1/2}$. Even above 60 MPa·m$^{1/2}$, most test results, in particular with low and medium sulphur RPV steels, were still below this curve as long as gross ligament yielding was avoided. The conservative nature of the approach was further confirmed by tests with PPU, where cessation of SCC was observed for long hold times (> 5 – 20 h) at constant load (see Figure 46 in Section 6.1.2) [36, 76, 128, 181]. Preliminary results indicated, however, that "Line 1" may be slightly exceeded at intermediate temperatures (180 – 270 °C) in RPV materials which show a distinct susceptibility to DSA (Figure 45) [36, 128, 139, 163]. Furthermore, sustained SCC with CGR significantly above "Line 1" was observed at 288 °C – not unexpectedly – when excessive hardness (> 350 HV5) (e.g., in bad weld HAZs) was present in the steel [36, 130], in particular in combination with a high steel sulphur content (Figure 78). Under reducing PWR or BWR/HWC (Figure 79) conditions no SCC crack growth was observed up to very high K_I values near to 100 MPa·m$^{1/2}$ or to K_{IJ} [9, 162].
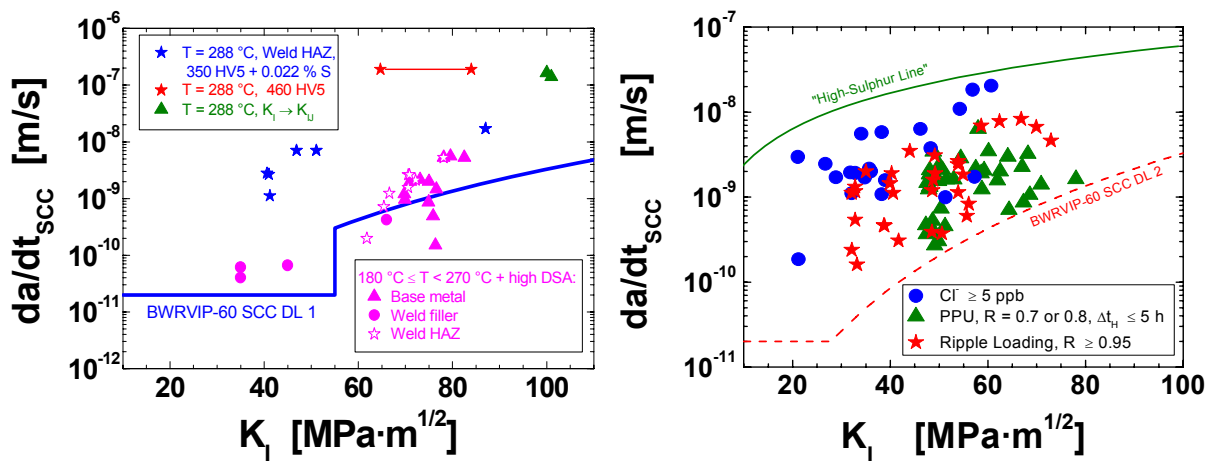
Figure 78: Test results [36, 128] with SCC CGRs above the BWRVIP-60 SCC DLs 1 and 2.
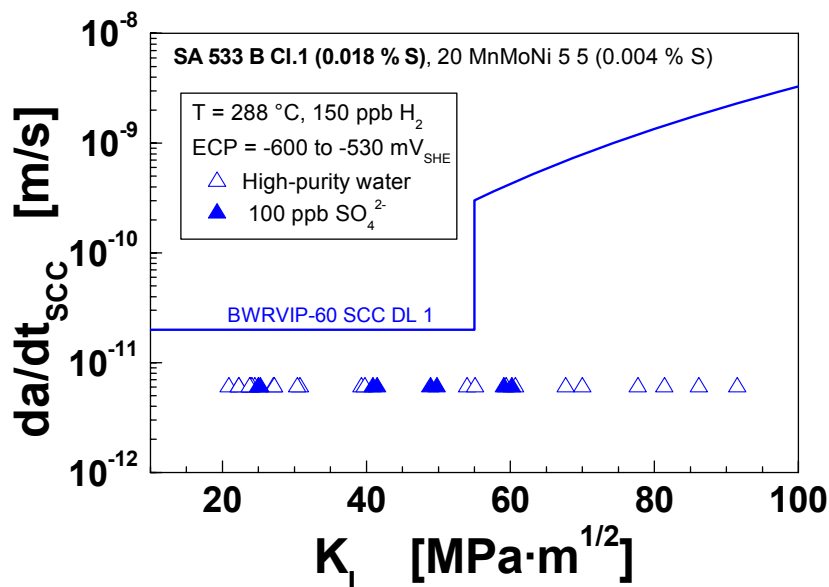
Figure 79: Comparison of SCC CGR under BWR/HWC conditions with BWRVIP-60 SCC DL 1.

Recent results revealed that the BWRVIP-60 SCC DL 2 may be significantly exceeded for the case of ripple loading (R > 0.95) [36, 128] (Figures 48 and 78) or with chloride transients (≥ EPRI action level 1 limit) [36, 67 – 69, 128] (Figures 16b and 78), even at fairly low stress intensity values around 20 to 30 MPa·m$^{1/2}$. After severe (≥ 20 ppb) and prolonged (≥ 100 h) chloride transients, sustained SCC with CGRs above the "Line 2" was also observed in preliminary tests for a significantly longer time interval than the 100 h period specified in BWRVIP-60 [36, 67 – 69, 128] in case of highly oxidizing conditions (ECP ≥ 50 mV$_{SHE}$). On the other hand, "Line 2" seemed to conservatively cover even very severe sulphate transients relevantly above the EPRI action level 3 values in both oxygenated and hydrogenated HT water (Figures 16a and 79) [36, 67 – 69, 76].

Laboratory experience has thus shown that fast SCC can only occur under some very specific conditions, which usually appear atypical for current BWR power operation practice or properly fabricated and heat-treated modern C & LAS components. Combinations of several of the following unfavourable factors can lead to sustained SCC with CGR above the BWRVIP-60 SCC DLs [16, 33 – 36, 67 – 69, 76, 130 – 132, 181 – 183]:

- A high corrosion potential ECP > +100 mV$_{SHE}$/high DO content (>> 200 ppb) and quasi-stagnant flow conditions.
- Cl$^-$ > EPRI action level 1 limit, SO$_4^{2-}$ >> EPRI action level 3 limit.
- A high steel sulphur content (> 0.020 wt.% S), in particular in combination with S-segregation zones.
- Intermediate temperatures (180 – 270 °C) in connection with distinct DSA susceptibility.
- A high hardness/YS level (> 350 HV5, YS > 800 MPa), e.g., in bad weld HAZs, in particular in conjunction with a high steel sulphur content.
- Loading close to K$_{IJ}$ or severe violation of SSY conditions.
- Ripple loading or relatively frequent PPU.

Under these unfavourable conditions, SCC CGRs can achieve rather high values, even up to a few m/year. The high-sulphur SCC line of the GE model [16, 156] gives a good estimate of the upper bound SCC CGR under such parameter combinations. Otherwise, the BWRVIP-60 SCC DL 1 is conservative and adequate for the RPV during transient-free, steady-state BWR power operation at temperatures in the range from 270 to 290 °C. Some areas of potential concern remain to be evaluated, such as the RPV feedwater nozzle and feedwater piping systems with lower operating temperatures (200 to 270 °C) together with the possible occurrence of small load fluctuations (→ ripple loading) and the case of chloride water chemistry transients.

9.2 ASME III Design Curves

9.2.1 Fatigue Design and ASME III Design Curves

C & LAS primary pressure-boundary components may (temporarily) be subjected to relevant fatigue loading, in particular during specific plant transients with pressure and temperature changes or with thermal stratification/striping. These phases are usually interrupted by long periods of stationary power operation, where pure static loading conditions prevail. Design against fatigue usually relies on the use of the ASME III design fatigue curves and endurance limits (derived mainly from strain-controlled LCF tests with small specimen in air), which do not explicitly consider corrosive effect of the specific environment, although the degree of included conservatism in the fatigue analysis may often offset this factor to a certain extent. [31]

Fatigue life in conventional fatigue design has been defined as the number of cycles required to form a fatigue crack, which can be detected by ND examinations during periodic in-service inspection (typically 5 mm long and 2 mm deep). Fatigue life can be divided into two stages: initiation, expressed as the cycles required forming microcracks on the surface; and propagation, expressed as cycles required to propagate the surface cracks to engineering size. During cyclic loading of smooth test specimens, surface cracks 10 μm or longer form quite early in life (i.e., < 10 % of life) at surface irregularities or discontinuities either already in existence or produced by slip bands, grain boundaries, second-phase particles, etc. [187, 188] Consequently, fatigue life may be considered to be composed entirely of propagation of cracks from 10 μm to few mm long. [31]

Cyclic loadings on a structural component occur because of changes in mechanical and thermal loadings as the system goes from one load set (e.g., pressure, temperature, moment, and force loading) to another. For each load set, an individual fatigue usage factor is determined by the ratio of the number of cycles anticipated during the lifetime of the component to the allowable cycles. Figures I-9.1 through I-9.6 of Appendix I, Section III of the ASME Boiler and Pressure Vessel Code specify fatigue design curves that define the allowable number of cycles as a function of applied stress amplitude. The cumulative usage factor (CUF) is the sum of the individual usage factors, and the ASME Code Section III requires that the CUF at each location must not exceed 1.

The ASME Code fatigue design curves, given in Appendix I of Section III, are based on strain-controlled tests of small polished specimens at room temperature in air. The design curves have been developed from the best-fit curves to the experimental fatigue-strain vs. life (ε–N) data that are expressed in terms of the Langer equation (9) of the form

$$\varepsilon_a = A_1 \cdot (N)^{-n_1} + A_2 \qquad (9)$$

where ε_a is the applied strain amplitude, N is the fatigue life, and A_1, A_2, and n_1 are coefficients of the model. Equation (9) may be written in terms of stress amplitude S_a instead of ε_a. The stress amplitude is the product of ε_a and elastic modulus E, i.e., $S_a = E \cdot \varepsilon_a$. The Code fatigue design curves are obtained from the best-fit curves of the experimental data by first adjusting for the effects of mean stress on fatigue life (according to Goodman) and then reducing the fatigue life at each point on the adjusted curve by a factor of 2 on strain (or stress) or 20 on cycles, whichever is more conservative.

The factors of 2 and 20 were intended to account for data scatter (including material variability) and differences in surface condition and size between the test specimens and actual components. The factors are not safety margins but rather adjustment factors that should be applied to the small-specimen data to obtain reasonable estimates of the lives of actual reactor components. They do not account for environmental effects in HT water!

Existing fatigue ε-N data illustrate potentially significant effects of LWR coolant environments on the fatigue resistance of C & LAS [29 – 31, 189] as well as austenitic stainless steels (SSs) (Figure 80) [31, 190]. Under certain environmental and loading conditions, fatigue lives of C & LAS can be a factor of 100 lower in the coolant environment than in air [191, 192]. Therefore, the margins in the ASME Code may be less conservative than originally intended.
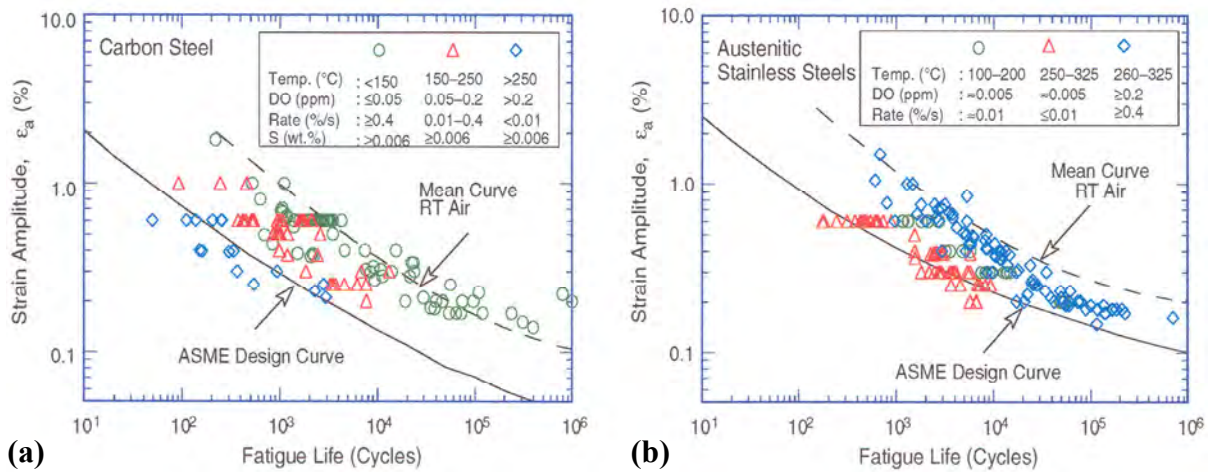
Figure 80: Fatigue ε-N data in water for carbon steels (a) and austenitic stainless steels (b) in water [31].

Extended research programmes have been performed in US at ANL and in Japan in the last two decades to study environmental effects on fatigue live. Based on these investigations, two approaches have been proposed for incorporating the environmental effects into ASME Section III fatigue evaluations for primary pressure-boundary components in operating nuclear power plants: (a) develop new fatigue design curves for LWR applications, or (b) use an environmental correction factor to account for the effects of the coolant environment. In the first approach, environmentally adjusted fatigue design curves are developed from fits to the experimental data in LWR environments following the same procedures used to develop the current fatigue design curves of the ASME Code [192 – 194]. The second approach, proposed by Higuchi and Iida [191], considers the effects of reactor coolant environments on fatigue life in terms of an environmental correction factor F_{en}, which is the ratio of fatigue life in air at room temperature to that in water under reactor operating conditions. To incorporate environmental effects into fatigue evaluations, the fatigue usage factor for a specific load set, based on the current Code design curves, is multiplied by the environmental correction factor [192 – 195].

Although the possibility of environmental effects on fatigue lives is undisputed, there has been an ongoing debate for many years as to whether such proposal should be included to ASME III or not. The industry has often taken the position that the current fatigue evaluation procedures contain a large degree of conservatism, which even covers possible environmental effects with sufficient margins.

In the next sections, environmental effects on fatigue live of C & LAS are briefly summarized followed by a short discussion of the major approaches for incorporating environmental effects to ASME III. Finally, the safety margins in ASME Code fatigue design considering potential environmental effects are critically reviewed.

9.2.2   *Environmental Effects on Fatigue Live of C & LAS*

In air, the fatigue lives of C & LAS depend on steel type, temperature, orientation (rolling or transverse), and strain rate. The fatigue life of carbon steels is a factor of ≈1.5 lower than that of LAS. For both steels, life is decreased by a factor of ≈1.5 when temperature is increased from room temperature to 288°C. In the temperature range of dynamic strain aging (100 – 350 °C), these steels show negative sensitivity to strain rate, i.e., cyclic stresses increase with decreasing strain rate. The effect of strain rate on fatigue life in air is not clear. For some heats, life may be unaffected or strongly decrease, but may increase for other heats.

The ASME mean curve for LAS is in good agreement with the experimental data. The corresponding curve for carbon steels is somewhat conservative, especially at strain amplitudes of < 0.2%. [29 – 31, 189 – 192]

The fatigue lives of C & LAS are reduced in LWR environments. Although the microstructures and cyclic–hardening behaviour of C & LAS differ significantly, the effects of the environment on the fatigue life of these steels are very similar. The magnitude of the reduction depends on temperature, strain rate, DO level in water, and S content of the steel. The decrease is significant only when four conditions are satisfied simultaneously, i.e., when the strain amplitude, temperature, and DO in water are above certain threshold values, and the strain rate is below a threshold value. For both steels, only a moderate decrease in life (by a factor of < 2) is observed when any one of the threshold conditions is not satisfied. The S content in the steel is also important; its effect on life appears to depend on the DO level in water. The threshold values and the effects of the critical parameters on fatigue life are summarized below. [29 – 31, 189 – 192]

Strain: The results indicate that environmental effects on fatigue life are significant primarily during the tensile-loading cycle. A minimum total applied strain is required above which environmental effects on life are significant [187, 189, 193]. Even within a given loading cycle, environmental effects are significant at strain levels greater than this threshold value. Limited data suggest that the threshold value is ≈ 20 % higher than the fatigue limit for the steel. Also (relatively short) hold periods during peak tensile or compressive strain have no effect on the fatigue life of the steels in high-purity water [187], but this might be different for very long hold periods (e.g., oxide-induced crack closure during the decreasing phase of the stress cycle) or in case of chloride, when SCC may occur.

Strain Rate: When all other threshold conditions are satisfied, fatigue life decreases according to a power law relationship with decreasing strain rate below 10^{-2} s^{-1} [191, 196]. The effect of strain rate usually saturates at ≈ 10^{-5} s^{-1} (Figure 81) [187, 189, 193], but in some other investigations in the DSA temperature range fatigue live did not saturate and further decreased monotonically down to the lowest tested strain rate of 10^{-7} s^{-1} [75]. When any one of the threshold conditions is not satisfied, e.g., DO < 0.04 ppm or temperature < 150 °C, the effects of strain rate are consistent with those observed in air. As a result, heats sensitive to strain rate in air show a decrease in life in water, although the decreases are smaller than those observed when the threshold conditions are met.

(a)　　　　　　　　　　　　　　　　　　　(b)
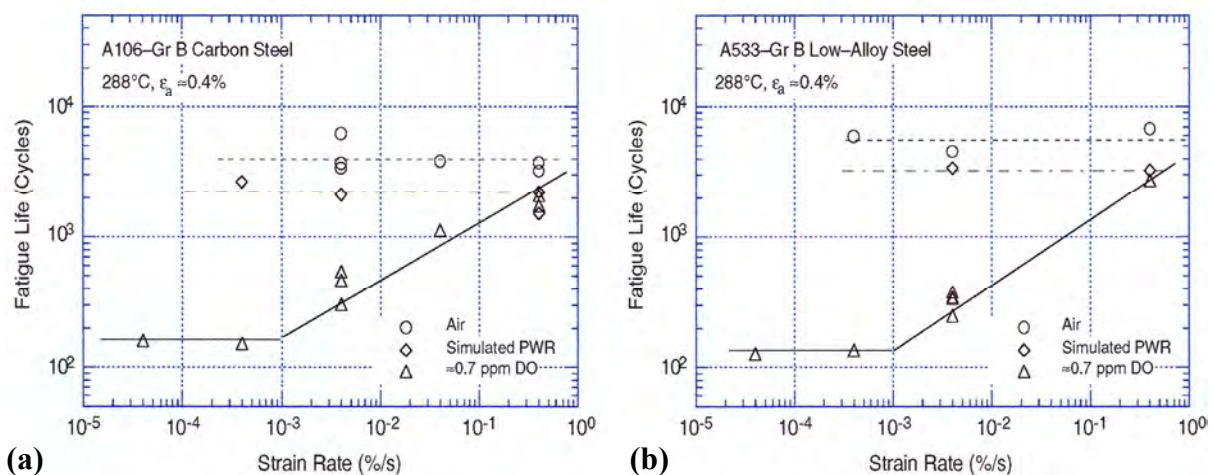
Figure 81: Dependence of fatigue lives of (a) carbon and (b) low-alloy steels on strain rate in HT water [31].

85

Temperature: (Limited) experimental data indicate a threshold temperature of 150°C, below which environmental effects on life either do not occur or are insignificant. When other threshold conditions are satisfied, fatigue life decreases linearly with temperature above 150°C and up to 320°C [191, 196, 197].

There is only very limited testing under non-isothermal conditions, which indicate that the fatigue life of non-isothermal tests were comparable to that of isothermal tests with an average temperature of thermal cycling (Figure 82). The fatigue life under in-phase condition was comparable to that of out-of-phase cycling in most tests, although one would rather expect a longer life for out-of phase tests [52, 53]. For service histories involving variable loading conditions, service temperature may be represented by the average of the minimum temperature or 150°C, whichever is higher, and the maximum temperature [52, 53].
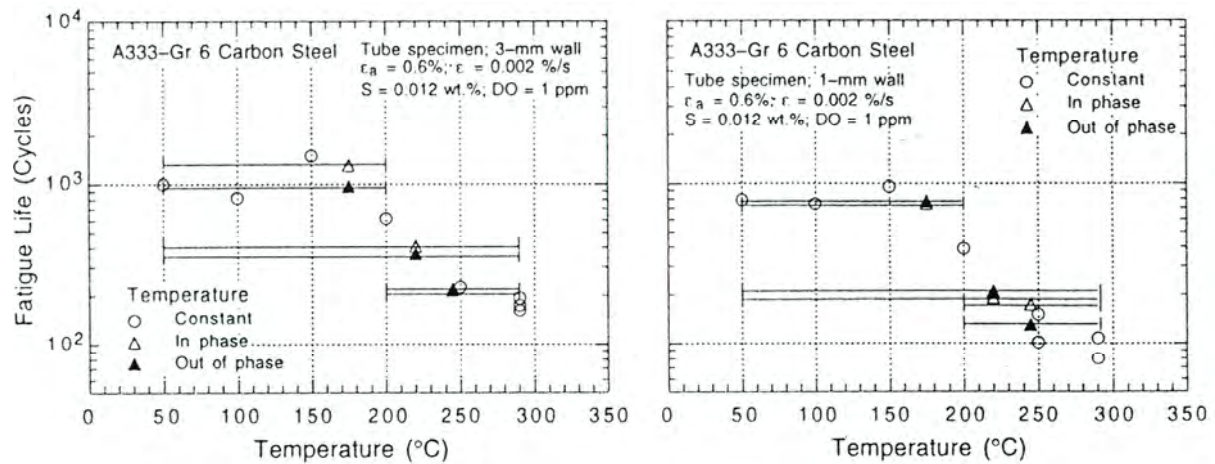
Figure 82: Reasonable correlation of LCF lives in tests with varying temperature and isothermal experiments at the average temperature of thermal cycling [52, 53].

The role of DSA in temperature effects on LCF live is not clear, but in the DSA temperature/strain rate range it could result in a further reduction of LCF live compared to a non-susceptible material with comparable sulphur content.

Dissolved Oxygen in Water: When the other threshold conditions are satisfied, fatigue life decreases with DO above 0.04 ppm (Figure 83); the effect saturates at ≈ 0.5 ppm DO. Only a moderate decrease in life, i.e., a factor of < 2, is observed at DO levels below 0.04 ppm. [196, 197]
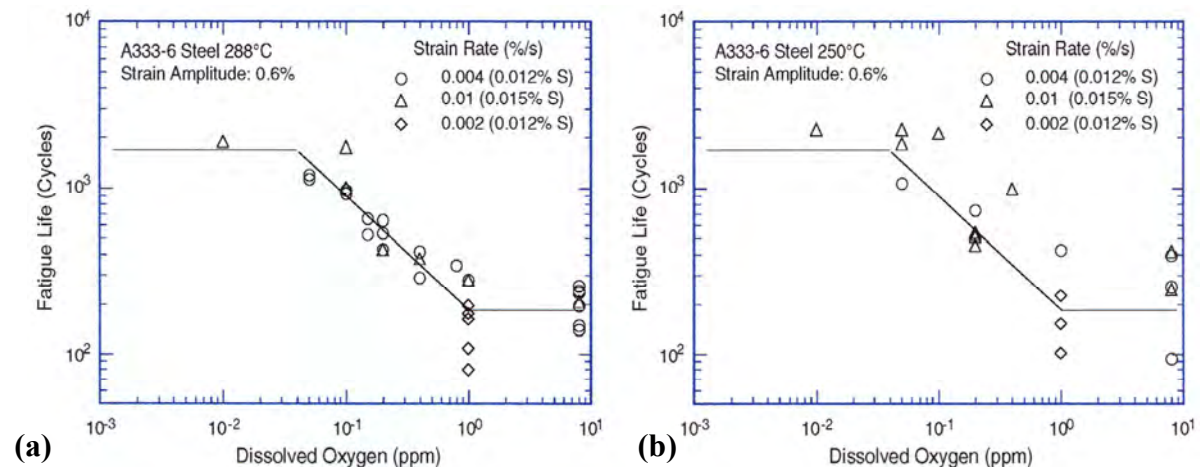
Figure 83: Dependence of fatigue lives on dissolved oxygen of carbon steels at 288 °C (a) and 250 °C (b) [31].

Water Conductivity/Anionic Impurity Concentration: The fatigue life of C & LAS decreases when the conductivity (or specific anionic impurities like chloride and sulphate) is increased [72 – 75]. The fatigue life of WB36 steel at 177 °C in water with ≈ 8 ppm DO decreased by a factor of ≈ 6 when the conductivity of water was increased from 0.06 to 0.5 μS/cm (Figure 84a) [73]. A similar behaviour has also been observed in studies on initiation of short cracks [74]. Limited testing using step changes in environmental conditions indicates that even a few cycles under aggressive water chemistry may have a disproportional strong effect on reducing fatigue live (Figure 84b) [72, 75].
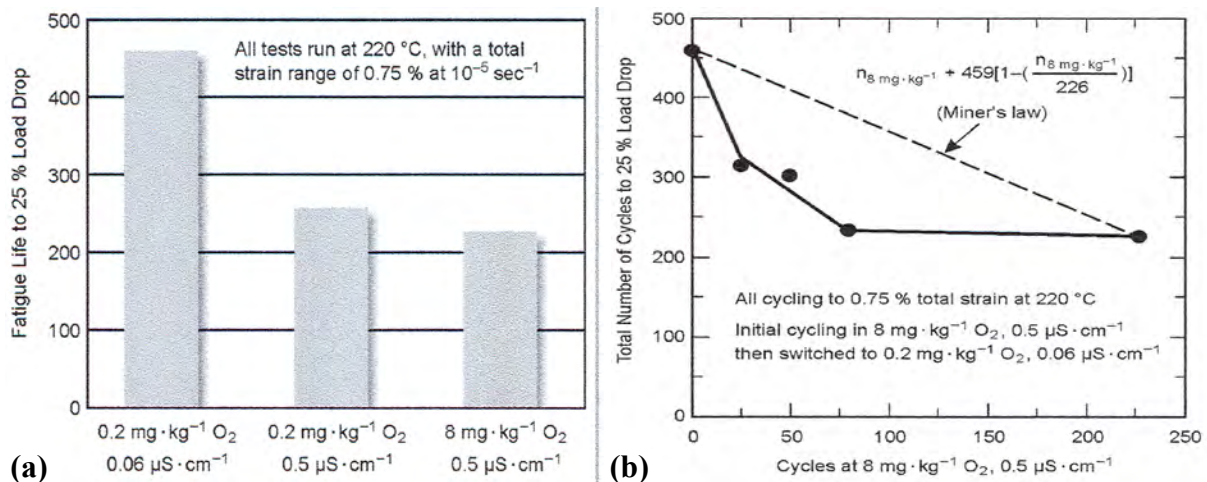
Figure 84: Importance of conductivity (concentration of sulphate) on the LCF behaviour of LAS in oxygenated HT water. (a) Comparison of effects of oxygen and conductivity in normal LCF tests. (b) Disproportionate effect of initial cycling at high conductivity on LCF life [72, 75].

Although BWR normally operate with high-purity water, during start-up increased levels of chloride and sulphate are usually observed under conditions, where relevant thermo-mechanical loading or stratification in horizontal piping may occur. Many early field EAC cracking incidents involved stagnant conditions, where the real conductivity of the water within the porous oxide/hydroxide layer immediately adjacent to the surface of the affected component might be expected to be much higher. Significantly, cracking has occurred in recent years in Germany in BWR feedwater lines, although the purity of the <u>bulk</u> medium was exceptionally high. Geometrically, however, it was clearly associated with areas in the lower part of horizontal sections of piping where corrosion products (primarily rust) and pitting had formed from water residues during prior (prolonged) shut-down. Thus it is possible that a local, "micro-environment" of much higher conductivity had existed during plant start-up (re-dissolution of precipitates), i.e., at the time when significant, dynamic straining at welds in the piping also occurred. [72]

Sulphur Content of Steel: The effect of S content on fatigue life appears to depend on the DO content of the water. When the threshold conditions are satisfied, the fatigue life decreases with increasing S content for DO levels ≤ 1.0 ppm. Limited data suggest that environmental effects on life saturate at an S content of ≈ 0.015 wt.% [187]. For DO levels >1.0 ppm, fatigue life seems to be relatively insensitive to S content in the range of 0.002 to 0.015 wt.% [195].

Flow Rate: Most tests were performed under quasi-stagnant conditions, whereas turbulent flow conditions prevail at most component locations. Recent data indicate that, under the environmental conditions typical of operating BWRs, environmental effects on the fatigue life

of carbon steels are a factor of at least 2 higher at high flow rates (7 m/s) than at 0.3 m/s or lower [84, 198, 199]. The beneficial effects of increased flow rate is small under mild conditions, but are greater for high-S steels and at low strain and strain rates, where environmental effects on fatigue live are more pronounced [198, 199] A factor of 2 increase in fatigue life at 240 °C has also been observed in component tests at KWU (Kraftwerk Union) laboratories using 180 ° bends of carbon steel tubing (0.025 wt.% S) where internal flow rates of up to 0.6 m/s were established [84]. For most plant transients environmental effects are not particularly severe, therefore mitigation effect of high flow rate is not very pronounced.

Effect of Surface Finish/Conditions and of Pitting: Although it is well known, that the surface state (roughness, residual stress, cold-worked surface layer, pitting (e.g., during shutdown periods), stillstand corrosion, oxide film, etc.) can have strong effect on fatigue initiation, in particular at small strain amplitudes, this aspect has not yet been studied much. The fatigue life of rough C & LAS is a factor of 3 lower in air compared with smooth specimens. In low-DO water the fatigue life of rough specimens is slightly lower than that of smooth specimens and in high-DO water, it is the same (Figure 85) [31]. The effect of pitting is not clear. Some investigations revealed a relevant reduction of fatigue live in pre-pitted specimens [75], others showed no significant effects [29], but this may be strongly dependent on strain amplitudes and other system conditions.
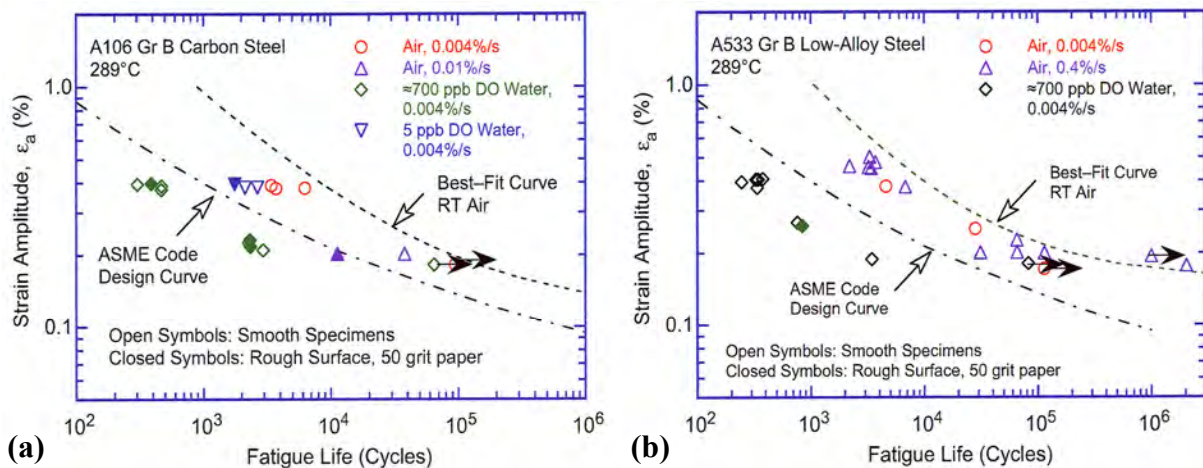
Figure 85: Effect of surface roughness on fatigue life of A106-Gr.B carbon steel (a) and A533 LAS (b) in air and high-purity water at 289 °C [204].

9.2.3 Proposals for Incorporating Environmental Effects

Two methods have been proposed for incorporating the effects of LWR coolant environments into the ASME Section III fatigue evaluations. In one case, new environmentally adjusted fatigue design curves are developed [187, 190, 193, 194]; in the other, fatigue life correction factors F_{en} are used to adjust the fatigue usage values for environmental effects [190, 195, 200, 201].

Fatigue Design Curves: Fatigue design curves for each given system conditions (i.e., combination of steel sulphur content, temperature, DO and strain rate) have been obtained from statistical models represented by equations (9) and (10) for C & LAS.

$$\ln(N) = B_1 - B_2 \cdot \ln(\varepsilon_a - B_3) + B_4 \cdot S^* \cdot T^* \cdot O^* \cdot d\varepsilon/dt^* \qquad (10)$$

The exact values of the parameters S^*, T^*, O^* and $d\varepsilon/dt^*$ depend on the steel sulphur content, temperature, DO and strain rate. To be consistent with the current ASME Code philosophy, the best-fit curves were first adjusted for the effect of mean stress by using the modi-

fied Goodman relationship. The adjusted curves were then decreased by a factor of 2 on stress and 20 on cycles to obtain design curves. Examples of fatigue design curves for LAS in LWR environments are shown in Figure 86.
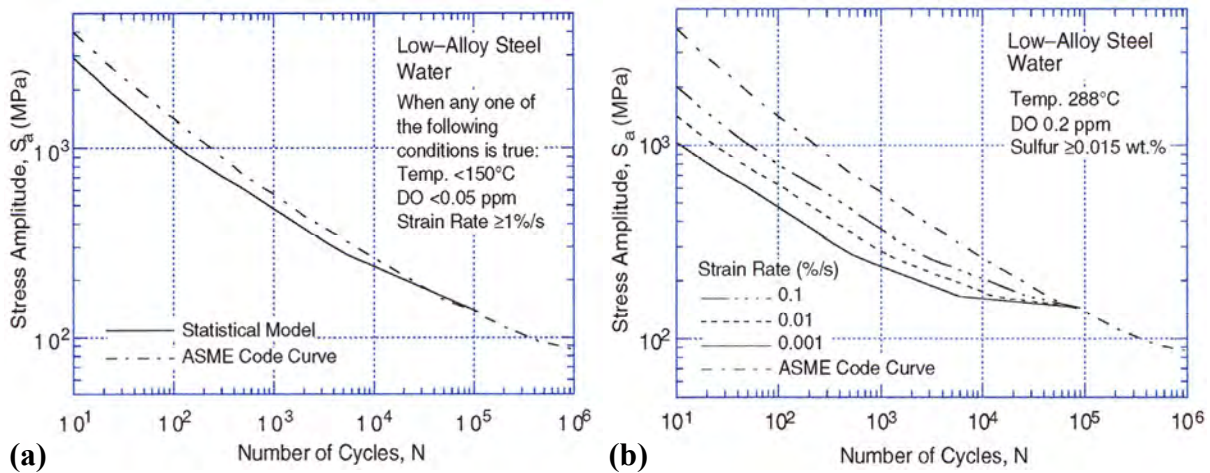
Figure 86: Examples of fatigue design curves developed from the statistical model for LAS in LWR environments under service conditions where one or more critical threshold values are not satisfied (a), and all threshold values are satisfied (b) [202].

For the environmentally adjusted fatigue design curves a minimum threshold strain is defined, below which environmental effects are modest. Based on the experimental data, the pressure vessel research council (PVRC) steering committee for cyclic life environmental effects (CLEE) [201] has proposed a linear variation for the threshold strain; i.e., a lower strain amplitude below which environmental effects are insignificant, a slightly higher strain amplitude above which environmental effects decrease fatigue life, and a linear variation of environmental effects between the two values. The two strain amplitudes are 0.07 and 0.08 % for C & LAS. These threshold values were used to develop the curves in Figure 86.

Fatigue Life Correction Factor: The effects of reactor coolant environments on fatigue life have also been expressed in terms of a fatigue life correction factor F_{en}, which is defined as the ratio of life in air at room temperature to that in water at the service temperature. Values of Fen can be obtained from the same statistical model, where

$$\ln(F_{en}) = \ln(N_{RT,air}) - \ln(N_{water}). \tag{11}$$

A strain threshold is also defined, below which environmental effects are modest; the values are the same as those used in developing the new fatigue design curves. To incorporate environmental effects into a Section III fatigue evaluation, the fatigue usage for a specific stress cycle based on the current Code fatigue design curve is multiplied by F_{en}.

The fatigue life correction factors for C & LAS developed by the ANL- (Chopra) and Japanese-model (Higuchi) are given in Table 9 [203]. Other models have been suggested by GE and EPRI [201, 202]. All models basically show similar trends [200, 203] and only differ in minor aspects (see also Figure 87).

In most plant transients both, strain rate, temperature, and sometimes water chemistry are continuously changing. The definition of these parameters for the individual cycles, as well as cycle definition and counting may have a strong impact on the calculated fatigue live. Furthermore, for many transients these parameters are not exactly known. Several proposals on parameter definitions or such transients have been defined [203] and were tested, e.g., under non-isothermal conditions [52, 53].

Latest Japanese Model (by Higuchi)		US ANL Model (by Chopra)	
(Carbon and low-alloy steels)		(Carbon steel)	$\ln(F_{en}) = 0.554 - 0.101\ S^*T^*O^*\varepsilon'^*$
$\ln(F_{en}) = -(0.199\ T^*O^* + 0.112)\ S^*\varepsilon'^*$		(Low-alloy steel)	$\ln(F_{en}) = 0.898 - 0.101\ S^*T^*O^*\varepsilon'^*$
$\varepsilon'^* = 0$	($\varepsilon' > 1.0$ %/s)	$S^* = 0.015$	(DO > 1 mg $\cdot$ kg^{-1} or S > 0.015 %)
$\varepsilon'^* = \ln(\varepsilon')$	($1.0 \geq \varepsilon' \geq 0.0004$ %/s)	$S^* = S$	(DO $\leq$ 1 mg $\cdot$ kg^{-1} & S = 0.015 %)
$\varepsilon'^* = \ln(0.0004)$	($\varepsilon' < 0.0004$ %/s)	$T^* = 0$	(T < 150 °C)
$T^* = 0.00531T - 0.7396$	(T $\geq$ 180 °C)	$T^* = T - 150$	($150 \leq T \leq 350$ °C)
$T^* = 0.216$	(T < 180 °C)	$O^* = O$	(DO < 0.04 mg $\cdot$ kg^{-1})
$O^* = \ln(DO/0.03)$	($0.03 \leq DO \leq 0.5$ mg $\cdot$ kg^{-1})	$O^* = \ln(DO/0.04)$	($0.04 \leq DO \leq 0.5$ mg $\cdot$ kg^{-1})
$O^* = 0$	(DO < 0.03 mg $\cdot$ kg^{-1})	$O^* = \ln(12.5)$	(DO > 0.5 mg $\cdot$ kg^{-1})
$O^* = \ln(0.5/0.3)$	(DO < 0.5 mg $\cdot$ kg^{-1})	$\varepsilon'^* = 0$	($\varepsilon' > 1$ %/s)
$S^* = 17.23\ S + 0.777$		$\varepsilon'^* = \ln(\varepsilon')$	($0.001 \leq \varepsilon' \leq 1$ %/s)
$F_{en} = 1.0$	($\varepsilon_a \leq 0.042$ %)	$\varepsilon'^* = \ln(0.001)$	($\varepsilon' < 0.0011$ %/s)
(ε_a of 0.042 % is the same strain amplitude at 10^6 cycles in the design curve)		$F_{en} = 1.0$	($\varepsilon_a \leq 0.07$ %)

Table 9: Summary of the latest Japanese and ANL Fen calculation [203].
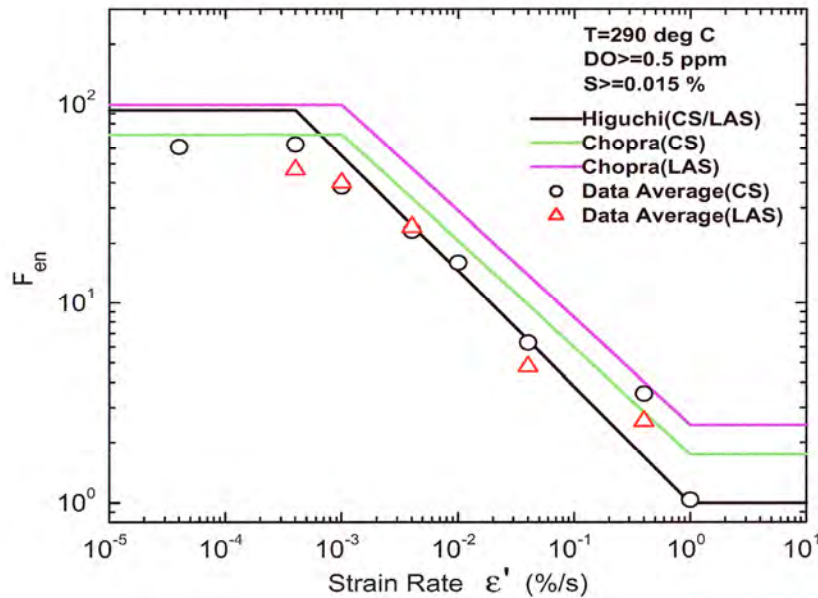
Figure 87: Similar strain rate effects on Fen in latest Japanese and ANL model [203].

9.2.4 *Margins in ASME Code Fatigue Design Curves*

Conservatism in the ASME Code fatigue evaluations may arise from (a) the fatigue evaluation procedures and/or (b) the fatigue design curves. The overall conservatism in ASME Code fatigue evaluations has been demonstrated in fatigue tests on components in air, which showed that the design margin for cracking exceeds 20, and for most of the components it is greater than 100, although for welds it may be far below 20. However some isolated other studies also indicate that the Code fatigue design procedures do not always ensure large margins of safety (Figure 88). [31]

The sources of conservatism in the procedures include the use of design transients that are significantly more severe than those experienced in service, conservative grouping of transients, and use of simplified elastic-plastic analyses that result in higher stresses/strains [31, 204]. With respect to real transients, the significantly higher strains of design transients usually compensate the smaller environmental reduction of fatigue live because of the higher

strain rates. However, the ASME Code permits new and improved approaches to fatigue evaluations (e.g., finite-element analyses, fatigue monitoring, and improved plastification factor K_e factors) that can significantly decrease the conservatism in the current fatigue evaluation procedures.
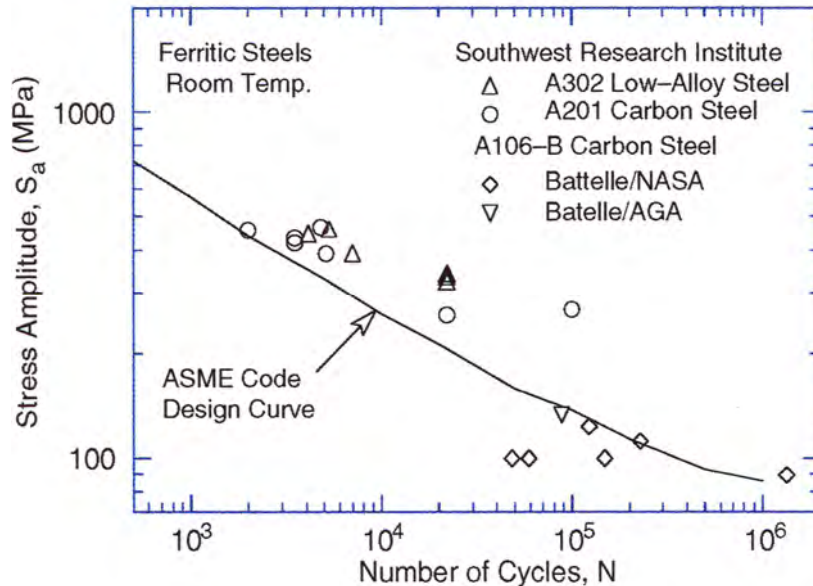
Figure 88: Fatigue data for C & LAS in component tests with no or very margins [31].

The design margins of 2 and 20 on stress and cycles in the ASME III design curve, respectively, were intended to cover the effects of variables that can influence fatigue life but were not investigated in the tests which provided the data for the curves. It is not clear whether the particular values of 2 and 20 that were chosen include possible conservatism. The contributions of four groups of variables, namely material variability and data scatter, size and geometry, surface finish, and loading sequence (Miner's rule; e.g.: The presence of a few cycles at high strain amplitude in a loading sequence causes the fatigue life at smaller strain amplitude to be significantly lower than that at constant amplitude loading), must be considered in developing the fatigue design curves that are applicable to components.

Data available in the literature have been reviewed by ANL to evaluate the margins on cycles and stress [31, 204]. The subfactors that are needed to account for the effects of various material, loading, and environmental variables on fatigue life are summarized in Table 10. These results in Table 10 suggest that the current ASME Code requirements of a factor of 2 on stress/strain and 20 on cycle to account for differences and uncertainties in fatigue life that are associated with material and loading conditions are quite reasonable (provided that components were fabricated and designed as required in the Codes), and do <u>not</u> contain excess conservatism that can be assumed to account for the effects of LWR environments. They thus provide appropriate margins for the development of design curves from mean data curves for small specimens in LWR environments. Therefore, in particular in the context of plant life extension, environmental effects should be incorporated into the current ASME III fatigue design procedure in an adequate way, otherwise, the current trend of applying improved and optimized fatigue evaluations approaches that can significantly decrease other sources of conservatism might result in a non-acceptable reduction of safety margins.

Parameter	Factor on Life (Air)	Factor on Life (Water) SS	Factor on Life (Water) CS/LAS	Factor on Strain
Material Variability & Experimental Scatter	2.0	3.0	3.0	1.2 – 1.7
Size Effect	1.4	1.4	1.4	1.25
Surface Finish	3.0	3.0	1.6	1.6
Loading History	1.5 – 2.5	1.5 – 2.5	1.5 – 2.5	1.3 – 1.6
Total Adjustment	12.5 – 21.0	19.0 – 31.0	10.0 – 17.0	1.6 – 1.7

Table 10: Factors on cycle and strain/stress, that have to be applied to mean ε-N curve to account for the effects of various parameters like material variability and surface finish, which are known to affect fatigue live [204].

9.3 ASME XI/Code Case N-643

9.3.1 *Current Status: ASME XI, Eason Proposal and PWR Code Case N-643*

The ASME BPV Code, Section XI, Appendix A, Article A-4300 contains a set of reference fatigue CGR (da/dN) curves for C & LAS in air ("air" curves) or in LWR reactor coolant environment ("wet" curves). The current ASME XI wet reference fatigue CGR curves (Figure 89) are based on lab data obtained prior to 1980. They depend explicitly on ΔK and R, but not on other variables that are known to be important, such as loading frequency (Figures 11 and 54), ECP/DO, or steel sulphur content. The same curves are used for different types of C & LAS and for BWR/NWC, BWR/HWC/NMCA and PWR primary or secondary side conditions. System conditions (or thresholds) where environmental effects on fatigue crack growth can be neglected or excluded are not defined in the present ASME Section XI Code.

In the meantime, several laboratories have conducted large testing programmes, including wide variation of controlled variables. Based on statistical analysis of the available laboratory database (PWR and BWR conditions), a proposal for new reference crack growth curves was made by Eason et al. [175, 176], taking into account the strong effect of strain rate/loading frequency (Figure 90). The BWR database for this proposal was relatively small and mainly based on tests with an ECP of $\leq +50$ mV$_{SHE}$, temperatures around 288 °C, rise times $\Delta t_R \leq$ 1000 s and base metal. There is still a lack of experimental data under BWR/HWC, at intermediate ECP (between BWR/NWC and PWR conditions) and for higher ECP values (characteristic, e.g., for the BWR/NWC RPV), low loading frequencies < 10^{-3} Hz, intermediate temperatures and weld filler/HAZ materials, as well as for very high load ratios R $\geq$ 0.95 and small ΔK (in particular close to EAC thresholds). This absence of data results in some uncertainty concerning the adequacy of the proposed reference curves for BWR/NWC and HWC conditions.
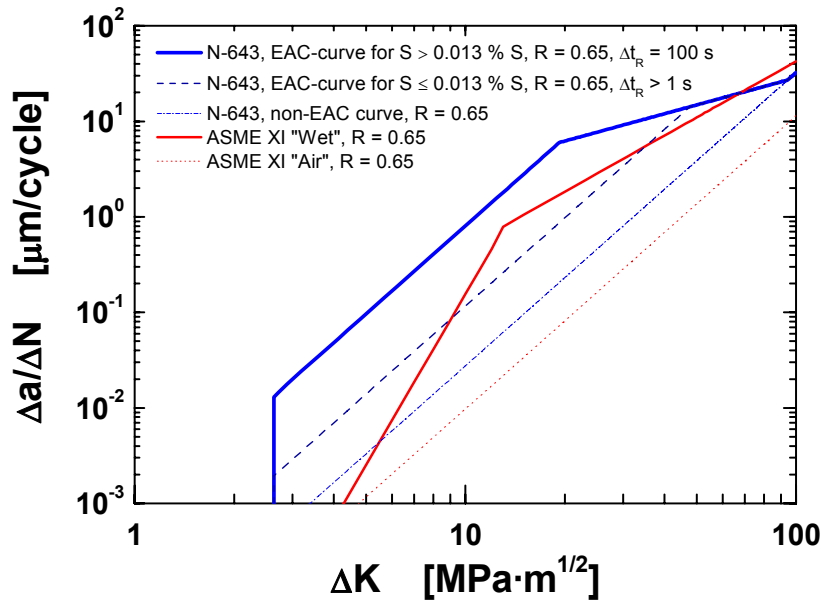
Figure 89: ASME XI air and wet curve and Code Case N-643 curves for high-(> 0.013 wt.% S) and low-sulphur (≤ 0.013 wt.% S) steels.
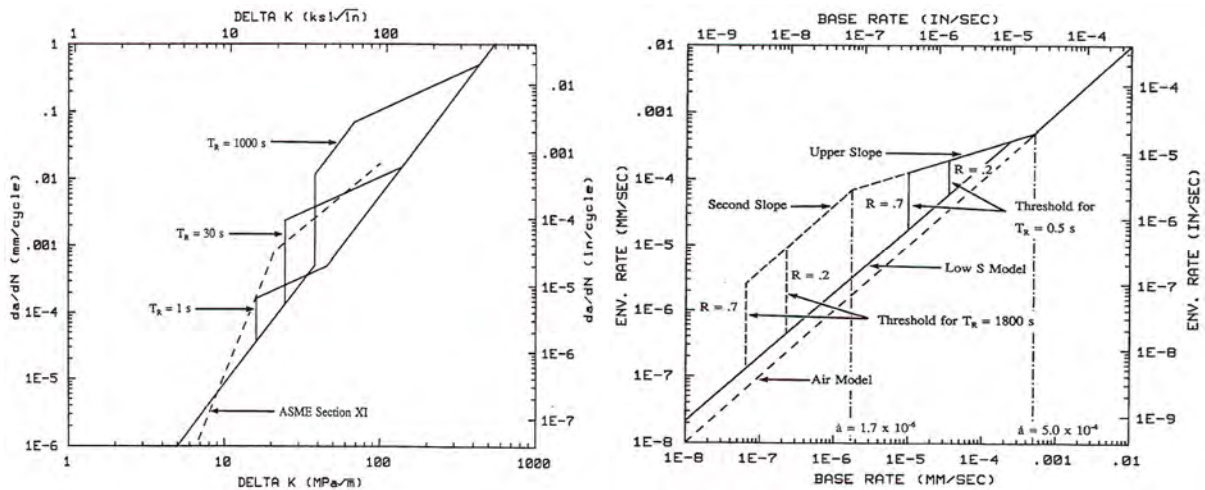
Figure 90: Eason model for CF in LAS in cycle-based and time-based from [175, 176].

Based on the EAC/air CGR curves developed by Eason [175, 176] and on the experimental work on threshold/susceptibility conditions for the onset/cessation of EAC crack growth by James [205] and Wire/Yin Li [206, 207], a new Code Case N-643 has been developed for fatigue crack growth in ferritic steels in <u>PWR</u> primary environments. This Code Case was approved in May 2000 and may be used as an alternative to the ASME XI wet reference fatigue CGR curves for this specific environment (Figure 89). This Code Case has been revised in 2003 to include new corrosion fatigue crack growth curves for low- and medium-sulphur steels (≤ 0.013 wt.% S) and to reduce sulphur threshold from 0.005 to 0.004 wt.% S, below which RPV steels are not susceptible to CF and the non-EAC curve may be applied [208]. The onset of EAC and the use of the corresponding EAC curves for high-sulphur (> 0.013 wt.% S) and low- and medium-sulphur steels (≤ 0.013 wt.% S) requires that both the incremental fatigue CGR da/dt and crack advance Δa have to simultaneously exceed critical values da/dt$_{crit}$ and Δa$_{crit}$, otherwise the non-EAC curve may be used. Depending on system conditions (fatigue CGR, crack advance and rise time of the load), the Code Case N-643 procedure predicts either lower or higher CGRs than the general ASME XI wet reference fatigue CGR curves. The main advantage of the new Code Case is that it contains criteria for the on-

set/cessation of EAC and that it considers frequency/loading-rate effects to a certain extent and therefore better reflects the experimentally observed cracking behaviour. These criteria (critical CGR and crack advance distance) are related to a critical sulphur-anion concentration in the crack-tip environment and there is both experimental and theoretical evidence for such behaviour [205]. There is no fundamental reason why this procedure could not be applied to BWR conditions, provided that appropriate criteria are experimentally developed and verified [205]. Based on the increasing number of BWRs operating with HWC (or HWC/NMCA), where lower EAC CGRs are anticipated, such an evaluation would appear justified.

9.3.2 *Assessment of the Fatigue CGR Curves in the Context of the Recent Test Result*

The adequacy of the current ASME XI wet reference fatigue CGR curves under PWR and BWR conditions has been evaluated for most combinations of loading, environmental and material parameters by several different laboratory investigations [5 – 13] and the observed trends were further supported by the predictions of the GE-model [16, 66, 114] (see Sections 6.3 and 10.6). Under PWR conditions, the curves were only exceeded under some very specific loading (e.g., frequencies around 10^{-3} to 10^{-2} Hz and very high ΔK) and material (high-sulphur steels) conditions. The same situation is expected for BWR/HWC conditions, although there is a lack of direct quantitative experimental data. Under BWR conditions (200 ppb DO), the curves were usually only exceeded either at low frequencies of 10^{-4} to 10^{-2} Hz and high ΔK or at high loading frequencies (e.g., $10^{-2} < \nu < 10$ Hz) and very small ΔK/high load ratios R. Above a loading frequency of 10^{-3} to 10^{-1} Hz, the CF crack growth behaviour of LAS with different sulphur contents was very similar under PWR and BWR conditions, therefore justifying one set of curves for all conditions in ASME XI. Under BWR conditions/in high-sulphur steels, a high-sulphur anion activity in the crack-tip environment, and therefore fast EAC, can be maintained down to significantly lower loading frequencies (10^{-4} to 10^{-2} Hz) than under PWR conditions/in low-sulphur steels. Above an upper critical frequency of approximately 10 Hz, and below the lower critical frequency ($\approx 10^{-4}$ to 10^{-2} Hz for BWR and 10^{-3} to 10^{-1} Hz for PWR conditions, depending on ECP, ΔK/R, steel sulphur content and temperature), no significant environmental acceleration of fatigue crack growth is observed. Based on these results, it was believed, that fast CF crack growth may not be sustained at loading frequencies $\leq \approx 10^{-4}$ Hz.

The most recent investigations [28, 51, 62, 76, 128] have been performed with higher ECP/DO (0 to +250 mV$_{SHE}$/0.4 to 8 ppm) levels than in most earlier lab experiments (0.2 or < 0.005 ppm DO). The increased oxygen (and sometimes conductivity) levels of these investigations were intended to simulate either a realistic ECP on the BWR RPV wall/feedwater nozzle, or the (local) conditions at some specific component locations/during special plant transients (piping with stagnant steam or non-degassed condensate, regions with possible shut-down corrosions, plant start-up, etc.). They may appear overly aggressive/conservative for many other LAS BWR pressure-boundary components (e.g., feedwater piping, piping carrying flowing steam) and operation conditions (stationary power operation, etc.). The CF CGRs $\Delta a/\Delta N_{EAC}$ in these fatigue tests under highly oxidizing, low-flow conditions significantly exceed the current ASME XI wet reference fatigue CGR curves (Figures 11 and 55) for loading frequencies < 10^{-2} Hz, $\Delta K \geq 2$ MPa·m$^{1/2}$ and temperatures > 150 °C in all investigated materials (base metal, weld filler, weld HAZ) for both low- and high-sulphur RPV steels, even in high-purity water ($\kappa < 0.06$ µS/cm). The excess difference to the ASME XI wet fatigue CGR curve increased with decreasing frequency, increasing load ratio and temperature with a maximum around 250 °C (Figures 11 and 55). Similarly, the proposed reference curves by Eason [175, 176] can be exceeded at low loading frequencies < 10^{-3} Hz for highly oxidizing (> 0 mV$_{SHE}$) and low-flow conditions at temperatures > 150 °C (Figure 91). All materials revealed quite similar EAC CGRs over a wide range of loading conditions. Significantly

lower ΔK thresholds were observed than predicted by the Eason [175, 176] or GE model [16, 66, 114]. Sustained, steady-state EAC crack growth was observed down to very low frequencies of around10^{-5} Hz (Figure 11) and ΔK values of 1.5 to 2 MPa·m$^{1/2}$ (Figure 55).

Preliminary tests under reducing HWC conditions [62, 63] and the few literature data with HWC [64] or NMCA [65] clearly indicated, that HWC/NMCA results in a significant reduction of CF CGR by a factor of 10 to 50 under LCF loading conditions and the cyclic CF CGRs $\Delta a/\Delta N_{EAC}$ dropped well below the ASME XI wet curve under HWC conditions (Figure 15). On the other hand, based on the GE-model or tests under PWR conditions above a loading frequency of 10^{-2} to 10^{-1} Hz, no or only a very moderate mitigation effect of HWC on CF CGR (see Figures 11 to 14) is expected.
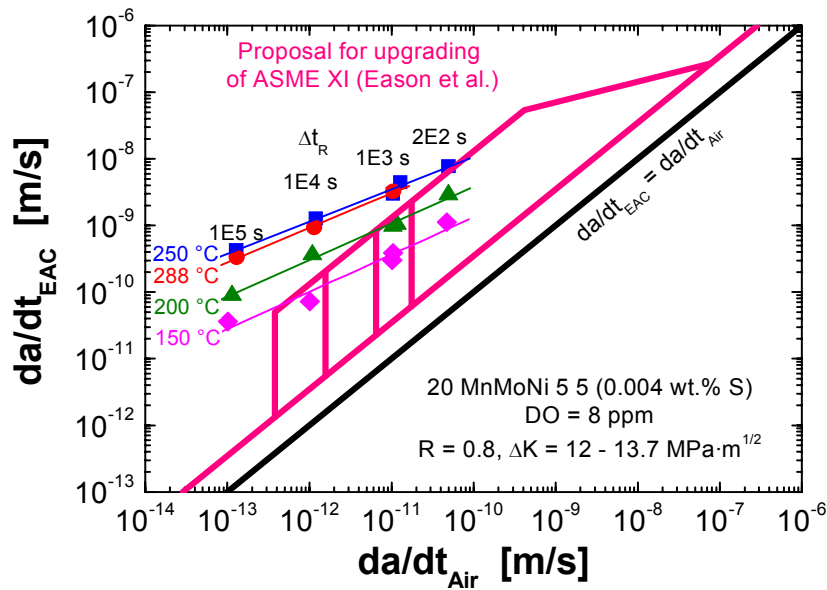
Figure 91: Comparison of time-based CGR da/dt$_{EAC}$ from CF tests under highly oxidizing conditions [28] with the Eason proposal [175, 176] for modifying ASME XI.

In summary, the current ASME XI wet reference fatigue CGR curves conservatively cover the CF CGR lab data under most combinations of loading, environmental and material parameters, even under BWR/NWC conditions, and have usually only been exceeded under some very specific BWR plant conditions. They might therefore be regarded as an adequate, general bounding curve, but they do not realistically describe and reflect the experimentally observed CF crack growth behaviour of LAS in oxygenated HT water (Figure 11). The curves either predict significantly too high (e.g., $\nu \leq 10^{-2}$ Hz and ECP < -200 mV$_{SHE}$ or 10^{-1} Hz < ν < 10 Hz and high ΔK) or too low CGRs (e.g., $\nu \leq 10^{-2}$ Hz and ECP > 0 mV$_{SHE}$ or 10^{-2} Hz < ν < 10 Hz and high R/small ΔK) [66, 128]. Furthermore, system conditions or thresholds (e.g., $\nu > 10$ Hz), where environmental effects on fatigue crack growth can be neglected or excluded, are not defined in ASME XI. For these reasons, modification of the ASME XI curves, or the development of a new code case for BWR/NWC, should be pursued. Any optimized procedure should adequately consider the strong effect of loading frequency and ECP (DO), but eventually could ignore material parameter effects for practical reasons, provided the necessary data are derived in a conservative way (e.g., with high-sulphur steels and materials with a high DSA susceptibility, etc.). Such procedures would have the potential to reduce both uncertainty and undue conservatism, but would also result in more complicated flaw tolerance evaluations than to date, since the loading frequency/strain rate of different transients

would have to be considered in an appropriate way. As discussed in [51, 62] and Section 6.3.3, a simple superposition model/time-domain evaluation method could be used for that purpose.

9.3.3 Status Concerning a New BWR/NWC Code Case

There is a good chance that the current ASME Code Case N-643 would also cover the CF crack growth in C & LAS under most BWR/HWC conditions. Therefore this Code Case should be further tested under these water chemistry conditions. Such a procedure could eliminate a lot of undue conservatism of the current ASME XI curves for HWC conditions.

A recent assessment of the currently available CF CGR data within an ongoing small EPRI/GE project [209] clearly revealed the need to re-visit the current ASME XI curves and the desire for a more realistic BWR/NWC codes case. A very preliminary corrosion fatigue/SICC analysis of BWR feedwater nozzles with a modified Code Case N-643 rise time approach indicated that a more realistic consideration of corrosion fatigue crack growth could eventually impact on current nozzle inspection intervals depending on the assumed transients [209]. In this ongoing work, it is suggested to exclude very long rise time results (where the Code Case N-643 EAC curve is usually not conservative under BWR/NWC conditions), if SCC growth rates under constant load were also included and considered in the analysis by the BWRVIP-60 SCC DL 1. If the BWR/NWC CF data base is corrected by this SCC contribution at high load ratio/high $K_{I \text{ values}}$, the overwhelming part of CF data is covered by the Code Case N-643 EAC curve.

Current models and methods such as the Eason model and the Code Case N-643 for PWRs do better reflect test data, but are difficult to apply for actual plant conditions. Clearly, simpler methods are needed that reflect recent BWR test data, but are still easy to apply. Ranganath and Hickling [210] suggest a simplified approach to the prediction of CF crack growth in BWR pressure vessels with a prescribed rise time, but which still does not require the knowledge of rise times for actual plant transients. For example, it is difficult to define rise time of specific transients, and often the rise time used in the ASME Code analysis (for conservatism in the stress prediction) may be much lower than the actual rise time of real transients. The appropriate CF CGR is a function of two competing parameters, the stress range due to the ΔT and the environmental enhancement of fatigue crack growth due to the longer rise time. A step change will lead to a higher stress and ΔK range, but the lowest environmental enhancement of fatigue crack growth. A slow rise time means lower stress, but potentially much higher environmental effects. Clearly there should be an intermediate point where the ΔT stress and the rise time environmental effect result in the highest actual CF CGR. It is reasonable to postulate that for a particular component geometry/plant transient it is possible to calculate an in-between limiting rise time that would adequately bound any variations in the predicted crack growth and simplify analyses. This could be pursued by considering the most important components and relevant transients with different rise times to define this "optimum" rise time. The final target of this ongoing work is to develop a simple relationship that reflects test data on environmental effects, but still does not require the knowledge of rise times for actual plant transients. Such a procedure may not necessarily be applied to feedwater nozzles where the stresses are mainly produced trough axial gradients.

10 Mechanisms and Models

In the following Sections, the most popular crack growth mechanisms (Section 10.1) and the role of DSA (Section 10.2) and of MnS-inclusions (Section 10.3) in EAC of C & LAS are briefly discussed on a mechanistic basis. In Section 10.4 it is briefly outlined how the local crack-tip strain rate and the activity of sulphur anion in the crack-tip environment synergistically control the EAC crack growth in C & LAS and how these local crack-tip parameters are governed by a system of interrelated and synergistic (macroscopic) corrosion system parameters. The basic concepts of occluded crack crevice (electro-)chemistry in C & LAS in HT water and the relation between the local crack-tip chemistry and the given bulk water chemistry outside the crack by mass transport process is discussed in more detail in Section 10.5. Finally, the basic ideas and fundamental equations and the relevant SCC and CF crack growth curves of the GE-model are summarized in Section 10.6. A more detailed discussion of mechanistic aspects of EAC and on crack electrochemistry can be found in [13, 16, 211 – 214] and [55, 214 – 217].

10.1 EAC Crack Growth Mechanisms in C & LAS in HT Water

It is widely accepted that there is a common mechanism for TG EAC of C & LAS under LWR conditions, in the sense that CF, SICC, and SCC are fundamentally related phenomena and governed by the same basic processes. The following potential cracking mechanisms have mainly been discussed in the literature:

- Film rupture/anodic dissolution (FRAD) [16, 66, 114, 156, 219, 222] (Section 10.1.1)

- Hydrogen-assisted EAC (HAEAC) [178, 218] (Section 10.1.2)

The controlling factors in EAC of C & LAS are well known (Sections 4 to 6), but the direct experimental evidence for a specific microscopic crack extension process is still weak. The exact crack growth mechanism is therefore still under discussion. None of the proposed mechanisms can satisfactorily explain all the experimentally observed aspects of cracking. Currently, the observed cracking behaviour can best be rationalized by a superposition/combination of these two fundamental cracking mechanisms. At lower temperatures (< 100 °C) and/or high YS/hardness levels (R_p > 800 MPa/> 350 HV5) and high strain rates (> 10^{-3} s^{-1}), hydrogen effects are more pronounced. At high temperatures (≥ 150 °C) and/or lower YS/hardness levels and slow strain rates (<10^{-3} s^{-1}), anodic dissolution seems to dominate.

10.1.1 Film Rupture/Anodic Dissolution Mechanism

The FRAD or slip dissolution model has been developed for SCC in stainless steels in HT water by Ford and Andresen, but has also been successfully adapted and applied to C & LAS [16, 66, 114,156, 215, 219, 222]. The basic ideas and critical steps of this cracking mechanism are shown in Figures 92 and 99.

In this cracking mechanism, the protective, but brittle oxide film, which is formed on C & LAS in HT water, is ruptured by plastic straining at the crack-tip. Once the oxide film is ruptured, the crack-tip advances by anodic dissolution of the bare metal matrix. The anodic dissolution is slowed down and finally stopped by the nucleation and reformation of the oxide film ("repassivation"). Thus, continued crack advance will depend on a further oxide rupture process due to the action of a strain rate at the crack-tip. Therefore, for given environmental and material conditions, the crack propagation rate is controlled by both the change in oxidation charge density with time and the frequency of oxide film rupture at the strained crack-tip. The first part is controlled by the anodic dissolution and repassivation kinetics, which are governed by the chemical composition of the local crack-tip electrolyte and the material. The second part is determined by the fracture strain of the oxide film and the crack-tip strain rate.
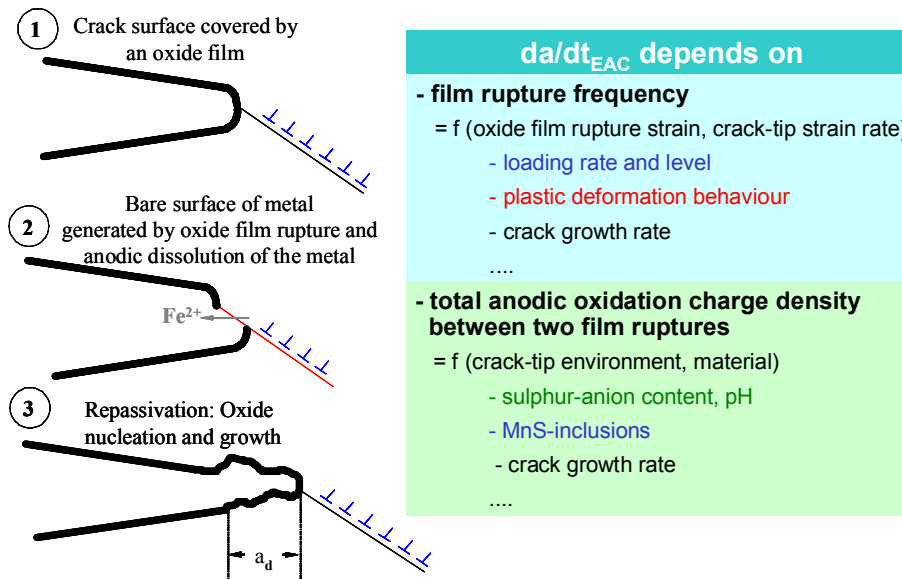
Figure 92: Basic steps of film rupture/anodic dissolution mechanism and major factors of influences.

Dissolution and repassivation kinetics are strongly affected by both anionic sulphur species as sulphate or sulphides and by pH [16, 166, 220, 221]. High concentrations of sulphur-anions (SO_4^{2-}, HS^-, S^{2-}) or a low pH relevantly retard repassivation and increase therefore the crack advance by anodic dissolution between two film rupture events. The dissolution of the MnS-inclusions which are intersected by the pre-existing crack and which will be exposed to the electrolyte by the crack growth itself and the concentration of sulphur-anions in the bulk environment outside the crack are the two sources of sulphur-anion species in the crack-tip environment. The crack-tip environment is related to the bulk environment by mass transport process (diffusion, migration, convection) and it is also dependent on the CGR itself.

Sources of dynamic crack-tip straining arise from external loading (loading rate and level), low-temperature creep and the crack growth into less strain-hardened regions itself [16]. Corrosion-deformation interactions (hydrogen, vacancies, etc.) and strain localisation by DSA may be further sources of crack-tip strain and strain rate.

10.1.2 Hydrogen-Assisted EAC Mechanism

Hydrogen embrittlement and HAEAC mechanisms are usually associated with high strength alloys because of the ease of attainment of high triaxial respectively hydrostatic stress conditions in front of the crack-tip and, thereby, the thermodynamic possibility of hydrogen supersaturation in this region [16, 214]. Once this supersaturation is achieved then localized crack initiation and propagation can occur by a variety of rupture mechanisms, e.g. hydrogen gas rupture, hydrogen absorption (surface energy), decohesion, brittle hydride phase formation, martensite formation and hydrogen enhanced local plasticity. In the last decades it has been increasingly proposed that hydrogen embrittlement may be also operating in lower strength alloys [223]. The transport of hydrogen by mobile dislocations during plastic deformation (which can be 10^3 to 10^6 times larger than by normal diffusion) with a sufficiently fast strain rate could result in hydrogen supersaturation under suitable dynamic equilibrium conditions at various hydrogen trapping sites.

Hänninen et al. [178, 218] have suggested that a hydrogen embrittlement mechanism is operating in the relatively ductile pressure vessel steels in water at 288 °C. The series of steps hypothesised to occur during the oxide film rupture/repassivation process at the strained crack-tip (similar to FRAD) in this system are shown in Figure 93.
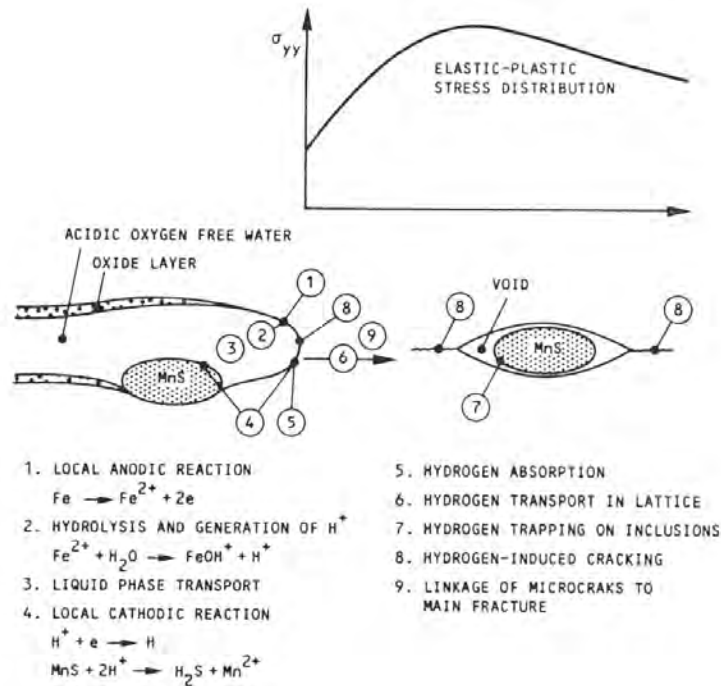
Figure 93: Schematic illustration of hydrogen-assisted EAC of pressure vessel steel in HT water according to Hänninen [218].

In the HAEAC-mechanism the hydrogen-induced micro-crack formation ahead of the crack-tip and linkage of these micro-cracks to the main crack are the main sources of EAC crack growth and result in discontinuous crack propagation (which may be superimposed to pure mechanical fatigue). The hydrolysis of metal cations from anodic dissolution is an important source of hydrogen, but in contrast to the FRAD-mechanism, anodic dissolution does not directly and remarkably contribute to crack advance.

Hydrogen transport in the electrolyte and in the metal lattice is believed to be fast. Therefore, the generation of bare metal surface by film rupture and the film reformation may be rate controlling steps in the cracking process and explain the strain rate dependence of EAC. The contribution of MnS-inclusions to EAC is rationalized in two ways:

- The dissolution of MnS intersected by the crack plane leads to an additional source of hydrogen by generation of H_2S and subsequent dissociation to HS^- and H^+. Furthermore H_2S and HS^- enhance hydrogen absorption through their adsorption on the bare surface. Additionally, they may retard repassivation and increase the hydrogen absorption.

- MnS-inclusions located in the plastic zone ahead of the crack are supposed to act as strong trapping sites for absorbed hydrogen. At a location near to the maximum hydrostatic stress this process aids in microcrack formation.

The prime experimental evidence for such a suggestion was the fractographical observation of "brittle" cracks in corrosion fatigue tests ($>10^{-3}$ Hz), which were associated with elongated MnS stingers ahead of the main crack-tip [177]. Moreover, the degree of environmental enhancement in fatigue CGRs could be directly correlated with the extent of these "brittle" fracture areas on the fracture surface. When environmental enhancement was observed in the cyclic CGR, brittle features in fracture morphology (brittle striations, or striationless cleavage-like fracture) were always seen to be associated with MnS-inclusions; brittle crack often spread like a fan from inclusion colony. The occurrence of EAC was accompanied by a transition from ductile to more brittle like fracture, whereas the corresponding striation spacing increased with this transition. Moreover, the quasi-brittle features observed were similar to the microscopic appearance of fracture generated in H_2 gaseous atmospheres at 95 °C [177].

99

10.1.3 FRAD vs. HAEAC Mechanism

Under crack-tip conditions (ECP, pH, anion content), which are relevant for C & LAS under LWR conditions, HAEAC and FRAD mechanisms are both thermodynamically and kinetically viable, and may be simultaneously active [114, 156, 218]. Depending on system conditions one of the two mechanisms may dominate. Furthermore, since both mechanisms may be controlled by the same rate limiting steps (for example oxide film rupture rate, repassivation kinetics, etc.), it is very difficult to differentiate experimentally between them. Both mechanisms are able to explain the observed, dominant effect of strain rate and of MnS-inclusions on EAC cracking behaviour. The HAEAC model may better explain some specific fractographic features, but – in contrast to the FRAD model – no quantitative, predictive formulation exists. However, unlike IG SCC (e.g., in sensitised SSs) there is no simple reason for the directed, anisotropic dissolution behaviour of LAS assumed in the FRAD model.

To date, there is a lack of direct experimental evidence for distinct hydrogen effects which would relevantly affect the cracking behaviour of C & LAS under LWR operating conditions at temperatures above 200 °C. Since hydrogen permeation rate through the oxide films and in the metal lattice is very rapid with respect to the hydrogen generation rate from corrosion reactions, radiolytic proton injection or transmutation, it is very difficult to generate a very high hydrogen fugacity and supersaturation in the metal [13, 224]. The most striking argument against such hydrogen effects in EAC at temperatures above 150 °C is that HAEAC should be enhanced by increasing the hydrogen fugacity of the environment, i.e., by decreasing the corrosion potential to more cathodic potentials and by catalytic surfaces. This is obviously not the case. In both cases, cracking susceptibility and EAC CGR in LAS with moderate strength levels (300 – 600 MPa) decrease rather than increase. Furthermore, no distinct effect of YS (< 600 MPa) on SCC growth has been observed and SCC CGRs increase with increasing temperature above 150 °C. For most hydrogen mechanisms, a higher EAC CGR would be expected for increasing YS levels because of the ease of attainment of highly triaxial and thus hydrostatic stress conditions in front of the crack-tip, and thereby the thermodynamic possibility of hydrogen supersaturation in this region. Because of thermal activation and the very high diffusivity of hydrogen, the hydrogen trapping efficiency of weak and strong trap centres is strongly reduced at temperatures above 150 to 200 °C. Both experimental observations are therefore hardly consistent with most hydrogen mechanisms. [13]

10.2 Role of DSA for EAC in C & LAS

EAC data strongly suggest that the susceptibility of C & LAS to EAC coincides with evidence of DSA, both in terms of temperature and strain rate [13, 26, 27] (Section 4.2.4). DSA generally results in an extension of the susceptibility region and may especially affect the temperature and strain rate dependence of EAC. The most pronounced effects of DSA on EAC are typically observed close to crack growth thresholds (e.g., for SCC under static load or for CF close to critical frequencies under cyclic load). Under system conditions, where fast EAC crack growth can be easily sustained, only minor or moderate effects of DSA are observed generally. DSA provides a possible, alternative explanation for strain rate thresholds and, more significantly, it may offer an explanation for the CGR peak and TG quasi-cleavage fracture appearance/increasing fracture surface roughness of EAC at intermediate temperatures. The concentration of free, interstitial nitrogen and carbon, which mainly govern the DSA susceptibility in LAS, might therefore be just as relevant for EAC susceptibility as the steel sulphur content and differences in DSA susceptibility of otherwise identical LAS may explain some of the observed data scatter and different temperature trends. EAC in LAS has been observed under temperature/strain rate conditions, or in materials, where no (or only minor) DSA effects were present. DSA is therefore not a pre-requisite for EAC and is best regarded as an additional contributor to the EAC growth process.

DSA is expected to be especially important for EAC in terms of dynamic crack-tip plasticity, since it influences yield strength [13, 27, 128], strain hardening exponent [13, 27] and low-temperature creep rate [141]. All of these are important factors affecting the crack-tip strain and strain rate [136 – 138]. DSA may thus result in the occurrence of a higher crack-tip strain and strain rate than for loading outside the DSA range, or in a material, which is not susceptible to DSA. The inhomogeneous localisation of plastic deformation (increase in dislocation density/planar deformation) by DSA [13, 27] may result in a reduction of the local fracture toughness and thus favour brittle crack extension. However, it could also assist in mechanical rupture of the protective oxide film and therefore favour crack advance by anodic dissolution/hydrogen embrittlement mechanism. Therefore, DSA may synergistically interact with either mechanism to increase EAC susceptibility.

The observed DSA (and YS) effects on EAC can be readily rationalized by the GE-model (see Section 10.6) and the effect of DSA on crack-tip strain rate (Figure 94). The most pronounced effects are expected close to the thresholds/transition from high- to low-sulphur EAC rates as it has been observed in experiments (see Section 4.2.4).
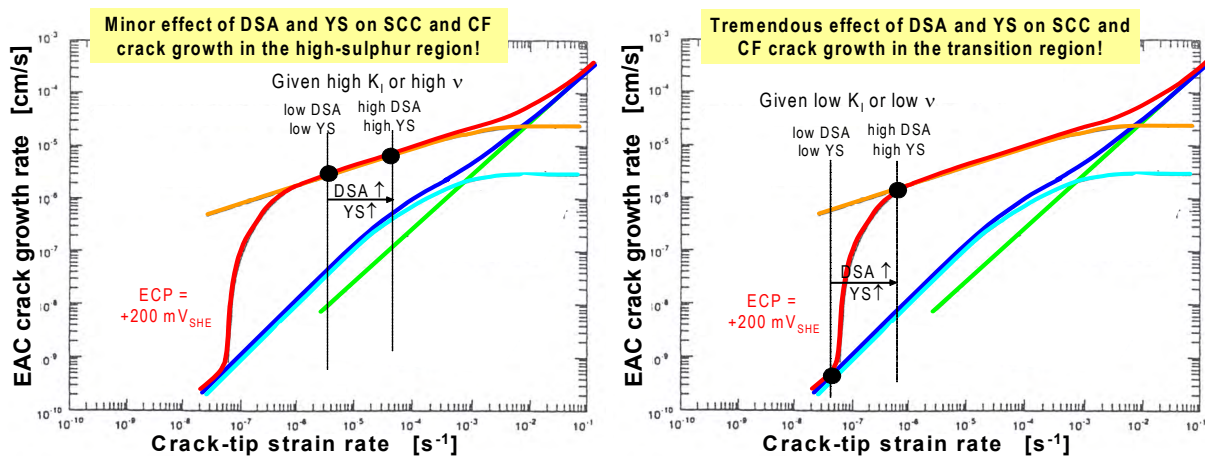
Figure 94: Explanation of the influence of DSA on EAC by the GE-model and the effect of DSA on crack-tip strain rate [136].

10.3 Role of MnS-Inclusions in EAC of LAS

The sulphur content of the steel, the size, type (chemical composition), morphology, and spatial distribution of MnS-inclusions are the material parameters having the strongest effect on EAC susceptibility (Section 4.2.1). The dissolution of MnS-inclusions to H_2S respectively HS^- and S^{2-} may contribute to EAC in the following ways:

Sulphur-anions as HS^-, S^{2-} and SO_4^{2-} may significantly retard repassivation after oxide film rupture and therefore increase crack advance by anodic dissolution in the FRAD-model (Section 10.1.1) and the HAEAC-model (Section 10.1.2). The retarded repassivation by the film-free surface and the adsorbed HS^-, S^{2-} or H_2S increase the hydrogen absorption to the metal lattice, and favour therefore HAEAC. Furthermore, the dissolution of MnS is a further potential source of hydrogen and MnS-inclusions in the region of maximum hydrostatic stress ahead of the crack-tip may act as strong hydrogen traps and HAEAC initiation sites.

The effects of steel sulphur content are <u>synergistic</u> with environmental variables, such as (sulphur-) anionic impurities in the bulk environment, ECP (DO content) and flow rate. This is believed to be due to the creation of a sulphur-rich crack-tip environment responsible for EAC, which arises from the dissolution of MnS intersected by the growing crack and by the transport of sulphur-anions by migration/diffusion/convection in the crack crevice (see Sections 10.4 to 10.6).

The dissolution rate of MnS is an important parameter for the EAC crack growth kinetics and depends on the type, size, morphology, and spatial distribution of MnS-inclusions in steel [116 – 121] which are influenced by the steel making and manufacturing process and the product form. The temperature, pH, and potential are further important factors, which govern dissolution kinetics and solubility. Finally, the CGR itself by the exposure of new fresh dissolvable MnS-inclusions can significantly affect the EAC behaviour.

Post-test fractography and metallography [177, 178], crevice experiments [225] and tests with microsampling [64, 70, 226] indicate, that dissolution of MnS-inclusions, which are intersected by the crack plane can and does occur under de-aerated crack-tip conditions. The detail of reaction mechanisms and kinetics are not known and several different chemical and electrochemical reactions have been proposed [13]. Based on microsampling [64, 70, 226] tests and other investigations, it seems that MnS-dissolution is rather slow. Under typical de-aerated crack-tip conditions (low ECP of $\approx$ - 500 mV$_{SHE}$, slight acidic pH shift of 1 to 2 units from neutral) H$_2$S respectively HS$^-$ and S^{2-} seem to be the thermodynamically stable dissolved sulphur products. Depending on crack-tip sulphur-anion activity, the stable film on the surface is either Fe$_3$O$_4$ or mixed Fe$_3$O$_4$/FeS/FeS$_2$. In fact, FeS and FeS$_2$ films respectively increased sulphur concentrations in the oxide films have been observed by post-test fractography in specimens which have shown fast EAC during the test. But it was not clear if precipitation of iron sulphides has occurred during the test or during cooling down. The iron sulphides and sulphur built-in into the oxide film may also act as a possible source of sulphur-anions and cause distinct hysteresis and asymmetric effects in EAC of C & LAS [13, 215, 222].

10.4 Control Factors and Conjoint Requirement for EAC Crack Growth

Both experimental data trends (Sections 4 to 6) and mechanistic models (Sections 10.1 and 10.6) reveal that EAC growth from incipient (long) cracks is essentially governed by two main local parameters: the crack-tip strain rate and the activity of sulphur- (or chloride-) anions (affecting repassivation/pH/oxide film stability) in the crack-tip environment [11 – 13, 16, 64, 66, 70, 156, 171, 214, 215, 222]. The onset and extent of EAC is crucially dependent on simultaneously maintaining a slow, positive crack-tip strain rate within the plastic zone and a critical sulphur-anion activity of about 1 to 5 ppm S^{2-} [16, 64, 70, 215, 222] in the crack-tip environment. If these two conjoint requirements are not met, no SCC and SICC, or only minor environmental acceleration of fatigue crack growth are generally observed. If the critical anion concentration is exceeded, the EAC CGR depends primarily on the crack-tip strain rate and increases with increasing external strain rate up to an upper critical limit around 10^{-3} to 10^{-2} s^{-1} (Figures 95 and 96) [13, 128]. Most EAC thresholds/cessation/pinning phenomena in the system C & LAS/HT water may be attributed to this conjoint requirement.

These two local factors are governed by a system of interrelated and synergistic corrosion system parameters such as the applied loading conditions (load level, loading rate/frequency), the ECP (or oxidant concentration in the water), the flow rate across the crack-mouth, and the bulk concentration of specific anionic impurities such as SO$_4^{2-}$ and Cl$^-$, as well as the MnS-inclusion content and morphology in the steel. Figure 97 shows schematically, how these factors synergistically shift SCC and CF crack growth thresholds to lower K$_I$ and ΔK/frequency (air CGRs) values.

The crack-tip strain rate is governed by the loading rate/level, the CGR into less strain hardened regions itself and the (visco-) plastic deformation behaviour of the material [13, 16, 214]. In general, the crack-tip strain rate increases with increasing loading rate/loading frequency (as well as load level), CGR, YS [137, 138] (see Section 4.2.2 on p. 35) and DSA susceptibility [136] (see Section 10.3). The crack-tip sulphur-anion activity is determined by the dissolution of the MnS inclusions (see Section 10.2) (which are intersected by the growing

crack and thus exposed to the electrolyte within the crack), by the concentration of sulphur-anions in the bulk environment outside the crack and by the time-dependent mass transport processes (diffusion along concentration gradients, migration by potential gradients, convection from external flow, or by cyclic pumping) between the crack-tip and the crack-mouth (see Section 10.5). Thus both crack-tip strain rate and crack-tip chemistry are strongly interrelated to CGR and vice-versa. This interrelation is one of the main reasons for hysteresis effects in tests with decreasing an increasing frequencies or ΔK and for retardation effects upon changing of test parameters. [13, 16, 64, 66, 70, 156, 171, 215, 222].
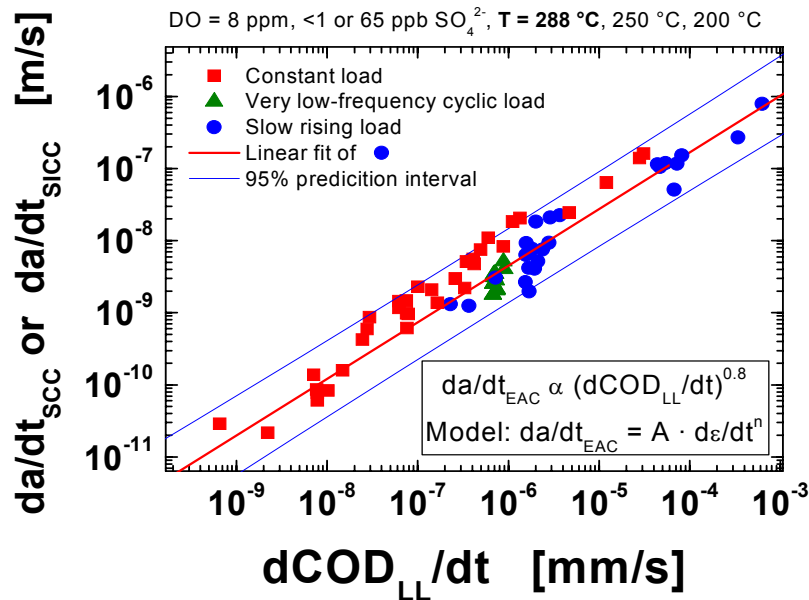
Figure 95: Experimental confirmation for basic relationship between EAC CGR and crack-tip strain rate (which is roughly proportional to the measured crack-opening displacement rate $dCOD_{LL}/dt$) for different loading conditions [128].
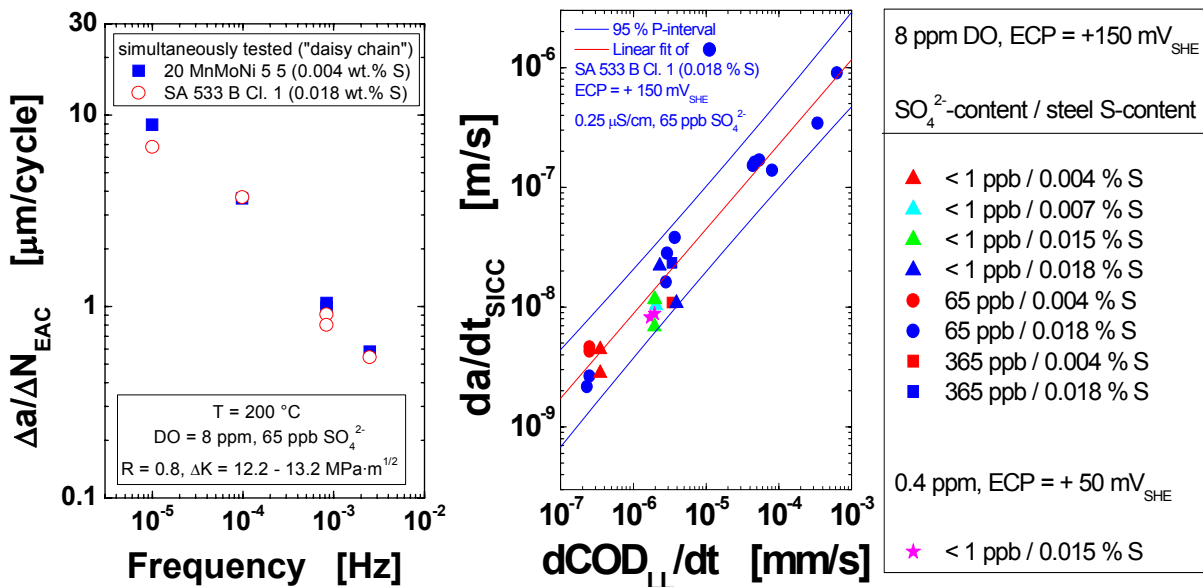
Figure 96: Experimental confirmation of conjoint requirement for EAC. If the conjoint requirement is satisfied and the crack-tip strain rate is $\leq 10^{-3}$ to 10^{-2} s^{-1} a power law relationship between CGR and crack-tip strain rate ($da/dt_{EAC} = A \cdot (d\varepsilon/dt_{CT})^n$) and similar EAC rates for different LAS and environmental conditions are observed [128].
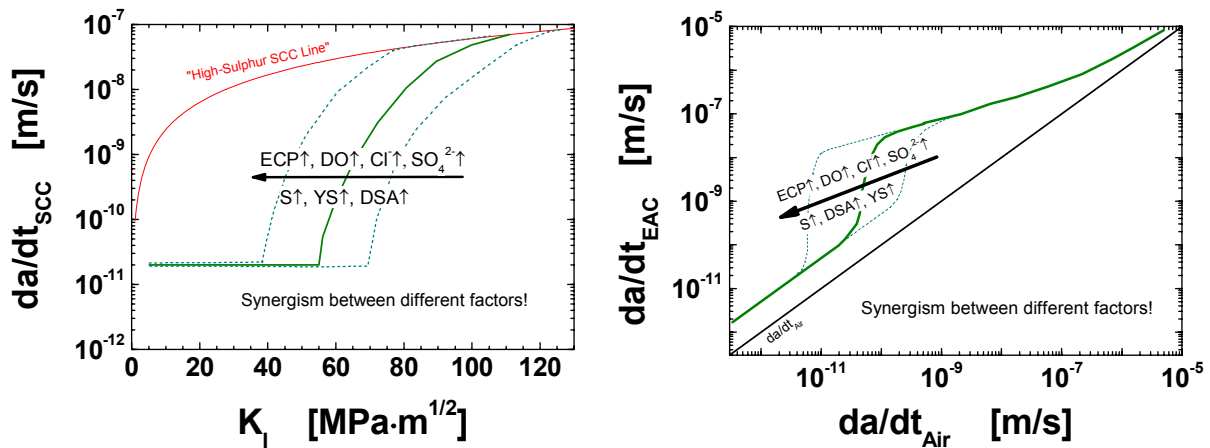
Figure 97: Synergistic effects of material, loading, and environmental parameters on SCC and CF crack growth [136].

Thus the threshold conditions for EAC (ECP_{crit}, ν_{crit}, ΔK_{EAC}, etc.) are directly related to crack-tip chemistry and CGR/crack-tip strain rate, rather than to loading parameters or bulk environmental conditions per se. E.g., suitable combinations of different system parameters may help to exceed the critical crack-tip sulphur-anion concentration (of 1 to 5 ppm S^{2-}) provided that there is at least one source of sulphur (MnS-inclusions or sulphur-anion in the bulk environment): a high ECP/DO (anion enrichment by migration), a high bulk sulphur-anion concentration, quasi-stagnant or low flow rate (no dilution by convection), a high steel sulphur content, local segregation zones with MnS-clusters in the steel, a long pre-existing crack with a large area of dissolvable MnS-inclusions, or a sufficiently high CGR/crack-tip strain rate/loading frequency (exposure of new, dissolvable MnS inclusions by crack growth). Any or all of these conditions favour the formation of a crack-tip environment rich in sulphur anions and therefore a high EAC CGR [13, 16, 64, 156, 171]. A high steel sulphur content or a high ECP (and large potential gradient) are therefore not mandatory for accelerated EAC. SICC has been even observed in extremely low-sulphur steels at high ECP and/or high bulk sulphur-anion contents [21, 22]. Furthermore, sustained, fast EAC may be observed at very low ECP (PWR) under suitable cyclic loading conditions [205 – 207] or at high bulk H_2SO_4 concentrations [64]. On the other hand, flushing/dilution of the aggressive crack-tip environment in high-purity BWR or PWR water by external flow (see Section 4.1.5 and Figure 23 on p. 27) can slow down CF crack growth with respect to quasi-stagnant conditions [13, 80].

Under PWR conditions, the sulphur enrichment mechanism by migration is absent. In pure PWR water, the crack-tip sulphur-anion concentration is governed by the balance between competing processes of sulphur-anion supply by the dissolution of MnS-inclusion and the loss of sulphur-anions by the diffusion out of the crack. To maintain a high crack-tip sulphur-anion activity, the growing crack has to expose a sufficient amount of new fresh dissolvable MnS-inclusion; otherwise the continuous diffusion will result in a continuous decrease of the crack-tip sulphur-anion activity and of EAC growth rate. A sufficiently high a growth rate may be achieved under suitable cyclic loading conditions (high ν and/or ΔK). The cessation of EAC in LAS under PWR conditions has been experimentally observed and discussed in three recent papers [205 – 207]. The concept of a critical crack-tip sulphur-anion activity for the occurrence of EAC has led to a new concept of a critical CGR and critical crack extension length which have to be simultaneously exceeded that sustained CF may be observed. If these conjoint conditions are not satisfied, only minor environmental acceleration of fatigue crack growth occurs. Time-domain EAC plots clearly reflect this behaviour (Figures 12, 14, 56, and 59). The critical CGR is expected to decrease with increasing steel sulphur content and increasing ECP/DO (see Figure 12, 14, 56, and 59).

10.5 Occluded Crack Electrochemistry and Crack-Tip Environment Conditions

10.5.1 Basic Concepts of Crack Electrochemistry in C & LAS under LWR Conditions

The evolution of occluded water chemistry in cracks with restricted mass transport is an important driving force for EAC and therefore outlined in the following Sections.

Mass Transport in the Crack Crevice: The concentration of a specific species in the crack-tip environment is governed by its bulk concentration outside the crack enclave, its production or depletion rate by homogeneous/heterogeneous reactions (e.g., dissolution of MnS-inclusions, precipitation of sulphides, etc.) and its transport into/out of the crack by the different mass transport mechanism. There are three different basic transport mechanisms, which can be simultaneously active in a crack/crevice:

- Diffusion of neutral and charged species due to their concentration gradients.

- Migration of charged species due to a potential gradient.

- Convection of neutral and charged species by water flow induced by external flow across the crack-mouth or by fatigue pumping by the relative displacements of the crack flanks between the maximum and minimum stress portions of a fatigue cycle.

The presence of high convection generally dominates all other transport mechanism and homogeneous concentration and potential conditions do generally exist in regions of high convection. Fatigue pumping becomes more important as cyclic frequencies are increased and as stress ratio is decreased. Under static or low-frequency fatigue loading conditions and for long cracks convection can be neglected, and then mass transport is dominated by diffusion (reducing PWR and BWR/HWC conditions) or diffusion and migration (oxidizing BWR/NWC conditions), respectively. The complete flushing out or dilution of the aggressive crack-tip environment by convection may completely suppress or relevantly slow down EAC crack growth in high-purity water (see Section 4.1.5).

Occluded Crevice Electrochemistry: Figure 98 shows the basic concepts of crack electrochemistry for EAC in C & LAS under LWR conditions. In oxygenated HT water (in BWRs) a differential aeration cell is formed in the crack-mouth region. Dynamic crack-tip straining may additionally result in oxide film rupture and the formation of a dissolution cell at the crack-tip. Both cells may exist without the other one. The evolution of the differential aeration cell only requires crevice geometry with restricted mass transport. Because of the limited conductivity under typical LWR conditions and the resulting high ohmic potential drops, the two cells are only coupled by mass transport but not by direct electronic coupling. [55]

Differential Aeration Cell at the Crack-Mouth: Oxygen reduction kinetics on oxide films is fast with respect to oxygen mass transport by diffusion in HT water. Therefore, in a high aspect ratio cracks with restricted mass transport, almost all oxygen is consumed over a short distance in the crack-mouth region resulting in a built-up of a differential aeration cell (oxygen concentration cell) at this location. The resulting potential drop between the aerated crack-mouth ($+0.1$ V_{SHE}) and the de-aerated remaining part of the crack (-0.5 V_{SHE}) and the additional mass transport of anions (cations) by migration towards the crack-tip (out of the crack enclave) were important factors for the evolution of the corresponding crevice and crack-tip water chemistry. The potential drop in the crack-mouth is acting as a pump for anionic impurities in the bulk environment towards the crack-tip and retains anionic impurities generated by (electro-)chemical reactions (dissolution of MnS-inclusions) in the crack-tip environment. If the bulk reactor water contains specific anionic impurities as SO_4^{2-} or Cl^-, the migration of these impurities towards the crack-tip and enrichment in the crack-crevice environment can result in acidic pH-shifts. The dissolution of MnS-inclusions (intersected by the crack flanks/front of the incipient and growing crack) and the hydrolysis of metal cations gen-

erated by anodic dissolution may be further reasons for pH-shifts under these conditions. The shifts in water chemistry increase exponentially with the potential gradient (see Section 10.6). The potential at the de-aerated crack-tip is always low and close to the equilibrium potential of the H_2/H_2O reaction. Therefore, the potential gradient decreases with decreasing dissolved oxygen content and corrosion potential at the crack-mouth. Under BWR/HWC or PWR conditions, there is only a small or virtually no potential gradient between the crack-mouth and crack-tip and mass transport is governed by diffusion only.

$$J_A = -D_A \Delta C_A - z\mu C_A F \Delta\phi + C_A V$$
$$\text{flux} = \text{diffusion} + \phi\text{-driven} + \text{convection}$$
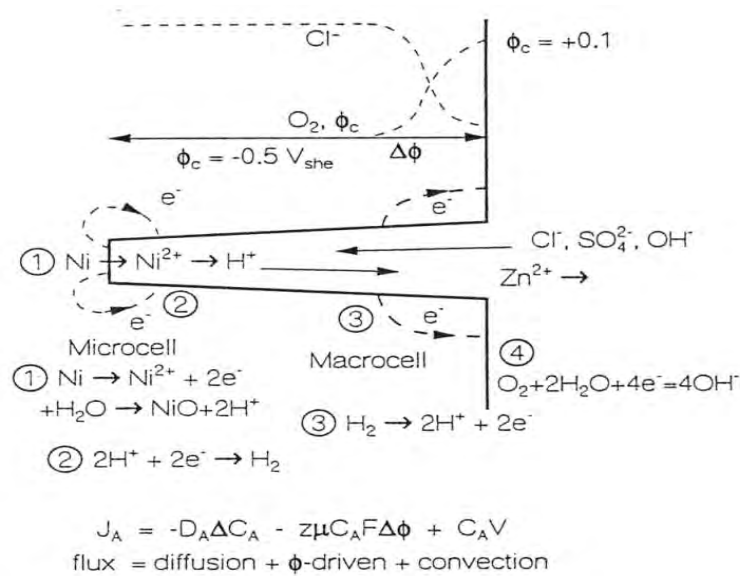
Figure 98: Schematic of crack electro and water chemistry showing the differential aeration cell at the crack-mouth (reaction 3 and 4) that establishes the crack-tip chemistry and the local microcell (reaction 1 and 2) associated with metal dissolution and crack advance. Because of the high ohmic resistance of the electrolyte, there is no direct coupling of electronic currents between these two cells. The potential gradient between the aerated crack-mouth (+0.1 V_{SHE}) and the de-aerated crack-tip (-0.5 V_{SHE}) results in an additional flux of anions/cations into/out of the crack enclave and an enrichments of anions and pH-shifts in the crack-tip environment in the case of non-OH⁻-anions in the bulk environment. (In the case of LAS, Ni/Ni^{2+} has to be replaced by Fe/Fe^{2+}). [55]

Dissolution Cell at the Crack-Tip: Mechanical straining results in the rupture of the protective oxide film at the crack-tip and in exposure of fresh bare metal to the de-aerated crack-tip electrolyte and in crack growth by anodic dissolution. The crack growth is stopped by the reformation of the protective oxide film (repassivation). Because of complete oxygen depletion in the crack enclave, anodic dissolution current on the very localized anode is balanced by the reduction of hydrogen or water on the crack walls in the absolute vicinity of the crack-tip. Hydrogen is always present in the crack-tip environment because of corrosion processes (oxide film formation) and hydrolysis of metal cations generated by anodic dissolution.

The limited conductivity results in high ohmic potential drops if currents were flowing and therefore strongly limits the spatial extension of local galvanic elements and is therefore avoiding direct electronic coupling between crack-tip and crack-mouth electrochemistry. Nevertheless, conductivity per se has a little direct effect on CGR. Certain species (e.g., NO₃⁻, BO₃⁻, F⁻) have a strong effect on conductivity but little or no effect on CGR. EAC crack growth in C & LAS is primarily controlled by the pH and the concentration of specific anionic impurities as sulphate/sulphides or chloride in the local crack-tip electrolyte, which have a strong influence on dissolution/repassivation kinetics or oxide film stability. Dissolution cell

current is limited by the repassivation kinetics rather than by cathodic reactions or ohmic polarisation. The balancing cathodic reactions never appears to be a limiting factor, undoubtedly because of the very high cathodic to anodic area at the crack-tip and since hydrogen or water reduction is always available at the crack-tip. This has been clearly confirmed by tests with microsampling technique and by repassivation measurements under simulated crack-tip conditions [55, 64, 70, 226, 227]. These tests clearly indicated further, that it is not the potential gradient per se, which enhances crack-tip dissolution, but the aggressive chemistry in the crack (activity of sulphur-anions and crack-tip pH) [55].

10.5.2 Typical Crack-Tip Electro- and Water Chemistry in LAS under LWR Conditions

Crack-Tip Potential and Potential Gradients: The ECP at the de-aerated crack-tip is always low (typically around -500 mV$_{SHE}$) even at extremely high bulk DO content of 42 ppm and/or high n/γ radiation levels and is similar for oxidizing BWR and reducing PWR conditions. The crack-tip ECP is governed by the H_2/H_2O-line, since oxygen is completely consumed in the crack enclave. This is confirmed by the low crack-tip ECP close to the equilibrium potential for H_2/H^+ reaction measured under aerated bulk conditions [228, 229]. Because of the lack of excessive hydrogen overpressure and LiOH under BWR bulk conditions, crack-tip ECP under BWR conditions are slightly more positive (100 to 250 mV) and crack-tip pH at temperature slightly more negative (1 to 2 units) than under PWR conditions [230].

Under BWR/NWC conditions, the ECP on the external surface outside the crack is high (typically -50 to +200 mV$_{SHE}$) and governed by the O_2/H_2O-line. The potential difference between the de-aerated crack-tip and the oxygenated crack-mouth region increases with increasing dissolved oxygen content and typically amounts 500 to 700 mV [55]. Under reducing PWR (or perfect BWR/HWC/NMCA) conditions there is virtually no potential gradient between crack-mouth and crack-tip.

Crack-Tip pH and Crack-Tip Sulphur-Anion Concentration: A slight acidification of the crack-tip environment with respect to the near neutral bulk reactor water is generally observed under BWR conditions, but the pH-shift is generally limited to maximal 1 to 2 units [55, 230]. Dissolution of MnS-inclusions (dominating factor in case of C & LAS) and hydrolysis of metal cations as well as the migration of specific anionic bulk impurities are the cause for this slight acidification. Under PWR conditions, the crack-tip pH at temperature is slightly more positive (1 to 2 units) than in BWR environment, because of the absence of any significant potential gradient and the pH buffering capability in PWR water.

Under aerated BWR conditions, crack-tip sulphur-anion activity is typically 20 to 30 x the bulk sulphur-anion activity. Under de-aerated PWR (or BWR/HWC/NMCA) conditions, where the mechanism of anion enrichment is not active, crack-tip sulphur activity is approximately 2 to 3 x higher than the bulk sulphur-anion activity and 10 x lower than under aerated bulk conditions under otherwise identical testing conditions [55, 64, 70]. At sufficiently high loading frequencies, higher sulphur-anion activities and high-sulphur CF CGRs can be achieved even under de-aerated PWR (or BWR/HWC/NMCA) conditions, since the sulphide generation rate by the dissolution of new fresh MnS-inclusions intersected by the fast growing crack may become higher than their transport rate out of the crack by ordinary diffusion.

Crack-Tip Conductivity: The solubility of corrosion products in near neutral HT water is very limited and only slightly changing for the observed small pH-changes [55, 230]. Precipitation reactions and the small solubility of most ionic impurities limit the concentration of cationic and anionic impurities respectively of the conductivity at the crack-tip. Crack-tip conductivity is probably at maximum 100 to 1000 x higher than in the bulk environment outside the crack, but still very small [55, 230].

10.6 General Electric EAC Crack Growth Model

The GE-model [16, 66, 114, 156, 219, 222], which is based on the FRAD mechanism, is the only quantitative model for C & LAS, which covers the whole spectrum of EAC. Its relative simplicity and its success in correctly explaining many different EAC crack growth data trends are the strongest arguments for its application. It has the potential to rationalize EAC CGR data over a very wide range of loading and environmental conditions and it has also been successfully applied to predict LCF initiation [219] in LAS. It therefore has good potential for data analysis and the definition of disposition lines/reference curves.

In the following Sections, the basic equations and major parameter trends of the GE-model are summarized followed by an assessment of the relevant SCC and CF crack growth curves of the GE-model by experimental data.

10.6.1 Basic Ideas, Equations and Parameter Trends of GE-Model

The basic ideas, fundamental equations, and parameter trends of the GE-model are summarized in Figures 100 to 102 and Tables 11 and 12. In the GE-model, the EAC crack growth through anodic dissolution is controlled by the crack-tip strain rate $d\varepsilon/d_{CT}$ <u>and</u> the sulphur-anion activity c_{CT} in the crack-tip electrolyte, which govern the oxide film rupture frequency and the dissolution/repassivation behaviour after the film rupture event (Figures 99 and 100). Based on the Faraday law and the assumed repassivation kinetics (Figure 99b), a simple power law relationship can be derived between EAC CGR and crack-tip strain rate. The exponent of this relationship is dependent on the repassivation kinetics and sulphur-anion activity in the crack-tip environment, respectively. According to this relationship, the EAC CGR increases with increasing crack-tip strain rate and saturates above a critical strain rate of 10^{-3} to 10^{-2} s^{-1} (continuous dissolution) (Figures 101 and 102, Table 11).

The crack-tip strain rate is dependent on loading conditions, (visco)-plastic deformation behaviour of material and CGR itself. Empirical formula between crack-tip strain rate and macroscopic loading parameters (Table 12), which have some mechanistic background, are used in this model [13, 16, 214]. The power law relationship between crack-tip strain rate and stress intensity factor for static loading conditions has originally been derived for stainless steels based on low-temperature creep experiments with compact tension specimens, and was then adjusted to LAS by fitting it to the SCC LAS data. For cyclic loading conditions it is assumed, that the crack-tip strain rate is proportional to the corresponding air fatigue CGR for given cyclic loading conditions. In SSR tests it is assumed that crack-tip strain rate is proportional to the applied strain rate. In all cases the parameters were determined by adjusting the model to experimental EAC data. DSA and YS effects are not directly considered.

The repassivation kinetics after oxide film rupture is strongly dependent on sulphur-anion-concentration in the crack-tip environment. Above a sulphide concentration of 0.02 ppm (low-sulphur threshold), the formation of a new, protective oxide layer is increasingly delayed by increasing sulphide content, which thus leads to a larger increment of crack advance by anodic dissolution per oxide-rupture event. Above a sulphide content of 20 ppm (high-sulphur threshold), the sulphide effect on repassivation saturates and a further increase in sulphide concentration does no cause any additional delay of repassivation (Figure 100). Based on this relationship between sulphur-anion activity and repassivation, derived experimentally under simulated crack-tip electrolyte conditions (Figure 100), a lower and an upper limiting EAC crack growth curve/equation (Figure 101 and Table 11) could be defined. The so-called low- and high-sulphur EAC lines represent a lower and upper bounding line for EAC crack growth in C & LAS in HT water. A critical high sulphur-anion content of approximately 2 to 20 ppm S^{2-} has to be maintained in the crack-tip electrolyte to sustain fast high-sulphur EAC CGRs, otherwise the CGRs quickly drop down to low-sulphur CGRs (Figures 101 and 102a).

The sulphur-anion concentration in the crack-tip environment from dissolution of MnS-inclusions is assumed to be proportional to the steel sulphur content and CGR (intersection rate of new dissolvable MnS-inclusions) and to increase exponentially with the potential gradient/ECP (based on crevice experiments and modelling) (Table 11). Similarly, sulphur-anion concentration in the crack-tip environment from the migration of sulphur-anions in the bulk environment outside the crack is proportional to their concentration and increases exponentially with potential gradient/ECP. The transition from high- to low-sulphur EAC CGRs is therefore shifted to lower crack-tip strain rates (or K_I values, loading frequencies) (Figures 56, 95, 102a, 103, and 105) exponentially with increasing ECP and linearly with increasing steel sulphur and sulphur-anion content in the bulk environment (see Table 11 and Figure 102b). Since the model directly considers the effect of crack growth on crack-tip environment chemistry and vice versa, it is therefore able to predict hysteresis effects, e.g., in decreasing-increasing loading frequency fatigue experiments [215, 222] as it has been observed by van der Sluys [77].

$da/dt_{EAC} = A \cdot (d\varepsilon/dt_{CT})^n$	$A, n = f(C_{CT})$	
High-Sulphur Line ($S^{2-} \geq 2$ ppm)	$d\varepsilon/dt_{CT} < 1E\text{-}4$ s^{-1}: $da/dt_{EAC} = 2.25E\text{-}6 \cdot (d\varepsilon/dt_{CT})^{0.35}$ $d\varepsilon/dt_{CT} > 1E\text{-}3$ s^{-1}: $da/dt_{EAC} = 2.3E\text{-}7$ m/s	
Low-Sulphur Line ($S^{2-} \leq 20$ ppb)	$d\varepsilon/dt_{CT} < 1E\text{-}4$ s^{-1}: $da/dt_{EAC} = 1E\text{-}4 \cdot (d\varepsilon/dt_{CT})$ $d\varepsilon/dt_{CT} > 1E\text{-}3$ s^{-1}: $da/dt_{EAC} = 3.7E\text{-}8$ m/s	
Transition Curves	= f (ECP, wt.% S, c_{CT}, history)	
Crack-tip strain rate $d\varepsilon/dt_{CT}$		
Loading rate/level, CGR, yield stress, visco-plasticity, DSA, CDI		
Constant Load	$d\varepsilon/dt_{CT} = A \cdot d\varepsilon/dt_{creep}(K_I) + B \cdot da/dt = 3.29E\text{-}17 \cdot K_I^4$	
Cyclic Load	$d\varepsilon/dt_{CT} = C \cdot dK_I/dt + D \cdot da/dt = 4E\text{-}4 \cdot da/dt_{air}$ $da/dt_{Air} = f(\Delta K, R, \nu)$, e.g., ASME XI air rates	
S-anion content in the crack-tip environment C_{CT}		
S-impurities in bulk environment, dissolution of MnS-inclusions in crack enclave, mass transport (diffusion, migration, convection), CGR		
Exposure rate of new fresh dissolvable MnS	$c_{CT} \propto da/dt$	
MnS-dissolution	$c_{CT} \propto$ wt.% S	
Migration $\Delta\Phi = \Phi_{Crack\text{-}mouth} - \Phi_{Crack\ tip} = f(DO, \ldots)$	$c_{CT} \propto c_{Bulk} \cdot \exp(\Delta\Phi)$	
Convection by external flow and by cyclic fatigue pumping = f (R, ν, ...)	$c_{CT} = f$ (Hydrodynamics)	

Table 11: Summary of basic equations of the GE-model (simplified). EAC crack growth is controlled by crack-tip strain rate $d\varepsilon/dt_{CT}$ and sulphur-anion concentration in crack-tip electrolyte c_{CT}. YS, DSA, lower temperatures, or flow rate effects are not explicitly considered. [16, 66, 114, 156, 219, 222]

Material Parameters
S $\uparrow$, MnS $\uparrow$ $\rightarrow c_{CT} \uparrow \rightarrow da/dt \uparrow$
YS $\uparrow$, work hardening $\uparrow$, DSA $\uparrow$, creep $\uparrow \rightarrow d\varepsilon/dt_{CT} \uparrow \rightarrow da/dt \uparrow$
Environmental Parameters
ECP $\uparrow$, DO $\uparrow$, SO$_4^{2-}$ $\uparrow \rightarrow c_{CT} \uparrow \rightarrow da/dt \uparrow$
Flow rate $\downarrow \rightarrow c_{CT} \uparrow \rightarrow da/dt \uparrow$
Loading Parameter
$K_I \uparrow$, $\Delta K \uparrow$ $\rightarrow d\varepsilon/dt_{CT} \uparrow \rightarrow da/dt \uparrow$
$dK/dt \uparrow$, $\nu \uparrow$ $\rightarrow d\varepsilon/dt_{CT} \uparrow \rightarrow da/dt \uparrow$

Table 12: Summary of major parameter trends according to the GE-model.
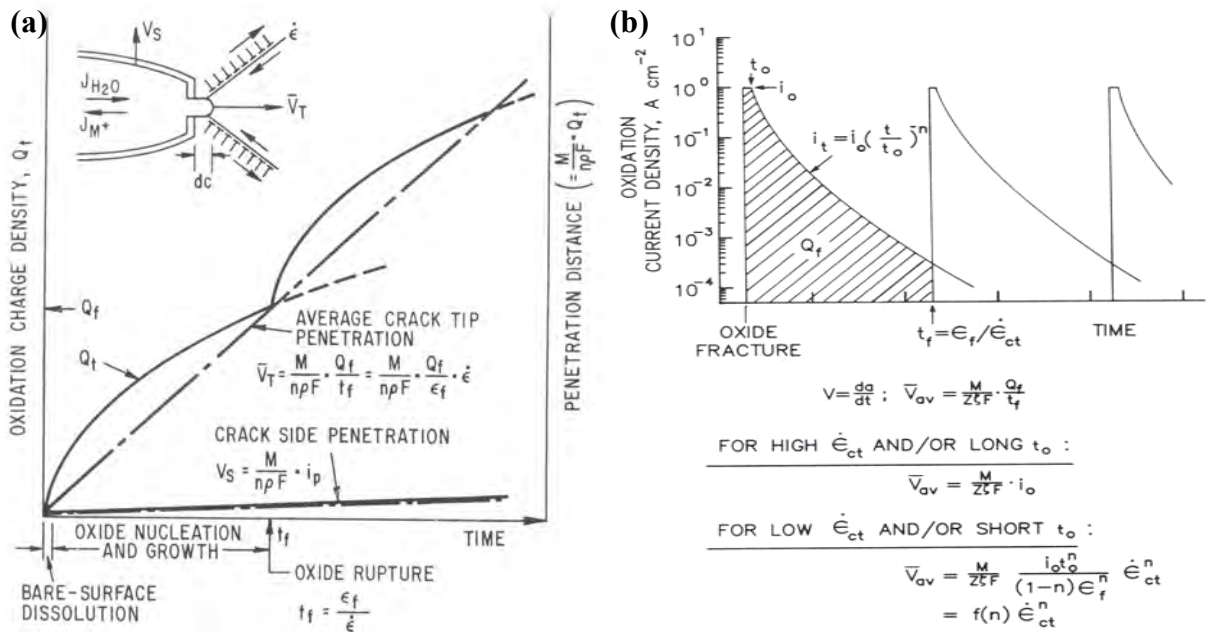
Figure 99: Schematic oxidation charge density/time relationship (a) and oxidation current density/time transients (b) for a strained crack-tip including the basic equations of the GE-model [16].
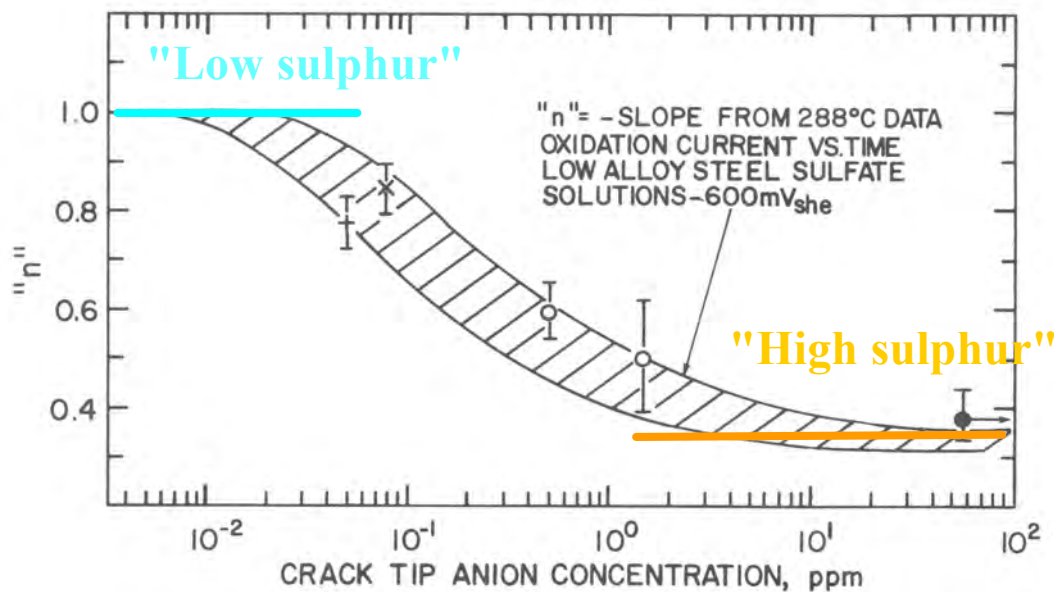
Figure 100: Relationship between "repassivation exponent" n (see Figure 99b) and sulphur-anion concentration in the crack-tip environment [16]. This relationship forms the basis for the low- and high-sulphur CGR-crack-tip strain rate equation.
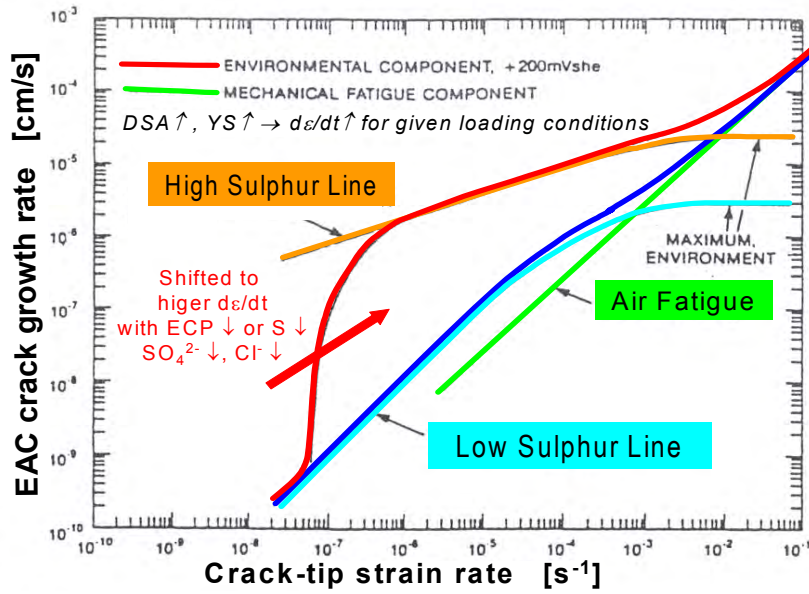
Figure 101: Basic EAC crack growth curves of the GE-model in an EAC CGR-crack-tip strain rate plot [16, 66, 114]. The transition from high- to low-sulphur EAC rates is shifted to lower crack-tip strain rates with increasing ECP, steel sulphur content and sulphur-anion content of the bulk environment. A higher DSA susceptibility or a higher YS result in a higher crack-tip strain rate for given loading conditions.
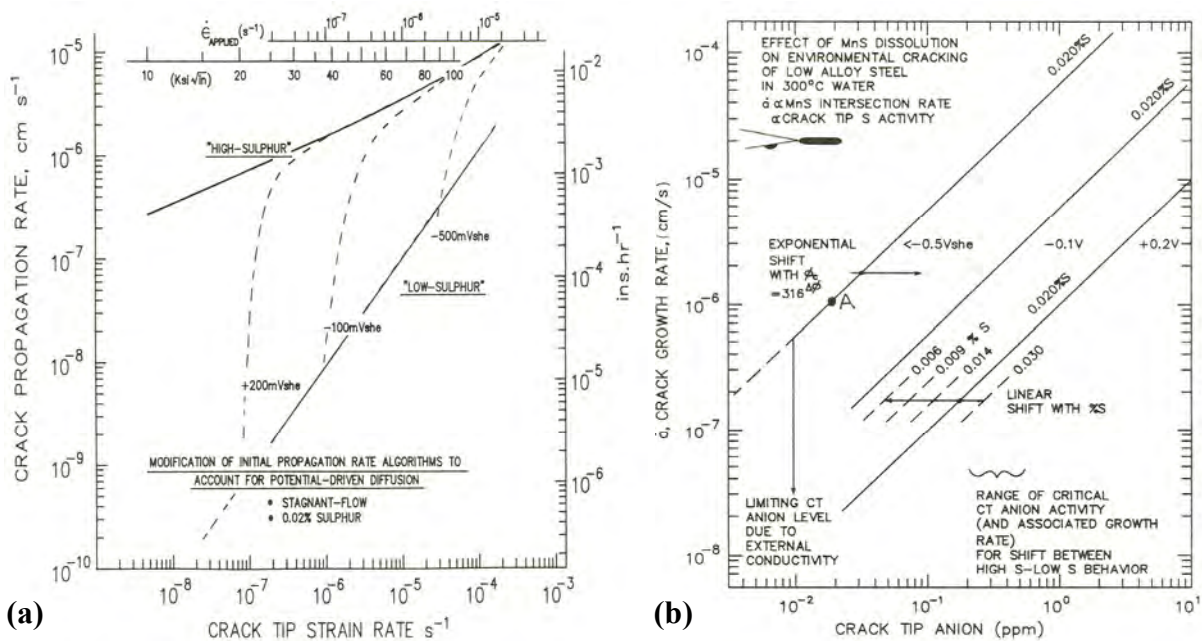
Figure 102: EAC CGR-crack-tip strain rate curves for different ECPs (a) and interrelation between sulphur-anion content in crack-tip environment, CGR, ECP, and steel sulphur content [16].

10.6.2 Assessment of SCC Crack Growth Prediction Curves

In Figure 103 the SCC crack growth predictions of the GE-model for a RPV steel with a sulphur content of 0.02 wt.% S in high-purity oxygenated HT water at different ECP levels are compared with corresponding PSI constant load tests results.

111
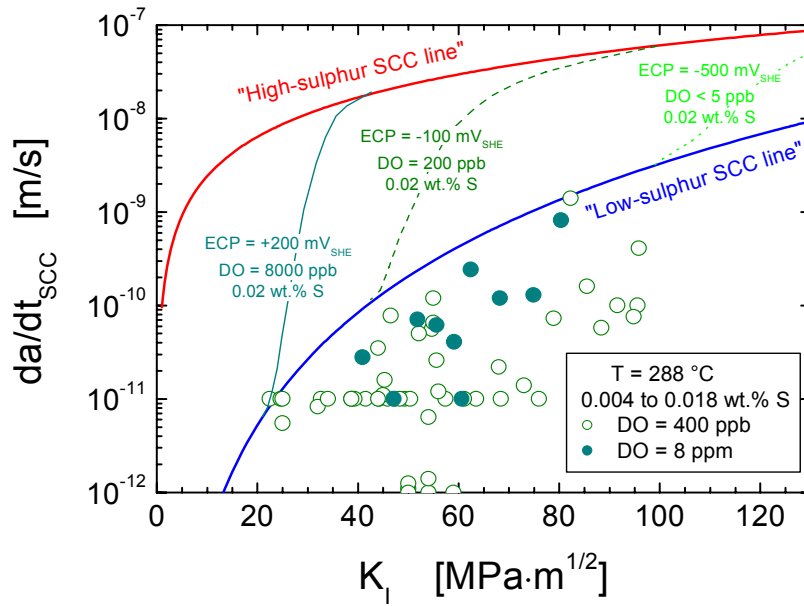
Figure 103: Comparison of constant load SCC test results in oxygenated HT water [35] with the predictions of the GE-model [16, 170, 171].

In contrast to corrosion fatigue, an apparently bad correlation was observed under constant load, where the model would predict much higher high-sulphur SCC CGR than typically observed in high-purity oxidizing water (Figure 103). This discrepancy may be rather related to the SCC cessation/crack pinning phenomena typically occurring at K_I levels < 60 MPa·m$^{1/2}$ than to a fundamental error in the model. These phenomena are related to the conjoint requirement and interrelation between crack-tip strain rate and CGR (and crack chemistry and CGR) [215, 222], and in particular, to the difficulty to maintain a sustained crack-tip strain rate at low K_I levels under constant load in C & LAS.

Under constant load no formulation exists for the computing of the balance and dynamic equilibrium between loss of dislocation sources by low-temperature creep exhaustion and the activation of new dislocation sources by the moving crack-tip. The empirical formula between crack-tip strain rate and stress intensity factor for constant load has originally been derived for stainless steels based on low-temperature creep experiments with compact tension specimens and was then adjusted to LAS by fitting it to the SCC LAS data, which were available at that time. Most of these tests involved some additional dynamic external loading (PPU for crack length measurement by compliance method), a poor water chemistry control with increased chloride levels (e.g., static autoclave tests) or specimens, where SSY conditions were clearly exceeded. It is therefore believed that this formula is generally unsatisfactory for application for stress intensity factor smaller than 40 to 60 MPa·m$^{1/2}$ in high-purity water under constant load [16] and the main reason for the apparent discrepancy between the model and experiments.

Under those few critical parameter combinations (excessive hardness/high YS, high DSA susceptibility), where fast sustained SCC was observed in high-purity water at K_I levels < 60 to 70 MPa·m$^{1/2}$, the SCC CGR reached up to the predicted high-sulphur SCC CGR of the GE-model (Figure 104) in some cases. A high YS [137, 138] or DSA susceptibility [27, 136] in the DSA temperature range result in a relevant increase of crack-tip strain/strain rate under otherwise identical loading conditions and may therefore help to overcome the dynamic crack-tip strain rate criteria. Similarly, if SSY conditions are significantly exceeded in small size specimens, the sustained low-temperature creep by gross ligament yielding also favours sustained SCC crack growth.
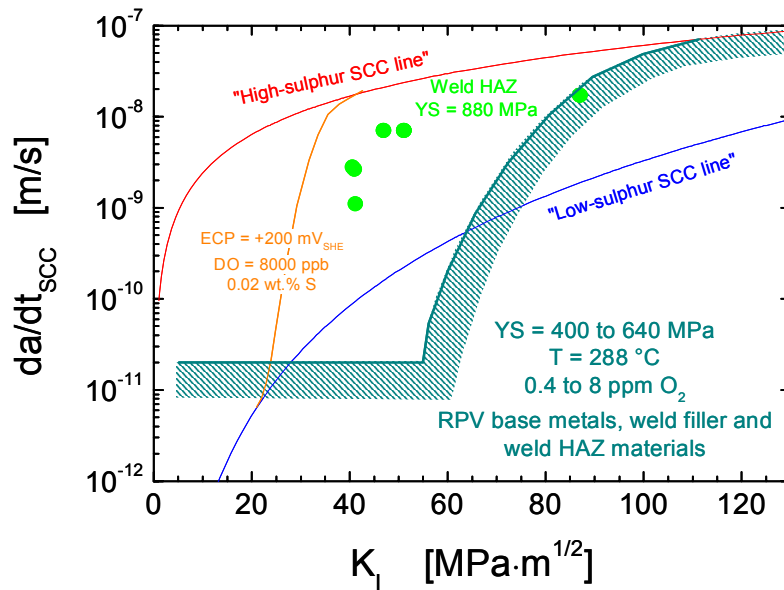
Figure 104: Comparison of constant load SCC CGRs of a weld HAZ with high hardness/YS in oxygenated HT water [36] with predictions of GE-model [16, 170, 171].

10.6.3 Assessment of CF Crack Growth Prediction Curves

A linear superposition of fatigue and EAC crack growth is assumed for CF crack growth [16, 66]. Characteristic cyclic CF crack growth prediction trends of the GE-model under BWR conditions are exemplary shown in Figures 53, 54 (cycle-based CGR), and 56 (time-based CGR). The CF CGR data of all materials were lying between the high- and low-sulphur CF line of the GE-model [16, 66] and were always conservatively covered by the high-sulphur CF line for all frequencies and temperatures (Figures 14, 23, 57, 59, and 105) [51, 62, 128]. The model readily predicts the effect of loading frequency and ΔK and the corresponding thresholds over a wide range of system conditions (Figures 14, 23, 57, 59, and 105). Under highly oxidizing BWR/NWC and reducing HWC conditions, the LFCF CGR ($\leq 10^{-3}$ Hz) were close to the high-sulphur and low-sulphur CF line, respectively (Figure 14). At ECPs ≤ -100 mV$_{SHE}$, the model seemed to reasonably well predict the experimentally observed critical frequency behaviour (Figure 105).

On the other hand, there is now some increasing experimental evidence that the transition curves between the low- and high-sulphur CF curve of the GE-model do not conservatively cover the results under highly oxidizing conditions (DO ≥ 0.4 ppm, ECP ≥ 0 mV$_{SHE}$) at very low loading frequencies $< 10^{-4}$ Hz (Figures 57 and 105). The model predicts too high critical frequencies ν_{crit}, air CGR da/dt$_{Air,crit}$, and ΔK_{EAC}-thresholds under these highly oxidizing conditions. DSA, which is not considered in the GE-model, may be one possible reason for this discrepancy at high ECP and very low loading frequencies. In susceptible materials, DSA may affect the EAC behaviour at temperatures from 150 to 300 °C in particular at slow strain rates/low loading frequencies $< 10^{-4}$ s^{-1}/$< 10^{-4}$ Hz by the strain localization and increase of YS/work hardening exponent, which increase with decreasing strain rate. Within the DSA temperature-strain rate range, DSA may thus result in a higher crack-tip strain and strain rate than for identical loading conditions outside the DSA range, or than in a material which is not susceptible to DSA. DSA may therefore have a similar effect as an increase in loading frequency or ΔK. At very low potentials ≤ -500 mV$_{SHE}$ the transition is in a crack-tip strain rate region of 10^{-4} to 10^{-3} s^{-1}, where DSA effects are absent or moderate and where crack-tip strain rate is completely dominated by the fast crack growth contribution.

113
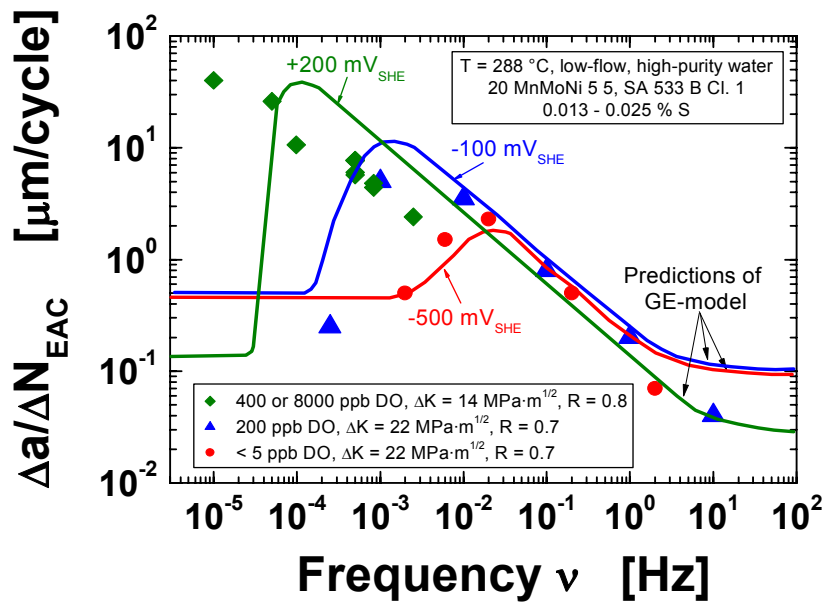
Figure 105: Comparison of the cycle-based CGR $\Delta a/\Delta N_{EAC}$ at different ECP/DO-levels [62] and frequencies with the predictions of the GE-model [16, 66].

During cyclic loading of smooth test specimens, surface cracks of 10 μm or longer form quite early in life (i.e., < 10 % of life) at surface irregularities or discontinuities either already in existence or produced by slip bands, grain boundaries, second-phase particles, etc. [187, 188]. Consequently, fatigue life may be considered to be composed entirely of propagation of cracks from 10 μm to few mm long [31]. Therefore, the GE-model has also been applied to predict LCF initiation in HT water [219]. Although the absolute prediction of N_i, is uncertain and depending on, for instance, the precise definition of "initiation" and the interactions between such phenomena as pitting or crack coalescence, the model predictions readily correlated with the experimental data trends (Figure 106) [219].
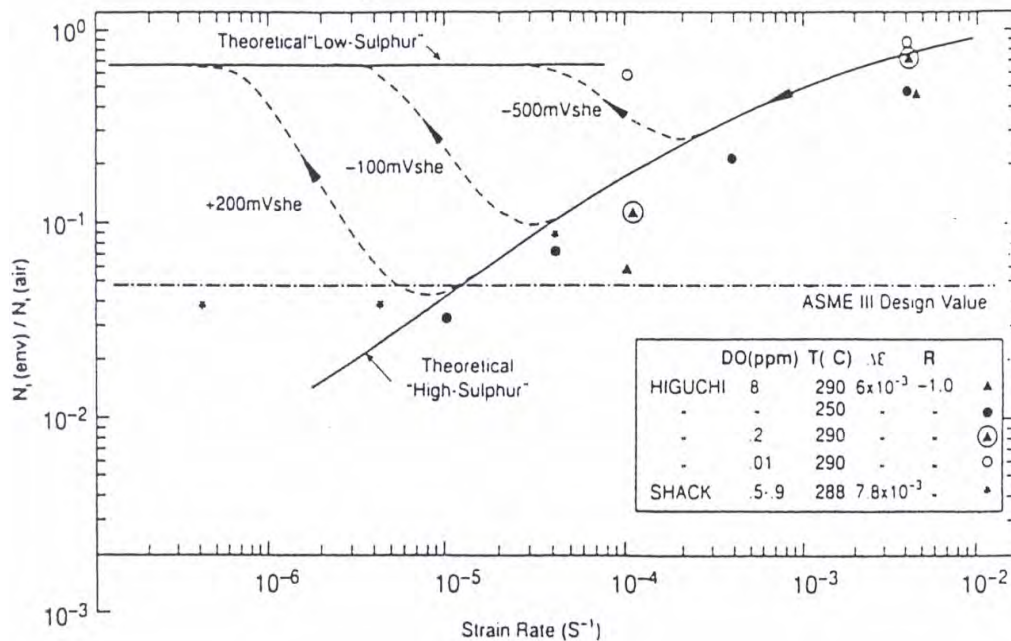
Figure 106: Fatigue life reduction in HT water in dependence of strain rate as measured in experiments and predicted by the GE-model [219].

114

11 Service Experience

11.1 EAC Cracking Incidents in BWR and PWR

The accumulated operating experience and performance of carbon and low-alloy primary pressure-boundary components in NPPs is very good worldwide [5 – 16]. Use of the current fatigue design and evaluation codes (ASME III and XI) has been successful in preventing fatigue cracks and failures in LAS components and the EAC curves in these would therefore seem to be adequate, or even conservative, under most operating circumstances. However, instances of EAC have occurred (particularly in BWR service), most often in LAS piping and, very rarely, in the RPV (where most locations are normally isolated from contact with the environment by a duplex or stabilised austenitic stainless steel weld overlay cladding). Oxidizing agents, usually DO, and relevant dynamic straining were always involved [9, 11, 13, 16]. These cases were attributed either to SICC or CF (Table 1). Cracking incidents with a major or relevant contribution of SCC to the total crack advance in properly manufactured and heat-treated low-alloy primary pressure-boundary components are not known to the authors [13, 128].

EAC has occurred in C or LAS covered by the designations SA 333 Gr.6, SA 106, SA 302 Gr.B, SA 533 B Cl.1 or SA 508 Cl.2/3 (and other national equivalents). Cracking was observed in base metal, as well as weld filler and weld HAZ materials, and has been predominantly TG in nature. In Germany, SICC was frequently observed in relatively high strength, fine-grained structural steels (WB 35, WB 36). These steels were widely used there, e.g., for the construction of pressure vessels and piping in BWRs and for the fabrication of feedwater tanks and heat exchangers in PWRs. This enabled the manufacture of relatively thin-walled components without stress relief treatment of welds.

The following carbon and low-alloy LWR pressure-boundary components have been affected [5 – 16, 72, 231 – 243]:

- Steam and feedwater piping and condensate systems of BWRs (mostly horizontal systems with stagnant or low flow and/or condensing steam or auxiliary condensates, intermittently-operated systems (flushing lines), mostly pipe to elbow joints and pipe bends, isolated cases of straight sections of piping at mechanical restraints).

- Feedwater nozzles of BWR RPVs (Figures 107 and 110).

- Feedwater piping/tanks and heat exchangers in the secondary circuit of PWRs, feedwater nozzles of PWR steam generators, steam generator girth welds.

These EAC incidents have been clearly associated with some combination of the following aspects [5 – 16, 72, 231 – 243]:

- **Severe dynamic straining,** due to global and local thermal stratification/striping (e.g., during hot-stand-by at low feedwater flow rate), or due to thermal and pressurisation cycles (e.g., plant-start-up/shut-down, hot stand-by, turbine rolls, etc.).

- **An oxidizing environment,** normally due to oxygen (in some few cases Cu^{2+}-cations from brass condensers helped to raise the ECP) and sometimes in conjunction with unspecified anionic impurities (Cl^-, SO_4^{2-}, etc.). Most PWR cracking incidents involved feedwater under specific operating conditions, or at special locations, where the normally low contents of oxygen <u>cannot</u> be assumed. The fact that cracking frequently occurred in BWR lines with stagnant steam or non-degassed condensate, but not in comparable lines carrying flowing steam, is another indication that oxygen concentration/corrosion potential are crucial parameters with respect to the occurrence of EAC, since such conditions are known to encourage the formation of a condensate film rich in dissolved oxygen.

- **High local stress around or above the HT yield stress, or high secondary/residual stress,** due, for instance, to local stress raisers, geometrical welding defects (misalignment of weld edges, excessive weld penetration leading to root notches and lack of fusion or incipient cracking in the root region), pipe bends in conjunction with inadequate pipe support or restraints, localized post-weld treatment and fit-up deformation.
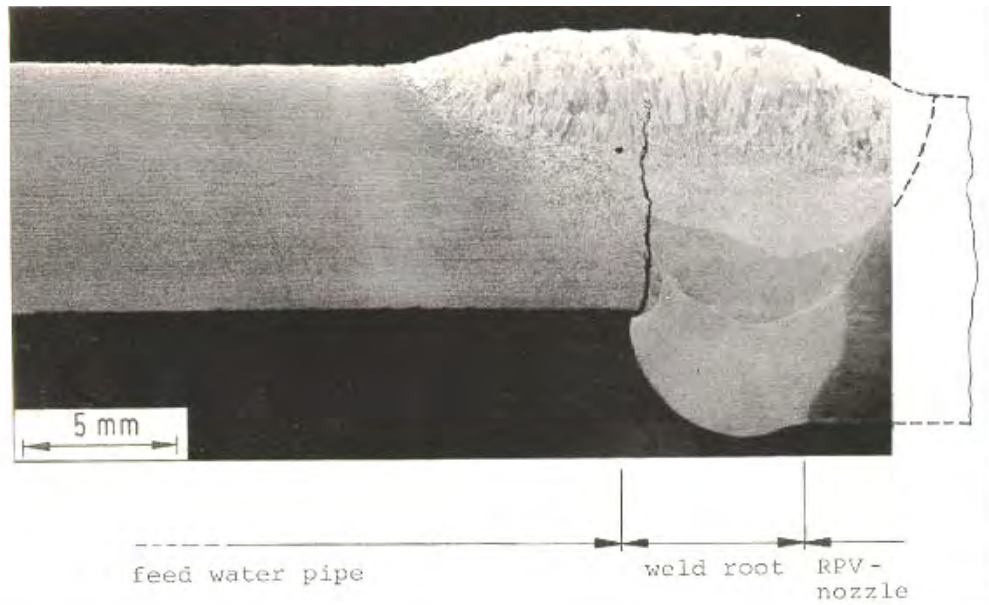
Figure 107: Circumferential SICC cracking at the feed water pipe to RPV nozzle weld of a German BWR unit, detected after about 11000 h of operation [15]. The major cracks initiated at weld root defects in the 12 o'clock position and had propagated up to a maximum depth of 80 % of wall thickness. They were located in the base metal, weld filler and HAZ material. Clear fatigue striations were observed in some areas of the fracture surface, thus confirming that cyclic loading was involved. Minor cracking was observed in the 6 o'clock position. The smaller cracks initiated from corrosion pits and showed less striations. In the initial operating phase, this component was subjected quite frequently to thermal shock by cold water injection and, in particular, to severe thermal stratification during start-up and hot stand-by or during plant transients with reduced feed water flow of less than 5 % of the normal flow capacity.

EAC damage was usually detected by non-destructive examination and seldom led to through-wall penetrations with leakage [13, 15]. In several of the reported incidents, EAC in LAS has occurred as a result of substantial departures from either design intentions or normal operation practice. These can be identified and can therefore be avoided [9]. Several incidents were related to unanticipated/unevaluated sources, frequency, and/or severity of thermal stress cycles in critical locations, thus indicating design inadequacies [5]. In many cases, fabrication or design deficiencies (e.g., welding defects) favoured local plastification and thus dynamic straining of the water-wetted material surface and sometimes resulted in an increased stress intensity (residual stress, weld geometries, hot cracks in weld cladding), or increased EAC susceptibility of the material (e.g., due to excessive hardness of LAS weld HAZs) [5, 9, 13, 15]. Reoccurrence of these cases was avoided, or significantly reduced, by improved design of the components or fabrication procedures and better quality control during the fabrication process, as well as by optimized operation procedures [5, 9, 13, 15, 237 – 243].

Cracks often initiated from water-wetted geometric discontinuities (which result in local stress concentrations) and/or in regions, where the formation of an aggressive, occluded water

chemistry was favoured (stagnant flow, crevice, etc.) [5, 9, 13, 15]. In many cases EAC cracks preferentially initiated from corrosion pits (Figure 108) and/or at MnS-inclusions intersecting the steel surface. In some cases, corrosion during shut-down periods (pitting, corrosion products (rust) close to the water line as a possible source of anionic impurities during start-up) was a further contributing factor [72]. In general, crack initiation has been more affected by high frequency, high-cycle fatigue due to local thermal stratification or thermal striping loads which were limited to near-surface regions. Crack propagation was often dominated by low-cycle fatigue from slower and less frequent transients, due, e.g., to global thermal stratification or operational power transients (start-up/shut-down, hot stand-by, etc.) [5].
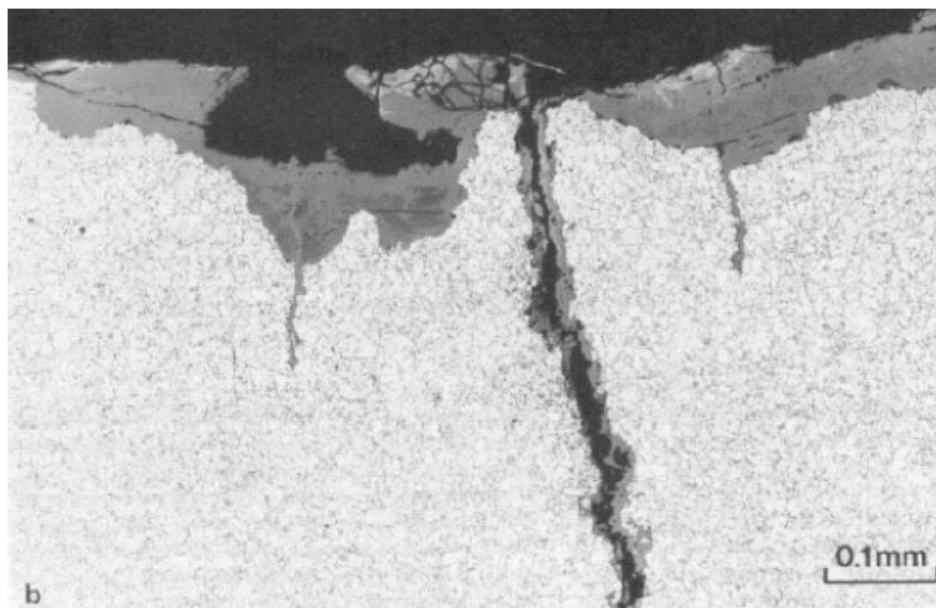
Figure 108: Axial SICC cracks in LAS pipe close to a pipe bend originating from corrosion pits [32].

A complete root cause evaluation has not always been performed in all cracking incidents. Therefore, identification of the cracking mode has not always been completely clear and, in particular, assessment of the relative contributions of EAC (SCC or SICC/CF) and pure mechanical fatigue to the total crack advance has often not been possible. Minor contributions to crack propagation through SCC cannot therefore be completely ruled out for some cracking incidents, but cases with major contributions of SCC to the total crack advance in properly manufactured and heat-treated, low-alloy, primary pressure-boundary components are not known to the authors. In contrast, certain incidents indicate excellent SCC resistance of the base metal under stationary power operation conditions, since no corrosion damage in the form of cracks has occurred either as a result of extensive surface contact with the operating environment (e.g., for unclad reactor heads or nozzle bore radii), or at the tips of cracks penetrating through the cladding to the low-alloy base metal [14].

11.2 Critical Components and Operation Conditions

Special attention should be paid to components, which are likely to undergo significant localized mechanical loading around or above the design/HT YS levels or which are related to increased oxygen contents/conductivities/quasi-stagnant flow conditions during operation [15]. Operational transients, which are associated with thermal stratification/high secondary strains (e.g., start-up, hot stand-by, etc.) or sufficiently slow, but relevant pressure and temperature changes should receive attention, in particular if they occur with a sufficiently high frequency. Critical components, for instance, are [15]:

117

- Pipelines, carrying nearly stagnant steam or non-degassed condensate during normal operation (or which are used only intermittently).

- Feedwater nozzles and adjacent sections of horizontal piping, if thermal stratification can occur.

- Components, which are likely to undergo significant localized mechanical loading over or above the design levels (e.g., thin-walled piping and pipe bends in conjunction with inadequate pipe supports or restraints).

11.3 Possible Mitigation Actions and Prevention Strategies

The common EAC mitigation strategy is to exclude large pre-existing defects by non-destructive (ND) examination and quality assurance (QA) measures during and after fabrication of components before they were put in operation and to avoid during operation those water chemistry/stress or strain combinations, which could lead to EAC crack initiation or accelerated crack growth. This procedure is complemented by periodic ND in-service inspection (ISI) of critical component locations. Based on the operating experience and laboratory background knowledge different short or long-term remedial measures have been successfully defined and applied [5, 13, 61, 65 – 68] for example by changing or optimising of manufacturing, design and operation related features. Operating conditions and component designs should be optimized to avoid dynamic straining and highly oxidizing/stagnant conditions. Temperature gradients/cycles, thermal stratification/stripping, oxygen enrichment and stagnant conditions should be reduced/avoided as far as possible. In summary EAC risks can be minimised by:

- Selection of suitable materials e.g. low sulphur steel (< 0.003 wt.% S) with low EAC and DSA susceptibility and optimized high toughness ($\rightarrow$ larger critical crack size).

- Selection of suitable manufacturing and fabrication practice to avoid welding defects and HAZ with high hardness (by suitable post-weld heat treatments) and to reduce residual stress (stress relieving, narrow gap welding).

- An improved design to reduce regions of high local stresses (by increased wall thickness, by internal flush grinding of joints and optimisation of welding technology, avoidance of discontinuities and constraints, optimized pipe supports).

- Reduction of the number of thermal and pressurisation cycles (thermal-stratification during hot stand-by, start-up/shut-down) and of temperature gradients by optimized operating procedure or an improved design of the affected component (thermal sleeve of feedwater nozzle, feedwater sparger).

- Avoiding stagnant conditions/crevices and reducing oxygen levels by optimized operation practice (for example modification of start-up procedures to reduce dissolved oxygen levels by better venting of piping, improvement of drainage in horizontal lines, etc.).

- An adequate water chemistry control (EPRI or VGB guidelines) and application of HWC/NMCA to reduce the ECP.

The current BWR operation practice is almost fully optimized with regard to water chemistry and fatigue. A further relevant reduction of the EAC risk may be obtained by the reduction of the ECP by hydrogen injection and noble chemical addition and by optimisation of ISI programmes with respect to EAC risks.

12 Service Experience vs. Experimental/Mechanistic Knowledge

12.1 Qualitative Assessment of Field Experience

Operating experience (Section 11) fits well to the accumulated experimental (Sections 4 to 9) and theoretical (Section 10) knowledge on EAC and pitting behaviour in the system LAS/HT water. Both operating and laboratory experience show the same qualitative parameter trends, e.g., for oxygen, flow rate and strain. They confirm the high SCC resistance of LAS under steady-state power operation and static loading conditions and clearly reveal that slow, positive (tensile) dynamic straining with associated plastic yielding and sufficiently oxidizing conditions are essential for EAC initiation and subsequent crack growth in high-purity, HT water. Since primary design stresses are generally limited to values below the elastic limit, (local) plastification at defect-free surfaces can only occur under special conditions with high secondary stresses (thermal stresses), or in regions of increased local stress (notches, weld defects, residual stress, etc.). Thermal-hydraulics (e.g., thermal stratification) and local stress raisers therefore played a key role for SICC/CF in the field and were generally more important than material or water chemistry aspects. EAC cracks often initiated from corrosion pits or MnS inclusions which intersected the steel surface. Pitting of LAS is strongly favoured under oxidizing conditions (high oxygen concentration), especially at low and intermediate temperatures, and by slow dynamic straining [6, 7, 13]. Quasi-stagnant or low-flow conditions promote the formation of an aggressive, occluded water chemistry at the base of the pit or within small surface defects, as well as the enrichment of oxygen in steam condensate, and therefore promote EAC initiation.

The conditions promoting SICC/CF susceptibility specified in Section 5 can be compared to typical LWR operational transients [10] in Table 13 and to the water chemistry conditions during BWR and PWR operation in Tables 14 to 16. Under PWR or BWR/HWC conditions, the oxygen threshold is only exceeded under some very specific operational conditions, or at special locations, where (temporary) increased DO levels cannot be fully excluded. Under BWR/NWC conditions, on the other hand, the ECP threshold criterion is always satisfied. For many BWR operational transients, the strain rate can be expected to lie in the critical range; nevertheless the frequency of cracking incidents has been relatively low. Most SICC cracking incidents in the field were related to significantly higher dissolved oxygen contents (> 300 ppb DO) than the laboratory thresholds of 20 to 100 ppb and to quasi-stagnant or low-flow conditions [5, 15].

Component	Operation	O_2 [ppb]	T [°C]	$\Delta\varepsilon$ [%]	$d\varepsilon/dt$ [s^{-1}]
PWR SG FW Nozzle	Start-up	5	230/RT	0.2 – 0.5	1E-4
BWR RPV FW Nozzle	Start-up	20/200	216/38	0.2 – 0.4	1E-4
BWR FW Piping	Start-up	20/200	216/38	0.2 – 0.5	1E-5 – 1E-4
BWR FW Piping	Start-up	20/200	288/38	0.067 – 0.1	4E-6 – 8E-8
BWR FW Piping	Turbine Roll	< 200	288/80	0.4	3E-6 – 6E-6
BWR FW Piping	Hot Stand-by	< 200	288/90	0.26	4E-6
BWR FW Piping	Cool-down	< 20	288/RT	0.2	> 6E-6
BWR FW Piping	Stratification	200	250/50	0.2 – 0.7	1E-6 – 1E-5

Table 13: Typical strain transients in LWR [10].

Parameter	Stationary Power Operation	Start-up sp: stationary power operation
κ [μS/cm]	0.08 to 0.1	1.0 $\rightarrow$ 0.1 (sp)
T [°C]	274 to 290	25 $\rightarrow$ 290 (sp)
pH_T	5.6	5.6 $\rightarrow$ 8.6 $\rightarrow$ 5.6 (sp)
O_2 [ppm]	0.2 (0.1 to 0.3)	8.0 $\rightarrow$ 0.02 (150°C) $\rightarrow$ 0.2 (sp)
H_2 [ppm]	0.015 (0.005 to 0.03)	0 $\rightarrow$ 0. 015 (sp)
H_2O_2 [ppm]	0 - 0.4*	0 $\rightarrow$ 1.0 (150 °C) $\rightarrow$ 0 $-$ 0.4 (sp)
Cl^- [ppb]	< 1	< 5 to 10 $\rightarrow$ < 1 (sp)
ECP(LAS) [mV_{SHE}]	0 to +150	no measured values

*Decrease of concentration with growing distance from reactor core (thermal and heterogeneous decomposition).

Table 14: Typical BWR/NWC reactor water conditions during stationary power operation and start-up. In C & LAS feedwater and steam piping different conditions prevail.

Parameter	Feed Water	Reactor Water
κ [μS/cm]	0.06 to 0.07	0.08 to 0.1
T [°C]	180 to 220	274 to 290
pH_T	5.6	5.6
O_2 [ppm]	0.08 (0.02 to 0.2)	0.2 (0.1 to 0.3)
H_2O_2 [ppm]	-	0 to 0.4
H_2 [ppm]	-	0.015 (0.005 to 0.03)
Cl^- [ppb]	< 1	< 1
ECP(LAS) [mV_{SHE}]	-200 to 0 mV_{SHE}	-50 to +150 mV_{SHE}

Table 15: Typical feed and reactor water conditions during stationary BWR/NWC power operation.

Parameter	BWR/NWC	BWR/HWC	PWR
Temperature	274 to 290 °C	274 to 290 °C	290 to 320 °C
Pressure	7.2 MPa	7.2 MPa	16 MPa
Flow rate	1 to 10 m/s	1 to 10 m/s	1 to 10 m/s
$pH_{300\,°C}$	5.65 (neutral)	5.65 (neutral)	6.8 – 7.4 (alkalic)
κ at 25 °C	$\leq$ 0.1 μS/cm	$\leq$ 0.1 μS/cm	10 to 40 μS/cm
Composition	O_2 + ½ H_2O_2 > H_2 High-purity water	H_2 >> O_2 + ½ H_2O_2 High-purity water	H_2 >> O_2 + ½ H_2O_2 H_3BO_3, LiOH
O_2 + ½ H_2O_2	200 to 600 ppb*	< 5 to 50 ppb*	< 10 ppb
H_2	5 – 30 ppb*	50 to 300 ppb* (1 to 2.5 ppm in feedwater)	2 to 5 ppm
Cl^-, SO_4^{2-}	< 1 ppb	< 1 ppb	< 1 to < 50 ppb
ECP (SS)	+50 to +250 mV_{SHE}	-500 to -200 mV_{SHE}**	-700 to -500 mV_{SHE}
ECP (LAS)	-50 to +150 mV_{SHE}	-600 to -200 mV_{SHE}**	-800 to -600 mV_{SHE}

* May strongly depend on reactor design and location within RPV
** In upper plenum always a high ECP of + 150 to +200 mV_{SHE} prevails.

Table 16: Typical reactor water conditions during stationary BWR and PWR operation.

By taking exact boundary conditions in lab tests and in the field into account, no major discrepancy between operating experience and trends in laboratory data could be found. The higher cracking frequency in lab tests may be easily explained by the beneficial effect in the field of a turbulent flow rate (which is characteristic for most component locations) on EAC

initiation and the conjoint threshold conditions for the onset of EAC with regard to ECP (or DO content), strain rate, strain and temperature. In general, for many transients/component locations, one or several threshold conditions are not satisfied. Even if all requirements were to be fulfilled, the SCC/fatigue initiation process may consume a long incubation period/ large number of fatigue cycles in the absence of pre-existing defects or cracks, in particular for small strains, and therefore extend over a significant part (or even the whole) of the plant lifetime. Most laboratory experiments start with a sharp, and relatively deep, pre-crack that is "ready" to propagate; this is significantly different from the situation in most components. [13, 18, 19]

12.2 Relevance and Adequacy of Lab Test Conditions

The majority of laboratory testing for data generation, which also form the main basis for EAC evaluation in LAS components, have been conducted with pre-cracked C(T) base metal specimens under isothermal and/or stationary water chemistry and either under pure static or cyclic loading conditions at rather high $\Delta K/K_I$ values. On the other hand, most CF and SICC related failures in service have occurred as a result of temporary thermal cycling, usually during plant transients, with typically biaxial stress generated under total strain control followed by long periods of static loading and isothermal conditions. Real cracks rather started from notches/geometrical discontinuities (e.g., welding defects) than from pre-cracks and revealed quite different crack shapes/configuration than in laboratory specimens. Furthermore, near-surface short crack growth behaviour under small $\Delta K/K_I$ (or $\Delta J/J$) conditions close to EAC and fatigue thresholds generally covered a large part of the lifetime. [5, 13, 18, 19]

In spite of some relevant differences between real field and simplified lab conditions, most experiments may still be regarded as representative or bounding for many specific plant/component situations. The overwhelming part of laboratory testing for data generation has generally been performed in a conservative way with respect to field conditions (e.g., experiments under quasi-stagnant or low-flow conditions in the temperature range of maximum EAC susceptibility, or loading and test histories, which result in the lowest feasible thresholds, etc.). These data therefore usually contain sufficient or even undue conservatism. As long as the boundary conditions in the field and lab tests are adequately known and carefully taken into account, these differences are not regarded as a critical point.

12.3 Assessment of Cracking Incidents by Flaw Tolerance Evaluations

Only few EAC flaw tolerance evaluations can be found in the literature [5, 16, 182, 209, 245]. Although these engineering assessments contain many simplifications and are strongly affected by the assumed boundary and initial conditions, they may give some indications concerning the real safety margins and the adequacy of the current inspection intervals of the periodic in-service inspection in case of EAC. As discussed below by some few examples, they generally confirm the excellent service record of C & LAS primary pressure-boundary components and are able to rationalize the few cracking incidents.

Within the BWRVIP-60 project [182], flaw tolerance evaluations were performed for circumferential and axial cracks in the vessel head and in the vessel around the vicinity of the shroud support plate to vessel weld in a BWR environment using the BWRVIP-60 SCC DL 1 (stationary, transient-free power operation). The evaluation results indicate that for both types of flaws, considerable time and sufficient margins with respect to the current inspection interval of 4 to 10 years exist for postulated initial through-clad flaws to reach the ASME Section XI allowable flaw size, thereby demonstrating substantial flaw tolerance for SCC in BWR pressure vessels. Field experience has shown, that no SCC induced damage has occurred in

BWR RPVs. All cracking in vessel cladding or attachment welds was usually confined to the weld metal and was often the result of manufacturing or fabrication defects.

Figure 109 shows selected results of a similar flaw tolerance analysis for SCC in a BWR RPV according to Blind [245], which is based on the low-sulphur line of the GE-model. This curve basically corresponds to the BWRVIP-60 SCC DL 2. Starting from a semi-elliptical axial surface crack in the cylindrical shell of the RPV, which just penetrates the cladding, the allowable ASME XI flaw size is just reached after more than 25 years of power operation even with this rather conservative SCC crack growth law. For the same initial axial crack configuration in the region of the highly stressed feedwater nozzle corner, the allowable flaw size is already reached after 2 to 3 years. In case of an uncladded feedwater nozzle corner and an axial semi-elliptical surface crack with an initial depth of 3 mm (which roughly corresponds to the NDT limit), the allowable ASME XI flaw size is reached after 12 years. Although these considerations were based on a rather conservative SCC crack growth curve, they clearly show, that in case of the highly stressed feedwater nozzle corner, there are significantly less margins than in the cylindrical RPV shell. Furthermore, it also has to be considered, that these component locations may be subjected to relevant fatigue load during plant transients.
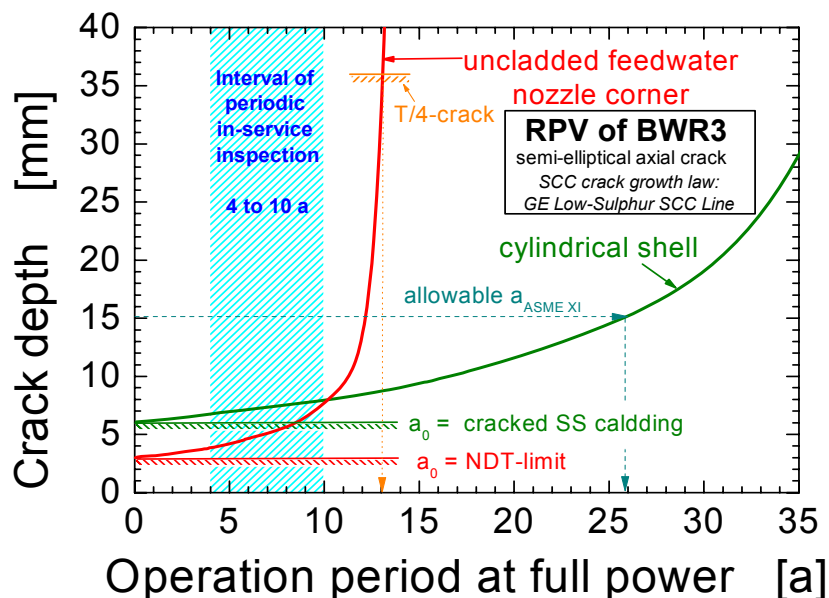
Figure 109: SCC flaw tolerance evaluation based on the GE low-sulphur SCC line for an axial semi-elliptical crack in the cylindrical shell and the uncladded feedwater nozzle corner of a BWR-3 according to Blind [245].

Because of the very low SCC CGRs up to relatively high K_I values of 50 to 60 MPa·m$^{1/2}$, the crack growth evaluations generally indicate a high flaw tolerance and large safety margins with respect to SCC in primary pressure-boundary components under transient-free steady-state power operation for small incipient crack depths in the range of typical NDT limits. These margins disappear in those situations, where high SCC rates can occur (e.g., for deep initial cracks or very high residual stress fields, chloride, ripple loading, intermediate temperatures and high DSA susceptibility, excessive hardness, etc.). Although most of these situations may appear as atypical for current power operation or properly manufactured and fabricated LAS primary pressure-boundary components, it should be reminded that at least in some specific or faulted situations relevant SCC crack extensions could occur in such components.

The EAC cracking incidents in some RPV feedwater nozzles in GE BWR [5, 14, 16], where cracking has been located in the bore and blend radius regions of the SA 508 nozzle (Figure 110) cladded by 308 (non-sensitised) duplex stainless steel could be explained by a sequence of high cycle thermal fatigue and EAC under low cycle conditions and was related to an inadequate thermal sleeve design, which allowed a leakage flow of cold feedwater in the annulus between the nozzle and the sleeve.
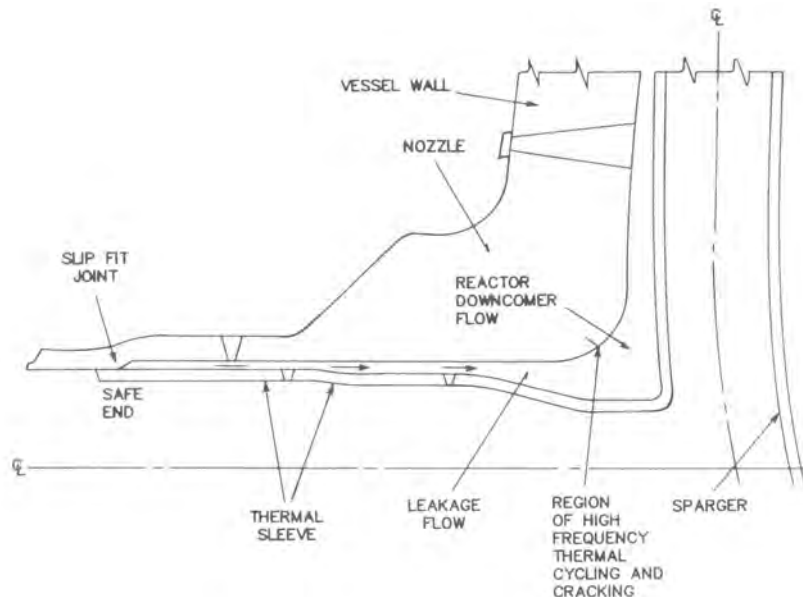
Figure 110: Schematic cross-section of feed water inlet nozzle/thermal sleeve/sparger assembly, indicating the region of cracking at the nozzle corner [5, 14].

The cracking was due to a sequence of high-cycle fatigue and EAC under low-cycle conditions and could readily rationalized by fatigue flaw tolerance evaluations based on ASME XI [5, 14]:

- A high frequency thermal fatigue mechanism (without relevant environmental contribution) initiated cracks in the stainless steel cladding, which subsequently propagated through the low-alloy steel. This mechanism [5, 14, 16] was attributed to turbulent mixing of the cold leakage flow (220 °C), past the slip fit joint of the safe end, and the hot downcomer flow (280 °C). The mixing fluid impinges on the nozzle wall, causing thermal cycling at frequencies in the range of 0.01 to 1 Hz. The thermal stress amplitude from this particular source degrades to zero when the crack propagates to an approximate 6 mm depth. An alternate thermal sleeve designs and removal of cladding by grinding, which minimise the high frequency thermal stresses, has been revealed as an adequate countermeasure.

- Further propagation of this crack in the LAS could be assigned to low frequency thermal and pressurization cycles associated with e.g., start-up/shut-down and feedwater on-off cycles, scrams, turbine rolls, etc. The cracking mechanism could be assigned to SICC or LFCF with relevant environmental acceleration of crack growth. SCC under static load during steady-state power operation seemed not to relevantly contribute to crack advance in these specific cases. This assumption is supported by the better correlation between the extent of cracking and the number of start-up/shut-down cycles than with the total operating period [5, 14]. This fatigue law tolerance evaluation is subjected to some uncertainty, since the ASME XI wet crack growth curves may be significantly exceeded under these low-frequency fatigue loading conditions (Section 9.3). An alternate analysis by Ford based on the GE-model model [16], which suggested that the SCC contribution to crack growth over extended operation periods could be in the same order as the crack advance accumulated

123

during shorter periods of cyclic loading associated with start-up/hut-downs and scrams, but the underlying SCC growth algorithms significantly overestimates SCC crack growth based on recent lab investigations.

So far no combined analysis, which includes corrosion fatigue, SICC and SCC and realistic crack growth curves have been performed. Such a combined analysis might result in a slightly different picture of the general situation, in particular if relevant SCC rates (e.g., high K_I values) will be involved.

13 Summary

13.1 Experimental Background Knowledge

13.1.1 Major Factors of Influence

The following synergistic environmental, material, and loading parameters have been observed to affect EAC initiation and growth in C & LAS:

- Temperature, ECP and DO, concentration of Cl^-, SO_4^{2-} and H_2S, flow rate.

- Steel sulphur content; size, type (chemical composition), morphology and spatial distribution of MnS-inclusions; dynamic strain ageing (DSA) in susceptible materials (high concentration of free N and C) in the DSA temperature/strain rate range (150 to 350 °C, 10^{-8} to 10^{-2} s^{-1}); yield stress/hardness if > 800 MPa/350 HV5.

- Loading rate/frequency (dK/dt, $d\varepsilon/dt$, ν, etc.) and load level (K_I, ΔK, σ, ε, etc.).

13.1.2 EAC Susceptibility Conditions

SCC Initiation: SCC initiation from smooth, defect-free surfaces under static load is generally only observed for stresses at the water-wetted surface above the HT yield stress, quasi-stagnant flow conditions and increased concentration levels of Cl^- or SO_4^{2-}.

SICC/CF Initiation: In high-purity water an increased SICC and CF susceptibility is only observed, if the following threshold conditions are simultaneously satisfied:

- **Corrosion potential ECP > ECP_{crit} = -200 mV_{SHE}.** Depending on flow rate, material and temperature, a DO content of 20 to 100 ppb is sufficient to exceed this threshold.

- **Strain rate in a critical range: $0 < d\varepsilon/dt_{crit,min} \leq d\varepsilon/dt \leq d\varepsilon/dt_{crit,max} = 10^{-3}$ s^{-1}.**

- **(Local) macroscopic strain above the elastic limit: $\varepsilon \geq \varepsilon_{crit}$ = 0.1 % ($\sigma_{crit} > R_p$).**

If one of these conjoint threshold conditions is not satisfied, SICC initiation is extremely unlikely and no or only minor environmental reduction of fatigue life is observed in HT water. SICC/CF susceptibility is usually low below 100 to 150 °C and for very low-sulphur steels (≤ 0.003 wt.% S). In high-purity water, a high flow rate may completely suppress SICC susceptibility and retard fatigue crack initiation compared to quasi-stagnant conditions. The range of system conditions where EAC crack growth from incipient cracks may occur is significantly extended compared to the initiation susceptibility conditions specified above.

13.1.3 EAC Crack Growth

SCC Crack Growth: For K_I values < 50 to 60 MPa·m$^{1/2}$ all C & LAS revealed a very low susceptibility to sustained SCC crack growth in BWR/NWC environment in the temperature range from at 274 to 288 °C with SCC CGRs well below 0.6 mm/year as long as the Vickers hardness/steel sulphur content were limited to values < 350 HV5 and < 0.02 wt.% and the water chemistry was maintained within current BWR/NWC operational practice (< EPRI action level 1 limit). Above 60 MPa·m$^{1/2}$ the SCC CGRs tended to increase with increasing K_I values, although in many cases they were still decaying with time following roughly a reciprocal time law. Under reducing PWR or BWR/HWC conditions no sustained SCC crack growth was observed up to very high K_I values close to 100 MPa·m$^{1/2}$.

Fast SCC was only observed under some very specific conditions, which usually appear atypical for current BWR and PWR power operation practice or properly fabricated and heat-treated modern C & LAS components. Under these unfavourable conditions, CGRs can achieve rather high values, even up to a few m/year. The high-sulphur SCC line of the GE-model gives a good estimate of the upper bound CGR under such parameter combinations.

SICC/CF Crack Growth: In contrast to the very low SCC crack growth susceptibility of C & LAS, very high time-based SICC (10^{-9} to $8 \cdot 10^{-7}$ m/s) and CF CGRs (10^{-10} to $5 \cdot 10^{-7}$ m/s) may be easily sustained in oxygenated high-purity water under suitable cyclic loading conditions. Under cyclic loading conditions in high-purity HT water, the CF CGRs were identical to those in air above an upper critical loading frequency of about 1 to 100 Hz. Below this upper critical frequency the cycle-based CGRs $\Delta a/\Delta N_{EAC}$ were similar for all ECP/DO/material conditions and were increasing with decreasing loading frequency down to a lower critical frequency, where a maximum in cycle-based CGRs $\Delta a/\Delta N_{EAC}$ and environmental acceleration of fatigue crack growth was observed. Below this lower critical frequency, no or only minor environmental acceleration (by factor of 2 to 5) was observed and cycle-based CGRs $\Delta a/\Delta N_{EAC}$ quickly dropped down close to air CGRs by further decreasing the loading frequency. This lower critical frequency was strongly dependent on DO/ECP and shifted to lower values with increasing ECP/DO, steel sulphur content and ΔK, as well as by decreasing temperatures (with a possible peak at intermediate temperatures). Depending on ΔK, R and material a critical frequency of 10^{-3} to 10^{-1} Hz (< 5 ppb DO, PWR, BWR/HWC), 10^{-4} to 10^{-2} Hz (200 ppb DO, BWR/NWC) and $< 10^{-5}$ to 10^{-6} Hz (DO $\geq$ 400 ppb, BWR/NWC transients or simulation of realistic in-pile ECPs) has typically been observed at 288 °C.

Under system conditions, where no or minor environmental acceleration of fatigue crack growth ($\leq$ a factor of 5) was observed (i.e., below the lower and above the upper critical frequency), a similar Paris-exponent m ($\Delta a/\Delta N_{EAC} = B \cdot \Delta K^m$) of $\approx$ 3 was observed in HT water as in air. The $\Delta a/\Delta N_{EAC}$ vs. ΔK curve was approximately parallel to the corresponding air fatigue CGR curve and hardly affected by loading frequency under these conditions.

Under system conditions, where strong environmental acceleration of fatigue crack growth ($\geq$ a factor of 10) was observed (i.e., between the lower and upper critical frequency), a plateau-like range was observed in the $\Delta a/\Delta N_{EAC}$ vs. ΔK curve above a plateau threshold ΔK_{EAC} with a relatively small Paris-exponent m between 1 and 2. This plateau intersected the air fatigue curve at high ΔK values. The plateau CGR $\Delta a/\Delta N_{EAC}$ and the plateau threshold ΔK_{EAC} increased with decreasing loading frequency. A power law relationship ($\Delta a/\Delta N_{EAC} = A \cdot v^n$) between plateau $\Delta a/\Delta N_{EAC}$ and loading frequency v was observed in this frequency range with a typical exponent of -0.5 to -0.6. The ΔK_{EAC} thresholds were strongly dependent on ECP/DO content and were decreasing with increasing load ratio, loading frequency and ECP/DO content. Under highly oxidizing BWR/NWC conditions (ECP $\geq$ +50 mV$_{SHE}$, DO $\geq$ 0.4 ppm) and suitable loading conditions, fast CF could be sustained down to the lowest tested loading frequency of $3 \cdot 10^{-6}$ Hz and to a CF threshold ΔK_{EAC} of 1.5 to 2 MPa·m$^{1/2}$.

13.1.4 Adequacy/Conservatism of Codes and Disposition Lines

BWRVIP-60 SCC Disposition Lines: The conservative character of the BWRVIP-60 SCC DL 1 for stationary, transient-free BWR power operation has been confirmed for 270 to 290 °C and RPV base ($\leq$ 0.02 wt.% S) and weld filler/HAZ materials (hardness < 350 HV5) if the water chemistry is maintained within current BWR/NWC operational practice (< EPRI action level 1 limit) and K_I value is below 60 MPa·m$^{1/2}$. Even above 60 MPa·m$^{1/2}$, most test results, in particular with low- and medium-sulphur RPV steels, were still below this curve. DL 1 may be exceeded at intermediate temperatures (180 – 270 °C) in C & LAS which show a distinct susceptibility to DSA and at 288 °C in case of excessive hardness (> 350 HV5). Under reducing PWR or BWR/HWC conditions no or very slow SCC crack growth well below DL 1 was observed up to very high K_I values close to 100 MPa·m$^{1/2}$.

The BWRVIP-60 SCC DL 2 for water chemistry/load transients conservatively covered the SCC crack growth during very severe sulphate transients relevantly above the EPRI action

level limit 3 or under periodical partial unloading conditions with constant load hold times > 5 to 20 h in both oxygenated (BWR/NWC) and hydrogenated HT water (BWR/HWC). Under BWR/NWC conditions (ECP ≥ 50 mV$_{SHE}$), the DL 2 may be significantly exceeded during chloride transients ≥ 5 to 10 ppb or in case of ripple loading (R > 0.95) in the frequency range from 10^{-3} to 0.1 Hz, even at fairly low stress intensity values around 20 to 30 MPa·m$^{1/2}$. After severe (≥ 15 ppb) and prolonged (≥ 200 h) chloride transients, sustained SCC with a CGR above the DL 2 was also observed in preliminary tests for a significantly longer time interval than the 100 h period specified in BWRVIP-60. Under BWR/HWC conditions, on the other hand, the SCC CGRs during chloride transients of 100 ppb (= EPRI action level 3 limit) and under ripple loading were conservatively covered by DL 2.

The BWRVIP 60 SCC DL 1 is therefore conservative and adequate for the RPV during transient-free, steady-state BWR or PWR power operation at temperatures in the range from 270 to 290 °C. Some areas of potential concern remain to be evaluated, such as the RPV feedwater nozzle and feedwater piping systems with lower operating temperatures (200 to 270 °C) together with the possible occurrence of small load fluctuations (→ ripple loading).

ASME III Design Curves: Fatigue design and evaluation according to the ASME III code have been successful in preventing fatigue cracks and failures in C & LAS components. The code would therefore seem to be adequate, or even conservative, under most operating circumstances. The ASME III design fatigue curves were derived form strain-controlled tests with small specimens in air and do not explicitly consider a corrosive effect of the specific environment, although the degree of included conservatism in fatigue evaluation procedures (e.g., use of design transients and simplified elastic-plastic analyses that result in higher stresses/strains) may often offset this factor.

Significant environmental reduction of fatigue lives of C & LAS in LWR coolant environments were observed in lab investigations, when the strain amplitude, temperature, and DO content in water were above certain threshold values, and when the strain rate was below a threshold value. If one of these threshold requirements was not satisfied, the environmental reduction of fatigue life was minimal and fatigue life was similar to that in air. Under certain environmental and loading conditions, fatigue lives of C & LAS can be a factor of 100 lower in the coolant environment than in air. Therefore, the margins in the ASME code may be less conservative than originally intended. Based on lab investigations, different methods (e.g., adjustment of fatigue usage by fatigue life correction factors F$_{en}$) have been proposed for incorporating the effects of LWR coolant environments into the ASME Section III fatigue evaluations.

Although the possibility of environmental effects on fatigue lives is undisputed, there has been an ongoing debate for many years as to whether environmental effects should be included to ASME III or not. The design margins of 2 and 20 on stress and cycles in the ASME III design curve were intended to cover the effects of variables (e.g., material variability and data scatter, size and geometry, surface finish, and loading sequence) that can influence fatigue life but were not investigated in the tests which provided the data for the curves. An analysis by ANL suggest that the current ASME code requirements of a factor of 2 on stress/strain and 20 on cycle are quite reasonable, and do <u>not</u> contain excess conservatism that can be assumed to account for the effects of LWR environments. Therefore, in particular in the context of plant life extension, incorporation of environmental effects into the current ASME III fatigue design procedure should be considered in an adequate way, otherwise, the current trend of applying improved and optimized fatigue evaluations approaches (e.g., FE analyses, fatigue monitoring, improved K$_e$ factors) that can significantly decrease other sources of conservatism, might result in a non-acceptable reduction of safety margins.

ASME XI/Code Case N-643: The current ASME XI wet reference fatigue CGR curves conservatively cover the CF CGR lab data under most combinations of loading, environmental and material parameters, even under BWR/NWC conditions, and have usually only been exceeded under some very specific BWR plant conditions. They might therefore be regarded as an adequate, general bounding curve, but they do not realistically describe and reflect the experimentally observed CF crack growth behaviour of LAS in oxygenated HT water. The curves either predict significantly too high (e.g., $\nu \le 10^{-2}$ Hz and ECP < -200 mV$_{SHE}$ or 10^{-1} Hz < ν < 10 Hz and high ΔK) or too low CGRs (e.g., $\nu \le 10^{-2}$ Hz and ECP > 0 mV$_{SHE}$ or 10^{-2} Hz < ν < 10 Hz and high R/small ΔK). Furthermore, system conditions or thresholds (e.g., ν > 10 Hz), where environmental effects on fatigue crack growth can be neglected or excluded are not defined in ASME XI.

Modification of the ASME XI curves or the development of a new code case for BWR/NWC, e.g., based on time-domain analysis/modelling, should therefore be pursued. Any optimized procedure should adequately consider the strong effect of loading frequency and ECP (DO content). Such procedures would have the potential to reduce both uncertainty and undue conservatism, but would also result in more complicated flaw tolerance evaluations than to date, since the loading frequency/strain rate of different transients would have to be considered in an appropriate way.

There is a lot of undue conservatism in the current ASME XI wet reference fatigue CGR curves for the overwhelming part of PWR and BWR/HWC conditions. The new Code Case N-643 for PWR primary side water chemistry readily reflects the observed CF cracking behaviour and eliminates a lot of undue conservatism, but is rather complicated for practical applications. There is a good chance that the current ASME Code Case N-643 would also cover the CF crack growth in C & LAS under most BWR/HWC or PWR secondary side water chemistry conditions. Therefore this Code Case should be further tested and evaluated under these water chemistry conditions.

13.1.5 *Metallographical and Fractographical Aspects of EAC*

Crack Initiation: SICC cracks usually initiate at MnS-inclusions, which intersect the steel surface or at corrosion pits. In contrast to SICC, environment appears to have little or no effect on formation of micro-cracks on the surface under most fatigue loading conditions and the reduction in fatigue life in HT water is primarily due to environmental effects on fatigue crack propagation. As in air, CF cracks primarily initiate and form along slip bands, carbide particles, or at the ferrite-pearlite phase boundary, but seldom at MnS-inclusions.

Crack Growth: The crack path in EAC of C & LAS in HT water is TG and perpendicular to the direction of maximum tensile stress. The general fracture appearance is similar for SCC, SICC and CF, thus confirming that EAC is governed by the same basic process for all three loading modes. In the temperature range from 150 to 320 °C the fracture surface usually has a TG quasi-cleavage appearance with feather morphology and terrace-like structure. Individual crack terraces are often fan-shaped, and sometimes initiate from MnS-inclusions, which intersect the crack front. The feather facets with a spacing of some few μm are parallel to the local crack growth direction and may be the result of plastic strain localization and shear processes. In case of cyclic loading, the fracture surface may also contain both ductile (irregular, deep) and brittle (regular, shallow, with feather facets/tear ridges parallel to local crack growth direction) fatigue striations, which are perpendicular to local crack growth direction. With decreasing loading frequency, the morphology is continuously changing from an air fatigue-like to a SICC/SCC-like appearance, i.e., the spacing between the striations becomes larger, the amount of ductile/brittle striations decreases/increases and the fracture surface becomes finally free of striations at < $5 \cdot 10^{-4}$ Hz.

13.2 Mechanistic Background Knowledge

13.2.1 EAC Crack Growth Mechanism

The film rupture/anodic dissolution (FRAD) and hydrogen-assisted EAC (HAEAC) mechanisms may be simultaneously active under typical crack-tip conditions in LWR environments and be controlled by the same rate limiting steps (for example oxide film rupture rate, repassivation kinetics, etc.). The EAC cracking behaviour of C & LAS in HT water can best be rationalized by a superposition/combination of the FRAD and HAEAC mechanisms. At lower temperatures (< 100 °C) and/or high YS/hardness levels (R_p > 800 MPa/> 350 HV5) and high strain rates (> 10^{-3} s^{-1}), hydrogen effects are more pronounced. At high temperatures (≥ 150 °C) and/or lower YS/hardness levels and slow strain rates (< 10^{-3} s^{-1}), anodic dissolution seems to dominate.

H$_2$S respectively HS$^-$ and S^{2-} as impurities in the bulk environment or from the dissolution of MnS-inclusions, which are intersected by the growing crack, may significantly retard repassivation after oxide film rupture and therefore increase crack advance by anodic dissolution. The retarded repassivation of the film-free surface and the adsorbed HS$^-$, S^{2-} or H$_2$S increase the hydrogen absorption to the metal lattice, and favour therefore also crack advance by HAEAC. Furthermore, MnS-inclusions in the region of maximum hydrostatic stress ahead of the crack-tip may act as strong hydrogen traps and HAEAC initiation sites.

Under certain combinations of temperature (100 to 350 °C) and strain rate (10^{-8} to 10^{-2} s^{-1}), DSA may synergistically interact with both mechanisms to increase EAC susceptibility and provide an additional contribution to the crack growth process. DSA may result in the occurrence of a higher crack-tip strain/strain rate than for loading outside the DSA range, or in a material, which is not susceptible to DSA. The localisation of plastic deformation/increase in planar deformation by DSA may support the mechanical rupture of the oxide film and result in a reduction of the local fracture toughness and thus favour brittle crack extension.

13.2.2 Control Factors for EAC Crack Growth

EAC growth from incipient cracks is essentially governed by the crack-tip strain rate and the activity of sulphur- (or chloride-) anions (affecting repassivation/pH/oxide film stability) in the crack-tip environment. The onset and extent of EAC is crucially dependent on simultaneously maintaining a slow, positive crack-tip strain rate and a critical sulphur-anion activity of about 1 to 5 ppm S^{2-} in the crack-tip environment. If these two conjoint requirements are not met, no SCC and SICC, or only minor environmental acceleration of fatigue crack growth are generally observed. If the critical anion concentration is exceeded, the EAC CGR depends primarily on the crack-tip strain rate and increases with increasing external strain rate up to an upper critical limit of around 10^{-3} to 10^{-2} s^{-1}. Most EAC thresholds and cessation/pinning phenomena may be directly attributed to this conjoint requirement.

These two local factors are governed by a system of interrelated and synergistic corrosion system parameters: In general, the crack-tip strain rate increases with increasing loading rate/loading frequency (as well as load level), CGR, YS and DSA susceptibility. The sulphur-anion activity in the crack-tip environment increases with increasing steel sulphur content, concentration of sulphur-anions in the bulk environment outside the crack, CGR (exposure of new fresh dissolvable MnS by the growing crack) and corrosion potential/DO content. The threshold conditions for EAC are directly related to crack-tip chemistry and CGR/crack-tip strain rate, rather than to loading parameters or bulk environment conditions per se. E.g., suitable combinations of different system parameters may help to exceed the critical crack-tip sulphur-anion concentration (of 1 to 5 ppm S^{2-}), provided that there is at least one source of sulphur (MnS-inclusions or sulphur-anion in the bulk environment).

13.2.3 General Electric EAC Crack Growth Model

The GE-model is based on the FRAD mechanism and correctly predicts most experimentally observed EAC crack growth data trends over a wide range of system conditions. Furthermore, it has also been successfully applied to predict LCF initiation. It therefore has good potential for data analysis and the definition of disposition lines. The high-sulphur line of the model conservatively covers almost all EAC CGR data. Recent results indicate that the transition curve between the low- and high-sulphur lines might be non-conservative under highly oxidizing BWR/NWC conditions (ECP $> 0\,mV_{SHE}$) and very low loading frequencies ($< 10^{-4}$ Hz). This might perhaps be related to DSA, which is not considered in the model. In high-purity water, the model predicts much too high SCC CGRs. This is related to the crack-tip strain rate formulation for static loading conditions, which was originally derived for stainless steels, and is generally unsatisfactory to applications at K_I levels $< 60\,MPa{\cdot}m^{1/2}$.

13.3 Service Experience and Practical Implications

13.3.1 Field EAC Cracking Incidents

The accumulated operating experience of C & LAS primary pressure-boundary components in NPPs is very good worldwide. Isolated instances of EAC have occurred (particularly in BWR service), most often in LAS piping and very rarely in the cladded RPV. EAC cracking has been observed in wrought, weld filler and weld HAZ materials and has been TG in nature. In BWRs, steam and feedwater piping as well as condensate systems and RPV feedwater nozzles have been affected. In the secondary circuit of PWRs, cracking has been observed in feedwater piping/tanks and heat exchangers, feedwater nozzles of PWR steam generators and steam generator girth welds. EAC damage was usually detected during in-service inspection and seldom led to through-wall penetrations with leakage.

These EAC incidents have been clearly associated with an oxidizing environment (usually due to oxygen), severe dynamic straining (due to global and local thermal stratification/striping or due to thermal and pressurisation cycles during plant transients), and high local stresses around or above the HT YS or high secondary/residual stress (due to, e.g., welding defects, pipe bends in conjunction with inadequate pipe support or restraints, localized post-weld treatment). Corrosion during shut-down periods (e.g., pitting) was sometimes a further contributing factor. Thermal hydraulics (thermal stratification/striping phenomena) and local stress raisers played a key role and were usually more important than water chemistry or material aspects. These cases were attributed either to SICC or CF. Cracking incidents with a major or relevant contribution of SCC to the total crack advance in properly manufactured and heat-treated low-alloy primary pressure-boundary components were not observed.

Cracks often initiated from water-wetted geometric discontinuities (e.g., welding defects) and/or in regions with stagnant flow or creviced geometry. In general, crack initiation has been more affected by high frequency, high-cycle fatigue due to local thermal stratification or thermal striping loads which were limited to near-surface regions. Crack propagation was often dominated by LCF from slower and less frequent transients, due to, e.g., global thermal stratification or operational power transients.

Several incidents were related to unanticipated/unevaluated sources, frequency, and/or severity of thermal stress cycles in critical locations. In many cases, fabrication or design deficiencies (e.g., welding defects) favoured local plastification of the water-wetted material surface and sometimes resulted in an increased stress intensity (e.g., residual stress) or increased EAC susceptibility of the material (e.g., excessive hardness of weld HAZs). Reoccurrence of this kind of cracking could be avoided by improved design of the components or fabrication procedures and better quality control during the fabrication process, as well as by optimized operation procedures.

13.3.2 Critical Components and Operation Conditions

Special attention should be paid to components, which are likely to undergo significant localized mechanical loading around or above the HT YS levels or which are related to increased oxygen contents/conductivities/quasi-stagnant flow conditions during operation. Critical components are, e.g., piping carrying nearly stagnant steam or non-degassed condensate during normal operation (or which are used only intermittently), feedwater nozzles, and adjacent sections of horizontal piping, if thermal stratification can occur and thin-walled piping and pipe bends in conjunction with inadequate pipe supports or restraints. Operational transients, which are associated with thermal stratification/high secondary strains (e.g., start-up, hot stand-by, etc.) or slow, but relevant pressure and temperature changes should receive attention, in particular if they occur with a sufficiently high frequency.

13.3.3 Possible Mitigation Actions and Countermeasures

Operating conditions and component designs should be optimized to avoid dynamic straining and highly oxidizing/stagnant conditions. Temperature gradients/cycles, thermal stratification/stripping, oxygen enrichment, and stagnant conditions should be reduced/ avoided as far as possible. In summary EAC risks can be minimised by:

- Selection of suitable materials, e.g., low-sulphur steel (< 0.003 wt.% S) with low EAC and DSA susceptibility and optimized high toughness ($\rightarrow$ larger critical crack size).

- Selection of suitable manufacturing and fabrication practice to avoid welding defects and HAZs with high hardness (by suitable PWHT) and to reduce residual stress (stress relieving, narrow gap welding).

- An improved design to reduce regions of high local stresses (by increased wall thickness, by internal flush grinding of joints and optimisation of welding technology, avoidance of discontinuities and constraints, optimized pipe supports).

- Reduction of the number of thermal and pressurization cycles (thermal-stratification during hot stand-by, start-up/shut-down) and of temperature gradients by optimized operating procedure or an improved design of the affected component (thermal sleeve of feedwater nozzle, feedwater sparger).

- Avoiding stagnant conditions/crevices and reducing oxygen levels by optimized operation practice (for example modification of start-up procedures to reduce DO levels by better venting of piping, improvement of drainage in horizontal lines, etc.).

- An adequate water chemistry control (EPRI or VGB guidelines) and application of HWC/NMCA to reduce the ECP.

- Optimized in-service inspection programmes with respect to EAC risks.

13.4 Service Experience vs. Experimental/Theoretical Background Knowledge

The operating experience fits well to the accumulated experimental/mechanistic background knowledge on EAC and pitting behaviour in the system C & LAS-HT water. Both show the same qualitative parameter trends, e.g., for oxygen, flow rate, and strain. They confirm the high SCC resistance of LAS under steady-state power operation and static loading conditions and clearly reveal that slow, positive (tensile) straining with associated plastic yielding and sufficiently oxidizing conditions are essential for EAC initiation in high-purity HT water. Since primary design stresses are generally limited to values below the elastic limit, thermal-hydraulics (e.g., thermal stratification) and local stress raisers therefore played a key role for SICC/CF in the field and were generally more important than material or water chemistry aspects. EAC cracks often initiated from corrosion pits or MnS-inclusions which intersected the steel surface. Pitting of LAS is strongly favoured under oxidizing conditions

(high oxygen concentration), especially at low and intermediate temperatures, and by slow dynamic straining. Quasi-stagnant or low-flow conditions promote the formation of an aggressive, occluded water chemistry at the base of the pit or within small surface defects, as well as the enrichment of oxygen in steam condensate, and therefore promote EAC initiation.

By taking the exact boundary conditions in lab tests and in the field into account, no major discrepancy between operating experience and trends in laboratory could be found. The EAC cracking incidents can be readily rationalized by the identified susceptibility conditions or by EAC flaw tolerance evaluations. The higher cracking frequency in lab tests may be easily explained by the beneficial effect of a turbulent flow rate in the field (which is characteristic for most component locations) for EAC initiation and the conjoint threshold conditions for the onset of EAC with regard to ECP (or DO), strain rate, strain and temperature. In general, for many transients/component locations, one or several threshold conditions are not satisfied. Even if all requirements would be fulfilled, the SICC/CF initiation process may consume a long incubation period/large number of fatigue cycles in the absence of pre-existing defects or cracks, in particular for small strains, and therefore extend over a significant part (or even the whole part) of the plant lifetime. Most experiments start with a sharp fatigue pre-crack that is "ready" to propagate; this is significantly different from the situation in most components.

13.5 Open questions and Possible Topics for Further Research

13.5.1 Assessment of the Current Situation

A high knowledge level on EAC in C & LAS in HT water has been gained during the last three decades, which readily correlates with the excellent service record of primary pressure boundary components. Several different remedial and mitigation actions have been qualified and successfully applied. Tools for incorporating environmental effects in fatigue design and EAC crack growth curves for engineering flaw tolerance evaluations and lifetime prediction have been developed and qualified. From a practical point of view, there is thus currently no major knowledge gap/uncertainty or actual failure-driven immediate need for large research programmes. Nevertheless, there are open questions and potentials for improvements in all fields, mainly in the context of evaluation of lifetime extension and assessment of safety margins, which are worth to be further evaluated.

13.5.2 Experimental Characterization of EAC

The SCC CGRs are usually small in C & LAS in LWR environments, but several parameter combinations have been identified, which can result in fast SCC. Although most of them appear atypical for current LWR power operation or properly manufactured C & LAS components, some of them might occur, at least temporarily during faulted operation conditions or in case of components with fabrications deficiencies (e.g., welding defects, repair welding, etc.). For safety, accelerated SCC crack growth over extended periods is more critical than the high SICC/CF CGRs, which might occur during specific in-frequent plant transients. From a safety perspective, the special emphasis should therefore be placed to those conditions, which can result in accelerated SCC and, in particular, to a better identification of the boundaries/thresholds for the transition from low to very high SCC CGRs.

In this context, the effect of chloride transients and the role of DSA, YS/hardness, and visco-plasticity in SCC crack growth of C & LAS in HT water, in particular under BWR/ NWC conditions should be further investigated. The role of these parameters is not sufficiently understood/characterized and not yet included in existing models. Weld filler and real or simulated weld HAZ materials should be increasingly included in such investigations. In case of HAZ materials, this may require special specimen designs (blunt notch C(T) or notched round tensile specimens). In case of DSA, a simple method/parameter has to be de-

veloped for identifying/measuring the DSA susceptibility of C & LAS and of operating components, which can be correlated with EAC susceptibility. In this context LCF, SSR, and fatigue crack growth tests should be performed both in air and HT water environment to carefully separate DSA and environmental effects and study their synergism. Investigations on chloride should focus on the possibility of long-term effects on SCC crack growth after temporary chloride excursions, as it has been observed in preliminary investigations after severe and prolonged chloride transients. Additionally, the mitigation effect of low potentials (BWR/HWC or NMCA) under these critical conditions should be investigated and quantified.

The following aspects (without prioritization) are not sufficiently characterized and worthy for further evaluation, in particular, with respect to code development, field assessment, and elimination of undue conservatism/reduction of minor uncertainties [18]:

All types of EAC:

- Role of DSA, YS and visco-plasticity in EAC of C & LAS.

- EAC behaviour of weld filler and weld HAZ materials.

- Effect of flow rate on EAC initiation and growth, in particular at small strain amplitudes/slow strain rates and with realistic crack-configurations (semi-elliptical surface cracks, including stainless steel or Inconel 182 cladding).

SCC:

- Evaluation of the possibility of long-term effects on SCC crack growth under BWR/NWC conditions after temporary chloride excursions.

- Effect DSA susceptibility and intermediate temperatures (100 to 250 °C) on SCC growth under BWR/NWC conditions.

- Effect of ripple loading (R > 0.95) in the frequency range of 10^{-2} to 10 Hz.

CF/SICC:

- Effect of non-isothermal conditions.

- Effect of anionic impurities (Cl^-, SO_4^{2-}) on CF/SICC initiation in particular at small strain amplitude/slow strain rates.

- Effect of surface condition (pitting, roughness, cold work, residual stress) on CF initiation.

- Effect of sequence/random loading, overloads (e.g., pressure test) and hold-time (SCC) mean stress/load ratio on CF initiation and growth.

- Quantification of mitigation effect of HWC or HWC/NMCA on CF initiation/growth.

- Determination of thresholds (critical CGR, frequency and ΔK_{EAC}) for the onset of accelerated CF as a function of ECP (in particular under BWR/NWC and HWC conditions).

- EAC crack growth behaviour in the low $\Delta K/K_I$ or $\Delta J/J$ region close to thresholds, in particular under high load ratio R conditions, for both (near-surface) short crack (growth) and long crack (growth) as well as for realistic crack configurations (semi-elliptical surface cracks).

13.5.3 Mechanism/Models

In the field of mechanism/models, the special emphasis should be placed on studies on the role of DSA and YS in dynamic crack-tip plasticity and on investigations on the interaction between chloride and oxide films/repassivation. Such investigations may contribute to a better mechanistic understanding of some important recent research results. The development of quantitative (macroscopic) correlations between crack-tip strain rate and macroscopic loading parameters <u>and</u> CGR, including DSA, YS and visco-plastic effects, in particular for static loading conditions, would drastically improve the predictive capabilities.

14 Conclusions

In the current status report, the most relevant aspects of research and service experience with EAC of C & LAS in high-temperature water have been reviewed, with special emphasis on the primary pressure-boundary components of BWRs.

Laboratory investigations revealed significant effects of simulated reactor environments on fatigue crack initiation/growth, as well as the possibility of SCC crack growth for certain specific critical combinations of environmental, material and loading parameters. During the last three decades, the major factors of influence and EAC susceptibility conditions have been readily identified. Most parameter effects on EAC initiation and growth are adequately known with acceptable reproducibility and reasonably understood by mechanistic models. Tools for incorporating environmental effects in ASME III fatigue design curves have been developed/ qualified and should be applied in spite of the high degree of conservatism in fatigue evaluation procedures. The BWRVIP-60 SCC DLs and ASME XI reference fatigue crack growth curves are usually conservative and adequate under most BWR operation circumstances, but there is both relevant potential for reduction of undue conservatism and need to eliminate/close some specific uncertainties/knowledge gaps.

The operating experience of C & LAS primary pressure-boundary components in LWRs is very good worldwide. However, isolated instances of EAC have occurred, particularly in BWR service, most often in piping and, rarely in the RPV itself. Oxidizing conditions, usually DO, and relevant dynamic straining were always involved. These cases were either attributed to SICC or CF and could be readily rationalized by the experimental background knowledge. Both service experience and experimental/mechanistic background knowledge confirm the high resistance of C & LAS to SCC under stationary power operation and static loading conditions and clearly reveal, that slow, positive (tensile) straining, with associated plastic yielding and sufficiently oxidizing conditions are essential for EAC initiation in HT water. Based on the experimental/mechanistic background knowledge and service experience different remedial and mitigation actions have been qualified and successfully applied, which further reduced the low EAC cracking frequency in the field.

In spite of the absence of SCC in the field, several unfavourable critical parameter combinations, which can lead to sustained, fast SCC with CGRs well above the BWRVIP-60 SCC DLs have been identified. Many of them appear atypical for current BWR plant operation with properly manufactured C & LAS components, but some might occur during service, at least temporarily under faulted conditions or in components with fabrication deficiencies. Although there are open questions and potentials for improvements in all fields, from a safety perspective, the special emphasis of research should be placed to these conditions, and in particular, to an improved identification/quantification of the boundaries/thresholds for the transition from low to high/accelerated SCC CGRs. In this context, research should be focused on the effects of chloride transients and DSA/YS on the SCC crack growth behaviour of C & LAS and of weld HAZ materials under BWR/NWC conditions. Additionally, the mitigation effect of HWC or NMCA should be evaluated under these critical conditions.

15 Acknowledgements

16 References

[1] **M.O. SPEIDEL, R.M. MAGDOWSKI,** *International Journal of Pressure Vessel & Piping*, **34**, pp. 119 – 142, 1988.

[2] **I. BENGTSSON, J. ERIKSSON,** "Final Report on Reactor Pressure Vessel Steel Testing in Oskarshamn 2 and Oskarshamn 3", ABB Atom Report SBR 99-020, November 1999.

[3] **U. EHRNSTÉN,** "Fractographic and Metallographic Investigations on Pressure Vessel Steel C(T) Specimens Tested in BWR Environment", VTT Research Report VAL62-001675, VTT, Espoo, Finland, September 2000.

[4] **H.P. Seifert, S. Ritter,** "Review and Assessment of SCC Experiments with RPV Steels in Oskarshamn 2 and 3 (ABB Report SBR 99-020)", SKI Report, SKI, Stockholm, Sweden, 2005 (to appear).

[5] **Y.S. GARUD, S.R. PATERSON, R.B. DOOLEY, R.S. PATHANIA, J. HICKLING, A. BURSIK,** "Corrosion Fatigue of Water-Touched Pressure Retaining Components in Power Plants", EPRI TR-106696, Final Report, November 1997.

[6] **Z. SZKLARSKA-SMIALOWSKA, D.D. MACDONALD, H. CHOI,** "The General and Localized Corrosion of Carbon and Low-Alloy Steels in Oxygenated High-Temperature Water", EPRI-NP-2853, EPRI, February 1983.

[7] **D. WEINSTEIN et al.**, "BWR Environmental Cracking Margins for Carbon Steel Piping", EPRI Report NP-2406, EPRI, Palo Alto, CA, USA, May 1982.

[8] **B. TOMKINS et al.,** *Int. Journal of Pressure Vessel and Piping,* **40**, pp. 331 – 403, 1989.

[9] **P. SCOTT, D. TICE,** *Nuclear Engineering & Design*, **119**, pp. 399 – 413, 1990.

[10] **F.P. FORD, S. RANGANATH, D. WEINSTEIN,** "Environmentally Assisted Fatigue Crack Initiation in Low-Alloy Steels – A Review of the Literature and the ASME Code Requirements", EPRI TR-102765, EPRI, Palo Alto, CA, USA, 1993.

[11] **L.A. JAMES,** *WRC Bulletin,* **404**, pp. 1 – 20, 1995.

[12] **L. A. JAMES, W.A. VAN DER SLUYS,** "The Effect of Aqueous Environments Upon the Initiation and Propagation of Fatigue Cracks in Low-Alloy Steels", NACE Corrosion 96, Proceedings of the CORROSION/96 Research Topical Symposia, pp. 176 – 209, NACE, Denver, USA, March 24 – 29, 1996.

[13] **H.P. SEIFERT,** "Literature Survey on the Stress Corrosion Cracking of Low-Alloy Steels in High-Temperature Water", PSI Report No. 02-06, February 2002.

[14] **B.M. GORDON et al.,** *ASM PVP,* **119**, pp. 9 – 17, 1987.

[15] **J. HICKLING, D. BLIND,** *Nuclear Engineering & Design*, **91**, pp. 305 – 330, 1986.

[16] **F.P. FORD,** "Environmentally Assisted Cracking of Low-Alloy Steels", EPRI NP-7473-L, EPRI, Palo Alto, CA, USA, January 1992.

[17] **E. TENCKHOFF et al.,** *Nuclear Engineering & Design*, **119**, pp. 371 – 378, 1990.

[18] **H.P. SEIFERT, S. RITTER, J. HICKLING,** "Environmentally Assisted Cracking of Low-Alloy RPV and Piping Steels under LWR Conditions", Proc. 11th Int. Conf. on Environmental Degradation of Materials in Nuclear Power Systems – Water Reactors, CD-ROM, NACE/TMS/ANS, Stevenson, WA, USA, August 10 – 14, 2003.

[19] **H.P. SEIFERT, S. RITTER, J. HICKLING,** *Power Plant Chemistry*, 6, 111 – 123, 2004.

[20] **T. SHOJI, H. TAKAHASI, T. KONDO, H. NAKAJIMA,** "Pre-Cracked Slow Strain-Rate Test (SSRT) on SA533B Steel in Hydrogen Gas, 85 °C and 288 °C Water Environments", Rep. Res. Inst. Strength & Fracture of Materials, Tohoku Univ., **17**, pp. 39 – 44, 1984.

[21] **T. ARAI, M. MAYUZUMI,** "Effect of Dissolved Oxygen Concentration and Material Factors on Stress Corrosion Cracking of Low-Alloy Steels", *NACE Corrosion 97*, Paper 90, pp. 90-1 – 90-13, NACE, USA, 1997.

[22] **T. ARAI, M. MAYUZUMI,** "Effects of Temperature, Dissolved Oxygen and Sulphur Content on SCC Behaviour of Low-Alloy Steels in High Temperature Water", Minutes of the 1998 Annual Meeting of the ICG-EAC, ICG-EAC-Meeting, Paper L4-1-L4-34, Hangzhou, China, April 19 – 24, 1998. (Referenced with the permission of the author).

[23] **E. LENZ, N. WIELING,** *Nuclear Engineering & Design*, **9**, pp. 331 – 344, 1986.

[24] **J. CONGLETON, T. SHOJI, R.N. PARKINS,** *Corrosion Science*, **25**, pp. 633 – 650, 1985.

[25] **M.E. INDIG et al.,** *Reviews on Coatings and Corrosion*, **5**, pp. 173 – 225, 1982.

[26] **J.D. ATKINSON, J. YU,** *Fatigue Fract. Engng. Mater. Struct.*, **20**, pp. 1 – 12, 1997.

[27] **H. HÄNNINEN, H.P. SEIFERT, Y. YAGODZINSKY, U. EHRNSTÉN, O. TARASENKO, P. AALTONEN,** "Effects of Dynamic Strain Ageing on Environment-Assisted Cracking of Low Alloy Pressure Vessel and Piping Steels" Proc. of 10th Int. Conf. on Environmental Degradation of Materials in Nuclear Power Systems – Water Reactors, NACE/TMS/ANS, CD-ROM, Paper No. 47, Lake Tahoe, Nevada, USA, August 6 – 10, 2001.

[28] **S. RITTER, H.P. SEIFERT,** *Power Plant Chemistry*, **5**, pp. 17 – 29, 2003.

[29] **O.K. CHOPRA, W.J. SHACK,** *Nuclear Engineering & Design,* **184**, pp. 49 – 76, 1988.

[30] **G. NAKAO, M. HIGUCHI, H. KANASAJI, K. IIDA, Y. ASASA,** "Effects of Temperature and Dissolved Oxygen on Fatigue Lives of Carbon and Low-Alloy Steels in LWR Environments", Effects of the Environments on the Initiation of Crack Growth, ASTM STP 1298, W.A. Van der Sluys, R.S. Piascik, and R. Zawierucha, Eds., ASTM, pp. 232 -244, 1997.

[31] **O.K. CHOPRA, W.J. SHACK,** "Review of the Margins for ASME Code Fatigue Design Curve – Effects of Surface Roughness and Material Variability", NUREG/CR-6815, ANL-02/39. US NRC, September 2003.

[32] **A. KRAUS,** "Stress Corrosion Cracking of Pressure Vessel Steels in High-Temperature Water", Ph.D. thesis, Diss. ETH Nr. 10644, ETH Zürich, 1994.

[33] **K. KUSSMAUL et al.,** *Nuclear Engineering & Design,* **168**, pp. 53 – 75, 1997.

[34] **J. HELDT, H.P. SEIFERT,** "Stress Corrosion Cracking of Low-Alloy Reactor Pressure Vessel Steels under Boiling Water Reactor Conditions" Proc. 9th International Symposium on Environmental Degradation of Materials in Nuclear Power Systems – Water Reactors, pp. 901 –909, NACE/TMS/ANS, Newport Beach, USA, August 1 – 5, 1999.

[35] **J. HELDT, H.P. SEIFERT,** *Nuclear Engineering & Design*, **206**, pp. 57 – 89, 2001.

[36] **H.P. SEIFERT, S. RITTER,** "New Observations About the SCC Crack Growth Behaviour of Low-Alloy RPV Steels Under BWR/NWC Conditions", Proc. 11th Int. Conf. on Environmental Degradation of Materials in Nuclear Power Systems – Water Reactors, CD-ROM, NACE/TMS/ANS, Stevenson, WA, USA, August 10 – 14, 2003.

[37] **R. MAGDOWSKI,** "Spannungsrisskorrosion von ferritischen Stählen in Wasser", Moderne Stähle, Reihe Ergebnisse der Werkstoff-Forschung, Ed.: J.P. Uggowitzer, Verlag Schweizerische Akademie der Wissenschaften, pp. 107 – 140, May 1987.

[38] **P.M. SCOTT, D.R. TICE,** "A Review of Stress Corrosion Cracking in Nuclear Reactor Pressure Vessel and Piping Steels", AEREG-G4616, March 1988.

[39] **E. LENZ, N. WIELING,** "Einflussgrössen auf die Rissinitiierung und auf das Risswachstum in niedriglegierten Feinkornbaustählen in Hochtemperaturwasser", 20th Session of DVM Team on Fracture Mechanics, DVM, March 17 – 18, 1988.

[40] J.D. Atkinson et al., *Nuclear Engineering & Design*, **184**, pp. 13 – 25, 1998.

[41] L.A. James, *Journal of Pressure Vessel Technology*, **116**, pp. 122 – 127, 1994.

[42] W.H. Cullen, K. Törrönen, M. Kemppainen, Effects of Temperature on Fatigue Crack Growth of A 508-2 Steel in LWR Environment", NUREG/CR-3230, US NRC, April 1983.

[43] E. Lenz, N. Wieling, H. Munster, "Influence of Variation of Flow Rates and Temperature on the Cyclic Crack Growth Rate under BWR Conditions", Proc. 3rd International Symposium on Environmental Degradation of Materials in Nuclear Power Systems – Water Reactors, pp. 283 – 288, TMS, 1987.

[44] J.D. Atkinson, T.C., Lindley, "The Effect of Frequency and Temperature on Environmentally-Assisted Fatigue Crack Growth below K_{ISCC} in Steels", Proc. of Conference on the Influence of Environment on Fatigue, pp. 65 – 74, Institution of Mechanical Engineers, London, 1977.

[45] Y. Katada, N. Nagata, *Corrosion Science*, **25**, pp. 693 – 704, 1985.

[46] D.R. Tice, D. Worswik, P. Hurst, H. Fairbrother, "Influence of Mean Stress and Temperature on Corrosion Fatigue Crack Growth of Reactor Pressure Vessel Steels", Proc. of the 6th International Conference on Environmental Degradation of Materials in Nuclear Power Systems – Water Reactors, pp. 19 – 27, R.E. Gold, E.P. Simonen, Eds., TMS, San Diego, California, August 1 – 5, 1993.

[47] J.D. Atkinson, "The Effect of Temperature on Corrosion Fatigue Crack Propagation in Reactor Pressure Vessel Steels", Proc. of the 6th International Conference on Environmental Degradation of Materials in Nuclear Power Systems – Water Reactors, pp. 29 - 34, R.E. Gold, E.P. Simonen, Eds., TMS, San Diego, California, August 1 – 5, 1993.

[48] T.A. Auten, S.Z. Hayden, R.H. Emanuelson, "Fatigue Crack Growth Rate Studies of Medium Sulphur Low-Alloy Steels Tested in High-Temperature Water", Proc. of the 6th International Conference on Environmental Degradation of Materials in Nuclear Power Systems – Water Reactors, pp. 35 – 41, R.E. Gold, E.P. Simonen, Eds., TMS, San Diego, California, August 1 – 5, 1993.

[49] L.D. Paul, R.H. Emanuelson, M.T. Miglin, *Pressure Vessel and Piping (PVP)*, **195**, pp. 21 - 28, 1990.

[50] P. Combrade, M. Foucault, "Crack-Tip Conditions Related to Environmentally Assisted Cracking in Pressure Vessel Steels", Proc. 5th International Symposium on Environmental Degradation of Materials in Nuclear Power Systems – Water Reactors, TMS, pp. 554 – 560, 1992.

[51] H.P. Seifert, S. Ritter, "Effect of Temperature and Loading Frequency on the SICC and Corrosion Fatigue Crack Growth Behavior of Low-Alloy RPV Steels under BWR/NWC Conditions", Proc. 11th Int. Conf. on Environmental Degradation of Materials in Nuclear Power Systems – Water Reactors, CD-ROM, NACE/TMS/ANS, Stevenson, WA, USA, August 10 – 14, 2003.

[52] H. Kanaski, M. Hayashi, K. Ida, Y. Asada, *Pressure Vessel and Piping (PVP)*, **306**, pp. 117 – 122, 1995.

[53] H. Kanasaki, A. Hirano, K. Ida, Y. Asada, "Corrosion Fatigue Behaviour and Life Prediction Method under Changing Temperature Conditions", Effects of the Environment on Initiation of Crack Growth, ASTM STP 1298, pp. 120 – 134, W.A. Van der Sluys, R.S. Piascik, R. Zawierucha, Eds., ASTM, 1997.

[54] L. A. James, *Nuclear Engineering & Design,* **172**, pp. 265 – 271, 1997.

[55] **P.L. ANDRESEN, L.M. YOUNG,** "Characterization of the Role of Electrochemistry, Convection and Crack Chemistry in Stress Corrosion Cracking", Proc. 7th Int. Symp. on Environmental degradation of Materials in Nuclear Power Systems – Water Reactors, CD-ROM, NACE, 1995, pp. 579 –596, 1995.

[56] **T. SHOJI,** "The Critical Cracking Potential of Reactor Pressure Vessel Steel in Pressurised High-Temperature Water", Proc. 3rd International Atomic Energy Agency Specialist's Meeting on Sub-critical Crack Growth, Technical Sessions II, II and IV, Vol. 2, NUREG/CP-0112, ANL-90/22, pp. 109 – 116, Moscow, USSR, 1990.

[57] **T. SHOJI, H. TAKAHASI, S. AIZAWA, M. SAITO,** "Effects of Sulphate Contamination, Sulphur in Steel and Strain-Rate on Critical Cracking Potential for SCC of Pressure Vessel Steels in Pressurized High-Temperature Water", Proc. 3rd Int. Symposium on Environmental Degradation of Materials in Nuclear Power Systems – Water Reactors, pp. 251 – 258, 1988.

[58] **P. HURST et al.,** *Corrosion Science,* **25**, pp. 651 – 671, 1985.

[59] **G. SUND,** "The Influence of Oxygen and Sulphate Contents of the Water on the Tendency to Stress Corrosion Cracking in Pressure Vessel Steels at 288 °C", Proc. 3rd International Atomic Energy Agency Specialist's Meeting on Subcritical Crack Growth, Technical Sessions II, II and IV, Vol. 2, NUREG/CP-0112, ANL-90/22, pp. 3 – 8, Moscow, USSR, 1990.

[60] **G. SUND, B. ROSBORG,** "The Influence of Impurities on the Tendency to Stress Corrosion Cracking of Pressure Vessel Steel A533-B in Water at 288 °C", Presentation at the ICG-EAC-Meeting 1991, Lake Placid, New York, USA, March 1991. (Referenced by permission of the authors).

[61] **G. NAKAO, H. KANASAKI, M. HIGUCHI, K. IIDA, Y. ASADA,** *Pressure Vessel and Piping (PVP),* **306**, pp. 123 – 128, 1995.

[62] **H.P. SEIFERT, S. RITTER,** "Corrosion Fatigue Crack Growth Behaviour of Low-Alloy RPV and Piping Steels under BWR Conditions", Proc. 3rd International Conference on Fatigue of Reactor Components, Session 3: Environmental Effects, CD-ROM, OECD/EPRI, Seville, Spain, October 3 – 6, 2004.

[63] **H.P. SEIFERT, S. RITTER,** "Mitigation Effect of Hydrogen Water Chemistry on SCC and Low-Frequency Corrosion Fatigue Crack Growth in Low-Alloy Steels", Proc. 12th Int. Conf. on Environmental Degradation of Materials in Nuclear Power Systems – Water Reactors, CD-ROM, NACE/TMS/ANS, Snowbird, Utah, USA, August 14 – 18, 2005.

[64] **P. L. Andresen, L. M. Young**, *Corrosion,* **51**, 223 – 233, 1995.

[65] **P. L. ANDRESEN, T. M. ANGELIU,** "The Effect of In-Situ Noble Metal Chemical Addition on Crack Growth Rate Behaviour of Structural Materials in 288 °C Water", Paper No.969084, *NACE Corrosion 96*, NACE, Houston, Texas, USA, 1996.

[66] **F.P. FORD, P.L. ANDRESEN,** "Corrosion Fatigue of A533B/A508 Pressure Vessel Steels in 288 °C Water", Proc. 3rd Int. IAEA Specialist's Meeting on Sub-critical Crack Growth, Vol. 1, pp. 105 – 124, W. Cullen, Ed., NUREG/CP-0112, Moscow, USSR, May 14 – 17, 1990.

[67] **S. RITTER, H.P. SEIFERT,** *Power Plant Chemistry,* **6**, pp. 748 – 760, 2004.

[68] **S. RITTER, H.P. SEIFERT,** "The Effect of Chloride and Sulfate Transients on the Stress Corrosion Cracking Behaviour of Low-Alloy RPV Steels Under Simulated BWR Environment", NACE Corrosion 2004, CD-ROM, Paper No. 04680, NACE, New Orleans, LA, USA, March 28 – April 1, 2004.

[69] **H.P. Seifert, S. Ritter,** *Chimia,* **59,** 2005 (to appear).

[70] **L.M. YOUNG, P.L. ANDRESEN**, "Crack-Tip Micro-Sampling and Growth Measurements in a 0.021% S Low-Alloy Steel in High-Temperature Water", Proc. 7th International Symposium on Environmental Degradation of Materials in Nuclear Power Systems – Water Reactors, Breckenridge, Colorado, Vol. 2, pp. 1193 – 1202, August, 1995.

[71] **J. HICKLING, U. REITZNER**, *VGB Kraftwerkstechnik*, **72**, pp. 359 – 367, 1992.

[72] **J. HICKLING**, "Strain-Induced Corrosion Cracking of Low-Alloy Steels under BWR Conditions: Are There Still Open Issues?", Proc. 10th Int. Conf. on Environmental Degradation of Materials in Nuclear Power Systems – Water Reactors, NACE/ANS/TMS, Lake Tahoe, Nevada, USA, August 6 - 10, 2001.

[73] **H.D. SOLOMON, R. E. DELAIR, A. UNRUH**, "Crack Initiation in Low-Alloy Steel in High-Temperature Water", in Effects of the Environment on the Initiation of Crack Growth, ASTM STP 1298, pp. 135 – 149, W.A. Van der Sluys, R.S. Piascik, R. Zawierucha, Eds., ASTM, 1997.

[74] **H.D. SOLOMON, R. E. DELAIR, A. TOLKSDORF**, LCF Crack Initiation in WB36 in High-Temperature Water, Proc. 9th International Symposium on Environmental Degradation of Materials in Nuclear Power Systems – Water Reactors, pp. 865 – 872, NACE/TMS/ANS, Newport Beach, USA, August 1 – 5, 1999.

[75] **H.D. SOLOMON, R. E. DELAIR, H.HOFFMANN**, "Influence of Environment and Strain Rate on the Low Cycle Fatigue Crack Initiation in Low Alloy Steel 15NiCuMoNb5 in High Temperature Water", Proc. 11th Int. Conf. on Environmental Degradation of Materials in Nuclear Power Systems – Water Reactors, CD-ROM, NACE/TMS/ANS, Stevenson, WA, USA, August 10 – 14, 2003.

[76] **A. ROTH et al.**, "The Effect of Transients on the Crack growth Behaviour of Low Alloy Steels for Pressure Boundary Components under Light Water reactor Conditions", Proc. 12th Int. Conf. on Environmental Degradation of Materials in Nuclear Power Systems – Water Reactors, CD-ROM, NACE/TMS/ANS, Snowbird, Utah, USA, August 14 – 18, 2005.

[77] **W.A. VAN DER SLUYS, R.H. EMANUELSON**, "Environmental Acceleration of Fatigue Crack Growth in RPV Materials and Environments", Environmentally-Assisted Cracking: Science and Engineering, ASTM STP 1049, pp. 117 – 135, 1990.

[78] **D. TICE**, *International Journal of Pressure Vessel & Piping*, **24**, pp. 139 – 173, 1986.

[79] **G. BRÜMMER et al.**, "Investigation on Environmentally Assisted Cracking Behaviour of a Ferritic Reactor Presure Vessel Steel under Simultaneous Influence of Simulated BWRE Coolant and Irradiation", Proc. 11th Int. Conf. on Environmental Degradation of Materials in Nuclear Power Systems – Water Reactors, CD-ROM, NACE/TMS/ANS, Stevenson, WA, USA, August 10 – 14, 2003.

[80] **P. ANDRESEN**, "Effects of Flow Rate on SCC Growth Rate Behaviour in BWR Water", Proc. 8th Int. Symp. on Environmental Degradation of Materials in Nuclear Power Systems – Water Reactors, pp. 603 – 614, ANS/TMS/NACE, Amelia Island, Florida, USA, August 10 – 14, 1997.

[81] **H. CHOI et al.**, *Corrosion*, **38**, pp.76 – 85, 1982.

[82] **J. HICKLING**, *Corrosion*, **40**, pp. 36 – 38, 1984.

[83] **A. HIRANO et al.**, *Pressure Vessel and Piping (PVP)*, 439, pp. 143 – 150, 2002.

[84] **E. LENZ, N. WIELING, H. MÜNSTER**, "Influence of Variation of Flow Rate and Temperature on the Cyclic Crack Growth Rate under BWR conditions", Proc. 3rd Int. Symposium on Environmental Degradation of Materials in Nuclear Power Systems – Water Reactors, TMS-AIME, pp. 283 – 288, 1988.

[85] P.M. Scott, A.E. Truswell, *Journal of Pressure Vessel Technology*, **105**, pp. 245 – 254, 1983.

[86] H. Kitigawa, K. Komai, H. Nakajima, M. Higuchi, "Testing Round Robin on Cyclic Crack Growth of Low and Medium Sulphur A533B Steels in LWR Environments", Transaction 9th SMIRT Conference, Vol. F, ,pp. 155 – 160, 1987.

[87] Y. Katada, N. Nagata, S. Sato, "Fatigue Crack Growth Behaviour and Corrosion Potential of A533B Steels in High Temperature Pressurized Water", Fatigue 90, Vol. III, Materials & Component Engineering Publications, pp. 1819 –1824, 1990.

[88] L. A. James et al., *Journal of Pressure Vessel Technology*, **117**, pp. 238 – 244, 1995.

[89] L. A. James et al., *Journal of Pressure Vessel Technology*, **119**, pp. 83 - , 1997.

[90] P. Hurst, P. Banks, G. Pemberton, A.S. Raffel, "Stress Corrosion Behaviour of A533B and A508-III Steels and Weldments in High Temperature Water Environments", Proc. 2nd International Symposium on Environmental Degradation of Materials in Nuclear Power Systems – Water Reactors, ANS, pp. 645 – 655, 1986.

[91] W.J. Shack et al., "Environmentally-Assisted Cracking in Light Water Reactors", NUREG/CR-4667, Vol. 5, 1989.

[92] P.M. Scott, A.E. Truswell, "The Influence of Water Chemistry on Fatigue Crack Propagation in LWR Pressure Vessel Steels"; Proc. 1st IAEA Specialists Meeting on Subcritical crack Growth, Vol. 1 / 2, NUREG CP-0044, p. 91 – 176, Freiburg, Germany, 1981.

[93] C.C. Lin et al., *Corrosion*, **53**, p. 618, 1996.

[94] Y. Kim, "Role of Hydrogen Peroxide and its Decomposition in BWRS", Proc. 10th Int. Conf. on Environmental Degradation of Materials in Nuclear Power Systems – Water Reactors, NACE/ANS/TMS, Lake Tahoe, Nevada, USA, August 6 - 10, 2001.

[95] P.L. Andresen, F.P. Ford, S.M. Murphy, J.M. Perkins, "State of Knowledge on Radiation Effects on Environmental Cracking in Light Water Reactor Core Materials", Proc. 4th International Symposium on Environmental Degradation of Materials in Nuclear Power Systems – Water Reactors, NACE, pp. 1/83 – 1/121, 1990.

[96] P. Andresen, F.P. Ford, A.J. Jacobs, "Life Prediction of LWR Core Internals Subjected to Stress Corrosion Cracking", VGB-Conference "Corrosion and Corrosion Protection in Power Plant Technology 1995", Attachment 13, Essen, November 29 - 30, 1995.

[97] L. A. James, *Nuclear Safety*, **18**, pp. 791 – 801, 1997.

[98] W.H. Cullen et al., *Journal of Nuclear Materials*, **96**, pp. 261 –268, 1981.

[99] W.H. Cullen, H.E. Watson, R.A. Taylor, F.J. Loss, H.A. Spencer, "Fatigue Crack Growth Rates of Irradiated Pressure Vessel Steels in Simulated Nuclear Coolant Environment", Proceedings of the IAEA Specialist's Meeting on Sub-Critical Crack Growth, NUREG/CP 0044, Vol. 1, pp. 89 – 108, May 1983.

[100] R.G. Lott, T.R. Mager, "Corrosion Fatigue of Irradiated Pressure Vessel Steels", Proc. 2nd International Symposium on Environmental Degradation of Materials in Nuclear Power Systems – Water Reactors, ANS, pp. 189 – 197, 1986.

[101] W.H. Cullen, "Fatigue Crack Growth of Irradiated Pressure Vessel Steels in LWR Environments", Proceedings of the 2nd IAEA Specialist's Meeting on Sub-Critical Crack Growth, NUREG/CP 0067, Vol. 1, pp. 357 – 378, April 1986.

[102] W.H. Cullen, "Fatigue Crack Growth in Pressure Vessel and Piping Steels in LWR Environments", NUREG/CR-4724, US NRC, March 1987.

[103] D. ANDERS, J. FÖHL, *Nuclear Engineering & Design*, **136**, pp. 265 – 276, 1992.

[104] M. RUSCAK, J. KYSELA, A. BROZOVA, O. ERBEN, M. POSTLER, G. BRUEMMER, H. HOFFMANN, U. ILG, W. RÜHLE, "Stress Corrosion Cracking Tests of RPV Steels under Simulated BWR Coolant and Irradiation Conditions", Proc. 9th International Symposium on Environmental Degradation of Materials in Nuclear Power Systems – Water Reactors, pp. 875 – 882, 1999.

[105] K. KUSSMAUL, E. ROOS, J. FÖHL, "Forschungsvorhaben Komponentensicherheit (FKS) – Ein wesentlicher Beitrag zur Komponentensicherheit", 23. MPA Seminar, pp. 2-1 – 2-21, October 1 - 2, 1997.

[106] H. GLADEN, H. KAESCHE, *Nuclear Engineering & Design*, **151**, pp. 463 – 472, 1994.

[107] H. FRIEDRICH, J. FRANK, H. GLADEN, M. STRATMANN, "Stress Corrosion Cracking of Low-Alloy Steels under High Pressure and High-Temperature Conditions", Corrosion 96, Baltimore, MD, USA, Paper 98, pp. 98-1 – 98-10, 1996.

[108] L.M. YOUNG, P.L. ANDRESEN, "Crack-Tip Microsampling and Growth Measurements in a 0.021%S Low-Alloy Steel in High-Temperature Water", Proc. 7th International Symposium on Environmental Degradation of Materials in Nuclear Power Systems - Water Reactors, Vol. 2, pp. 1193 – 1202, Breckenridge, Colorado, August, 1995.

[109] J. KUNIYA, H. ANAZAI, I. MASAOKA, *Corrosion*, **48**, pp. 419 – 425, 1992.

[110] J.D. ATKINSON, "The Role of MnS-Inclusions in the Development of Environmentally Assisted Cracking of Nuclear Reactor Pressure Vessel Steels", Proc. 2nd IAEA Specialist's Meeting on Sub-critical Crack Growth, Sendai, Japan, NUREG/CP-0067, Volume II, pp. 153 – 178, May 15 – 17, 1986.

[111] K. RIPPSTEIN, H. KAESCHE, *Corrosion Science*, **29**, pp. 517 – 534, 1989.

[112] H. GLADEN, "Untersuchungen zur Spannungsrisskorrosion von Feinkornbaustählen in Hochdruck-Hochtemperatur-Wasser", PhD thesis, Erlangen, April 1994.

[113] H. HÄNNINEN, I. AHO-MANTILA, K. TÖRRÖNEN, "Environment Sensitive Cracking in Pressure-Boundary Materials of Light Water Reactors", CSNI Report 141, 1987.

[114] F.P. FORD, *Journal of Pressure Vessel Technology*, **110**, pp. 113 – 128, 1988.

[115] C.E. SIMS, *Transactions Metallurgical Society of the AIME*, **215**, pp. 367 – 393, 1995.

[116] J. BULLOCH, *Res. Mechanica*, **8**, pp. 331 – 354, 1986.

[117] W.A. LOGSDON, P.K. LIAW, J.A. BEGLEY, "Fatigue Crack Growth Rate Properties of SA508 and SA533 Pressure Vessel Steels and Submerged Arc Weldments in a Pressurized Water Environment", Fracture Mechanics: 19th Symposium, ASTM STP 969, pp. 830 – 867, 1998.

[118] P.K. LIAW et al., *Metallurgical Transactions*, **20**, pp. 2069 – 2085, 1989.

[119] G. WRANGLÉN, *Corrosion Science*, **14**, pp. 331 – 349, 1974.

[120] W.H. BAMFORD, "A Summary of Environmentally-Assisted Crack Growth Studies Performed at Westinghouse Electric Power Corporation: Under Funding from the HSST-Programme", NUREG/CR-5020, US NRC, May 1988.

[121] J.H. BULLOCH, "Environmental Assisted Cracking Phenomena in Reactor Pressure Vessel Steel – the Role of Manganese Sulphide Segregation", Proc. 3rd International Symposium on Environmental Degradation of Materials in Nuclear Power Systems – Water Reactors, TMS, pp. 261 – 268, 1987.

[122] W.H. BAMFORD, I.L.W. WILSON, "Characterization of the Environmental Cracking Behavior of High Sulphur Steel Plates", Proceedings of the 2nd IAEA Specialist's Meeting on Sub-Critical Crack Growth, NUREG/CP 0067, Vol. 1, pp. 317 – 338, April 1986.

[123] T. KONDO, J. KUNIYA, H. TAKAKU, K. TOKIMASA, M. ARII, M. KURIHARA, "Recent Studies on Cyclic Crack Growth of Reactor Pressure-Boundary Materials in High Temperature Water Environments in Japan", Proceedings of the 2nd IAEA Specialist's meeting on Sub-Critical Crack Growth, NUREG/CP 0067, Vol. 1, pp. 219 – 249, April 1986.

[124] W.A. VAN DER SLUYS, R.H. EMANUELSON, "Environmental Acceleration of Fatigue Crack Growth in Reactor Pressure Vessel Materials and Environments", Environmentally-Assisted Cracking: Science and Engineering, ASTM STP 1049, pp. 117 – 135, 1990.

[125] G. SUND, "Quantifying Manganese Sulphide Inclusions in Pressure Vessel Steels", SKI Report 94:23, 1994.

[126] H. CHOI et al., *Corrosion*, **38**, pp. 136 – 144, 1982.

[127] J. KUNIYA, *Journal of Pressure Vessel Technology*, **107**, pp. 430 – 435, 1985.

[128] H.P. SEIFERT, S. RITTER, U. INEICHEN, U. TSCHANZ, B. GERODETTI, "RIKORR-I – Risskorrosion in druckführenden Komponenten des Primärkreislaufes von SWR", PSI Report No 03-10, Switzerland, April 2003.

[129] J. HICKLING, "Strain-Induced Corrosion Cracking: Relationship to Stress Corrosion Cracking/Corrosion Fatigue and Importance for Nuclear Service Life", 3rd IAEA Specialist's Meeting on Sub-Critical Crack Growth, Moscow, NUREG/CP-0112, ANL-90/22, Vol. 2, pp. 9 – 26, May 14 - 19, 1990.

[130] J. HICKLING, "Wasserstoffinduzierte Spannungsrisskorrosion in niedriglegierten Stählen", Beitrag Nr. 7, 4. MPA-Seminar, Stuttgart, October 4 – 5, 1978.

[131] M.O. SPEIDEL, "Ursachen und Geschwindigkeit des umgebungsabhängigen Bruches in metallischen und nichtmetallischen Werkstoffen", Umgebungsabhängiges Bruchverhalten: Werkstoffschädigung und Bauteilsicherheit in korrosiven Medien und bei erhöhter Temperatur, Vorträge zur 17. Metalltagung, M. Schaper, J. Barthel, Eds., Dresden, Germany, October 29 – 31, 1990.

[132] M.O. SPEIDEL, "Stress Corrosion Cracking and Corrosion Fatigue Fracture Mechanics", Corrosion in Power Generating Equipment, Proceedings of the 8th Int. Brown Boveri Symposium, pp. 85 – 132, Plenum, New York, USA, 1984.

[133] M. TSUBOTA, H. SAKAMOTO, R. TSUZUKI, "Intergranular Stress Corrosion Cracking of Low-Alloy and Carbon Steels in High-Temperature Water", Proc. 6th International Symposium on Environmental Degradation of Materials in Nuclear Power Systems - Water Reactors, pp. 53 – 58, TMS, San Diego, California, USA, August 1- 5, 1993.

[134] H.P. SEIFERT, S. RITTER, "SCC of Low-Alloy RPV steels under BWR Conditions – New Observations -", Minutes of the ICG-EAC 2001 Meeting, Paper LAS-4, Kyongju, South Korea, April 23 – 27, 2001.

[135] E. LENZ, N. WIELING, *VGB Kraftwerkstechnik,* **66**, pp. 481 – 485, 1986.

[136] H.P. SEIFERT, S. RITTER, "The Role of DSA, Yield Stress and Low-Temperature Creep in EAC of LAS - Preliminary Experimental Observations and Interpretation", Minutes of the 2005 Annual Meeting of the International Co-operative Group on Environmentally-Assisted Cracking of Water Reactor Materials, CD-ROM, Ed.: J. Hickling, Low Alloy Steel Session, Paper LAS10, Antwerp, Belgium, April 10 – 15, 2005.

[137] **L.M. YOUNG, P. ANDRESEN,** "Crack Tip Strain Rate: Estimates Based on Continuums Theory and Experimental Measurement", NACE Corrosion 2001, Paper 01131, NACE, 2001

[138] **Q. PENG, T. SHOJI,** *Journal of Nuclear Materials,* **324**, pp. 52 – 61, 2004

[139] **A. ROTH,** "Investigation of Dynamic Strain Ageing Effects of Low Alloy Steels and Their Possible Relevance for Environmentally-Assisted Cracking in Oxygenated High-Temperature Water", Proc. 11th Int. Conf. on Environmental Degradation of Materials in Nuclear Power Systems – Water Reactors, CD-ROM, NACE/TMS/ANS, Stevenson, WA, USA, August 10 – 14, 2003.

[140] **R. SCHELLENBERGER,** "Einfluss des Niedertemperaturkriechens auf das Korrosionsriss-wachstum ferritischer Stähle", Techn. wiss. Ber. MPA Stuttgart, Heft 99-02, 1999.

[141] **S.M. HAN, O.G. KWON,** *Journal of Material Science,* **39**, pp. 6555 – 6559, 2004.

[142] **D.J. GOOCH,** *Materials Science and Engineering,* **64**, pp. 183 – 196, 1984.

[143] **D.J. GOOCH,** *Materials Science and Engineering,* **83**, pp. 17 – 27, 1987.

[144] **D.J. GOOCH,** *Materials Science and Engineering,* **91**, pp. pp. 45 – 54, 1987.

[145] **J.G. NEATE,** *Material Science & Technology,* **3**, pp. 14 – 22, 1987.

[146] **A. SHIBLI,** *Material Science & Technology,* **3**, pp. 110 – 117, 1987.

[147] **E.J. H. BULLOCH,** *Theoretical and Applied Fracture Mechanics,* **212**, pp. 142 – 155, 1994.

[148] **W.R. CORWIN et al.,** "Thermal Embrittlement of Reactor Pressure Vessel Steels", Transactions of the 13th SMIRT Conference, pp. 345 - 350, Porto Alegre, Brazil, August 13 – 18, 1995.

[149] **S. RITTER, H.P. SEIFERT,** "Effect of a Chloride Transient on the EAC Crack growth Behaviour of Low-Alloy RPV Steels under Simulated BWR Operating Conditions", PSI Report No. 02-23, ISSN 1019-0643, November 2002.

[150] **X.Q. WU, Y. KATADA,** *Corrosion,* **60,** pp. 1045 - , 2004.

[151] **A. CELOVSKY, M.D. WRIGHT, T.S. GENDRON, S.A. USMANI, J. SLADE,** "S08: Investigation and Repair of a Cracked Feeder at Point Lepreau", 4th Int. Conf. CANDU Maintenance, pp. 97-109, Toronto, Canada, CNS, 1997.

[152] **A. SHIBLI,** *International Journal of Pressure Vessel & Piping,* **24**, pp. 303 – 336, 1986.

[153] **R. WU et al.,** *Journal of Nuclear Materials,* **336**, pp. 279 – 290, 2005.

[154] **W.A. VAN DER SLUYS,** "Evaluation of the Available Data on the Effect of the Environment on the Low Cycle Fatigue Properties in Light Water Reactor Environments", Proc. 6th Int. Symp. on Env. Degr. of Mat. in Nucl. Power Systems – Water Reactors, pp. 1 – 4, NACE/TMS/ANS, San Diego, California, USA, August 1 – 5, 1993.

[155] **T. SHOJI et al.,** *Journal of Engineering Materials and Technology,* **103**, pp. 298 – 304, 1981.

[156] **F.P. FORD, P.L. ANDRESEN,** "Corrosion Fatigue of A533B/A508 Pressure Vessel Steels in 288 °C Water", Proc. 3rd Int. IAEA Specialist's Meeting on Subcritical Crack Growth, Vol. 1, pp. 105 – 124, W. Cullen, Ed., NUREG/CP-0112, Moscow, USSR, May 14 – 17, 1990.

[157] **B. ISKLUTH,** "Beitrag zur Spannungsrisskorrosion am Beispiel eines niedriglegierten warmfesten Feinkornbaustahles in sauerstoffhaltigem Hochtemperaturwasser", Ph.D thesis, Staatliche Materialprüfungsanstalt, Universität Stuttgart, 1989.

[158] **T.A. Prater,** *Journal of Engineering Materials and Technology*, **108**, pp. 2 – 9, 1986.

[159] **W.A. Van der Sluys, R. Pathania,** "Studies of Stress Corrosion Cracking in Steels used for Reactor Pressure Vessels", Proc. 5th International Symposium on Environmental Degradation of Materials in Nuclear Power Systems – Water Reactors, pp. 571 – 578, TMS, Monterey, California, USA, 1991.

[160] **D. Blind et al.,** "European Round Robin on Constant Load EAC Tests of Low Alloy Steel under BWR Conditions", Proc. 9th Int. Conf. on Environmental Degradation of Materials in Nuclear Power Systems – Water Reactors, pp. 911 – 919, ANS/NACE/TMS, Newport Beach, CA, USA, August 1 – 5, 1999.

[161] **U. Ehrnstén et al.,** "Inter-laboratory Crack Growth Test on Pressure Vessel Steel 20 MnMoNi 5 5 in Simulated BWR Environment", Proc. 11th Int. Conf. on Environmental Degradation of Materials in Nuclear Power Systems – Water Reactors, CD-ROM, NACE/TMS/ANS, Stevenson, WA, USA, August 10 – 14, 2003.

[162] **G.J. Loyd,** "Constant Load and Constant Displacement Stress Corrosion in Simulated Water Reactor Environments", Proc. of the 2nd International Atomic Energy Agency Specialist's Meeting on Sub-Critical Crack Growth, NUREG/CP-0067, Vol. I, pp. 423 – 437, Sendai, Japan, May 15 – 17, 1986.

[163] **S. Ritter, H.P. Seifert,** "Stress Corrosion Cracking Behavior of Low-Alloy Reactor Pressure Vessel Steels and of a Weld Filler Material under Simulated BWR Environment", NACE Corrosion 2003, CD-ROM, Paper No. 03664, March 16 – 20, 2003.

[164] **H.M. Chung et al.,** "Environmentally Assisted Cracking in Light Water Reactors", NUREG/CR-4667, Vol. 14, Argonne National Laboratory, August 1992.

[165] **H.P. Seifert, S. Ritter,** "Einfluss von kleinen Lastfluktuationen auf das Korrosionsrisswachstum in RDB-Stählen unter SWR/NWC-Bedingungen", Handout of Presentation at the "52. Sitzung des RSK-Ausschusses Druckführende Komponenten und Werkstoffe", BMU, Bonn, Germany, March 30, 2005.

[166] **V. Läpple,** "Untersuchungen zum korrosionsgestützten Rißwachstum ferritischer Stähle in sauerstoffhaltigem Hochtemperaturwasser", Technisch-wissenschaftlicher Bericht der MPA Stuttgart 96/02, Staatliche Materialprüfanstalt Universität Stuttgart, 1996.

[167] **J. Hickling,** "Evaluation of Acceptance Criteria for Data of Environmentally-Assisted Cracking in Light Water Reactors", SKI Report 94:14, Statens Kärnkraftinspektion, September 1994.

[168] **P.M. Scott,** "Recommended Test Procedure for Studies on Crack Growth in Simulated LWR Water Environments", Proc. 3rd International Atomic Energy Agency Specialist's Meeting on Sub-Critical Crack Growth, Vol. 2, NUREG/CP-0112, ANL-90/22, pp. 117 – 128, Moscow, USSR, 1990.

[169] **P.L. Andresen,** "Effects of Testing Characteristics on Observed SCC Behaviour in BWR", NACE Corrosion 98, Paper No. 137, pp. 137.1 - 137.16, San Diego, CA, USA, 1998.

[170] **F.P. Ford et al.,** "Stress Corrosion Cracking of Low Alloy Steels under BWR Conditions; Assessments of Crack Growth Rate Algorithms", Proc. 9th Int. Conf. on Environmental Degradation of Materials in Nuclear Power Systems – Water Reactors, pp. 855 – 863, ANS/NACE/TMS, Newport Beach, CA, USA, August 1 – 5, 1999.

[171] **F.P. Ford, P. L. Andresen,** "Stress Corrosion Cracking of Low-Alloy Steels in 288 °C Water", NACE Corrosion 89, Paper No. 498, pp. 498-1 – 498-19, NACE, New Orleans, Houston, USA, 1989.

[172] G. GABETTA, C. RINALDI, M.M. RADAELLi, "Stress Corrosion Tests in Water at 288 °C, using the Unloading Compliance Technique", Proc. ECF 8, pp. 1083 – 1089, Turin, October 1 – 5, 1990.

[173] G. GABETTA, C. RINALDI, "Environmentally Assisted Cracking of A533B RPV Steel", Proc. 3rd International Atomic Energy Agency Specialist's Meeting on Sub-Critical Crack Growth, NUREG/CP-0112, ANL-90/22, Vol. 2, pp. 145 – 154, Moscow, USSR, 1990.

[174] R. SCHELLENBERGER, P. DEIMEL, Nuclear Engineering & Design, 151, pp. 449 – 461, 1994.

[175] E. EASON et al., Nuclear Engineering & Design, 184, pp. 89 – 111, 1998.

[176] E. EASON et al., WRC Bulletin, 404, pp. 38 – 51, 1995.

[177] K. TÖRRÖNEN, M. KEMPPAINEN, H. HÄNNINEN, "Fractographic Evaluation of Specimens of A533B Pressure Vessel Steel", EPRI-Report, EPRI-NP-3483, Final Report, May, 1984.

[178] H.HÄNNINEN et al., Corrosion Science, 23, pp. 663 –679, 1983.

[179] K. MABUCHI et al., Corrosion, 47, pp. 500 – 508, 1991.

[180] P.M. YUKAWICH, C.W. HUGHES, Practical Metallography, 20, pp. 1 – 12, 1997.

[181] R. PATHANIA et al., "Stress Corrosion Cracking in Low Alloy Steels", EPRI Report RPC 102-4, EPRI, Palo Alto, CA, USA, February 1994.

[182] BWRVIP-60, "Evaluation of Stress Corrosion Crack growth in Low Alloy Steel Vessel Materials in the BWR Environment (BWRVIP-60) ", Final Report, EPRI TR 108709, March 1999.

[183] G. BRÜMMER et al., "Beschreibung einer einhüllenden Risswachstumskurve zum Spannungsrisskorrosions-verhalten von ferritischen Reaktordurckbehälter (RDB)-Stählen unter Siedewasser (SWR)-Bedingungen", Proc. of 28th MPA Seminar, Safety and Reliability in Energy Technology, Vol. 1, Paper No.13, pp. 13.1 – 13. 30, Stuttgart, Germany, October 10 and 11, 2002.

[184] B. CHENG et al., "BWR Water Chemistry Guidelines – 1996 Revision", EPRI Report TR-103515-R1, Palo Alto, December 1996.

[185] M. LASCH, U. STAUDT, VGB-Kraftwerkstechnik, 75, pp. 745 – 750, 1995.

[186] Personal communication with B. AGHILI (SKI).

[187] O.K. CHOPRA, W. J. SHACK, "Effects of LWR Coolant Environments on Fatigue Design Curves of Carbon and Low–Alloy Steels", NUREG/CR–6583, ANL–97/18, March 1998.

[188] D.J. GAVENDA, P. R. LUEBBERS, O. K. CHOPRA, "Crack Initiation and Crack Growth Behavior of Carbon and Low–Alloy Steels", Fatigue and Fracture 1, Vol. 350, pp. 243 – 255, S. Rahman, K. K. Yoon, S. Bhandari, R. Warke, and J. M. Bloom, Eds., ASME, New York, 1997.

[189] O.K. CHOPRA, W. J. SHACK, Journal of Pressure Vessel Technology, 121, pp. 49 – 60, 1999.

[190] O.K. CHOPRA, Pressure Vessel and Piping (PVP), 439, pp. 119–132, 2002.

[191] M. HIGUCHI, K. IIDA, Nuclear Engineering & Design, 129, pp. 293 – 306, 1991.

[192] O.K. CHOPRA, W. J. SHACK, "Effects of LWR Coolant Environments on Fatigue Design Curves of Carbon and Low-Alloy Steels", NUREG/CR–6583, ANL–97/18, March 1998.

[193] **O.K. CHOPRA, W. J. SHACK,** "Environmental Effects on Fatigue Crack Initiation in Piping and Pressure Vessel Steels", NUREG/CR–6717, ANL–00/27, May 2001.

[194] **O.K. CHOPRA,** "Effects of LWR Coolant Environments on Fatigue Design Curves of Austenitic Stainless Steels", NUREG/CR–5704, ANL–98/31, 1999.

[195] **K. IIDA, K., T. BANNAI, M. HIGUCHI, K. TSUTSUMI, K. SAKAGUCHI,** *Pressure Vessel and Piping (PVP),* **419**, pp. 73 - 82, 2001.

[196] **G. NAKAO, H. KANASAKI, M. HIGUCHI, K. IIDA, Y. ASADA,** *Pressure Vessel and Piping (PVP),* **306**, pp. 123 - 128, 1995.

[197] **Y. KATADA, N. NAGATA, S. SATO,** *ISIJ International.* **33**, pp. 877 - 883, 1993.

[198] **A. HIRANO, M. YAMAMOTO, K. SAKAGUCHI, K. IIDA, T. SHOJI,** *Pressure Vessel and Piping (PVP),* **410**, pp. 13 - 18, 2000.

[199] **A. HIRANO, A., M. YAMAMOTO, K. SAKAGUCHI, T. SHOJI, K. IIDA,** *Pressure Vessel and Piping (PVP),* **439**, pp. 143–150, 2002.

[200] **H.S. MEHTA, S. R. GOSSELIN,** *Nuclear Engineering & Design,* **181**, pp. 175 - 197, 1998.

[201] **H.S. MEHTA,** *Pressure Vessel and Piping (PVP),* **386**, pp. 183 - 193, 1999.

[202] **O.K. CHOPRA, W. J. SHACK,** "Evaluation of Effects of LWR Coolant Environments on Fatigue Life of Carbon and Low–Alloy Steels, in Effects of the Environment on the Initiation of Crack Growth", ASTM STP 1298, W. A. Van Der Sluys, R. S. Piascik, and R. Zawierucha, Eds., ASTM, Philadelphia, pp. 247 - 266, 1997.

[203] **M. HIGUCHI,** "Development of Evaluation Method of Fatigue Damage on Operating Plant Components in Considering Environmental Effect of LWR Coolant", Proc. 3rd International Conference on Fatigue of Reactor Components, Session4: Code Rules and Guidelines, CD-ROM, OECD/EPRI, Seville, Spain, October 3 – 6, 2004.

[204] **O.K. CHOPRA, W.J. SHACK,** "Effects of LWR Coolant Environments on Fatigue crack Initiation in Carbon and Low-Alloys Steels and Austenitic Stainless Steels", Proc. 3rd International Conference on Fatigue of Reactor Components, Session 3: Environmental Effects, CD-ROM, OECD/EPRI, Seville, Spain, October 3 – 6, 2004.

[205] **L. A. JAMES,** *ASM-PVP,* **307**, pp. 207 – 230, 1998.

[206] **G.L. WIRE,** *Nuclear Engineering & Design,* **197**, pp. 25 – 44, 2000.

[207] **Y. YIN LI,** *Nuclear Engineering & Design,* **197**, pp 45 – 60, 2000.

[208] **E. EASON, G.B. HEYS,** "Fatigue Crack Growth Rate of Medium and Low Sulfur Ferritic Steels in Pressurized Water Reactor Primary Water Environments", ASME Pressure Vessel and Piping Conference 2003, Cleveland, Ohio, USA, July 20 – 24, 2003.

[209] **H. METHA, R. HORN,** "Low Alloy Steel EAC Corrosion Fatigue Relationships for BWR Envrionment", Proc. 3rd International Conference on Fatigue of Reactor Components, Session 3: Environmental Effects, CD-ROM, OECD/EPRI, Seville, Spain, October 3 – 6, 2004.

[210] **S. RANGANATH, J. HICKLING,** "Development of a Possible Bounding Corrosion Fatigue Crack Growth Rate relationship for Low Alloy Steel Pressure vessel Materials in BWR Environments", Proc. 3rd International Conference on Fatigue of Reactor Components, Session 3: Environmental Effects, CD-ROM, OECD/EPRI, Seville, Spain, October 3 – 6, 2004.

[211] **R.H. JONES, R.E. RICKER,** "Mechanism of Stress Corrosion Cracking, in Stress Corrosion Cracking", R.H. Jones, Ed., ASM International, pp. 1 – 40, 1993.

[212] **A.TURNBULL,** *Corrosion Science,* **34**, pp. 921 – 960, 1993.

[213] T.Magnin, *Material Science Forum*, **202**, 1995.

[214] F.P. FORD, "The Crack-Tip System and its Relevance to the Prediction of Cracking in Aqueous Environments", Environment-Induced Cracking of Metals, R.P. Gangloff, M.B. Ives, Eds., NACE, pp. 139 – 166, Houston 1996.

[215] P.L. ANDRESEN, "Modelling the Effect of Sulphur on the Threshold Environmental Cracking Rate of Steels in High Temperature Water", Proc. 3rd Int. Conf. on Fatigue and Fatigue Thresholds, Midlands, UK, pp. 1189 – 1200, 1987.

[216] M.J. PSAILA DOMBROWSKI, M.J. Psaila Dombrowski, "Modelling of Crack and Crevice Chemistry in Light Water Reactor Environments", PhD Thesis, MIT, 1990.

[217] A. TURNBULL, "Crack-Tip Electrochemistry", Corrosion Sous Contrainte, D. Desjardins, R. Oltra, Eds, Bombanes, France, Les Editions de Physique, pp. 75 – 100, 1990.

[218] H. HÄNNINEN, K. TÖRÖNNEN, W.H. CULLEN, "Comparison of Proposed Cyclic Crack Growth Mechanisms of Low-Alloy Steels in LWR Environments", Proc. 2nd Int. IAEA Specialist's Meeting on Sub-Critical Crack Growth, NUREG/CP-0067, Vol. 2, pp. 73 – 97, Sendai, Japan, Mai 15 – 17, 1985.

[219] F.P. FORD, "Predicition of Corrosion-Fatigue Initiation in Low-Alloy Steel and Carbon-Steel/Water Systems at 288 °C", Proc. 6th Int. Symp. on Env. Degr. of Mat. in Nucl. Power Systems – Water Reactors, pp. 9 – 17, NACE/TMS/ANS, San Diego, California, USA, August 1 – 5, 1993.

[220] F.P. FORD, P. COMBRADE, "Electrochemical Reaction Rates on Bare Surfaces and their Use in a Crack Prediction Model for the Low-Alloy Steel/Water system", Proc. 2nd Int. IAEA Specialsist's Meeting on Sub-critical crack Growth, NUREG/CP-0067, Vol. 2, pp. 231 – 268, Sendai, Japan, Mai 15 – 17, 1985.

[221] F.P. FORD, "Mechanism of Environmental Cracking in Systems Peculiar to the Power Generation Industry", EPRI-Report EPRI NP-2589, 1982.

[222] P. ANDRESEN, "Modelling of Water and Material Chemistry Effect on Crack-Tip Chemistry and Resulting Crack Growth Kinetics", Proc. 3rd Int. Symp. on Environmental Degradation of Materials in Nuclear Power Systems - Water Reactors, TMS-AIME, pp. 301 – 312, 1988.

[223] A.W. THOMPSON, I. W. BERNSTEIN, "The Role of Metallurgical Variables in Hydrogen Assisted Environmental Fracture", Rockwell Science Center Report, SCPP-75-63.

[224] P. ANDRESEN et al., "Mechanism and Kinetics of SCC in Stainless Steels", Proc. of 10th Int. Conf. on Environmental Degradation of Materials in Nuclear Power Systems – Water Reactors, NACE/TMS/ANS, CD-ROM, Paper No. 47, Lake Tahoe, Nevada, USA, August 6 – 10, 2001.

[225] H. HÄNNINEN, H. ILLI, K. TÖRRÖNNEN, M. VULLI, "On the Electrochemical and Chemical Conditions in Corrosion Fatigue Cracks of Low-Alloy Steels in High Temperature Water", Proc. 2nd IAEA Specialist's Meeting on Sub-Critical Crack Growth, NUREG/CP-0067, Vol. 2, pp. 179 – 200, Sendai, Japan, 1985.

[226] Y. LEE, T. SHOJI, K.S. RAJA, "Evaluation of Crack-Tip Solution Chemistry of Low-Alloy Steels in Oxygenated High-Temperature Water", Proc. 9th International Symposium on Environmental Degradation of Materials in Nuclear Power Systems - Water Reactors, pp. 893 – 898, Newport Beach, USA, August 1999.

[227] F.P. FORD, "Overview of Collaborative Research into Mechanisms of Environmentally Controlled Cracking in the Low-Alloy Pressure Vessel Steel/Water System", Proc. 2nd Int. IAEA Specialist's Meeting on Sub-Critical Crack Growth, NUREG/CP-0067, Vol. 2, pp. 3 – 71, Sendai, Japan, 1985.

[228] G. GABETTA, "Measure of Chemical and Electrochemical Parameters inside an Environmentally-Assisted Growing Crack", Proc. 3rd Int. IAEA Specialist's Meeting on Sub-Critical crack Growth, W. Cullen, Ed., NUREG/CP-0112, Vol. 2, pp. 129 – 143, Moscow, USSR, 1990.

[229] G. GABETTA, *Fatigue of Engineering Materials & Structures*, **5**, pp. 215 – 220, 1982.

[230] P.L. ANDRESEN, "Conceptual Similarities and Common Predictive Approaches for SCC in High Temperature Water Systems", NACE Corrosion 96, Paper No. 258, pp. 258-1 – 258-15, NACE, 1996.

[231] W.H. BRAMFORD et al., *ASM-PVP*, **119**, pp. 19 – 29, 1987.

[232] C.J. CZAJKOWSKI, *Int. Journal of Pressure Vessels and Piping*, **26**, pp. 97 – 110, 1986.

[233] B. VYAS et al., *Nuclear Technology*, **55**, pp. 525 – 537, 1981.

[234] K. KUSSMAUL et al., *Int. Journal of Pressure Vessel and Piping*, **17**, pp. 83 – 104, 1984.

[235] J.F. ENRIETTO et al., *Int. Journal of Pressure Vessel and Piping*, **9**, pp. 421 – 443, 1981.

[236] K. KUSSMAUL et al., *Int. Journal of Pressure Vessel and Piping*, **25**, pp. 111 – 135, 1986.

[237] E. LENZ et al., "CERT-Data and Their Relevance for Corrosion Assessments of Cases", *Proc. 2nd IAEA Specialists' Meeting on Sub-critical Crack Growth*, NUREG/CP-0067, Vol. 2, pp. 455 – 473, Sendai, Japan, May 15 – 17, 1985.

[238] M. MIKISCH et al., *Nuclear Engineering & Design*, **84**, pp. 179 – 187, 1985.

[239] E. LENZ, N. WIELING, *VGB Kraftwerkstechnik*, **66**, pp. 481 – 485, 1986.

[240] M. ERVE et al., *Nuclear Engineering & Design*, **96**, pp. 217 – 224, 1986.

[241] K. Kussmaul et al., *VGB Kraftwerkstechnik*, **64**, pp. 1115 – 1129, 1984.

[242] E. LENZ, A. SEIBOLD, "Dehnungsinduzierte Risskorrosion; Erfahrungen mit ferritischen Komponenten; Abhilfe- und Vorbeugungsmassnahmen gegen Schäden", VDI-Schadenstagung, Munich, FRG, pp. 125 – 130, 1985.

[243] G. ENGELHARD et al., "Neuere Werkstoff- und schweisstechnische Entwicklungen im Rohrleitungsbau", VGB Konferenz "Werkstoffe und Schweisstechnik im Kraftwerk", Essen, FRG, 1987.

[244] J. HICKLING, H.P. SEIFERT, S. RITTER, *Power Plant Chemistry*, **7**, pp. 4 – 15, 2005.

[245] D. Blind, "Zur Korrosionsrissbildung in druckführenden Kraftwerkskomponenten infolge Einwirkung von Hochtemperaturwasser", Habilitationsschrift, Universität Stuttgart, June 1991.

www.ski.se